Studies on the Aggregation Characteristics of Selected Surfactants and Surface Active Ionic Liquids

A Thesis submitted to the University of North Bengal

For the Award of

Doctor of Philosophy

in

Chemistry

By

Gulmi Chakraborty

Supervisor

Professor Swapan Kumar Saha
Department of Chemistry
University of North Bengal

Department of Chemistry
University of North Bengal
Darjeeling-734013
West Bengal
November-2017

Dedicated to my parents

DECLARATION

I declare that the thesis entitled **"Studies on the aggregation characteristics of selected surfactants and surface active ionic liquids"** has been prepared by me under the guidance of Dr. S. K. Saha (Supervisor), Professor of Chemistry, University of North Bengal. No part of this thesis has formed the basis for the award of any degree or fellowship previously.

Gulmi Chakraborty

Gulmi Chakraborty
Department of Chemistry
University of North Bengal
Darjeeling-734013
West Bengal
India

Date: 02.11.2017

University of North Bengal

Dr. S. K. Saha
Emeritus fellow (UGC)
DEPARTMENT OF CHEMISTRY
il: ssahanbu@hotmail.com

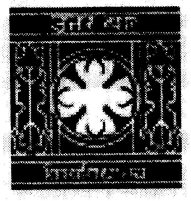

Ph: (0353) 2776 381
Fax: (0353) 2699 001
P.O. North Bengal University
Raja Rammohunpur
Dt. Darjeeling.
PIN – 734 013
Dated:

Ref.

CERTIFICATE

This is to certify that the thesis entitled "***Studies on the aggregation characteristics of selected surfactants and surface active ionic liquids***" submitted by **Ms Gulmi Chakraborty**,who got her name registered on 5th June, 2014 for the award of, Ph.D. (Science, new ordinance) degree of University of North Bengal, is absolutely based upon her own work under my supervision and that neither this thesis nor any part of it has been submitted for either any degree/diploma or any other academic award anywhere before.

Dr. S. K. Saha
Emeritus fellow (UGC)
Department of Chemistry
University of North Bengal
Darjeeling-734013
West Bengal
India

Date: 02.11.2017

ACKNOWLEDGEMENT

Firstly, I would like to convey my deepest gratitude and thankfulness towards my supervisor, Prof. S. K. Saha, for accepting me as his Ph.D student and giving me the opportunity to learn under his guidance. This thesis would not have been possible without him.

I sincerely thank all the faculty members, of our department, especially Prof. A. Misra, Prof. A. K. Nanda, Dr. S. Das, Prof. B. Basu and Prof. P. Ghosh who have always been very supportive providing their invaluable suggestions numerous times regarding DFT calculations, NMR studies and organic syntheses.

I also thank my lab mates, Dr. Soumik Bardhan, Madhurima Paul Chowdhury and Barnali Kar who have always been there for the scientific discussions besides making the work environment ambient. My special thanks to Dr. Tamal Goswami and Dr. Debasish Sengupta for their immense help in discussion and execution of theoretical calculations and organic syntheses.

I thank all the non-teaching members of our department for the office support they provided whenever necessary.

I would also like to specially acknowledge my friends Debolina, Sumit, Arpita, Pinaki, Swarnali and Dr. Biplab Panigrahi, for their unconditional love and support.

Finally, I am thankful to the Almighty for blessing me with my family. My parents have been the greatest support, pillar of strength and everything that I needed to make this journey possible. At times, when confidence gave away, they always pulled me up and showed the way to focus. My little sister is that never ending boost of energy, I always look up to. I also cannot thank Almighty enough for giving the companionship of Mr. D. Guha. He has been that person who never gave up on me and have always lifted me up in this incredible journey and beyond.

This work is financially supported by United Grants Commission, (UGC) New Delhi through the Basic Scientific Research (BSR) fellowship scheme (Award number: F.4-1/2006(BSR)/7-133/2007(BSR))

Gulmi Chakraborty

ABSTRACT

In this dissertation, detailed investigation of characteristics of molecular self-assembly of different surfactant systems have been explored via surface tensiometry, conductivity, UV-Visible spectroscopy, fluorescence steady state emission spectroscopy, fluorescence anisotropy, one dimensional proton nuclear magnetic resonance (^{1}H NMR) study, two dimensional nuclear Overhauser effect spectroscopy (2D NOESY) study, two dimensional rotating frame nuclear Overhauser effect (2D ROESY) study, small angle neutron scattering (SANS) study, density functional theory (DFT) calculations, dynamic light scattering study (DLS), rheometry, high resolution transmission electron microscopic (HRTEM) study and cryogenic transmission electron microscopic (cryo-TEM) study.

In **Chapter I**, the concept of molecular self-assembly has been introduced. The different types of molecular aggregates and the related systems have been presented with special emphasis on worm-like micelles. Application of self-assembled structures and important research advancements in related fields have been elaborately discussed.

In **Chapter II** the scope of research on molecular aggregates in the field of surface chemistry and the objectives of the present dissertation have been discussed.

In **Chapter III**, influence of head group geometry of cationic surfactants Cetyltrimethylammonium bromide (CTAB) and Cetylpyridinium bromide (CPB) on interaction with aromatic π-conjugated systems (additives) 1 Naphthol, 2 Naphthol and 2,3 Dihydroxynaphthalene have been explored as function of temperature and composition. It has been found that the aromatic π-conjugated systems behave as cosurfactant and synergistically reduce the critical micellization concentration (cmc) of both CTAB and CPB. Interaction parameter (β) evaluated on basis of regular solution theory showed that the naphthalene derivatives interacted more strongly with the pyridinium head group of CPB compared to quaternary ammonium head group of CTAB. SANS study revealed a morphology transition in spherical aggregates of CTAB and CPB to elongated cylindrical aggregates in presence of the aromatic additives. Rheometric study of the viscoelastic gels of the surfactant-additive systems have been presented as function of temperature. The observed characteristics have been discussed in light of cation-π and π-π interactions with the aid of ^{1}H NMR and NOESY study.

In **Chapter IV** the nature of transition from ordinary micelles (of nanometer length scale) of surface active ionic liquid 1-Hexadecyl-3-methylimidazolium chloride, to wormlike micelles (WLM) (micrometer length scale), mediated by 1 Naphthol, 2 Naphthol and 2,3 Dihydroxynaphthalene (2,3 DHN) in salt free condition have been studied under Newtonian as well as non-Newtonian flow regimes. Conductance and tensiometry showed that the additives lower the critical micelle concentration (cmc) of the ionic liquid surfactant. The interaction parameter (β) of the systems at different mole fractions evaluated on basis of Rubingh's Regular solution approach were negative at all SAIL/Additive compositions. UV-Vis spectroscopy showed that micelle-bound additives formed hydrogen bonds with interfacial water molecules. Location of the π-conjugated hydroxy aromatic derivatives within the SAIL micelles was ascertained via UV-Vis and ^{1}H NMR study. At higher concentration (100mM, 1:1), systems formed transparent viscoelastic gel. Rheological study of the viscoelastic gels showed that their zero shear viscosity is a function of temperature. 2,3 DHN interacted most strongly with the SAIL micelles, both in Newtonian and non-Newtonian regimes. This was corroborated by DFT study of binding energy. The study sheds light on understanding the molecular interactions behind the structural change from spherical to elongated micelles, in both microscopic and macroscopic scale, triggered by hydroxy naphthalenes under salt-free condition. The metal tolerance of the gels have been studied which has huge application prospects as fractured fluids in oil-mining industry.

In **Chapter V**, synthesis of hydrophobic derivatives of tyrosine and tryptophan viz., octyl and dodecyl esters of tyrosine and octyl ester of tryptophan have been presented and their interfacial and bulk properties in aqueous media as models for the membrane proteins are investigated. Molecular modelling by density functional theory (DFT) method is carried out in order to understand molecular conformation and geometry for the purpose of determining the packing parameters. Water induced molecular folding of the esters of both tyrosine and tryptophan, as observed by rotating frame nuclear Overhauser effect spectroscopy (ROESY), indicated that segregation of hydrophobic and the hydrophilic blocks in water is the key to the development of fascinating interfacial property displayed by the aromatic aminoacid esters. The unusually high order morphology of the aggregates, as observed under high resolution transmission electron microscopy (HRTEM), is highly uncommon for single chain amphiphiles and points to the fact that the self-assembly behavior of the present systems resembles that

of block copolymers. The study of the growth of mesosized hollow aggregates with internal bilayer structures from tyrosine and tryptophan based model systems would add to the understanding of biochemistry and biotechnology relevant to cell membrane. The promise of the biocompatible nanostructured motifs as the drug carriers have been discussed. The highly functional role played by the aromatic aminoacids at the membrane-water interface is considered with the present amphiphilic models for future perspective.

In **Chapter VI** influence of the long chain aromatic aminoacid residue of tyrosine, viz.,L-Tyrosineoctyl ester (TYOE) and L-Tyrosinedodecyl ester (TYDE) in modifying the surface characteristics of the model-membrane interface viz., spherical micellar aggregates of cationic amphiphile Cetyltrimethylammonium bromide (CTAB) have been investigated via tensiometric study. The surface property of the cationic micellar interface appear highly modified in presence of the long chain tyrosine residues. Interaction parameters suggest synergistic interaction between the quaternary ammonium group of the cationic model-membrane monomers and the phenolic moiety of TYOE and TYDE. SANS study revealed strong sequestering of the electrostatic charge of the cationic micelles in presence of the tyrosine derivatives and unidimensional growth of the spherical aggregates. The relative position of TYOE and TYDE w.r.t the membrane interface have been ascertained from study of micropolarity of the membrane interface by monitoring the dissociation equilibrium of the hydroxy functionality within the CTAB micelles. The results have been further corroborated by ^{1}H NMR and 2D NOESY study. The transition in the model membrane curvature as function of composition of the tyrosine derivative and their chain length have been investigated by rheometry and HRTEM study. Results highlight the specific role of the hydroxy functionality and hydrophobicity of the alkyl chain length of TYOE and TYDE in modifying the membrane curvature. Micellar morphology transition from cylindrical to rod/wormlike micelles via charge screening of the headgroups by π-electrons of aromatic aminoacid is indeed interesting in view of the abundance of zwitterionic phosphatidylcholine in bio-membranes and the ubiquitous feature of transmembrane proteins to localize tyrosine and tryptophan at the interface. Since the interplay between lipids and proteins is the key to how cells control membrane shape during many vital events including cellular fission, fusion and virus entry, the observed tuning of micellar surface curvature by tyrosine analogue is thought provoking and opens up avenue for

new physical chemistry research on a vital biological phenomena. The end-cap geometry of the cylindrical/wormlike micelles formed via charge screening of the cationic micelles is discussed and found to be flat-cap in shape for the first time.

In **Chapter VII,** local bending of membrane curvature of model membrane system composed of spherical micelles of cationic surfactant Cetyltrimethylammonium bromide, (CTAB) in presence of long chain (octyl) derivative of aromatic aminoacid Tryptophan have been studied via tensiometry, fluorescence steady state emission, ^{1}H NMR, 2D ROESY, rheometry and DFT study. The lowering of the membrane curvature mediated by the tryptophan residues have been discussed in the light of cation-π interaction and the high promise of fine tuning of the tryptophan residues to achieve desirable rigidity of membrane interface have been discussed. Calculation of interaction parameter provide support in favor of non-ideal mixing of the CTAB and TROE molecules, yielding negative magnitude of β, which shows that this interaction is attractive and synergistic in nature. Fluorescent behavior of TROE reveals progressive binding of TROE molecules to CTAB. NMR spectroscopy provided considerable evidence of strong cation-π interaction to take place between the quaternary ammonium head groups of CTAB and the electron rich π conjugated indole face of TROE. The CTAB-TROE system showed marked change in their physical property at increased concentration. Highly viscoelastic gels comprised of linear as well as wormlike micelles were observed via HRTEM microscopy. The study demonstrates high efficiency of TROE, which is an important model representing membrane bound tryptophan residues, in tuning the morphology of CTAB micelles. The system mimics the microenvironment of lipid membranes through cation-π interaction as well as hydrogen bond.

PREFACE

Surface active agents or Surfactants constitute a unique class of compounds having amphiphilic nature that are capable of forming molecular aggregates in solution without any external aid. The shape and size of the aggregates are functions of parameters such as chemical nature of the surfactant, nature of the additives and the solvent polarity. Morphology transition of surfactant assemblies have been the subject of intensive investigation from both theoretical and experimental points of view during the past three decades. The interest in the micellar morphology originates not only from the variety of supramolecular structures (such as micelles, vesicles, wormlike micelles etc.) formed by the surfactant, but also from the industrial application due to segregation of polar and nonpolar domains with particular characteristics in a given system.

Lipids are one of the vital components in biological systems. Aggregation of lipid molecules into bilayers forms the structure of the bio-membranes. Beside this, surfactants are also present in the gastrointestinal tract and lungs as well. Natural surfactants have also been found in crude oil. Synthetic surfactants, on the other hand, have a wide range of domestic and industrial use. Examples include cosmetic products, dyestuff, mineral processing, oil field industry, pharmaceuticals, paints etc.

A comprehensive understanding of the process of surfactant aggregation in solution is pivotal in the field of surfactant chemistry in order to develop surfactant systems with adaptive functionality. This thesis aims to explore the aggregation characteristics of various surfactants in solution, their biological relevance, compatibility and their applicability.

Table of Contents

LIST OF TABLES

Page No.

LIST OF SCHEMES

Page No.

Chapter III

Chapter IV

Chapter V

Chapter VI

LIST OF FIGURES

Page No.

Chapter I

Chapter III

Chapter IV

Chapter V

Chapter VI

Chapter VII

LIST OF APPENDICES

Appendix A

Surface activity and modifying effects of 1 Naphthol, 2 Naphthol and 2,3 Dihydroxynaphthalene on self-assembled nanostructures of 1-Hexadecyl-3-methylimidazolium chloride

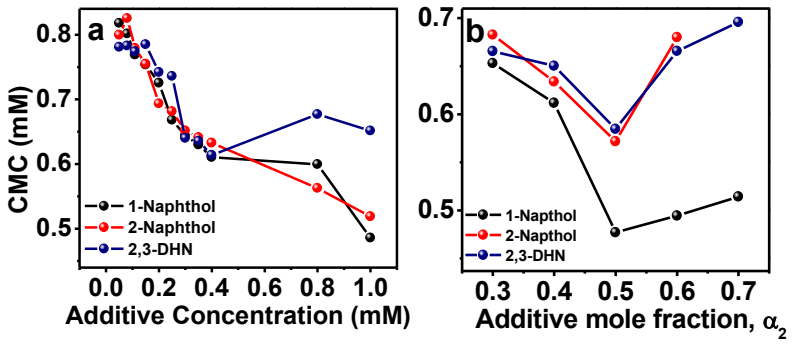

Figure S1. (a) Variation of CMC of C_{16}-3-MeImCl with additives concentration at 303 K. (b) Variation of CMC of C_{16}-3-MeImCl/Additive systems as a function of mole fraction of additives at 303 K

1.1. Mixing behavior of π-conjugated additives with SAIL under Newtonian flow regime

Decrease in surface tension is caused by orientation of surface active agents at the air-water interface. The various surface parameters underlining the surface behavior is calculated via Gibbs adsorption equation. For aqueous surfactant mixtures, the Gibbs surface excess of surfactants per unit area of surface is related to the surface pressure, Π [where Π = surface tension of water (γ_0) surface tension of surfactant solution (γ)] by the equation[1]

$$d\Pi = \sum \nu \Gamma_i RT \, d \ln a_i \quad (1)$$

where ν is the number of ions per surfactant molecule, Γ_i is the surface excess or adsorption density, a_i is the activity of the i^{th} component in the mixed adsorbed film, while T and R are the absolute temperature and universal gas constant, respectively. When the composition of the components of the surfactants in the aqueous solution is constant and C is the total surfactant concentration in solution,

$$\Gamma_{max} = \frac{\nu}{2.303RT}\left[\frac{d\Pi}{d\log C} + d\log f_{\pm}\right]_{T,P} \quad (2)$$

where f is the mean activity coefficient of the surfactant in solution. The maximum surface excess (Γ_{max}^{tot} in mol/m^2) and the minimum area per molecule of a surface active compound (A_{min}^{tot} in nm^2/molecule) can be estimated from the relationships

$$\Gamma_{max}^{tot}=\frac{1}{2.303RT}\, lim_{C\to CMC}\left[\frac{d\Pi}{d\log C}\right] \quad (3)$$

and

$$A_{min}^{tot} = \frac{10^{18}}{N.\Gamma_{max}^{tot}} \quad (4)$$

where N is the Avogadro number. Since the surfactant solutions were always dilute in within the regime studied, dlog $f_{\pm}$ was neglected.

1.2. Interaction parameters

According to the approach of the Regular Solution Theory (RST), the parameters - mole fraction of surfactant (α_1), CMC of the mixture, (CMC); CMC of the surfactant (CMC_1), CAC of the additives (CAC_2) and mole fraction of the surfactant within the micelles, (X_1), are related as follows:[2]

$$\beta = \frac{\ln\{(CMC.\alpha_1)/(X_1.CMC_1)\}}{(1-X_1)^2} \quad (5)$$

X_1 is evaluated iteratively using the relation:

$$\frac{[X_1^2.\ln(CMC.\alpha_1/CMC_1.X_1)]}{(1-X_1)^2}\ln\left[\frac{CMC\,(1-\alpha_1)}{CAC_2(1-X_1)}\right] = 1 \quad (6)$$

The activity coefficients f_1 and f_2 of the surfactant and respective additives are related to β as

$$f_1 = \exp\{\beta\,(1-X_1)^2\} \quad (7)$$

$$f_2 = \exp\{\beta\,.X_1{}^2\} \quad (8)$$

2. UV spectroscopy

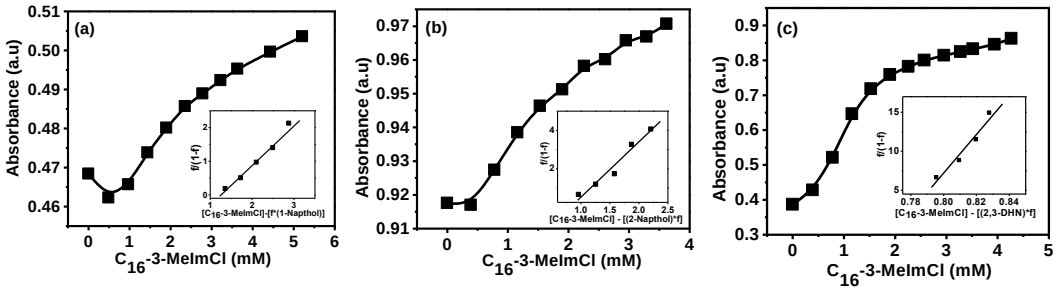

Figure S2. Plot of absorbance of (a) 0.5 mM 1 Naphthol, (b) 0.5 mM 2 Naphthol, (c) 0.5 mM 2,3 Dihydroxynaphthalene (2,3 DHN) against the concentration of aqueous C_{16}-3-MeImCl at 25^{0}C. The value of K_s (binding constant) are determined from the slope of the plot in the inset.

Surfactant – Probe Binding Equilibria

The binding constant K_s of the probe molecules viz, 1 Naphthol, 2 Naphthol and 2,3 Dihydroxynaphthalene (2,3 DHN) with cationic micelle of 1-Hexadecyl-3-methylimidazolium chloride (C_{16}-3-MeImCl) are determined from the study of the effect of surfactant addition on the absorption spectra of the probe employing following relation[3] (Table S1):

$$f/(1 - f) = K_s \{ [D_m] - [S_t]. f\} - K_s . cmc. \quad (9)$$

Where, $f = [S_m]/ [S_t]$ and $D_m = [D_t] - cmc$ (suffix t refers to total). Above relationship is drawn assuming following equilibrium hold between aqueous solubilisate (S_w) and the surfactant (D_m) to form the micelle embedded substrate (S_m),

$$S_w + D_m = S_m \quad (10)$$

Experimentally, f is calculated by, $f = (A - A_w) / (A_m - A_w)$, where A, A_W , and A_m are absorption intensities in surfactant, in water and at complete micellization of substrate, respectively. A plot of $f / (1 - f)$ against $\{ [D] - [S_t].f\}$ shows discontinuity at two critical points. Above plots give good straight lines, from the slope of which the binding constant K_s is obtained.

Table S1. Binding constant of 1 Naphthol, 2 Naphthol and 2,3 DHN with C_{16}-3-MeImCl.

Probe	Surfactant	K_s
1 Naphthol	C_{16}-3-MeImCl	1552
2 Naphthol	C_{16}-3-MeImCl	3476
2,3 DHN	C_{16}-3-MeImCl	6952

The binding constant for 2,3 DHN is substantially larger than that of 1 and 2 Naphthol and this result is consistent with the fact that 2,3 DHN is more efficient in tuning microstructural transition of C_{16}-3-MeImCl micelles compared to 1 and 2 Naphthol.

3. Rheology

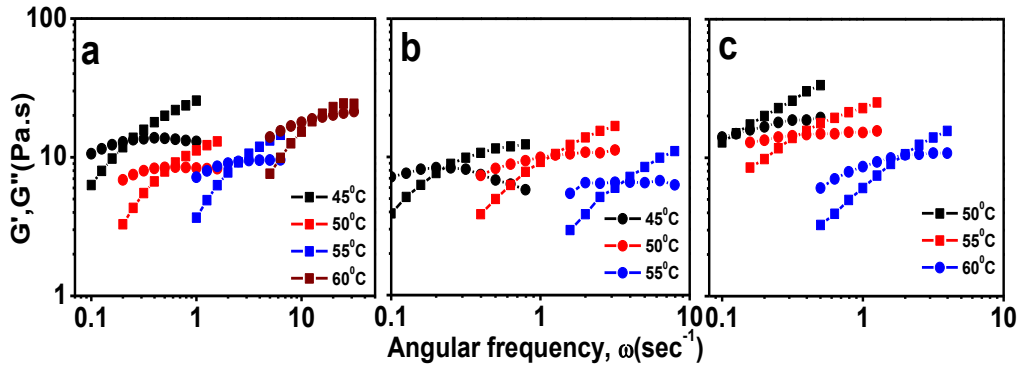

Figure S3. Dynamic rheology of C_{16}-3-MeImCl/Additive systems (1:1, 100 mM) as function of temperatures. Specification: a) 1 Naphthol, b) 2 Naphthol, c) 2,3 DHN, solid squares-G″, solid circle-G´.

3.1. Living polymer model for Maxwell fluids

According to this model the relaxation of the viscoelastic micelles involves two time scales viz., reptation time (τ_{rep}) corresponding to curvilinear diffusion of a wormlike micellar chain along its own contour and breaking time(τ_b) which is the result of micellar chain scission. When $\tau_b << \tau_{rep}$, there occurs many breakages and recombination before the chain segment relaxes by reptation. The system is then defined by a single stress relaxation time,

$$\tau_R = (\tau_{rep}.\tau_b)^{1/2} \quad (11)$$

and is characterized as a Maxwell Fluid. The sinusoidal deformation on the system, at an angular frequency, ω, causes the response stress, which remains out of phase with the applied strain. The strain ɣ(t) is given by:[4]

$$\gamma(t) = \gamma_0 \exp(i\omega t) \tag{12}$$

where γ_0 denotes the amplitude of strain, and t is the time.

The response stress will also be sinusoidal and will have a phase difference of δ, i.e

$$\sigma(t) = \sigma_0 \exp\{i(\omega t + \delta)\} \tag{13}$$

The complex modulus (G*) thus obtained is defined as

$$G^* = \sigma(t)/\gamma(t) = \frac{\sigma_0}{\gamma_0}(\cos\delta + i\sin\delta) = G' + iG'' \tag{14}$$

where G_0 is the storage modulus at high frequency, where it exhibits a plateau, also called the plateau modulus.

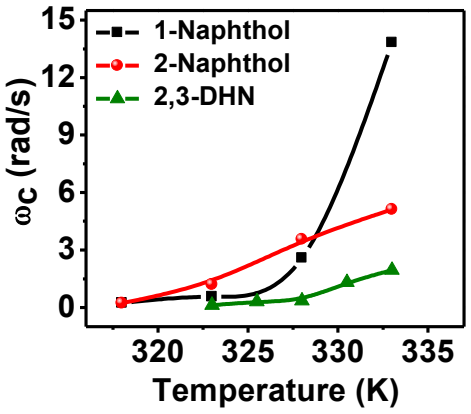

Figure S4. Crossover frequency (ω) profile as a function of temperature for C_{16}-3-MeImCl/Additive (1:1, 100 mM) systems.

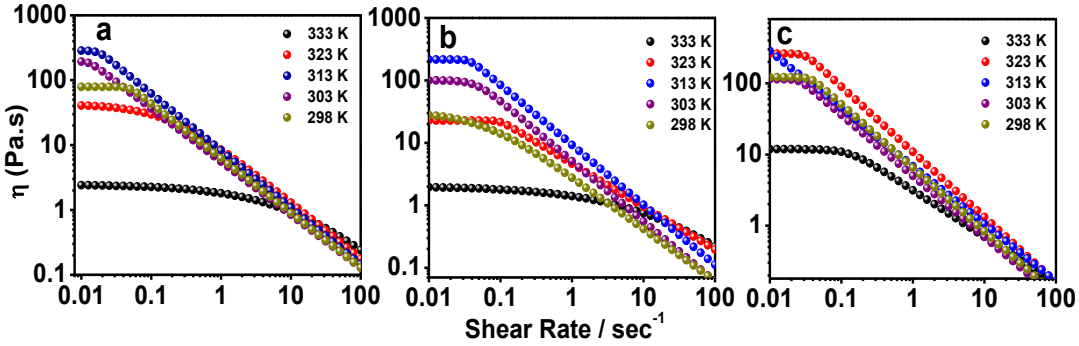

Figure S5. Shear viscosity (η) profile of C_{16}-3-MeImCl/Additive (1:1, 100 mM) systems as a function of temperature. Specification: a) 1 Naphthol, b) 2 Naphthol, c) 2,3 DHN.

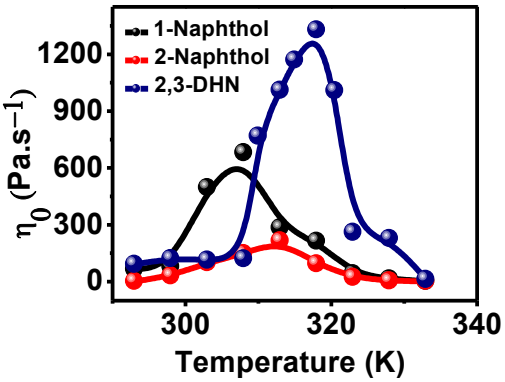

Figure S6. Corresponding zero shear viscosity (η_0) of C_{16}-3-MeImCl/Additive (1:1, 100 mM) systems at various temperatures.

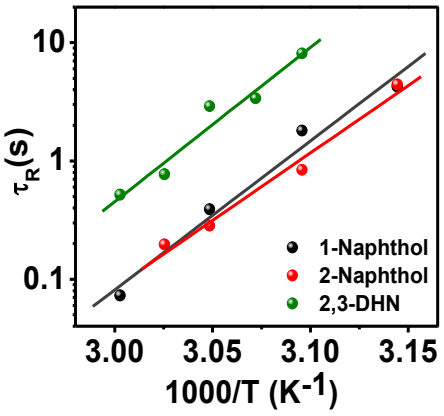

Figure S7. Arrhenius semilog plots of relaxation time (τ_R) as function of 1/T for C_{16}-3-MeImCl/Additive (1:1, 100 mM) systems

3.2. Packing parameter

P is a dimensionless fundamental parameter, which determines the shape of molecular aggregates and is defined as:[5]

$$P = {}^{V_c}/_{(A_0.L_c)} \quad (15)$$

where V_c is the volume occupied by the alkyl chain of the aggregate monomer, L_c is the alkyl chain length and A_0 is the area occupied the surfactant monomer head group. V_c and L_c are characteristics of the ionic liquid monomer and are therefore rigid quantities

4. ^{1}H NMR study

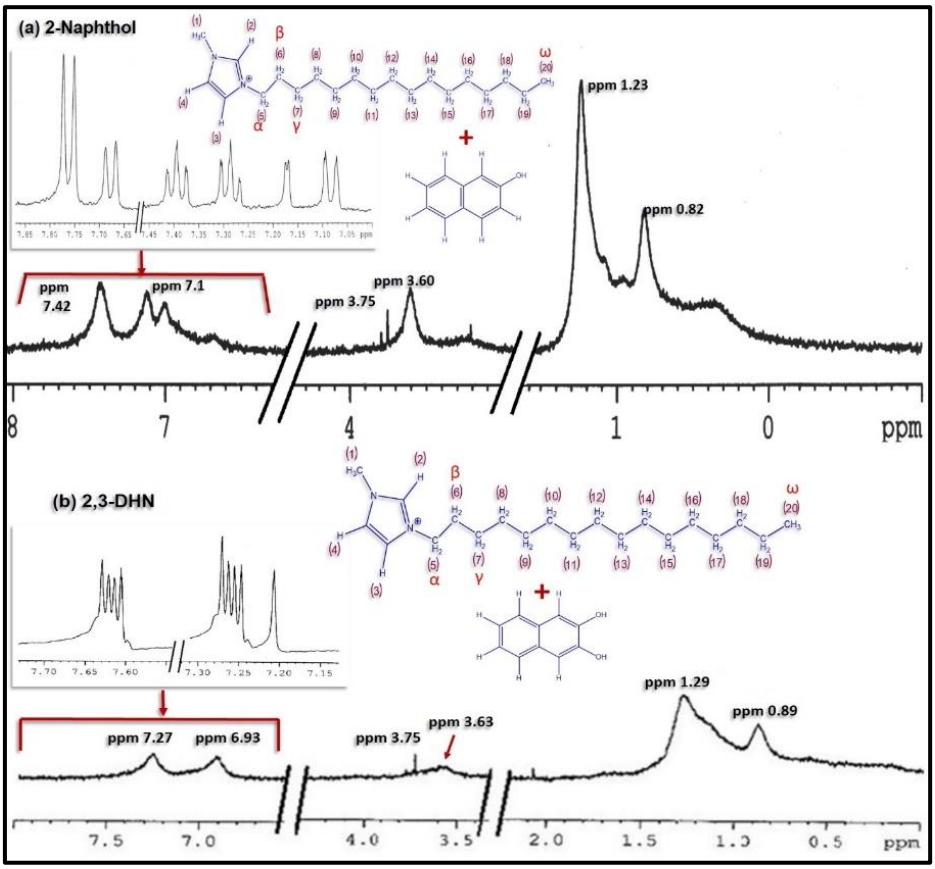

Figure S8 (a) ^{1}H-NMR spectra of 10 mM C_{16}-3-MeImCl and 10 mM 2 Naphthol in D_2O at 25^{0}C, (b) ^{1}H-NMR spectra of 10 mM C_{16}-3-MeImCl and 10 mM 2,3 DHN in D_2O at 25^{0}C.

5. DFT Study

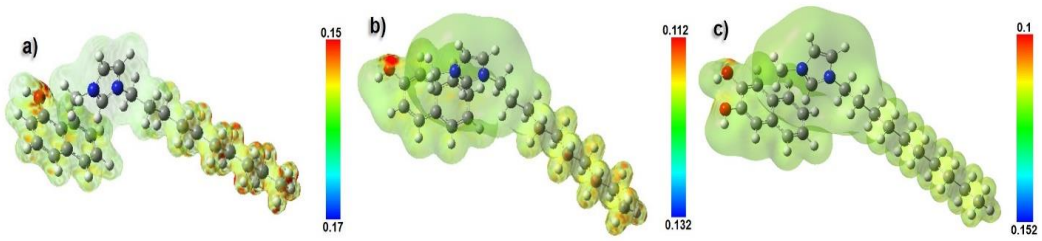

Figure S9. UB3LYP/6-31G (d, p) electrostatic potential, in Hartrees, at the 0.004 e Bohr^{-3} isodensity surfaces of (a) 1 Naphthol, (b) 2 Naphthol and (c) 2,3 DHN with C_n-3-MeImCl (n=10).

References

1. Ghosh, S., Surface Chemical and Micellar Properties of Binary and Ternary Surfactant Mixtures (Cetyl Pyridinium Chloride, Tween-40, and Brij-56) in an Aqueous Medium. *Journal of Colloid and Interface Science* **2001,** *244* (1), 128-138.

2. Rosen, M. J., Molecular Interactions and Synergism in Mixtures of Two Surfactants. In *Surfactants and Interfacial Phenomena*, John Wiley & Sons, Inc.: 2004; pp 379-414.

3. Ali, M.; Jha, M.; Das, S. K.; Saha, S. K., Hydrogen-Bond-Induced Microstructural Transition of Ionic Micelles in the Presence of Neutral Naphthols: pH Dependent Morphology and Location of Surface Activity. *The Journal of Physical Chemistry B* **2009,** *113* (47), 15563-15571.

4. Cates, M. E.; Candau, S. J., Statics and dynamics of worm-like surfactant micelles. *Journal of Physics: Condensed Matter* **1990,** *2* (33), 6869.

5. Platz, G., J. H. Clint: Surfactant Aggregation, Blackie Publishing Group, Glasgow, London, 1992,. *Berichte der Bunsengesellschaft für physikalische Chemie* **1992,** *96* (5), 742-742.

Appendix B

Solvent induced molecular folding and self-assembled nanostructures of Tyrosine and Tryptophan analogues in aqueous solution: Fascinating morphology of high order

1.1. Single point energy calculation

The electronic energy (E_e), the zero point energy (ZPE) of the aminoacid esters were computed in order to evaluate the total thermal internal energy (E_{tot}) given by-

$$E_{tot} = ZPE + E_{transational} + E_{rotational} + E_{vibrational} \quad (1)$$

and the enthalpy, H, is given by-

$$H = E_e + E_{tot} + RT \quad (2)$$

at 298.15 K and 1 atm pressure with rigid rotor and harmonic oscillation approximation.[1] The total entropy, S_{tot}, was calculated as

$$S_{tot} = S_{transational} + S_{rotational} + S_{vibrational}. \quad (3)$$

The results are summarized in Table S1.

Table S1. B3LYP/6-31G Calculated electronic energy, E_e (Hartree), Zero point energy, ZPE (kCal.mol^{-1}), standard enthalpy, H^o (kCal.mol^{-1}), standard Gibbs free energy, G^o (kCal.mol^{-1}),standard entropy, S^o (Cal.mol^{-1}.K^{-1}), specific heat capacity at constant volume, C_V (Cal.mol^{-1}.K^{-1}) and total thermal internal energy, E_{tot} (kCal.mol^{-1}) at 298.15 K and 1 atm pressure.

Amino acid ester	E_e	ZPE	$H^o_{298K, 1\ atm}$	$G^o_{298K, 1\ atm}$	$S^o_{298K, 1\ atm}$	C_V	E_{tot}
TYOE	-944.25	265.67	+15.42	-37.46	177.37	85.44	280.51
TYDE	-1101.47	337.87	+18.19	-42.08	204.12	104.51	356.06
TROE	-1000.59	282.31	+15.83	-37.29	178.17	89.31	297.55

1.2. Surface parameters

For any surface active moiety, the Gibbs surface excess per unit area of surface is related to the surface pressure, Π [where Π = surface tension of water (γ_0) surface tension of solution (γ)] by the equation[2]

$$d\Pi = \sum \nu \Gamma_i RT\ d \ln a_i \quad (4)$$

where ν is the number of ions per surface active molecule, Γ_i is the surface excess or adsorption density, a_i is the activity of the i^{th} component in the adsorbed film, while T and R are the absolute temperature and universal gas constant, respectively and C is the total surfactant concentration in solution,

$$\Gamma_{max} = \frac{\nu}{2.303RT}\left[\frac{d\Pi}{d\log C} + d\log f_{\pm}\right]_{T,P} \quad (5)$$

f is the mean activity coefficient of the surfactant in solution. The maximum surface excess (Γ_{max} in mol/m^2) and the minimum area per molecule of a surface active compound (A_{min} in nm^2/molecule) can be estimated from the relationships:[3]

$$\Gamma_{max} = \frac{1}{2.303RT}\lim_{C\to CMC}\left[\frac{d\Pi}{d\log C}\right] \quad (6)$$

and

$$A_{min} = \frac{10^{18}}{N.\Gamma_{max}^{tot}} \quad (7)$$

where N is the Avogadro number. Since the solutions were always dilute within the regime studied, $d\log f_{\pm}$ was neglected.

1.2.1. Thermodynamics

The standard free energy change of aggregation, (ΔG^0_{agg}), standard free energy change of interfacial adsorption (ΔG^0_{ads}), standard enthalpy change of aggregation (ΔH^0_{agg}), standard entropy change of aggregation (ΔS^0_{agg}) are related to the cac and temperature (T) as follows:[4]

$$\Delta G^0_{agg} = RT\ln X_{cac} \quad (8)$$

$$\Delta H^0_{agg} = -RT^2\frac{d\ln X_{cac}}{dT} \quad (9)$$

$$\Delta S^0_{agg} = \frac{(\Delta H^0_{agg} - \Delta G^0_{agg})}{T} \quad (10)$$

$$\Delta G^0_{ads} = \Delta G^0_{agg} - \frac{\Pi_{cac}}{\Gamma_{max}} \quad (11)$$

The enthalpy-entropy compensation temperature, T_C, and the enthalpy of compensation, ΔH^*_{com} are related as:[5]

$$\Delta H^0_{agg} = \Delta H^*_{com} + T_C . \Delta S^0_{agg} \quad (12)$$

T_C indicates the solvation part of the aggregation phenomenon and is obtained from the slope of the ΔH^0_{agg} *v/s* ΔS^0_{agg} plot while ΔH^*_{com} accounts for the solute-solute interactions within the system and is obtained from the respective intercept.[3] ΔH^*_{com} obtained from Figure S3 and Equation 12 are -13.5 kJ.mol^{-1}, -14.1 kJ.mol^{-1} and -30.3 kJ.mol^{-1} for TYOE, TYDE and TROE respectively.

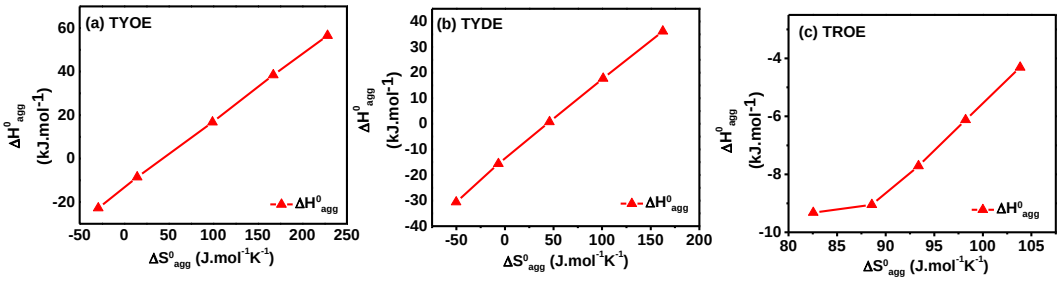

Figure S1. Enthalpy entropy compensation curves for (a) TYOE, (b) TYDE and (c) TROE

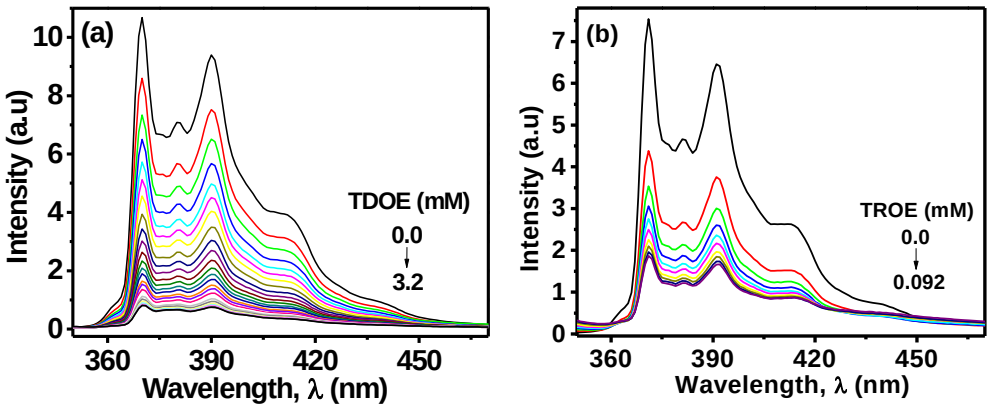

Figure S2. Variation of emission intensity of 2µM aqueous Pyrene as a function of (a) TYDE, (b) TROE concentration at 25^{0}C.

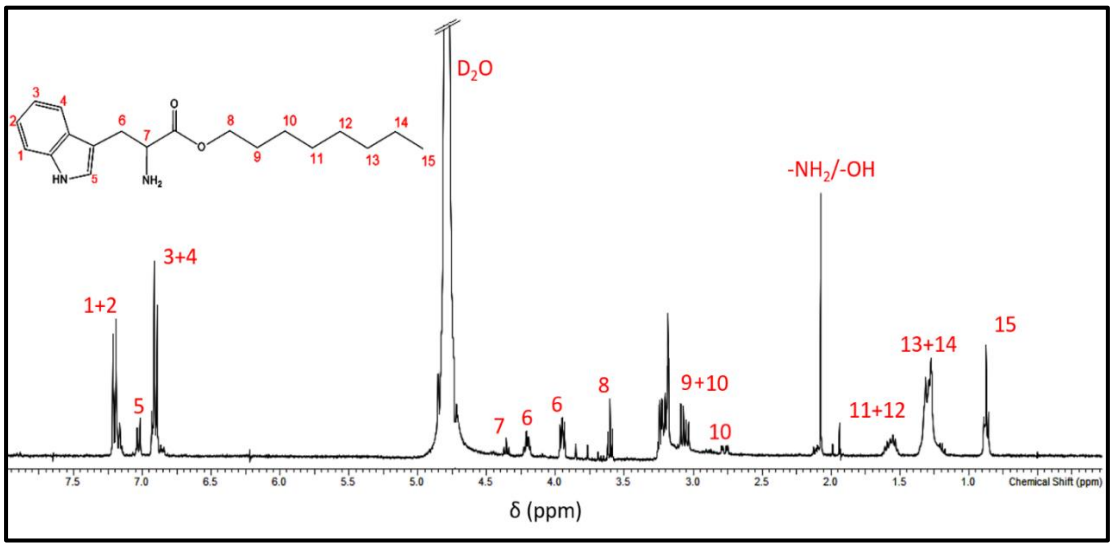

Figure S3 (a) ^{1}H NMR Spectra of TROE in D_2O

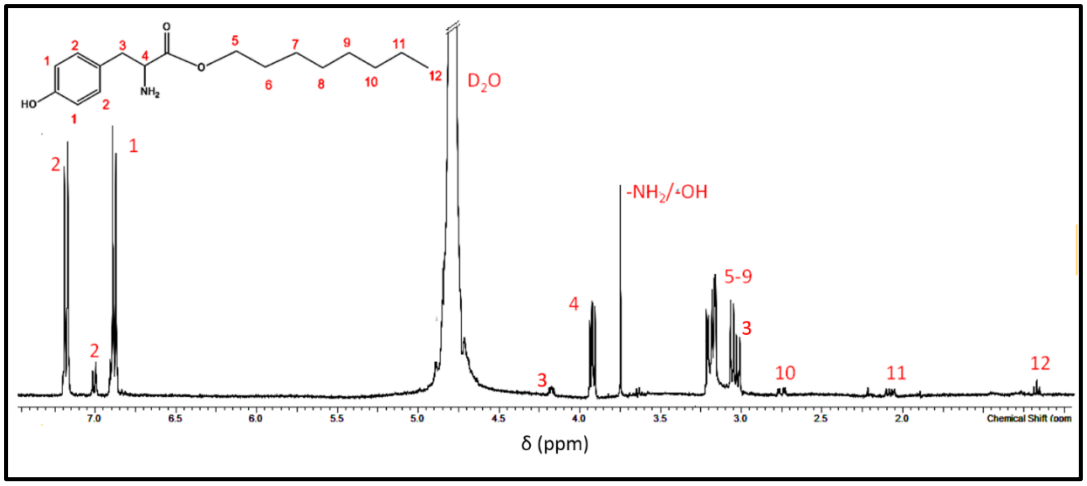

Figure S3 (b) ^{1}H NMR Spectra of TYOE in D_2O

References

1. Lee, J. E.; Choi, W.; Mhin, B. J., DFT Calculation on the Thermodynamic Properties of Polychlorinated Dibenzo-p-dioxins: Intramolecular Cl−Cl Repulsion Effects and Their Thermochemical Implications. *The Journal of Physical Chemistry A* **2003,** *107* (15), 2693-2699.

2. Sarmoria, C.; Puvvada, S.; Blankschtein, D., Prediction of critical micelle concentrations of nonideal binary surfactant mixtures. *Langmuir* **1992,** *8* (11), 2690-2697.

3. Ghosh, S.; Das Burman, A.; De, G. C.; Das, A. R., Interfacial and Self-Aggregation of Binary Mixtures of Anionic and Nonionic Amphiphiles in Aqueous Medium. *The Journal of Physical Chemistry B* **2011,** *115* (38), 11098-11112.

4. Chatterjee, A.; Moulik, S. P.; Sanyal, S. K.; Mishra, B. K.; Puri, P. M., Thermodynamics of Micelle Formation of Ionic Surfactants: A Critical Assessment for Sodium Dodecyl Sulfate, Cetyl Pyridinium Chloride and Dioctyl Sulfosuccinate (Na Salt) by Microcalorimetric, Conductometric, and Tensiometric Measurements. *The Journal of Physical Chemistry B* **2001,** *105* (51), 12823-12831.

5. Carnero Ruiz, C.; Díaz-López, L.; Aguiar, J., Self-assembly of tetradecyltrimethylammonium bromide in glycerol aqueous mixtures: A thermodynamic and structural study. *Journal of Colloid and Interface Science* **2007,** *305* (2), 293-300.

Appendix C

Interaction of tyrosine analogues with quaternary ammonium head group at micelle/water interface and their influence on aggregation characteristics of cationic micelles

1. Interaction parameters.

The strength and nature of interaction between two components in a binary surfactant mixture is given by the interaction parameter, β, obtained on basis of Rubingh's Regular solution theory. According to this approach, the parameters- mole fraction of surfactant CTAB i.e α_1; experimental critical aggregation concentration of the mixed system of the mixture, cac; critical aggregation concentration of CTAB, cac_1 and mole fraction of the surfactant within the micelles, X_1, are related as follows:[1]

$$\beta = \frac{\ln\{(cac.\alpha_1)/(X_1.cac_1)\}}{(1-X_1)^2} \quad (1)$$

X_1 is evaluated iteratively using the relation:[2]

$$\frac{[X_1^2.\ln(cac.\alpha_1/cac_1.X_1)]}{(1-X_1)^2} \ln\left[\frac{cac\,(1-\alpha_1)}{cac_2(1-X_1)}\right] = 1 \quad (2)$$

The respective activity coefficients f_1 and f_2 of the surfactant and respective hydrotopes are related to β as

$$f_1 = \exp\{\beta\,(1-X_1)^2\} \quad (3)$$

$$f_2 = \exp\{\beta\,.X_1{}^2\} \quad (4)$$

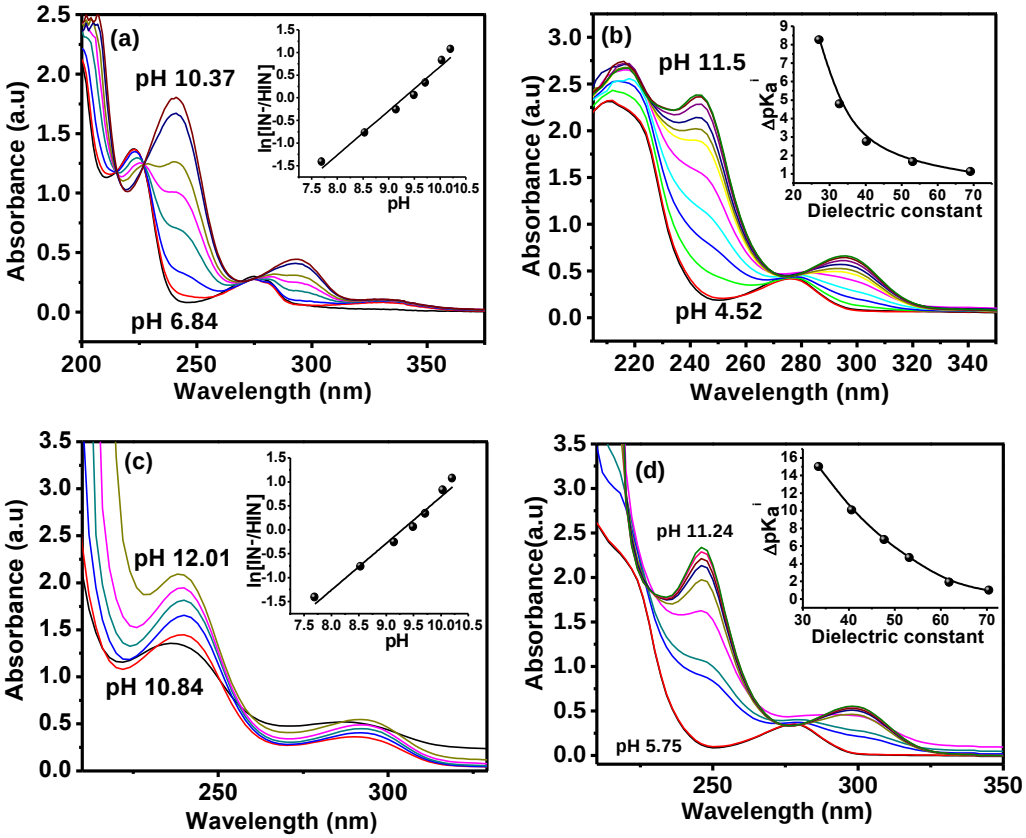

Figure S2. (a) Absorption spectra of 0.2 mM TYOE in aqueous medium as function of pH at 298 K, Inset display plot of ln [IN$^-$/HIN] vs pH, (b) Absorption spectra of 0.2 mM TYOE in presence of 100 mM aqueous CTAB solution at varying pH at 298 K, Inset display plot of ΔpK_a^i vs dielectric constant at 298 K, (c) Absorbtion spectra of 0.2 mM TYDE in aqueous medium as function of pH at 298 K, Inset display plot of ln [IN$^-$/HIN] vs pH, (d) Absorption spectra of 0.2 mM TYDE in presence of 100 mM aqueous CTAB at varying pH at 298 K, Inset display plot of ΔpK_a^i vs dielectric constant at 298 K.

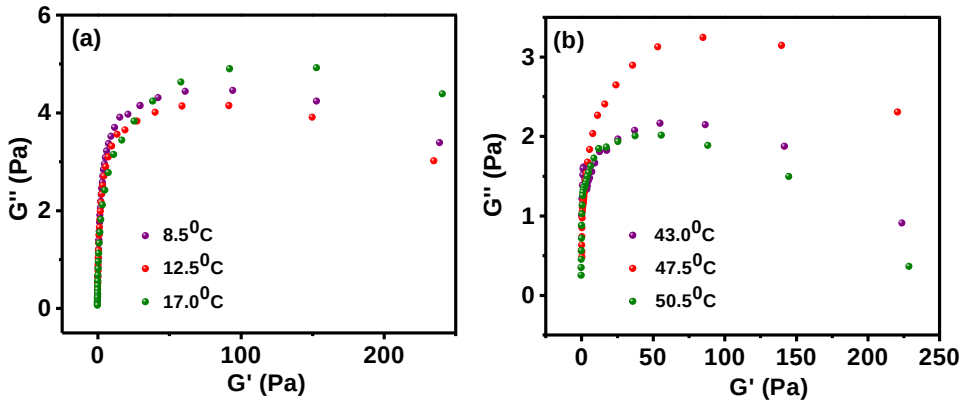

Figure S2. Cole-Cole plots of (c) CTAB (75 mM)-TYOE (37 mM) as function of temperature and (d) CTAB (75 mM)-TYDE (37 mM) as function of temperature.

References

1. Carnero Ruiz, C.; Díaz-López, L.; Aguiar, J., Self-assembly of tetradecyltrimethylammonium bromide in glycerol aqueous mixtures: A thermodynamic and structural study. *Journal of Colloid and Interface Science* **2007,** *305* (2), 293-300.
2. Rosen, M. J., Micelle Formation by Surfactants. In *Surfactants and Interfacial Phenomena*, John Wiley & Sons, Inc.: **2004**, 105-177.

Appendix D

Interaction of a tryptophan analogue with quaternary ammonium head group at micelle/water interface and its influence on aggregation characteristics of cationic micelles

1.1.Behavior of TROE at air-water interface

Decrease in surface tension is caused by orientation of surface active agents at the air-water interface. The various surface parameters underlining the surface behavior is calculated via Gibbs adsorption equation. For a surface active moiety, the Gibbs surface excess per unit area of surface is related to the surface pressure, Π [where Π = surface tension of water (γ_0) surface tension of solution (γ)] by: [1]

$$d\Pi = \sum \nu \Gamma_i RT \, d \ln a_i \quad (1)$$

where ν is the number of ions per surface active molecule, Γ_i is the surface excess or adsorption density, a_i is the activity of the i^{th} component in the adsorbed film, while T and R are the absolute temperature and universal gas constant, respectively and C is the total surfactant concentration in solution,

$$\Gamma_{max} = \frac{\nu}{2.303RT}\left[\frac{d\Pi}{d\log C} + d\log f_{\pm}\right]_{T,P} \quad (2)$$

f is the mean activity coefficient of the surfactant in solution. The maximum surface excess (Γ_{max} in mol/m^2) and the minimum area per molecule of a surface active compound (A_{min} in nm^2/molecule) can be estimated from the relationships:

$$\Gamma_{max} = \frac{1}{2.303RT}\lim_{C \to CMC}\left[\frac{d\Pi}{d\log C}\right] \quad (3)$$

and

$$A_{min} = \frac{10^{18}}{N.\Gamma_{max}^{tot}} \quad (4)$$

where N is the Avogadro number. Since the solutions were always dilute within the regime studied, $d\log f_{\pm}$ was neglected.

1.2. Energetics of Micellization and Interfacial Adsorption.

The standard free energy of aggregate formation per mole of monomer unit for TROE in aqueous medium is evaluated based of Mass action model. The standard free energy change of aggregation, ($\Delta_{agg}G^0$), standard free energy change of interfacial adsorption ($\Delta_{ads}G^0$), standard enthalpy change of aggregation ($\Delta_{agg}H^0$), standard entropy change of aggregation ($\Delta_{agg}S^0$) are related to the critical aggregation concentration (CAC) and temperature (T) as follows:[2]

$$\Delta_{agg}G^0=RT\ln X_{CAC} \quad (5)$$

$$\Delta_{agg}H^0 = -RT^2 \frac{d\ln X_{CAC}}{dT} \quad (6)$$

$$\Delta_{agg}S^0 = \frac{(\Delta_{agg}H^0-\Delta_{agg}G^0)}{T} \quad (7)$$

$$\Delta_{ads}G^0 = \Delta_{agg}G^0-\frac{\Pi_{CAC}}{\Gamma_{max}} \quad (8)$$

2.1. UV-Vis absorption

UV-Vis study was carried on Jasco V 530 Spectrophotometer fitted with a tungsten filament. A matched pair of glass cuvette of optical length 1cm was used for control and sample solutions. The solutions were allowed to equilibrate for 10 minutes before each measurement.

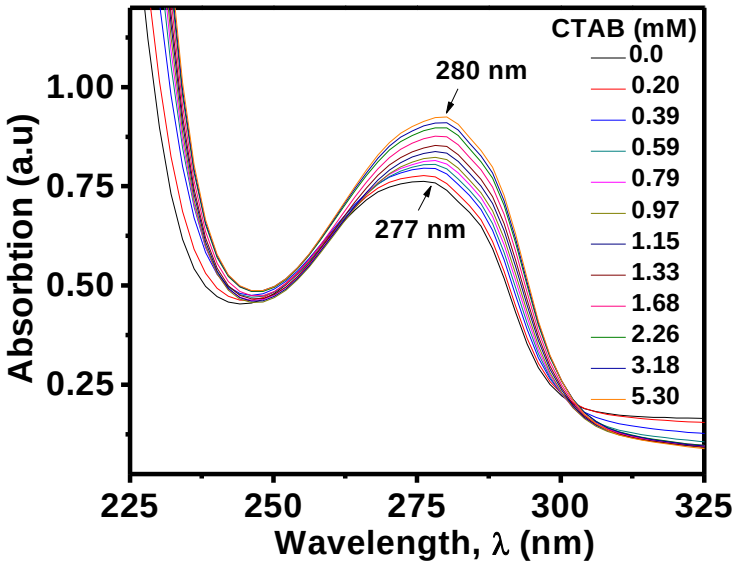

Figure S1. Absorption spectra of 0.2 mM TROE as function of CTAB concentration at 298 K.

Reference

1. Platz, G., J. H. Clint: Surfactant Aggregation, Blackie Publishing Group, Glasgow, London, 1992, ISBN In *Berichte der Bunsengesellschaft für physikalische Chemie*, Wiley-VCH: **1992**; *96*, 742-742.

2. Chatterjee, A.; Moulik, S. P.; Sanyal, S. K.; Mishra, B. K.; Puri, P. M., Thermodynamics of Micelle Formation of Ionic Surfactants: A Critical Assessment for Sodium Dodecyl Sulfate, Cetyl Pyridinium Chloride and Dioctyl Sulfosuccinate (Na Salt) by Microcalorimetric, Conductometric, and Tensiometric Measurements. *The Journal of Physical Chemistry B* **2001,** *105* (51), 12823-12831.

Appendix E

List of publication(s)

1. **Gulmi Chakraborty**, Madhurima Paul Chowdhury, Soumik Bardhan, Swapan K. Saha, Surface activity and modifying effects of 1 Naphthol, 2-Naphthol and 2,3-Dihydroxynaphthalene on self-assembled nanostructures of 1-Hexadecyl-3-methylimidazolium chloride. *Colloid Surfaces A.*, **2017**, 516, 262-273

   (Based on findings of Chapter IV)

2. **Gulmi Chakraborty**, Madhurima Paul Chowdhury, Swapan K. Saha, Solvent-Induced Molecular Folding and Self-Assembled Nanostructures of Tyrosine and Tryptophan Analogues in Aqueous Solution: Fascinating Morphology of High Order. *Langmuir*, **2017**, 33, 6581-6594

   (Based on findings of Chapter V)

3. Interaction of tyrosine analogues with quaternary ammonium head groups at micelle/water interface and contrasting effect of molecular folding on hydrophobic outcome and end-cap geometry
   (*Manuscript under preparation*)

4. Interaction of a tryptophan analogue with quaternary ammonium head group at micelle/water interface and its influence on aggregation characteristics of cationic micelles
   (*Manuscript under preparation*)

5. Modification of aggregation characteristics of cationic surfactants by hydroxy aromatic derivatives of naphthalene under salt-free condition
   (*Manuscript under preparation*)

Appendix F

List of seminar(s) and symposia attended

1. Participated in "Workshop in Diversities and Frontiers in Chemistry" held at University of North Bengal during August 07-08, 2013.
2. Participated in "5th Asian Conference on Colloid and Interface Science" held at University of North Bengal during November 20-23, 2013.
3. Participated in National seminar or "Frontiers in Chemistry-2014" held at University of North Bengal during March 11-12, 2014.
4. Presented a scientific paper (oral presentation) in International Conference on "Emerging trends in Science and Technology" held at Biratnagar, Nepal, during March 22-23, 2014.
5. Presented a scientific paper (poster presentation) in National symposium on "Recent trends and perspectives in Chemistry" held at Department of Chemistry, National Institute of Technology, Sikkim during January 23-24, 2015.
6. Presented a scientific paper (oral presentation) in 22nd West Bengal Science and Technology Congress 2015, held at University of North Bengal during February 28-March 01, 2015.
7. Presented a scientific paper (poster presentation) in "19th CRSI National Symposium in Chemistry" held at University of North Bengal during July 14-16, 2016.
8. Participated in National seminar or "Frontiers in Chemistry 2017-2018" held at University of North Bengal on September 04, 2017.

Chapter I

Introduction and review of previous works

1.1. Self-assembly of amphiphilic molecules : An overview

Self-assembly refers to spontaneous organization of molecules in solution driven by noncovalent interactions into stable aggregates. Self-assembly is highly recognized in biological systems, e.g., lipid bilayers, the DNA duplex, and tertiary and quaternary structure of proteins. The process of spontaneous aggregation of single molecules in solution into larger structures with a certain order is also an important phenomenon in every-day-life as well as in science. The best-known example of aggregation in every-day-life is the formation of micelles by detergent molecules. The most important type of aggregation, which is essential to life, is the formation of the lipid bilayer membrane by phospholipids. It has inspired chemists and physicists to study and mimic this and other types of aggregates.[1] Aggregation of molecules often occurs at the borderline of solubility. An important molecular property in this respect is polarity, for which solubility follows the rule 'like dissolves like'. Polar (hydrophilic) compounds are well soluble in polar solvents, e.g. salt in water, and the same goes for apolar (hydrophobic) compounds and solvents, e.g. vitamin E in oil. Furthermore, polar compounds are insoluble in apolar solvents and vice versa. Interestingly, there is a major class of compound which are amphiphilic in nature, i.e. these contain a polar as well as an apolar part. The polar part is called “head” and the apolar part, usually a long chain hydrocarbon, is called “tail” (Figure 1).

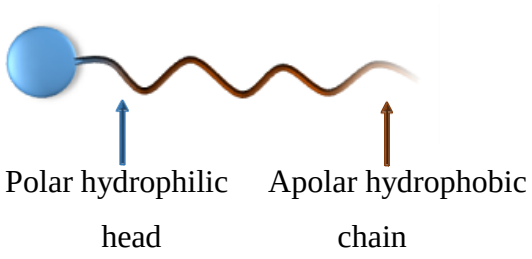

Figure 1. Representation of a surfactant molecule

These compounds are most comfortable in a situation when each part is located in an appropriate environment, which is only possible at the interface between two media. Therefore, amphiphilic compounds are also called surface-active agents, or in short,

surfactants.[2] The hydrophobe is usually the equivalent of 8 to 18 hydrocarbon, and can be aliphatic, aromatic, or a mixture of both. The source of hydrophobes are normally natural fats and oils, petroleum fractions, relatively short synthetic polymers, or relatively high molecular weight synthetic alcohols. The hydrophilic group gives the primary classification to surfactants, and are anionic, cationic and nonionic in nature. The anionic hydrophiles are the carboxylates (soaps), sulphates, sulphonates and phosphates. The cationic hydrophiles are usually quaternary ammonium, pyridinium, imidazolium cations etc. The nonionic hydrophiles are dominated by long chain ethoxylates. These hydrophiles associate with water at the ether oxygens of a polyethelene glycol chain. There are some surface active amphiphilic molecules that contain both anionic and cationic centres at the head group. These are called zwitterionic surfactants. Surfactants can also have two hydrocarbon chains attached to a polar head and are called double chained surfactants. On the other hand, surfactants containing two hydrophobic and two hydrophilic groups are called "gemini" surfactants. Amphiphilic molecules can also have two head groups (both anionic, both cationic or one anionic and the other cationic) joined by hydrophobic spacer.[1] These type of molecules are termed "bola-amphiphiles" commonly known as "bolaforms". Surface activity of these molecules depend on both the hydrocarbon chain length and the nature of the head group(s).

1.2. Classifications of diverse self-organized assemblies on the basis of packing parameter

The concept of molecular packing parameter has been widely cited in chemistry, physics, and biology literature because it allows a simple and intuitive insight into the self-assembly phenomenon.[3] The packing parameter approach permits indeed to relate the shape of the surfactant monomer to the aggregate morphology.[4-6] The molecular packing parameter P is defined as the ratio $\nu/(a_o.l_c)$, where ν and l_c are the volume and the extended length of the surfactant tail, respectively and a_o is the *equilibrium* area per molecule at the aggregate interface (or mean cross-sectional (effective) head-group surface area), as illustrated in Figure 2. If we consider a spherical micelle with a core radius R, made up of N_{agg} molecules, the volume of the core is $V = N_{agg} \times \nu = 4\pi R^3/3$, the surface area of the core $A = N_{agg} \times a_o = 4\pi R^2$. Hence, it can be deduced that $R = 3\nu / a_o$, from simple geometrical relations. If the micelle core is packed with surfactant tails without any empty space, then the radius R cannot exceed the extended length lc of the

tail. Introducing this constraint in the expression for R, one obtains $0 \leq v / a_o.l_c \leq 1/3$, for spherical micelles. These geometrical relations, together with the constraint that at least one dimension of the aggregate (the radius of the sphere or the cylinder, or the half-bilayer thickness, all denoted by R) cannot exceed l_c, lead to the following well-known connection between the molecular packing parameter and the aggregate shape[4]: $0 \leq P \leq 1/3$ for sphere, $1/3 \leq P \leq 1/2$ for cylinder, and $1/2 \leq P \leq 1$ for bilayer. Inverted structures are formed when P>1.

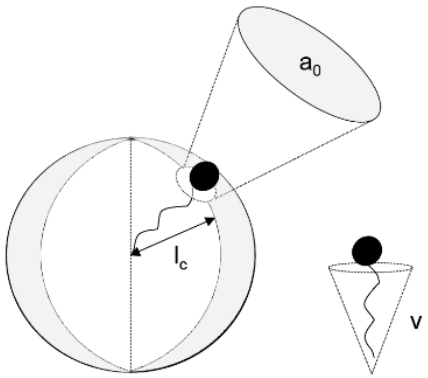

Figure 2. The critical packing parameter P (or surfactant number) relates the head group area, the extended length and the volume of the hydrophobic part of a surfactant molecule into a dimensionless number $P=v/(a_o l_c)$

Therefore, if the molecular packing parameter is known, the shape and size of the equilibrium aggregate can be readily identified as shown below (Table 1). It is noteworthy that a_o is often referred to as the "headgroup area" in the literature. However, for all practical purposes this has led to the erroneous identification of a_o as a simple geometrical area based on the chemical structure of the headgroup in many papers, although a_o is actually an equilibrium parameter derived from thermodynamic considerations.[3] Needless to say, that for the same surfactant molecule, the area a_o can assume widely different values depending on the solution conditions such as temperature, salt concentration, additives present, etc.; hence, it is meaningless to associate one specific area with a given head group. For example, sodium dodecylbenzene sulfonate forms micelles in aqueous solution whereas bilayer structures are formed when alkali metal chlorides are added.[7] Moreover, the role of the surfactant tail has been virtually neglected. This is in part because the ratio v / l_c appearing in the molecular packing parameter is independent of the chain length for common surfactants (0.21 nm^2 for single tail surfactants) and the area a_o depends only on the head group interaction parameter. Nagarajan showed that the tail length

influences the head group area (consideration of tail packing constraints) and thereby the micellar shape.[8]

Table 1. Schematic representation of surfactant structures and shapes derived from various packing parameters

Possible surfactant type		P(=v/$a_o l_c$)	Shape	Structures formed
Single-tail surfactants with large headgroups	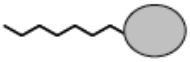	< 1/3	cone 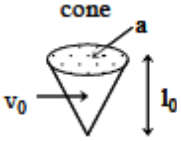	spherical micelles 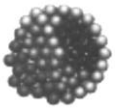
Single-chain surfactants with small headgroups		1/3<P<1/2	truncated cone 	cylindrical micelles 
Double-chain surfactants with large headgroups and flexible chains	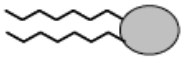	1/2<P<1	truncated cone 	flexible bilayers, vesicles 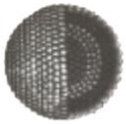
Double-chain surfactants with small headgroups or rigid, immobile chains		P~1	cylinder 	planar bilayers 
double-chain surfactants with small headgroups, and bulky chains	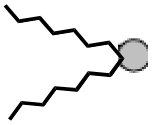	P>1	inverted truncated cone or wedge 	inverted micelles 

1.2.1 Micelles

The most intensely studied and debated molecular self-assembly and perhaps the simplest in terms of the structure of the aggregate is the micelle. Micelles formed by ionic amphiphilic molecules in aqueous solution are dynamic associations of surfactant molecules that achieve segregation of their hydrophobic portions from the solvent via self-assembly. They are loose, mostly spherical aggregates above their critical micellization concentration (cmc) in water or organic solvents.[1] Also, micellar aggregates are short-lived dynamic species, which rapidly disassemble and reassemble.[9] Hence, only average shape and aggregation numbers of micelles can be determined. Micellization of surfactants is an example of the hydrophobic effect. In micellization there are two opposing forces at work. The first is the hydrophobicity of the hydrocarbon tail, favoring the formation of micelles and the second is the repulsion between the surfactant head groups. The mere fact that micelles are also formed from ionic surfactants is an indication of the fact that the hydrophobic driving force is large enough to overcome the electrostatic repulsion arising from the surfactant head groups. Figure 3 represents a spherical micelle formed in aqueous solution, where the hydrophobic chains are directed towards the interior of the aggregate and the polar head-groups point towards water, hence allowing the solubility / stability of the aggregate (no phase separation).

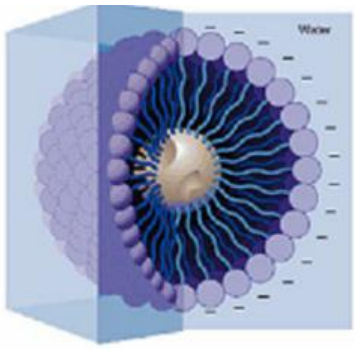

Figure 3. Schematic representation of a spherical micelle in aqueous solution.

Micelles are also known to be disorganized assemblies whose interiors consist of mobile, non-stretched hydrophobic chains.[10] Water molecules can penetrate partially into the micelle core to interact with surfactant hydrophobic tails.[11] There are a huge number of publications related to the micelles, micelle structures, and the thermodynamics of micelle formation. A huge amount of experimental and theoretical work devoted to the understanding of the aggregation of surface-active molecules has

been carried out.[12-14] Micelles are formed by cationic, anionic, zwitterionic as well as surfactants having short alkyl chains. The environment of a micelle varies in a regular manner as a function of distance from the center of the micelle, going from a relatively dense aliphatic medium near the center to a relatively diffuse region known as either Stern layer in ionic micelles, or as palisade layer in neutral micelles[15-17] where the headgroups, bound counterions, and solvent molecules coexist. The remaining counterions are contained in the Gouy-Chapman portion of the double layer that extends further into the aqueous phase. Fluorescence probe studies have indicated that micellar core is nonpolar, but less fluid than hydrocarbon solvents of equivalent chain length.[18] On the other hand, the Stern layer has polarity equal to that of alcohols.[19]

When a nonpolar group is introduced into an aqueous solution, the hydrogen bonding network formed by the existing water molecules is disrupted and the water molecules order themselves around the nonpolar entity to satisfy hydrogen bonds (Figure 4 (a)). This results in an unfavorable decrease in entropy in the bulk water phase. As additional nonpolar groups are added to the solution, they self-associate thus reducing the total water-accessible surface of the complex relative to the monodisperse state. (Figure 4 (b))

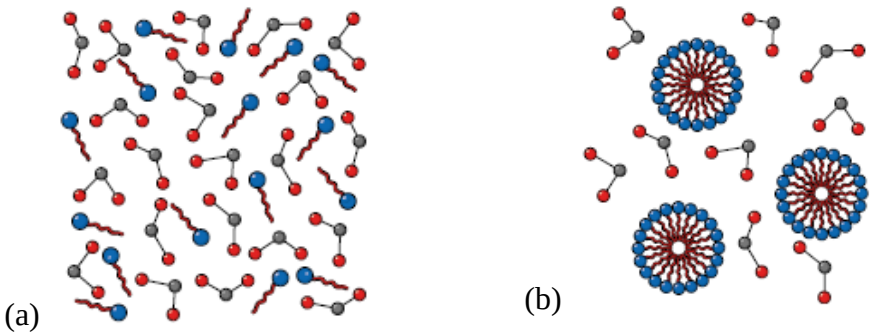

Figure 4. (a)Water molecules ordered around surfactant monomers, (b) Loss of total water-accessible surface as a result of micellization.

Now, fewer water molecules are required to rearrange around the collection of nonpolar groups. Therefore, the entropy associated with the complex is less unfavorable than for the monodisperse detergents. In short, hydrophobic association and the formation of micelles is driven by the favorable thermodynamic effect on the bulk water phase. An extensive compilation of the cmc's of surfactants in aqueous media has been published.[20]

1.2.2 Vesicles

Vesicles are closed bilayered or hollow spherical structures similar to those of the lamellar phase characterized by two distinct water compartments, one forming the core and other the external medium. Like micelles, the formation of vesicles is a result of energetically favorable hydrophobic association of the hydrocarbon tail(s) of an amphiphilic molecule. However, unlike micelles, two distinct domains are present in vesicles: a lipophilic membrane and the aqueous interior cavity. Precisely, the surface of micelles is a lipid monolayer, while that of liposomes is a lipid bilayer. Whereas, the inner core of micelles is composed of hydrocarbon chains, and that of vesicles is an aqueous phase.[21,22] Vesicles are dynamic supramolecular structures generally composed of amphiphilic molecules that form bilayers enclosing a small aqueous compartment. Besides the common phospholipids, synthetic amphiphiles can also form vesicles and bilayers that encapsulate an aqueous compartment. Due to the close analogy of synthetic vesicles with biological membranes, research on vesicles have been undertaken extensively giving rise to a blossoming field of biomimetic membrane chemistry.[4,23] Specific molecules can bind to the bilayer membrane and mediate interactions between the vesicles or, in selected cases, can be transported across the membrane. For this reason, synthetic vesicles are versatile model systems for protein and carbohydrate mediated recognition, fusion, adhesion and transport phenomena that are known from ion and water channels, endocytosis, viral infection, cell adhesion and the development of tissue from individual cells.[24] Vesicles are differentiated on basis of size and structure as follows: small unilamellar vesicles (SUVs,<100 nm), large unilamellar vesicles (LUVs, 100 -1000 nm), giant unilamellar vesicles (GUVs, >1 μm), multilamellar vesicles (MLVs, >1 μm) and multivesicular liposomes (MVLs, >1 μm). The term ‘‘liposome’’ is generally used for vesicles composed of natural phospholipids, while the term ‘‘vesicle’’ includes vesicles composed of synthetic amphiphiles, phospholipids, and other components. A schematic representation is shown in Figure 5.

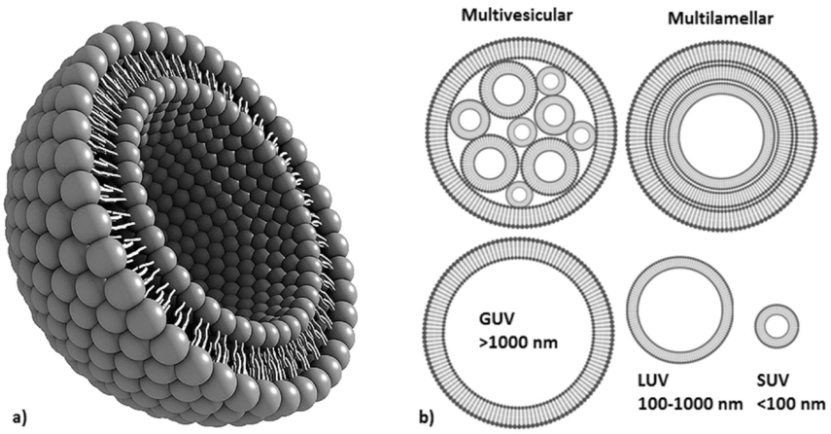

Figure 5. Schematic representation of (a) liposome with assembly of phospholipids in a bilayer showing both inner aqueous and outer lipid compartments within the structure and (b) various forms and sizes of vesicles; small unilamellar vesicles (SUVs), large unilamellar vesicles (LUVs), giant unilamellar vesicles (GUVs), multilamella and multivesicular liposomes.[25]

Vesicles can also be formed by mixing a single-tailed cationic surfactant with an aromatic acid. This is similar to the mixtures of surfactants because the surfactant and the aromatic acid tend to bind very strongly. The difference is that only one of the two components in the mixture is a surfactant. Mixtures of CTAB and 5-methyl salicylic acid (5mS) have been previously studied by Davis et al.[26] Surprisingly, at a molar ratio around 1.1, it was found that their solution contained unilamellar vesicles. Cryogenic transmission electron microscopy (cryo-TEM) was employed, which showed that vesicles were around 100 nm in diameter. Zheng, Zakin and co-workers[27] also used cryo-TEM to infer the presence of vesicles in mixtures of CTAB and the sodium salt of 3-methyl salicylic acid (3mS). These vesicles transformed into cylindrical micelles upon shearing. In the system studied by Manohar et al., a surfactant was obtained by mixing of CTAB with sodium 3-hydroxynaphthalene-2-carboxylate (SHNC) in equimolar amounts, followed by removal of excess counterions.[28] In aqueous solutions, at room temperature, the surfactant molecules assembled into MLVs with diameter around 1 - 10 μm.[29] Due to the formation of these large MLVs, highly turbid and viscous solutions were obtained (viscosities ca. 100 times that of water). On increasing the temperature, the samples transformed into clear solutions containing wormlike micelles (discussed later), thereby leading to an increase in viscosity by about an order of magnitude. Davies and co-workers, using turbidimetry, rheological techniques, and small-angle neutron scattering (SANS) measurements, have demonstrated that the aromatic derivative, 5-methyl salicylic acid (5mS), can induce the cationic surfactant,

CTAB, to form either wormlike micelles or unilamellar vesicles depending on the solution composition.[30] Eisenberg and Zhang reported the formation of vesicles from self-assembly of polystyrene-poly (acrylic acid) (PS-PAA) block copolymer.[31] Due to the wide array of intramolecular and intermolecular interactions within block copolymer assemblies, the block copolymer vesicles (or polymerosomes) has superior mechanical and physical properties, compared to the lipid based vesicles (or liposomes).[32] Following this, hundreds of papers and reviews have been published reporting the formation of vesicles from single, di-block and tri-block copolymers.[33-37]

Biocompatible vesicles show high promise in applications for the in vivo delivery of anti-cancer drugs for tumour treatment[38] and even in the treatment of degenerative brain conditions.[39] Vesicles with responses to pH stimulus also exhibit applications for the rapid and non-cytotoxic cellular delivery of DNA sequences, which opens the possibilities for efficient gene-delivery for the treatment of specific genetic diseases.[40,41] Polymer vesicles has also been used as synthetic nano-reactors[42] for several biological connotations.[43] Furthermore, the potential applications of polymer vesicles as synthetic intra-cellular organelles have been the basis for several striking reports, with possibilities for the treatment of genetic diseases caused by either enzyme inactivity or deficiency.[44]

1.2.3. Worm like micelles

Under specific conditions like salinity, pH, counter ion variation etc., micelles can grow into ‘polymer-like’ elongated and flexible aggregates, referred to as ‘wormlike’ (or ‘threadlike’) micelles (Figure 6).

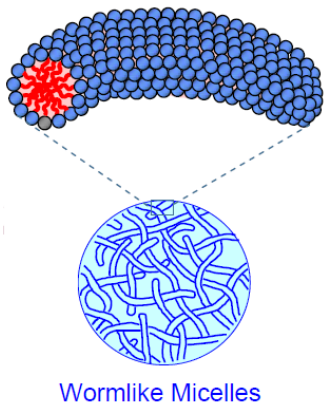

Figure 6. Microstructure of a typical wormlike micelle.

The formation of worm like micelles is a consequence of the system minimizing the excess free energy by reducing the number of end caps as the spontaneous curvature of the end caps is higher than the curvature along the cylindrical body. The dynamics of these systems are particularly interesting, because subtle changes in the surfactant, counterion and added electrolyte alter the dimensions, flexibility and interactions of the micelles which lead to marked effects on the macroscopic rheological behavior.[45] The rheological behavior of these surfactant solutions is known to follow "reaction-reptation model" which is an extension of the reptation model of polymer relaxation to cylindrical micelles of surfactant molecules undergoing reversible scission and recombination processes.[46] Wormlike micelles have drawn considerable interest over the past three decades, both from a theoretical viewpoint as well as for industrial and technological applications, the range of which keeps expanding. From a fundamental perspective, wormlike micelles are of specific interest, as they are a model of 'equilibrium polymers' (or 'living' polymers)[47-49]: extended linear objects that constantly break and reform. Due to their transient nature, they exhibit novel static and dynamic properties on time-scales both long and short compared to their finite lifetime.[49-51] The unique viscoelastic properties of worm like micelles have been exploited to tune the rheology in various applications without the use of polymers or additives.[52] Industrial significance include their use as heat-transfer fluids, hard-surface cleaners, drag reduction agents,[53-56] fracturing fluids in oil fields,[57] solids transports and personal care products,[58] for which both their high viscosity and elastic properties are exploited. Several theoretical approaches and simulations[59-61] have been proposed to predict structure-property relationships and understand how the structural features of the aggregates can be tuned by specific control parameters, and how these dictate the bulk properties. The bulk properties and dynamics have been measured by rheological measurements, recently by microrheology and neutron spin-echo while detailed structural information is typically obtained by small-angle neutron scattering (SANS), static and dynamic light scattering (LS), and cryogenic transmission electron microscopy (cryo-TEM).[62]

1.3. Rheology of viscoelastic fluids

Rheology is the science of deformation and flow. The term originates from Greek 'rheos' meaning 'to flow'. One common factor between solids, liquids, and all materials

whose behavior is intermediate between solids and liquid is that if we apply a stress or load on any of them they will deform or strain. The response of materials towards the externally applied strain or deformation describes its rheological behavior. The experimental characterization of a material's rheological behavior is known as rheometry. Typically, materials are either elastic or viscous. Elasticity is the tendency of solid materials to return to their original shape after forces are applied on them. An ideal elastic material stores all imposed deformation energy and recovers totally on release of stress. Viscosity is a measure of a fluid's resistance to flow. An ideal viscous material is unable to store any deformation energy. It is irreversibly deformed when subjected to stress i.e., it flows and the deformation energy is dissipated as heat resulting in rise in temperature. Materials whose properties are intermediate between viscous and elastic are known as viscoelastic i.e., they store some of the deformation energy in their structure while some is lost by flow. The relationship between stress and strain of viscoelastic materials depends on time or, in the frequency domain, on frequency. One of the way of characterization of materials is by its relaxation time- i.e. the time required to reduce the stress in the material by its flow. Some of the typical relaxation time for materials are- gas $<10^{-6}$ sec, liquid $10^{-6\ -\ 2}$ sec, solid $> 10^{2}$ sec. Figure 7 represent the difference in viscous, elastic and viscoelastic fluids in terms of relaxation time.

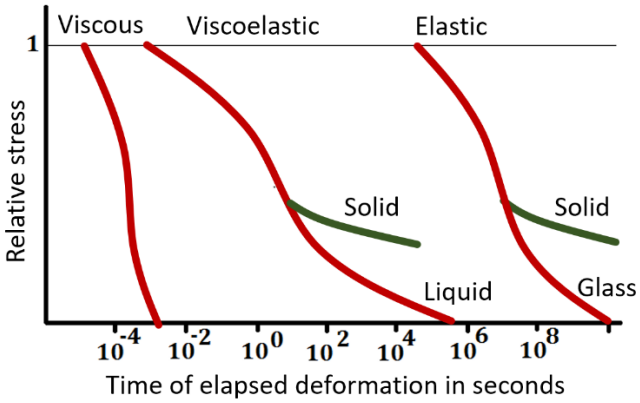

Figure 7. Curves showing the differences between viscous, viscoelastic and elastic materials when subjected to deformation.[63]

Shearing of a substance is the key to the knowledge of its flow behavior and structure. A sheared flow is achieved through: (a) flow between two parallel plates, (b) rotational flow between two coaxial cylinders, of which one is stationary and other is rotating, (c) telescopic flow through capillaries and pipes (d) torsional flow between parallel plates. Depending on their viscosity behavior as a function of shear rate, stress, deformation,

fluids are characterized as Newtonian or non-Newtonian. Newtonian fluids are named after Sir Issac Newton (1642 - 1726) who described the flow behavior of fluids with a simple linear relation between shear stress [mPa] and shear rate [1/s]. This relationship is now known as Newton's Law of Viscosity, where the proportionality constant η is the viscosity [mPa.s] of the fluid:

$$\sigma = \eta * \dot{\gamma} \quad (1)$$

Where, σ is the shear stress, $\dot{\gamma}$ is the shear rate and η is the viscosity.

Newtonian fluids are characterized by a single co-efficient of viscosity and thus they have constant viscosity dependent on temperature but independent of shear rates. Typical examples are water, mineral and vegetable oils and pure sucrose solutions. In reality most fluids are non-Newtonian, i.e., their viscosity is dependent on shear rate (Shear Thinning or Thickening) or the deformation history (Thixotropic fluids). In contrast to Newtonian fluids, non-Newtonian fluids display either a non-linear relation between shear stress and shear rate (Figure 8), have a yield stress, or viscosity that is dependent on time or deformation history or a combination of all the above.

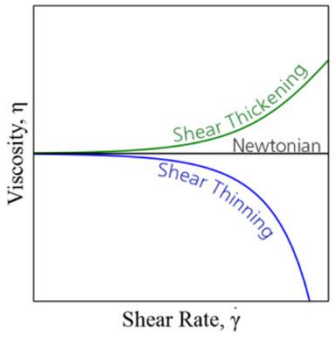

Figure 8. Viscosity of Newtonian, shear thinning or shear thickening fluids as function of shear rate.

A fluid is shear thickening if the viscosity of the fluid increases as the shear rate increases (Figure 8). A common example of shear thickening fluids is a mixture of cornstarch and water. Fluids are shear thinning if the viscosity decreases as the shear rate increases. Shear thinning fluids, also known as pseudo-plastics, are ubiquitous in industrial and biological processes. Common examples include ketchup, paints and blood. A fluid while flowing under constant stress may show some elastic properties as well. When such bodies are subjected to a sinusoidally oscillating stress, the strain is neither exactly in phase with the stress (as it would be for a perfectly elastic solid) nor 90 degrees out of phase (as it would be for a perfectly viscous liquid) but rather exhibits a strain that lags the stress at a value between zero and 90 degrees:

The sinusoidal deformation (strain) can be expressed as

$$\gamma(t) = \gamma_0 \exp(i\omega t) \quad (2)$$

Where, γ_0 is the amplitude of the strain, ω is the angular frequency and t is the time.

The shear stress developed will also be sinusoidal with a phase angle δ, thus

$$\sigma(t) = \sigma_0 \exp(i[\omega t + \delta) \quad (3)$$

For an oscillatory shear, we can define a complex shear modulus G* as:

$$G^* = \frac{\sigma(t)}{\gamma(t)} = \frac{\sigma_0 \, (cos\delta + isin\delta))}{\gamma_0 \exp(i\omega t)}$$

or, $G^* = G' + iG''$ (4)

G′ and G′′ are referred as the storage or elastic modulus and loss or viscous modulus respectively and are measure of the elastic or viscous property of the system.

Oscillatory shear measurements are a convenient way to measure viscoelasticity of entangled wormlike micelles formed in various surfactant solutions. Wormlike micelles have two principal mechanisms of stress relaxation: first, reptation occurs when the system is sufficiently concentrated to be entangled, as for classic polymers.[64] Reptation describes how a polymer chain escapes from the tube formed by the surrounding entangled chains. The characteristic time of stress relaxation by reptation, τ_{rep}, is directly proportional to $\frac{L^2}{D_c}$ with L the micellar contour length and D_c the curvilinear diffusion constant of the micelle. Second, micelle breaking (scission) and recombination is expressed by the characteristic time τ_{br}, which is inversely proportional to L.[47]When the system is sufficiently entangled, reptation is much slower than breaking. In this fast breaking limit ($\tau_{br} << \tau_{rep}$) several scission and recombination events take place within the reptation time scale. In this limit, the stress relaxation is close to that of a Maxwell fluid, with a single exponential stress decay,[47,48] characterized by one relaxation time, τ_R:

$$\tau_R = (\tau_R . \tau_{rep})^{1/2} \quad (5)$$

The viscoelastic behaviour of giant micelles is often close to that of a Maxwell fluid, for which G´and G'' are related as:

$$G'(\omega) = \frac{G_0 \omega^2 \tau_R^2}{(1+\omega^2 \tau_R^2)} \quad (6)$$

$$G''(\omega) = \frac{G_0 \omega \tau_R}{(1+\omega^2 \tau_R^2)} \quad (7)$$

where G_0 is the elastic modulus extrapolated to infinite frequency, also referred to as the plateau

modulus. G_0 is proportional to the number density of the entanglement points, therefore it characterizes the network structure whereas τ_R is a measure of the time required for the original state to be reestablished after the application of a stress and therefore characterizes the dynamics of the system. The zero shear viscosity, η_0 , for Maxwell fluids is given by:

$$G_0 = \eta_0 . \tau_R \quad (8)$$

The network mesh size of the entangled wormlike micelles is characterized by ξ, the hydrodynamic correlation length. This length scale can be obtained directly from the plateau modulus G_0:[65]

$$\xi = \left(\frac{k_B.T}{G_0}\right)^{1/3} \quad (9)$$

ξ is related to the persistence length,l_p, of the micelles and the entanglement length, l_e the average distance along the micelle between two entanglement points in the micellar network as:

$$l_e = \frac{\xi^{1/3}}{l_p^{2/3}} \quad (10)$$

The entanglement length can be determined from measurements of viscoelasticity using[66]

$$\frac{G_0}{G''_{min}} = \frac{L_{avg,}}{l_e} \quad (11)$$

where $L_{avg,}$ is the average micelle length and G''_{min} is the local minimum of the G'' curve at frequencies above $1/\tau_R$. The ratio $L_{avg,}/l_e$ defines the average number of entanglements per micelle.

Quantitative rheological measurements show that this viscoelasticity is characterized by a single relaxation time, a property which is rather unusual for fluids with complex

microstructures.[67] This rule is indeed so general that it is now admitted that a single relaxation time in the linear mechanical response is a strong indication of the wormlike character of self-assembled structures. The kinetics of the micelle formation and breakdown above the cmc is based on multiple equilibria, in which the micelles grow or shrink by stepwise incorporations or dissociations of monomers.[19,68,69] For surfactant showing preferentially the cylindrical aggregation, the end-cap energy, E, denotes the excess in packing energy (between a spherical and a cylindrical environment) for the molecules located in the two hemispherical end-caps. The growth laws for neutral and polyelectrolyte micelles are presented as follows.

Neutral micelles

The end-cap energy E is here equivalent to the scission energy necessary to create two new chain ends. For a dispersion of micelles of length L and molecular weight distribution c(L), the minimization of a free energy that takes into account the end-cap energy and the translational entropy yields for the average micellar length, L_{avg},[70-72]

$$L_{avg} = \frac{2}{n_0} c^{1/2} \exp\left(\frac{E}{2k_B T}\right) \quad (12)$$

where n_0 is the number of surfactant per unit length of the linear aggregate. n_0 (in Å^{-1}) is of the order of unity. The distribution in length c(L) is broad and given by:

$$c(L) = \frac{c}{L_{avg}{}^2} \exp\left(-\frac{L}{L_{avg}}\right) \quad (13)$$

where c(L)dL denotes the number density of chains of length comprised between L and L + dL.

Polyelectrolyte Micelles

MacKintosh and coworkers have proposed a model to demonstrate that the electrostatic interactions reduce the scission energy and favor the breaking of micelles.[73,74] For polyelectrolyte

micelles, the end-cap energy is not equivalent to the scission energy. The electrostatic contribution to the free energy results in a broad dilute regime. There, the micelles are rather monodisperse and their length increases very slowly with concentration. The overlap concentration, c* between the dilute and semidilute regimes depends on the effective linear charge density, ν, through the relationship:

$$c' = \left(\frac{k_B T l_b R_c \nu^2}{E}\right)^2 \quad (14)$$

where l_b is the Bjerrum length (l_b= 7.15 Å in water) and $R_c$the radius of the cylinder. Above the overlap threshold, which also corresponds to the screening of the electrostatic interactions by the counterions, the micelles grow more rapidly according to:

$$L_{avg} = \frac{2}{n_0} c^{1/2} \exp\left(\frac{E}{2k_B T}\left[1 - \left(\frac{c'}{c}\right)^{1/2}\right]\right) \quad (15)$$

The predictions for the dynamics of growth of neutral and polyelectrolyte micelles agree qualitatively with experiments. For instance, it is known that the addition of salt to a solution of polyelectrolyte micelles can result in a strong increase of viscosity, the solution passing from a viscous fluid to a viscoelastic gel.[75]

1.4. Formation and Physical Chemistry of Wormlike Micelles

Wormlike micelles can form spontaneously at ambient temperature using cationic surfactants, e.g., with 16 carbon atoms in the aliphatic chain. This is the case for cetyltrimethylammonium bromide (CTAB)[76,77] and cetylpyridinium bromide (CPBr).[78] The growth of the aggregates can be promoted however if cosurfactants or other low molecular weight additives are incorporated to the solutions. These additives are short alcohol chains, strongly binding counterions, oppositely charged surfactants etc. the different classes of surfactants and cosurfactants/additives which form such structure. These are discussed elaborately as follows.

(a) Surfactant and simple salt. The addition of simple salts such as sodium chloride (NaCl) or potassium bromide (KBr) to ionic surfactant solutions results in the screening of the electrostatic interactions between the charges, and thus in the growth of the aggregates. The archetype system of class A is CTAB with KBr.[49,79-83] Other well-known examples are sodium dodecyl sulfate (SDS) with monovalent[84-90] or multivalent counterions.[91,92]

(b) Surfactant and cosurfactant, where the cosurfactant is a short alcohol chain. Classical examples are the ternary systems sodium alkylsulfate-decanol (Dec)-water, Sodiumdecyl sulfate (SdS)-Dec[93-96] and Sodiumdodecyl sulfate (SDS)-Dec[97-99] and cetylpyridinium chloride (CPC)-hexanol-Hexanol (Hex)-brine.[100-104] In these systems,

the ratio between the alcohol and surfactant concentrations controls the polymorphism of the self-assembly.

(c) Surfactant and strongly binding counterion. Strongly binding counterions are small molecules of opposite charge with respect to that of the surfactant. They are sometimes called hydrotopes. Well-known examples of hydrotopes are salicylate, tosilate and chlorobenzoate counterions, which all contain an aromatic phenyl group. CTAB and CPC with sodium salicylate (NaSal) have been probably the most studied micellar systems during the last two decades.[105-120] Contrary to simple salts (class A), a large proportion of these counterions (~ 80 %) is assumed to be incorporated into the micelles. It was found that in CPC-NaSal, long wormlike micelles are immediately formed at the cmc (0.04 wt. %), without passing through any intermediate spherical morphology.[105,106,121]

(d) Amphoteric surfactant. Amphoteric surfactants are surface active molecules that contain positive and negative charges in the head group. Betaine-type molecules with quaternary ammonium and carboxylate groups are the representatives of this class. They associate at low concentrations and aqueous solutions exhibit strong gel-like properties. These properties are attributed to the existence of an entangled network of micelles.[122,123]

(e) Gemini surfactants and surfactant oligomers. The covalent linking of amphiphilic moieties at the level of the head group yields to Gemini surfactants and surfactant oligomers.[124] In aqueous solutions, these molecules present a broad polymorphism of aggregation.[125-129] Gemini surfactants are one of the rare examples for which cylindrical micelles close on themselves spontaneously, forming loops or rings. This property has been attributed to large end-cap energies.[130]

(f) Cationic and anionic surfactant mixtures. Oppositely charged surfactants have shown synergistic enhancements of rheological properties, and notably through the formation of mixed wormlike micelles. The growth of the micelles is assumed to arise from the charge neutralization of the surface potential and from the related increase of the ionic strength (as in type (a)). Recent examples studied are the mixtures of sodium dodecylsulfate (SDS) and dodecyltrimethylammonium bromide (DTAB)[131,132] or the mixtures made from cetyltrimethylammonium tosilate and sodium dodecyl benzenesulfonate.[133, 134]

(g) Block copolymers. Cylindrical self-assembly have also been reported in aqueous solutions of low molecular weight block copolymers.[135-137] The system investigated is poly(ethylene oxide)-poly(butadiene) with a weight fraction around 50 % for the first block.[135,136] "Giant" micelles have been found by cryo-transmission electron microscopy and the cylindrical morphology of the poly(butadiene) core was confirmed by neutron scattering. Beside the ionic sufactants, non-ionic surfactants such as polyoxythelene ethers such as $C_{12}E_5$,[138] $C_{10}E_{51,}$[139] and $C_{16}E_6$[140] are also reported to form worm like micelles in presence of co-surfactants. Lecithin (or phosphatidylcholine),[141-144] is one of the most widely studied lipid-based surfactant forming wormlike micelles and is used in pharmaceutical formulations as it is well-tolerated and non-toxic. Since the past decade, an increasing number of studies have been focusing on wormlike micelles made from biocompatible or biodegradable surfactants, which could find potential applications as drug-delivery systems. Examples include block-copolymers based on methoxypoly(ethylene glycol) and poly(caprolactone-b-L-lactide)[145] and biomimetic glycopolymer–polypeptide triblock copolymers for site-specific drug delivery.[146]

1.5. Morphology transition in presence of aromatic hydrotropes/counterions

Organic π-conjugated molecules are effective tuners in the formation of various nanostructured materials, and the entailed route is potentially facile and efficient for the development of functional materials of technological and biological importance.[147-150] Microstructural transitions of micellar aggregates, especially the nature of transition from ordinary micelles to long worm-like giant micelles and the vesicles, mediated by organic π-electron systems are of fundamental scientific interest and have been investigated. Interactions of aromatic hydroxy compound, phenol (PhOH) with micellar aggregates of CTAB in aqueous solutions have been investigated by means of titration calorimetry, solution conductimetry, and ^{1}H NMR spectroscopy.[151, 152] Results indicate that PhOH molecules can interact directly with CTAB micelles formed either in H_2O or D_2O and reside both at palisade layer[152] as well as at the hydrophobic core of the micelles.[151] The strongly negative enthalpy change of micellization, The ΔH^0_{mic},values measured for the PhOH/CTAB/H_2O system suggest that the main driving force of phenol solubilization is the increased PhOH - CTAB interaction upon transfer from the unmicellized aqueous phase. Influence of electrolyte on the interaction between the micelles of CPC and phenol was studied by Xu et. al.[153] Compared with sodium chloride

(NaCl) and sodium sulfate (Na_2SO_4), the presence of sodium carbonate (Na_2CO_3) promoted the solubilization of phenol in CPC micelle significantly due to the enhancement in degree of dissociation of phenol. The addition of Na_2CO_3 produced more (phenolate ion) $C_6H_6O^-$ at the same phenol concentration. The ion interaction between $C_6H_6O^-$ and (pyridinium ion) $C_5H_5N^+$ played more important role in the solubilization of phenol in CPC micelle than the polar interaction between phenol and CPC micelle in the presence of Na_2CO_3. A thermo-responsive phase transition from a viscoelastic wormlike micelle solution to an elastic hydrogel in a mixture of an imidazole-type surfactant, 1-hexadecyl-3-methylimidazolium bromide (C_{16}mimBr), and sodium salicylate (NaSal) was repoted by Lin. et al.[154] They speculated that π-π interactions between aromatic groups may play a key role in the observed thermo-responsive phase transition. You et. al.[155] reported the structural transitions of wormlike micelles triggered by pH in system comprised of ionic liquid (IL) *N*-hexadecyl-*N*-methylpyrrolidinium bromide (C_{16}MPBr) and anthranilic acid (AA). For 80mM C_{16}MPBr/80 mM AA composition, highly entangled wormlike micelle were observed at pH 5.01 which disappeared at pH 2.03 as well as at pH 7.03. The p*K*a values of the AA are 2.14 and 4.92 and its isoelectric point is 3.2. When pH value increases from ~2 to ~5, an increased binding of AA on the headgroups of C_{16}MPBr occurred due to reduced electrostatic repulsion, which led to the morphology of aggregates transit from spherical micelles to WLMs. The structural transitions occurring with change in pH for aqueous mixtures of CTAB and NaSal were further investigated by Umeasiegbu et. al. at various temperatures using dynamic light scattering and small-angle neutron scattering study.[156] Beside structural transition from rigid cylindrical micelles at neutral pH to spherical micelles at ~ pH 2 upon protonation of salicylate molecules; an unanticipated reversion to flexible cylindrical micelles with further decrease in pH was observed. Their results suggested that, in addition to the well-described electrostatic and hydrophobic interactions in cationic surfactant−hydrotrope mixtures, the pH-induced microstructural changes are potentially governed by complementary cation−π and hydrogen bonding interactions. The effect of extended aromatic π-conjugated compounds 1 and 2-Naphthols on the shape transition of CTAB and cetylpyridinium bromide (CPB) micelles were studied by Saha et. al.[157] They revealed that in the absence of charge screening of surfactant head groups, H bonding among micelle embedded naphthol molecules probably played the key role in micellar shape transition. While fluorescence quenching via H-bond strengthening was not observed in the

micellar phase, UV absorption spectra demonstrated the presence of inter molecular H bond in micelle-embedded naphthols in their ground electronic states, which was confirmed by FTIR. In a subsequent paper,[158] they established that the success of naphthols in effecting microstructural transition of micelles lie in their unique ability to form H-bonds with interfacial water molecules, which have shown unusual H-bond donating properties compared to bulk water. They reported that OH groups of micelle-embedded naphthols remain protruded toward the Stern layer through ~1 Å and the dielectric constant of OH sites has been measured as 45 ± 2 by observing the pKa shift of acid-base equilibrium of naphthols at the interface relative to that in bulk water. This observation was significant in relation to orientation of aromatic moieties in biological membrane. In studying the the location, orientation, and dynamics of small hydrophobes 1 naphthol and 1-methylnaphthalene in lipid dimyristoylphosphatidylcholine (DMPC) membrane, via ^{1}H- nuclear overhauser effect spectroscopy (NOESY) and molecular dynamics simulation, Shintani et. al. have shown that 1-naphthol exhibits a slight preference for pointing its OH group toward the hydrophilic domain of the membrane while no definite preference was concluded for the orientation of 1-methylnaphthalene.[159] Stronger NOE was observed for 1-naphthol due to the restricted motion of the OH group along with the slowdown of the 1-naphthol motion within the lipid membrane. Study on 1-hexadecyl-3-methylimidaozlium cation,$[C_{16}mim]^{+}$ with aromatic anions, 4-hydroxybenzesulfonate, $[HBS]^{-}$, benzenesulfonate, $[BS]^{-}$, and p-toluenesulfonate $[PTS]^{-}$ have shown that the ILs exhibited 2-3 fold lower cmc values as compared to that of conventional surfactants or ILs having inorganic anions as counterions.[160] The high promise and applicability of aromatic π-conjugated systems in promoting structural transition and their industrial and biological relevance have been explored in this dissertation.

1.6. Need for innovation in novel surfactant development

Besides the constant challenge of finding ways to minimize the manufacturing cost for existing surfactants, the market pull for ‘greener’ products is the overriding driving force for surfactants development. Some recent methodology that are being followed are - to synthesize the surfactant from natural building blocks; to insert one or more weak bonds into the structure in order to speed up the degradation, such surfactants are sometimes referred to as ‘cleavable surfactants’; to use starting materials – natural or synthetic – that give proper rate of biodegradation and to make more efficient

surfactants, i.e., surfactants that can be used in lower amounts; gemini surfactants are examples of that approach. With the rising challenges of environmentally benign chemical processing, ionic liquids (ILs), consisting of a large organic cation and a corresponding small anion, have emerged in recent years as discussed earlier. ILs have drawn increasing interest for their promising role as alternative media in a variety of catalytical, separation, and electrochemical processes as a result of their unique chemical and physical properties.[161-163] According to the generally accepted definition, these salts are liquid below 100°C, and have a negligible vapor pressure.[164] They have been shown to be excellent candidates in the fields of catalysis, nanostructure materials, organic synthesis, electrochemistry, and liquid/liquid extraction.[165-169] More importantly, their chemical and physical properties can be effectively and easily tailored by changing the cation, anion, and substituent components.[170] ILs bearing long alkyl chain can be regarded as a novel category of amphiphiles. ILs are considered environment friendly compounds, mainly because they are non-flammable and non-volatile. Additionally, enhanced reaction rates obtained in ILs allows the reduction of solvent volumes in the given technological process, thus reducing costs, risks and possible waste. These properties prompt the interest to replace common volatile organic solvent with ILs. The opportunity of cation modification and anion selection as well as enormous number of their possible combinations let to improve their physical and chemical properties. This, in turn, fulfills technological demands and provides for contemporary technology and especially chemical industry, novel so called task-specific media.[171] The high interest is also due to the capability of ILs to form a wider range of intermolecular interactions than typical volatile organic solvents. This includes interactions of the type: strong and weak ionic, hydrogen bonding, van der Waals, dispersive, n-π and π-π interactions.[172,173] A number of ILs also exhibit surface activity at air/water interface and due to this inherent nature, they are called surface-active ionic liquids (SAILs), and they can form aggregates with specific structures, shapes, and properties. The aggregation behavior of SAILs has therefore been extensively investigated in the field of colloid and interface chemistry.[174,175] Bowers et al. investigated the aggregation behavior of three ionic liquids based on the 1-alkyl-3-methyl-imidazolium cation, 1-butyl-3-methylimidazolium tetrafluoro-borate ([BMIM][BF_4]), 1-methyl-3-octylimidazolium chloride and iodide ([OMIM][Cl] and [OMIM][I], respectively) in aqueous solutions by means of surface tension, conductivity, and small angle neutron scattering (SANS) measurements.[176] Their

results revealed that SAILs behaved like short chain surfactants in aqueous solutions and formed micelles at concentrations higher than their respective cmc. The conductivity data for the [OMIM][Cl] and [OMIM][I] also indicated the possible presence of aggregates at concentrations below the cmc. Fluorescence quenching technique was used by Vanyur et. al to determine the aggregation number of long chain imidazolium based ionic liquids viz., 1-dodecyl-3-methyl-imidazolium bromide ([DDMIM][Br]), 1-methyl-3-tetradecyl-imidazolium bromide ([TDMIM][Br]) and 1-hexadecyl-3-methyl-imidazolium bromide ([HDMIM][Br]).[177] They observed that the aggregation number of the micelles were smaller than values characteristic for parallel alkyltrimethylammonium bromide (C_nTAB) surfactants containing the same chain length. The fluorescent behavior of pyrene probe indicated higher polarity in [C_nMIM][Br] micelles than in the corresponding C_nTAB micelles. A novel class of zwitterionic SAIL N-alkyl-N-carboxymethylimidazolium inner salts ([N-C_n, N´-CO_2-Im], n = 10, 12, 14) was synthesized and reported by Wang. et. al.[178] They showed that these class of SAIL exhibited higher surface active property and lower cmc than conventional imidazolium based SAILs. Detailed experimental and theoretical investigations on another newly synthesized halogen-free and low-cost alkylcarboxylate-based anionic SAIL namely, 1-butyl-3-methylimidazolium alkylcarboxylates ([C_4mim][$C_nH_{2n-1}O_2$], n = 8, 10, 12) was reported by Cheng et. al.[179] An interesting study on C_{16}mimBr, with an azobenzene derivative, sodium azobenzene 4-carboxylate (AzoCOONa) in aqueous solution was done by Yu et.al. Initially, viscoelastic wormlike micelles with a viscosity of 0.65 Pa·s were constructed in the C_{16}mimBr/AzoCOONa system. Upon irradiation by UV light (365 nm), the wormlike micelles become much longer and more entangled, exhibiting a high viscosity of 6.9 Pa.s.[180] This can be attributed to photoisomerization of the AzoCOONa molecule from trans to cis form. It is the first time that, with exposure to UV or visible light, the aggregate type of the photoresponsive system has been found to remain unchanged, with only a change of internal property parameters. The cation−π interaction prevailing over the hydrophobic interaction and electrostatic interaction between C_{16}mimBr and AzoCOONa molecules was supposed to be responsible for this peculiar phase behavior. Apart from these, a large number of reports on aggregation of different imidazolium based surface active ionic liquids are available in literature.[181]

The diverse application of the self-assembled aggregates of molecules has also led to the research in increasing the extent of adaptiveness of these aggregates towards different chemical and physical environment. Modification in adaptive nature of self-assembly of molecules towards parameters like temperature, pH, pressure, moisture etc. have also been a major field of interest. The environmental adaptiveness, including smart self-assemblies adaptive to pH, temperature, pressure, and moisture; special chemical adaptiveness, including nanostructures adaptive to important chemicals, such as enzymes, CO_2, metal ions, redox agents, explosives, biomolecules; field adaptiveness, including selfassembled materials that are capable of adapting to external fields such as magnetic field, electric field have been extensively researched in the past and ongoing decade.[182]

Amino acids, on the other hand, are natural products and the linkage between the amino acid residue and the hydrophobic tail is often an ester or an amide bond. Such bonds are easily degraded by the action of hydrolytic enzymes such as lipases and peptidases. This means that the majority of amino acid-based surfactants are readily biodegradable and non-toxic, especially to marine organisms. In addition, the most common of the amino acid-based surfactants have proven to be mild to the skin and non-sensitizing. Long chain N-alkyl derivatives of amino acids are amphoteric surfactants. There has been an interest in N-alkyl cysteine-based surfactants because of the possibilities that the thiol group in the polar head can provide.[183,184] Task specific surfactants based on l-glycine, l-alanine, l-valine, l-glutamic acid, and l-proline having superior surface activity compared to conventional surfactants, were prepared by Trivedi et al.[185] Amino acid-based surfactants have many of the characteristics that are needed for surfactants in consumer products. The transmembrane domains of integral membrane proteins show an astounding accumulation of the aromatic amino acids tyrosine and tryptophan residues, especially in the region of the highest lipid density. It has been found that these residues perform vital antioxidant functions inside lipid bilayers and protect cells from oxidative destruction.[186] Long-chain acylated tyrosine and tryptophan, but not phenylalanine or short-chain acylated derivatives, are potent inhibitors of lipid peroxidation and oxidative cell death. Statistical analyses of amino-acid distribution patterns in integral membrane proteins reveal a pronounced enrichment of tyrosine and tryptophan in the transmembrane domains of all major classes of membrane proteins: Single-span as well as multi-span membrane proteins, proteins of the a-helix bundle as

well as of the β-barrel type.[187-189] Tyrosine and Tryptophan are especially enriched in the region contacting the membrane zone of the highest lipid density, which comprises the inner portion of the lipid headgroups and the beginning of the hydrocarbon tails. The antioxidant functions of tyrosine and tryptophan provide a specific explanation for (a) their unique transmembrane distribution pattern and (b) the high vulnerability of low-protein neuronal membranes to oxidative stress, as seen in neurodegenerative disorders. With the growing concern about the biological effects of chemicals it is likely that the class of amino acid surfactants will become even more important in the future.

References are provided in BIBLIOGRAPHY under “References for Chapter I” (Page 155-168)

Chapter II

Scope and object

The self-aggregation of amphiphilic molecules, either in the simplest form of monolayers or in the form of micelles, vesicles and liposomes, all provide unique opportunities to bring other molecules closer together, to orient them in specific way and to alter their reactivities. Normal micelles that form within aqueous surfactant solutions above a certain surfactant concentration (or a concentration range), usually called critical micelle concentration (cmc), are a topic of major interest due to their unusual physicochemical properties as a result of surfactant aggregation. Although some work has been done in this field, a complete understanding of the micellization phenomena, its fundamental aspects, use of related studies for technological developments, and understanding molecular behavior requires a comprehensive knowledge of the forces and factors controlling the said process. One approach that is widely being practiced for this knowledge has been the study of effect of additives especially electrolytes, on the micellization characteristics of ionic surfactants. The alteration or modifications of important physicochemical properties of aqueous surfactant solutions is highly desirable as far as potential applications of such systems are concerned. Modification of forces operating within the surfactant micelles has led to formation of sophisticated aggregates such as wormlike micelles, which have physical characteristics that are entirely different from that of the spherical micelles. Wormlike micelles are long, flexible, cylindrical chains with contour lengths of the order of a few micrometers. The rheological properties of entangled wormlike micellar solutions are similar to those of semidilute polymer solutions with the difference that the micelles are dynamic in nature (breaking and recombining rapidly). The formation of wormlike micelles is linked to the emergence of viscoelasticity in the solution. Due to their viscoelastic properties, wormlike micelles have found applications in many areas, such as home and personal care products and in oil field industry. Frequently, they are also used as drag reducing agents for district heating.[1] Fluids those viscosify or gel upon heating are of high interest for biomedical and drug delivery applications, for flow control and separation using micro-fluidic devices and as hydraulic fracturing fluids in enhanced oil recovery. The simplicity, low cost and ease of preparation of these systems might make it attractive for some of these applications. Understanding

how the micellar structure is connected to the chemical composition and geometry of the surfactants, and how the structural features of the aggregates can be tuned by specific control parameters, and how these dictate the bulk properties of the solution, offers a considerable challenge. Although it is generally believed that micellar entanglement and transient network formation are responsible for developing shear induced viscoelasticity, precise knowledge regarding the nature of interaction in micellar entanglement and shear induced structure formation of such complex fluids is still lacking. In view of the fact that most of the previous works on the micellar shape transition involved systems containing cationic surfactants in presence of hydrophobic salts as the triggering agents, the primary aim of the present work is to attempt for morphology transition under salt-free condition. The major objectives of this dissertation are, therefore, as follows:

The objective of this work is to understand how the molecular geometry of surfactants determine their interaction with the class of π-conjugated aromatic additives viz., 1 Naphthol, 2 Naphthol and 2,3 Dihyroxynaphthalene (2,3 DHN) in order to apply these compounds as triggering agents under salt-free condition. The surfactants chosen for this study are cetyltrimethylammonium bromide (CTAB) and cetylpyridinium bromide (CPB). Both CTAB and CPB are very important ionic surfactants from scientific as well as industrial points of view. Moreover, the quaternary ammonium head group of CTAB resemble the choline moiety, which also consist of quaternary ammonium group and are present in phosphocholine, the most abundant phospholipid found in plant and animal membranes. Both CTAB and CPB have identical hydrophobic chain length consisting of 16 carbon atoms in the linear hydrocarbon chain but they differ in charge type and size of the polar head groups. The naphthalene derivatives have been chosen since these aromatic compounds have shown promise of structural modification of cationic micelles via charge screening through their electron-rich aromatic skeleton and also because they resemble the aromatic aminoacid tyrosine, which is present abundantly in lipid membrane interface. To precisely understand the role of the OH group, all the three naphthalene derivatives, viz.,1 Naphthol, 2 Naphthol and 2,3 DHN, which only differ in the relative position of the OH group in their molecular architecture, have been investigated.

The second objective is the detailed investigation on the surface properties of the individual naphthalene derivatives, viz., 1 Naphthol, 2 Naphthol and 2,3 DHN, in order

to understand their unique behaviour as triggering agents of morphology transition of the cationic micelles. These compounds will be studied to understand their interaction with the novel surface active ionic liquid (SAIL) 1-hexadecyl-3-methylimidazolium bromide (C_{16}-3-MeImCl) as well. SAIL belonging to the imidazolium class, have superior surface property compared to conventional surfactants.[2] Moreover, the imidazole ring has found application as bio-reagent due to its ability to bond to metals as ligands.[3-7] In order to have a more comprehensive idea on the interaction with hydroxynaphthalene, C_{16}-3-MeImCl, is chosen in particular, because its hydrocarbon chain is identical to CTAB and CPB. The scope of industrial application of the C_{16}-3-MeImCl-hydroxynaphthalene systems will be explored and metal tolerance of viscoelastic gel will be examined because of the possibility of its application as fractured fluids in oil-fields under neutral and salt-free conditions.

Biological membranes exhibit various function-related shapes, and the mechanism by which these shapes are created is largely unclear. It is generally believed that the changes of membrane topology is produced as a result of a complex interplay between membrane proteins, lipids and certain physical forces. In an attempt to understand the specific role of interfacial aromatic aminoacids in tuning spontaneous membrane curvature, a physico-chemical investigation on a model system of charged micelle/water interface, loaded with aromatic aminoacids, is proposed.

The scope of understanding the precise functioning of the aromatic amino acid viz., tyrosine and tryptophan would also be explored. Lipid membrane interface contain unusually high concentrations of residues of tyrosine and tryptophan, especially in the region where lipid density is maximum and it has been found that these residues perform vital antioxidant functions.[8] With an objective to understand this preference of nature towards these two aminoacids in particular, aminoacid amphiphiles based of tyrosine and tryptophan will be synthesised and characterised. Attempts will be made to understand their molecular conformation in vacuum as well as in aqueous medium. Octyl and dodecyl esters of tyrosine and tryptophan in presence of cationic micelles of CTAB will be employed as the models for bio-membrane in order to study their surface and interfacial properties. Influence of Tyrosine and Tryptophan esters in modification of these properties at different concentration regimes will be explored. The rheology of

the systems will be examined in view of the possibility of unidimensional growth of the micelles and subsequent development of complex fluidic nature of the system

References are provided in BIBLIOGRAPHY under “References for Chapter II” (Page 169)

Chapter III

Modification of aggregation characteristics of cationic surfactants by hydroxy aromatic derivatives of naphthalene under salt-free condition

1. Introduction

Ever since the interests are generated in scientific community on micellar shape transition phenomenon and the formation of long wormlike micelles (WLM) more than 40 years ago, a number of triggering agents for tuning the micellar surface curvature leading to sphere to rod transition, especially those of cationic micelles, have been in the center of attention. Some of these agents are highly efficient compared to others. For some cationic surfactants, wormlike micelles are formed even at low salt concentrations by using specific strongly binding aromatic anions, such as salicylate, tosylate, chlorobenzoate and naphthalene sulfonate. The research on WLM has drawn considerable interest because its rheology is challenging due to the presence of multiple pertinent length scales and stress relaxation mechanism. This relatively new material has many applications using that of fractured fluids in the oil field, efficient drag reducing agent in hydrodynamic engineering and home care; personal care and cosmetic products. A large number of study in micellar shape transitions in cationic, anionic and catanionic surfactant systems have been reported in the literature, but almost all the investigations engaged organic and inorganic salts and involved charge screening of the head groups via electrostatic interactions. Surprisingly, attempt to promote micellar morphology transition under salt-free condition is meagre in the literature.

Organic π-conjugated molecules are effective tuners in the formation of various nanostructural materials and the entailed route is potentially facile and efficient for the development of functional materials of technological and biological importance. Microstructural transitions of micellar aggregates, especially the nature of transition from normal spherical micelles to long wormlike micelles mediated by organic π-electron systems are of fundamental scientific interest and have been reported recently. It has been shown that along with hydrophobic interactions, cation-π interaction is principally involved and the success of 1 and 2 Naphthols in effecting microstructural

transition of micelles like CTAB and CPB lies also in their unique ability to form H-bonds with interfacial water molecules, which have shown unusual H-bond donating properties compared to bulk water.

Studies on the effect of neutral naphthols and methoxynaphthalenes on CTAB micelles that showed the formation of cylindrical micelles with the former but not the later point to the importance of the hydroxyl (OH) group of salicylate molecules as well. It is argued that the cation-π interaction is one of the most important driving force in tuning the surface curvature via charge screening of the head group in the case of salicylate promoter as well. 1 and 2 Naphthols triggered wormlike micelle formation on CTAB and CPB. However, in the case of salicylate, it is believed that the ionized salicylate molecules are positioned in an inner location of the micelle-water interfacial region (palisade layer) for effective electrostatic interaction between the cationic head group of surfactant molecule and COO^- group of salicylate molecule. It has further been argued that with decreasing pH and consequent protonation, salicylate molecules are positioned at an outer location of the micelle water interface with the cationic head group perpendicular to their π-face, resulting in stronger cation-π interaction. In general, these studies bring new fundamental insight into the driving molecular forces behind wormlike micelle formation in cationic surfactant/hydrotopes solutions (including 1 and 2 Naphthols), showing that in addition to the hydrophobic effect and electrostatic interactions, the importance of H-bonding and cation-π interactions are also vital importance. Further investigations might provide deeper insights into the molecular mechanism through which H-bonding and cation-π interactions contribute to the equilibrium microstructure and associated rheological behavior of cationic surfactant-hydrotrope mixtures.

Interests in the micellar morphology transitions in presence of organic π-conjugated systems as above also stem from another important point of view; the biological relevance of cation-π interaction and the fact that the self-assembled aggregates of surfactants viz., micelles, vesicles etc. are considered as simple models of biological membrane including cell membranes. It is indeed interesting to further note that in structural biology, the importance of quaternary ammonium ion is well recognized. For example, Dougherty and co-workers found that the anionic cyclophane (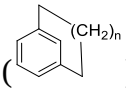

) is a

better receptor for quaternary ammonium and iminium ions in aqueous borate buffer than for corresponding neutral molecules.

Some of the strongest support for cation-π interactions at acetylcholine binding sites comes from studies of the nicotinic acetylcholine receptor (nAChR). Even without an X-ray structure, the evidence for a key role for aromatic residues at the ACh-binding site, and hence for the possible involvement of a cation-π interaction, is very strong.

Further, biological membranes exhibit various function-related shapes, and the mechanism by which these shapes are created is largely unclear. It is generally believed that the changes of membrane topology is produced as a result of a complex interplay between membrane proteins, lipids and certain physical forces. In view of the abundance of zwitterionic phosphatidylcholine in biomembranes and the ubiquitous feature of transmembrane proteins to localize aromatic aminoacids near the membrane-water interface, present study on the interaction of cationic head groups with aromatic π-systems definitely add to the understanding the tuning of surface curvature of biophysical membranes in presence of transmembrane proteins.

From the ongoing discussion it is amply clear that a completely new driving force is operational viz., cation-π interaction in presence of cationic head group (including quaternary ammonium ion (CTAB)) and the π-electron face of aromatic π-system along with hydrophobic interaction and H-bonding. This lead to highly efficient tuning of surface curvature of cationic micelles resulting in sphere-to-rod/ wormlike micelles transitions under salt-free condition. As have been already mentioned, further study would contribute to the deeper insights into the molecular mechanism by which H-bonding and cation-π interaction lead to the microstructure transition of micellar aggregates. Surprisingly, only a few works in this direction are reported.

In the present chapter, a detailed study of the interaction of CTAB and CPB micelles with the aromatic systems viz., 1 Naphthol, 2 Naphthol and 2,3 Dihydroxynaphthalene (2,3 DHN) have been undertaken along with the subsequent microstructural transition from spherical to WLM. Molecular level picture have been obtained from 2D NMR study. The morphology transitions have been investigated by means of SANS and the detail rheological aspects have been explained dynamic rheological investigation.

2. Materials and Methods

Materials

Cetylpyridinium bromide (CPB) and Cetyltrimethylammonium bromide (CTAB) were purchased from Across chemicals (USA) and was used as received. 1 and 2 Naphthols (Fluka, Germany) and 2,3 Dihydroxynaphthalene (Fluka, Germany) were further purified by vacuum sublimation followed by crystallization from 1:1 aqueous methanol. Methanol was distilled prior to use. Double distilled water (conductance below 2 μS/cm, pH ~6.5-7) was used for all experimental purposes. D_2O was purchased from Aldrich, USA (Purity >99.9%).

Methods

2.2.1. Specific conductivity measurements- The specific conductivity measurements were carried out in Metler Toledo Digital Conductivity bridge (MC226) (accuracy 0.1%) using a dip-type immersion cell with cell constant 1.0 (±0.05) cm^{-1}. 5 min equilibrium time was allotted before each reading. Constant temperature was maintained during the experiments with Remi ultra-thermostat (CB-700) with precision ± 0.1K. The uncertainty of the measurements was ±0.01μS.cm^{-1}.

2.2.2. Small Angle Neutron Scattering (SANS). The SANS measurements were carried out using small angle neutron scattering diffractometer at the Dhruva reactor, Bhabha Atomic Research Centre, Trombay, India. The diffractometer uses a beryllium oxide filtered beam with a mean wavelength (λ) of 5.2 Å. The angular distribution of the scattered neutrons is recorded using a one-dimensional (1D) position-sensitive detector (PSD). The accessible wave vector transfer ($Q = 4\pi \sin\theta/\lambda$, where 2θ is the scattering angle) range of the diffractometer is 0.017-0.35 $Å^{-1}$. The PSD allows simultaneous recording of data over the full Q. The samples were held in a quartz sample holder of 0.5 cm thickness. The measured SANS data have been corrected and normalized to absolute unit (as cross-section per unit volume), using standard procedures.

2.2.3. Nuclear Magnetic Resonance Spectroscopy (NMR). ^{1}H-NMR experiments were performed in Bruker (Germany) ADVANCE spectrometer operating at 300 MHz frequency (for characterization) and at 600.13 MHz for 2D Nuclear overhauser spectroscopy (NOESY) study. Signals are quoted as δ values in ppm using residual

protonated solvent signals as internal standard (D_2O: δ 4.79 ppm). Respective solutions were made in D_2O and 0.6 mL of the same was used for each measurement. Data are reported as chemical shift. 2D NOESY spectra was studied using Brucker standard software acquisition program noesyphpr in phase-sensitive mode using 5 mm BBO probe. An acquisition time of 0.085 sec and relaxation delay of 2 sec was used between the scans. The mixing time was 300 milisec. A total number of 2048 complex point were collected. Number of 16 scans were undertaken.

2.2.4. Rheology. The rheological experiments were done using cone-plate geometry with 4^0 truncation angle, with diameter 25 mm and 0.105 mm sample gap in MCR 302 (Anton Paar, Germany) equipped with Peltier temperature control system. The samples were initially stirred at 60^0C for three hours for homogenization and equilibrated for 72 hrs. During measurement, samples were equilibrated for 10 mins at each temperature.[1]

2.3. Analysis of SANS data

For a system of monodispersed interacting particles, the differential scattering cross-section per unit volume ($d\Sigma/d\Omega$) may be expressed as a function of scattering vector Q as:

$$\frac{d\Sigma}{d\Omega} = n\,(\rho_m - \rho_s)^2\, V^2\, [\langle F(Q)^2\rangle + \langle F(Q)\rangle^2 (S(Q)-1)] + B \qquad (1)$$

where n is the number density of micelles, ρ_m and ρ_s are the scattering length densities of the micelle and the solvent, respectively, and V is the volume of the micelle. F(Q) denotes the single-particle form factor which is the characteristic of specific size and the shape of the scatterer, and S(Q) denotes the interparticle structure factor. B is a constant, which represents the incoherent scattering background. The F(Q) is calculated by treating the micelles as prolate ellipsoids, using the equations: [2]

$$\langle F(q)^2\rangle = \int_0^1 [F(q,\mu)]^2\, d\mu \qquad (2)$$

$$\langle F(q)\rangle^2 = \int_0^1 [F(q,\mu)\, d\mu]^2 \qquad (3)$$

$$F(q,\mu) = \frac{3(\sin x - x\cos x)}{x^3} \qquad (4)$$

$$x = q[a^2\mu^2 + b^2(1-\mu^2)} \qquad (5)$$

where a and b are the semimajor and semiminor axes of an ellipsoidal micelle, respectively, and μ is the cosine of the angle between the directions of a and the wave vector transfer Q. The interparticle structure factor S(Q) identifies the correlation between the centers of different micelles, and it is the Fourier transform of the radial distribution function g(r) for the mass centers of the micelle. S(Q) is calculated using expressions derived by Hayter and Penfold from the Ornstein-Zernike equation and using the rescaled mean spherical approximation.[3] To simplify the calculation of S(Q), the micelle is assumed to be a rigid equivalent sphere of radius $\sigma = (ab^2)^{1/3}$ interacting through a screened Coulomb potential.

3. Results and Discussion

3.1. Surface activity of aromatic π systems and their influence on surface and bulk properties of cationic surfactants

The influence of head group architecture of the cationic surfactants CTAB and CPB on their interaction with the aromatic π conjugated hydroxy naphthalenes viz., 1 Naphthol, 2 Naphthol and 2,3 Dihydroxynapthalene (2,3 DHN) is studied via conductometry. Upon addition of the hydroxy aromatic derivatives, there is a gradual decrease in the cmc values of both CTAB and CPB. While 1 Naphthol lowers the cmc of the surfactants in a linear fashion (Figure 1(a)), a non-linear or exponential trend is exhibited by both 2 Naphthol and 2,3 DHN as a function of concentration, which is more prominent in the case of CPB. Moreover, it is striking that the cmc of CPB is lowered to a greater extent compared to the others, i.e., CTAB. The lowering of cmc values indicates that the micellization of both the cationic surfactants are facilitated due to presence of the additives.

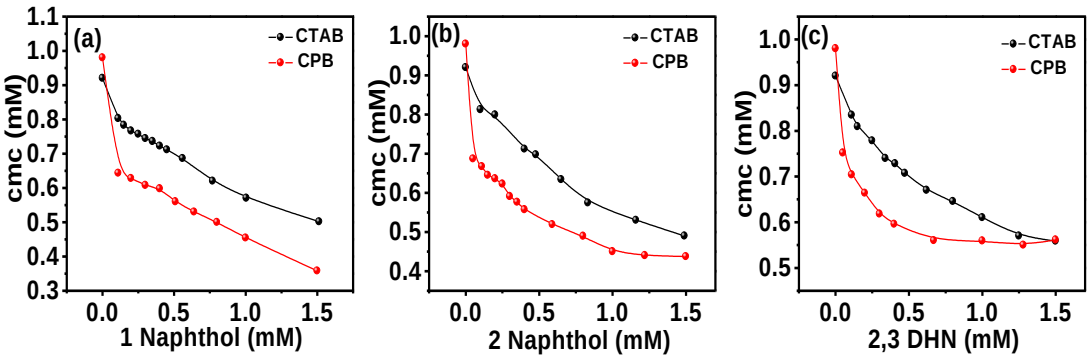

Figure 1. Variation of cmc of the surfactant-additive systems as function of (a) 1 Naphthol, (b) 2 Naphthol and (c) 2,3 DHN concentration at 303 K.

In a similar study, influence of phenol on micellization characteristics of CTAB have been reported previously.[4] A gradual decrease in cmc of CTAB was observed with increase in phenol concentration. The cmc of CTAB decreased from 0.93 mM in aqueous solution to 0.63 mM in presence of 10 mmol.kg^{-1} phenol. It was concluded that the decrease is cmc values was due to decreased electrostatic repulsion between the cationic head group of the CTAB micelle and salting out of the surfactant monomers. In the present study, it is evident that the lowering of cmc of CTAB as well as CPB occur at much lower concentration of the naphthalene derivatives. This stronger synergism may be attributed to the presence of the extra benzene moiety in the hydroxy naphthalene molecules and the extended conjugation therein.

In the present study, it is evident that the lowering of cmc of CTAB as well as CPB occur at much lower concentration of the naphthalene derivatives. This stronger synergism may be attributed to the presence of the extra benzene moiety in the hydroxy naphthalene molecules and the extended conjugation therein. In another study on Cetylpyridinium chloride (CPC)-Phenol interaction at different pH, it was found that at lower phenol concentration (0.5 mM, 1.0 mM), phenol was solubilized at the micelle-water interface driven by the interaction between the phenolate ion ($C_6H_6O^-$) and the pyridinium cation ($C_5H_5N^+$).[5] At higher phenol concentration (>2 mM), upon saturation of the micelle-water interface, $C_6H_6O^-$ is intercalated deeper into the palisade layer of the micelles. In the present case, the additives (aromatic π systems) remain in their protonated form, since the solution pH was maintained in the range 6.8-7.2 which is far below the pKa of the individual additives (viz., pK_a of 1 Naphthol is 9.34, pK_a of 2 Naphthol is 9.51, pK_a of 2,3 DHN is 9.10)[6] yet, they strongly interact with the surfactants thereby reducing the electrostatic head group repulsion between the cationic head groups and facilitating micellization. It is evident that interaction between the naphthalene moieties is stronger with CPB compared to that in CTAB, possibly due to the aromatic head group architecture of the latter. To obtain the composition of optimum interaction, the cmc of the systems are measured as function of different surfactant:additive molar ratios and displayed in Figure 2.

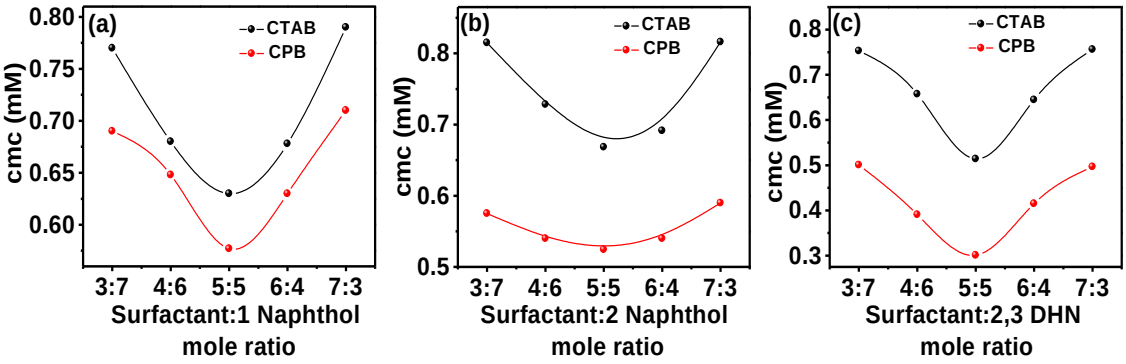

Figure 2. Variation of cmc of surfactant-additive systems at different surfactant:additive mole ratio, at 303 K.

It may be seen that for both CTAB and CPB, minimum value of cmc is obtained at equimolar composition of the surfactant and the respective additives. Theoretical calculations based on regular solution theory,[7] showed a similar cmc-concentration profile for mixtures of ionic and non-ionic surfactants with similar head group sizes.[8] The electrostatic free energy of mixing as a function of reduced charge density, S, assuming S>>1 have been expressed as:[8]

$$S = \frac{\sigma}{\sqrt{c_t.\epsilon_0\epsilon_r N_A kT}} \qquad (6)$$

Where, $\sigma = \frac{e_{el}}{a_{ch}}$ is the surface charge density, e_{el} is the elementary charge and $a_{ch}$is the area per charge at the aggregate surface. ϵ_0 and ϵ_r are the electric permeability in a vacuum and the relative permeability, respectively, N_A is the Avogadro constant, *k* is the Boltzmann constant and *T* is the temperature. Therefore, the synergistic effect observed between CTAB/CPB and the additives is due to electrostatic interaction governed by entropy of mixing of the surfactant and additive molecules with the solvent and as well as among themselves.[8] The increase in the cmc values beyond equimolar composition may be due to the self-interaction between the surfactants and thus becomes predominant at higher surfactant compositions and over-rules the synergism between surfactant and the additive.[9]

More insight on the strength and nature of interaction between the two components of the mixed systems is found out by calculating the interaction parameter, β, obtained on the basis of Rubingh's Regular solution theory.[10] According to this theory, the excess energy of mixing of the components in a mixed surfactant system is zero. The parameters viz., mole fraction of surfactant CTAB or CPB, α_1, experimental critical

aggregation concentration of the mixed system of the mixture, cac, critical aggregation concentration of CTAB, cac_1 (the cmc of CTAB in the mixed systems is now renamed as cac) and mole fraction of the surfactant within the micelles, X_1, are related as follows:[11]

$$\beta = \frac{\ln\{(cac.\alpha_1)/(X_1.cac_1)\}}{(1-X_1)^2} \quad (7)$$

X_1 is evaluated iteratively using the relation:[11]

$$\frac{[X_1^2.\ln(cac.\alpha_1/cac_1.X_1)]}{(1-X_1)^2}\ln\left[\frac{cac\,(1-\alpha_1)}{cac_2(1-X_1)}\right] = 1 \quad (8)$$

The respective activity coefficients f_1 and f_2 of the surfactant and respective hydrotopes are related to β as:

$$f_1 = \exp\{\beta\,(1-X_1)^2\} \quad (9)$$

$$f_2 = \exp\{\beta\,.{X_1}^2\} \quad (10)$$

All the π-conjugated additives viz., 1 Naphthol, 2 Naphthol and 2,3 DHN are reported to be surface active with well-defined critical aggregation values (Discussed in detail in Chapter IV). Therefore the surfactant-additive systems in the present study have been treated as mixed surfactant systems and the interaction between the head groups of the surfactant components are evaluated (Table 1). It is noteworthy that negative values of β are obtained for all the surfactant-additive systems implying that their interaction is essentially attractive and synergistic in nature. The hydroxy aromatic compounds interact more strongly with the aromatic pyridinium head group of CPB compared to quaternary ammonium head group of CTAB as evident from higher negative values of β observed for the CPB-additive systems at all the compositions (Table 1 as well). This result corroborates the lower cmc values observed in CPB-2,3 DHN system (Figure 2(c)). Moreover, among all the systems, the extent of head group interaction is the highest in between CPB and 2,3 DHN and lowest in between CTAB-2 Naphthol system. Most of the systems exhibit maximum value in β at or near the equimolar composition (except CTAB-2,3 DHN system and CPB-2 Naphthol system) implying that in most of the systems, entropically this composition is more favored compared to the others.

Table 1. Interaction parameter (β), activity coefficients (f_1 and f_2) of CTAB and CPB with 1-Napthol, 2-Napthol and 2,3 DHN at 303 K (Prefix 1 indicate surfactant, 2 indicate additive).

CTAB												
α_{Surf}	1-Napthol				2-Napthol				2,3 DHN			
actant	cmc	β	f_1	f_2	cmc	β	f_1	f_2	cmc	β	f_1	f_2
0.3	0.77	-4.14	0.06	0.27	0.81	-3.37	0.09	0.37	0.75	-3.49	0.08	0.37
0.4	0.68	-4.11	0.07	0.24	0.73	-3.41	0.11	0.32	0.66	-3.45	0.09	0.34
0.5	0.63	-4.11	0.08	0.21	0.66	-3.46	0.11	0.27	0.51	-4.49	0.05	0.21
0.6	0.68	-3.78	0.12	0.18	0.69	-3.31	0.15	0.24	0.64	-4.76	0.08	0.11
0.7	0.79	-2.66	0.29	0.24	0.81	-2.32	0.34	0.29	0.75	-2.59	0.27	0.27
CPB												
	cmc	β	f_1	f_2	cmc	β	f_1	f_2	cmc	β	f_1	f_2
0.3	0.69	-4.72	0.04	0.24	0.57	-5.03	0.03	0.24	0.50	-5.01	0.02	0.27
0.4	0.65	-4.43	0.05	0.22	0.54	-4.81	0.04	0.22	0.39	-5.77	0.02	019
0.5	0.57	-4.86	0.05	0.16	0.52	-4.75	0.05	0.19	0.30	-6.69	0.11	0.12
0.6	0.63	-5.53	0.05	0.08	0.54	-4.35	0.07	0.19	0.41	-5.44	0.03	0.14
0.7	0.71	-3.57	0.16	0.17	0.59	-3.87	0.11	0.18	0.49	-4.56	0.07	0.15

3.2. Nuclear magnetic resonance (NMR) study

3.2.1. ^{1}H NMR

To ascertain the location of the solubilized additives within the surfactant micelles, ^{1}H NMR study is undertaken. The molecular architecture of the additives viz., 1 Naphthol, 2 Naphthol and 2,3 DHN are similar, differing only in the position of the OH functionality in the aromatic ring. The hydroxy proton being labile, does not provide signals which could be worthwhile for NMR analysis. Therefore, the study is focused on determining the location of residence of the aromatic naphthalene ring with respect to the surfactant molecules. The collective ^{1}H NMR spectra of 2 Naphthol in D_2O, CTAB in D_2O and mixture of 10 mM CTAB and 10 mM 2 Naphthol in D_2O, alongwith the respective proton numbering, are presented in Figure 3. The spectra exhibit several interesting features. Firstly, considering the resonances for the aromatic moiety, it may be seen that the signals of 2 Naphthol in D_2O appear highly spilt displaying the most downfield and most upfield resonances at 7.86 and 7.18 ppm respectively (Figure 3(a)). However, in the CTAB-2 Naphthol mixture (Figure 3 (c)), the aromatic proton signals

are broadened and appear heavily merged and shielded, the most downfield and upfield resonances being at 7.46 and 7.06 ppm respectively. This upfield shift essentially imply a non-polar environment around the aromatic protons.[12] The broadening of signals are indicative of possible hydrogen bonding associated with the protons.[12] Secondly, the N-methyl protons of CTAB (C1) which normally resonate at 3.11 ppm in D_2O, also appear greatly shifted to lower ppm value i.e., 2.78 ppm ($\delta_{initial} - \delta_{final} = \Delta\delta = 0.33$ ppm).

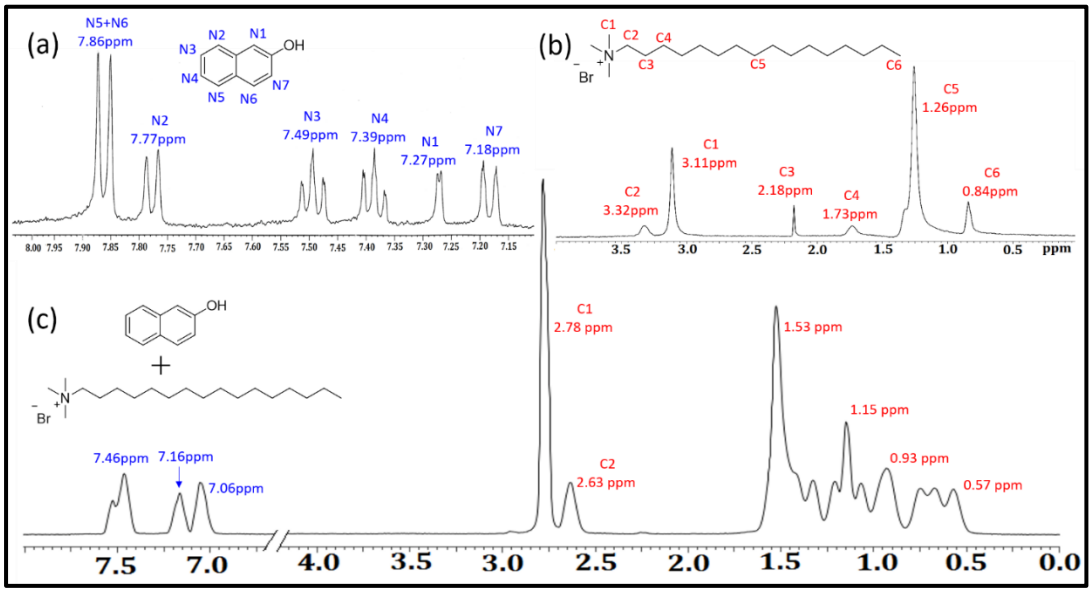

Figure 3. ^{1}H NMR spectra of (a) 5 mM 2 Naphthol in D_2O, (b) 10 mM CTAB in D_2O and (c) mixture of 10 mM CTAB and 10 mM 2 Naphthol in D_2O, at 298 K.

The most significant upfield shift is observed in the C2 protons, $\Delta\delta = 0.69$ ppm.[13] The resonances for the alkyl chain protons viz., C3, C4 and C5 as well as the terminal protons viz., C6, merge together and appear as multiplet ranging from 1.53 ppm to 0.57 ppm. It is striking that the intense signal corresponding to C5 protons appears at 1.26 ppm in D_2O (Figure 3 (b)), while in the CTAB-2 Naphthol mixture (Figure 3(c)), it appears at 1.53 ppm i.e., a downfield shift of $\Delta\delta = -0.27$. A similar upfield shift in the NMe (C1) as well as C1 and C2 proton resonances of CTAB has been reported in presence of phenol which has been shown to be the evidence in favor of radial penetration of the aromatic ring of phenol into the palisade layer of the CTAB micelles.[4] The presently observed shielding effect on the CTAB protons, may, therefore, be thought to be induced by the effect of ring current of the naphthalene ring of 2 Naphthol, which intercalates into the palisade layer and its location remains in the vicinity of the CTAB head group.[14,15] The huge perturbation of the alkyl proton resonances (Figure 3(c)) demonstrates interaction between naphthalene ring and the chain protons and this

further suggests much higher penetration depth of 2 Naphthol compared to that of phenol.[4] This leads to the concomitant upfield shift in the aromatic resonances. Intercalation of the extended benzene ring into micelle causes the hydrocarbon chains of CTAB to mutually move away apart causing an increase in the spatial distribution of the alkyl protons creating a relatively less non-polar environment in the vicinity which ultimately resulted in the downfield shift of the C5 resonances.[4,16]

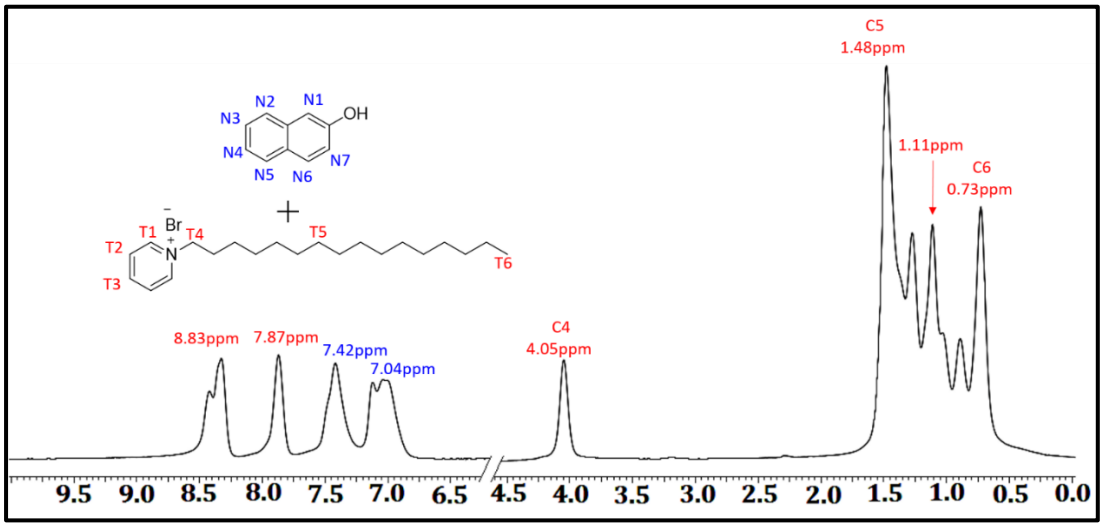

Figure 3 (d). ^{1}H NMR spectra of mixture of 10 mM CPB and 10 mM 2 Naphthol in D_2O, at 298 K.

The aromatic resonances for the pyridinium moiety of CPB in D_2O resonate highly downfield, in between 8-9 ppm[5] but in the CPB-2 Naphthol system (Figure 4 (d)), a merged broad peaks appear within 7.04 ppm to 8.83 ppm due to resonances of aromatic protons of both CPB and 2 Naphthol. It is apparent that the more downfield resonance is exhibited by pyridinium protons due to stronger deshielding of the same.[5] Therefore, a qualitative assignment of the aromatic resonances has been presented in Figure 5(d). The spectral line width of the aliphatic proton signals of CPB in the CPB-2 Naphthol mixed system is high, and these appear as multiplets, because of which specific assignment of proton resonances becomes less straightforward in this case. 2D NMR is, therefore, applied for achieving better insight on the molecular interactions.

3.3.2. NOESY

Nuclear Overhauser effect spectroscopy (NOESY) is a 2D NMR technique which presents correlation via dipolar interaction, between protons which are closer than 5 Å in space. Intensity of NOESY cross-peaks is a direct measure of extent of magnetization transfer and the internuclear distance between the protons.[17] The NOESY spectrum of

(10 mM) CTAB and (10 mM) 2 Naphthol and that of (10 mM) CPB and (10 mM) 2 Naphthol shows several cross-peaks correlating CTAB and the aromatic protons of 2 Naphthol as well as that of CPB and the aromatic protons (Figure 4).

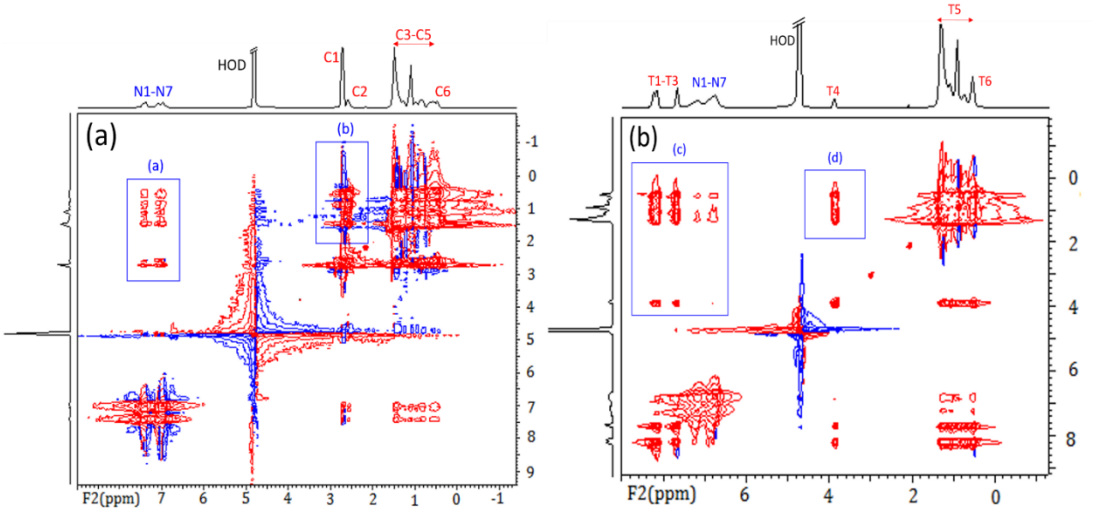

Figure 4. 2D NOESY spectrum of (a) 10mM CTAB and 10 mM 2 Naphthol in D_2O and (b) 10mM CPB and 10 mM 2 Naphthol in D_2O at 303 K.

The intense cross-peak N1-N7/C4 highlights the correlation between the NMe protons of CTAB with that of the aromatic ring. The presence of cross-peaks N1-N7/C1 and N1-N7/C2 (highlighted in the box (b) in Figure 4 (a)) which correlates the quaternary ammonium protons of CTAB with the terminal as well as some other aliphatic protons of the same is indeed interesting. This is indicative of apparent self-interaction within the CTAB molecule, which generally occur if the molecule remain in highly coiled conformation. This is, however, not likely to occur in our present system because of the presence of strong hydrophobic interactions between the hydrocarbon chain and the naphthalene moiety, indicated by the intense cross-peaks viz., N1-N7/C5-C6 which correlate the NMe protons as well as the chain protons of CTAB with the aromatic ring of 2 Naphthol (highlighted in box (a) in Figure 4(a)). This observation indicates the simultaneous proximity of the aromatic protons with the chain protons as well and provides evidence in favor of much deeper intercalation of the naphthalene moiety towards the micellar core as suggested from the ^{1}H NMR study.[4] Therefore, the apparent self-interaction between the head group and chain protons of CTAB is likely to originate from different CTAB molecules with different orientations. In all probabilities, this may occur near the end-cap regions of the rod/worm-like micelles. In

the case of CPB, cross-peaks indicating correlation between the aromatic protons of both 2 Naphthol (N1-N7) and CPB (T1-T3) with the α methylene protons of CPB (T4) are evident. Contrary to that observed in the case of CTAB, intensity of the N1-N7/T4 cross-peak is significantly less, which suggests a greater distance between the T4 and N1-N7 protons. Moreover, key cross-peaks indicating interaction between the alkyl and terminal protons with the naphthalene as well as pyridinium moiety, is apparent (Highlighted in box (c)), although intensity corresponding to interaction with 2 Naphthol is relatively low. Moreover, similar to that observed in the case of CTAB-2 Naphthol system, the self-interaction between the T4 and the T5-T6, is also apparent in CPB-2 Naphthol system.

The origin of the observed interactions in NOESY spectra may be understood by considering the different forces operating within the systems. Spectroscopic investigations of CTAB-1 Naphthol system in aqueous solutions has revealed that naphthols have the unique ability to form hydrogen bonds with the interfacial water molecules at its vicinity, in which the proton atoms of its hydroxy groups act as the donors.[12] This is considered as the driving force behind the embedding of the 2 Naphthol molecules in between the CTAB monomers within its micelle. A similar argument may be adopted to explain the observed interactions in the present CTAB-2 Naphthol system. The restructuring of water molecules at the micelle-water interface causes the OH functionality of 2 Naphthol to orient outward from the micellar interface, while the aromatic rings are embedded in between head groups of CTAB. 2D ROESY analysis show that this orientation is favored by strong cation-π interaction between the quaternary ammonium head group and the π-electron cloud of the naphthalene moiety and also by hydrophobic interactions between the aromatic protons and the alkyl chain protons.[12,18,19] This interaction largely neutralizes the positive charge on head group of CTAB monomers and facilitates micellization which is reflected in the conductometric study. The π-π interactions, on the other hand, are known to control diverse phenomenon like stabilization of the DNA double helical structure,[20] tertiary structure of proteins,[21] packing of aromatic molecules in crystal,[22] etc. This interaction results if the attractive interaction between π-electron and σ- framework outweigh the repulsive interaction between two π-electron system.[23] CPB is essentially an electron deficient aromatic system with a positively charged nucleus surrounded by delocalized π-electron cloud, while 2 Naphthol is a neutral electron rich aromatic system with

extended π-electron conjugation. The CPB-2 Naphthol system is likely to be dominated by the π-π interaction instead of the cation-π interaction as observed in CTAB-2 Naphthol system.[20] The electrostatic complementarity between the π-electron rich 2 Naphthol and the π-electron deficient CPB head group can lead to strong face-to-face stacking and thereby screening the head group charge of the CPB molecule because of which the micellization is favored.[24] Due to this interaction along with the rigid anchoring of the OH moiety to the interfacial water and further due to the larger head group size of pyridinium ring, the naphthalene moiety does not penetrate deep inside the micelle for which the relatively less intense cross-peaks correlating the aromatic naphthalene protons and CPB chain protons are observed in the NOESY spectra (Figure 3 (b)). A schematic representation of the molecular orientation in the CTAB-2 Naphthol and CPB-2 Naphthol systems is proposed in Scheme 1. Due to stronger cation-π interaction, the naphthalene additive shield the electrostatic charge of the CTAB head groups more efficiently, compared to π-π interaction which is further corroborated in the SANS study (Discussed later).

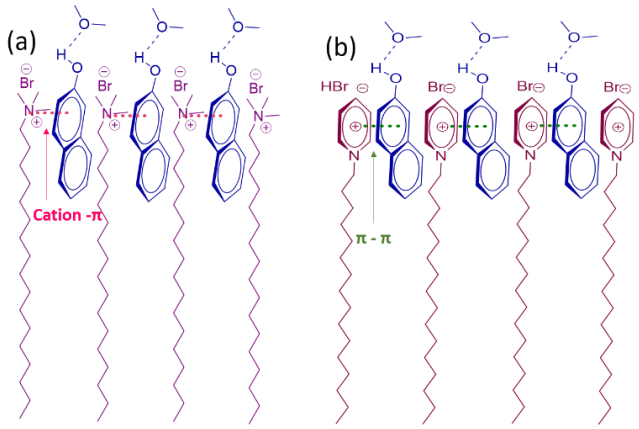

Scheme 1. Schematic representation of possible molecular orientation in the (a) CTAB-2 Naphthol system and (b) CPB-2 Naphthol system.

Due to the effective shielding of the head group charges via intercalation of the naphthalene moiety in between the surfactant monomers in micelles, the effective head group area, a_0, of the surfactant is decreased, which eventually increase the packing parameter, P of the surfactant. P governs the aggregate morphology and is given by:[25]

$$P = \frac{v}{a_o.l_c} \tag{11}$$

where ν and l_c are the volume and the extended length of the surfactant tail, respectively. For spherical micelles, $P > \frac{1}{3}$, while for elongated or worm-like micelles,

$\frac{1}{2} > P > \frac{1}{3}$.[25] The ellipsoidal or wormlike micelles in the present surfactant-additive systems are thus formed as the consequence of the electrostatic shielding of the head group charge.[26] To minimize the end cap energy, long wormlike micelles are formed with cylindrical body and nearly spherical end caps. Due to spatial congestion near the endcaps and higher density of the surfactant molecules, intermolecular interaction between the surfactants are likely to be predominant at the end cap and this may be responsible for the corresponding cross-peaks observed in the NOESY spectrum (Figure 4(a), (b)) as mentioned before. These aspects have been discussed in further detail in Chapter VI.

3.3. Small angle neutron scattering (SANS) study

The structural aspects of surfactant aggregates in solution may be obtained via SANS study.[27] In a SANS experiment, the sample is subjected to a beam of neutrons and the intensity of the scattered neutrons are measured in different directions. To obtain larger scattering intensity, samples are made in deuterated solvents. The SANS profile of the surfactant-additive systems are provided in Figure 5. The SANS spectra of the surfactant in the presence of the additives show a rise in the low Q region, while scattering in the high Q region is independent of the surfactant type and is nearly identical for CTAB and CPB in case of all the additives. The SANS spectra of CTAB in D_2O[26] and CPB in D_2O[28] show a characteristic correlation peak at the intermediate Q region, signifying the presence of inter-particle electrostatic interaction. In presence of 1 Naphthol, no correlation peak is evident in either CTAB or CPB (Figure 5 (a)) which demonstrates that the electrostatic repulsions between the charged head group of CTAB as well as CPB is efficiently reduced due to the presence of 1 Naphthol.[26] There is a rise in intensity at the low Q region for CTAB compared to CPB, in case of all three additives which signifies a growth in the micellar structure for CTAB compared to CPB in all the three cases.[2]

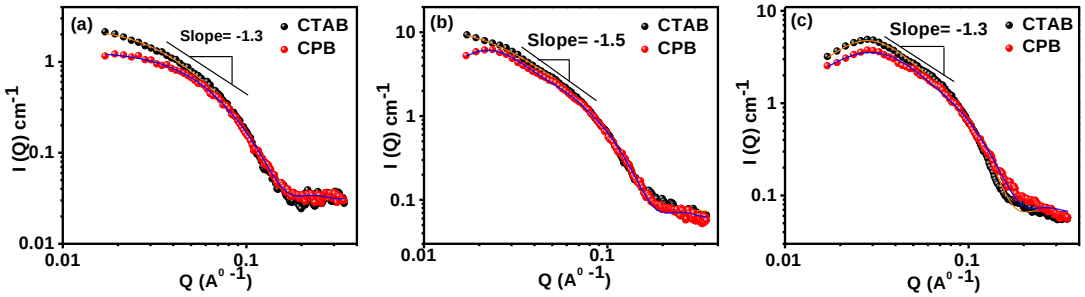

Figure 5. SANS distribution profile of 25 mM CTAB and 25 mM CPB in the presence of (a) 25 mM 1 Naphthol, (b) 25 mM 2 Naphthol and (c) 25 mM 2,3 DHN at 303 K. Solid circles represent experimental curve, solid lines represent theoretical fit for prolate ellipsoid micelle model.

The spectra of CTAB in presence of 2 Naphthol (Figure 5 (b)) is similar to that in the presence of 1 Naphthol, while, a correlation peak is evident in spectra of CPB meaning that electrostatic repulsion is present in this system, i.e., the screening of CPB head group repulsion by 2 Naphthol is less efficient than that in the case of CTAB. In presence of 2,3 DHN, distinct correlation peak is evident for CTAB and CPB (Figure 5 (c)). The peak appear at higher Q value for CPB compared to 2 Naphthol. The correlation peak generally occur at $Q \approx \frac{2\pi}{d}$, where d is the average distance between the aggregates present in the sample.[2] Thus, the observation imply a decrease in correlation length in the surfactant-2,3 DHN systems, ξ, given by $\xi = 2\pi/Q_{max}$.[26] The nearly identical Q_{max} for CTAB and CPB (Figure 5 (c)) imply that aggregate density in both the systems is identical. The SANS data are fitted to the prolate ellipsoid micellar model and it is found that the model is in excellent agreement with the experimental curves (Solid lines in Figure 5). This interestingly signifies that a structural modification of the spherical micelles of both CTAB and CPB is mediated by the hydroxy aromatic derivatives. The slope of the intensity vs Q at the intermediate Q region is obtained as -1.3, -1.5 and -1.3 for 1 Naphthol, 2 Naphthol and 2,3 DHN respectively and may be taken as an indication of presence of wormlike or rod like structures in the system.[28] Table 2 represents the structural dimension of the surfactant-additive systems obtained on fitting the experimental data to prolate ellipsoidal micellar model.

Table 2: Dimension of wormlike micelles of CTAB and CPB in presence of 1 Naphthol, 2 Naphthol and 2,3 DHN at 303 K, as obtained from SANS study.

	CTAB		CPB	
	Semi minor axis (Å)	Semi major axis (Å)	Semi minor axis (Å)	Semi major axis (Å)
1 Naphthol	23	92	22	59
2 Naphthol	26	122	21	110
2,3 DHN	22	74	19	72

It is apparent that the micelles of the system are rod like having length about five times of the radius. Longest worm like micelles are formed in CTAB-2 Naphthol system while shortest worms are formed in CPB-1 Naphthol system. Nevertheless, the result indicate that the hydroxy aromatic derivatives steer the transition of morphology of spherical aggregates of both CTAB and CPB, to elongated worm like.

3.4. Rheology of the wormlike micelles

On minimizing head group repulsion, surfactant micelles are capable of forming linear wormlike aggregates which have characteristic property of a viscoelastic gel, i.e., these giant molecules can withstand external stress up to a critical extent (Newtonian behavior) beyond which they become viscous or fluid-like.[29] Rheology is an important tool to measure the viscoelastic traits of such systems. On the application of an external stress, the system undergoes deformation followed by relaxation in order to regain its equilibrium state. According to the living polymer model of Cates[30] the relaxation of the viscoelastic micelles involves two time scales viz. reptation time (τ_{rep}) corresponding to curvilinear diffusion of a chain along its own contour and breaking time (τ_b) which is the result of chain scission. When $\tau_b << \tau_{rep}$, there occurs many breakages and recombination before the chain segment relaxes by reptation. The system is then defined by a single stress relaxation time, τ_R, given by $\tau_R=(\tau_{rep.}\ \tau_b)^{1/2}$ and is characterized as a Maxwell Fluid. The sinusoidal deformation on the system, at an angular frequency ω, causes the response stress, which remains out of phase with the applied strain.

The sinusoidal deformation (strain, $\gamma(t)$) can be expressed as:

$$\gamma(t) = \gamma_0 \exp(i\omega t) \tag{12}$$

where, γ_0 is the amplitude of the strain, ω is the angular frequency and t is the time.

The response stress will also be sinusoidal and will have a phase difference of δ, i.e.

$$\sigma(t) = \sigma_0 \exp(i[\omega t + \delta) \quad (13)$$

The complex modulus (G*) thus obtained is defined as:

$$G^* = \frac{\sigma(t)}{\gamma(t)} = \frac{\sigma_0 (cos\delta + isin\delta))}{\gamma_0 \exp(i\omega t)}$$

or, $G^* = G' + iG''$ (14)

where G' is the storage modulus and G'' is the loss modulus and these reflect the respective extent of elastic and viscous property of the system. For a fluid with near-Maxwell character, the elastic (or storage modulus), G' and viscous (or loss modulus), G'' are related to angular frequency, ω as: [31]

$$G'(\omega) = \frac{G_0 \omega^2 \tau_R^2}{(1+\omega^2 \tau_R^2)} \quad (15)$$

$$G''(\omega) = \frac{G_0 \omega \tau_R}{(1+\omega^2 \tau_R^2)} \quad (16)$$

where G_0 is the storage modulus at high frequency, where it exhibits a plateau, also called the plateau modulus. It is proportional to the number density of the entanglement points and hence characterize the network structure.[32] τ_R is obtained from inverse of crossover frequency, i.e. the frequency where G' and G'' intersects. Furthermore, Cole-Cole plot i.e the plot of G'' *v/s* G' is expected to yield a semicircle at low frequency region for a Maxwell fluid.[31]

3.4.1. Dynamic oscillatory measurements

Oscillatory measurements were carried out to characterize the flow behavior of the viscoelastic gels. Figure 6 presents the variation of G' and G'' with ω, for the surfactant-additive systems at different temperature. The response of G' and G'' as function of ω is typical to that observed in viscoelastic fluids comprised of wormlike micelles.[26,32,33] At lower ω, systems are predominantly viscous with G″ predominating over G′ while at high ω, G′ > G″ and the systems exhibit elastic behavior. There exists a distinct cross over point, ω_c, at which $G' = G''$. With rise in temperature, the frequency spectra shifts to the right, exhibiting higher ω_c.

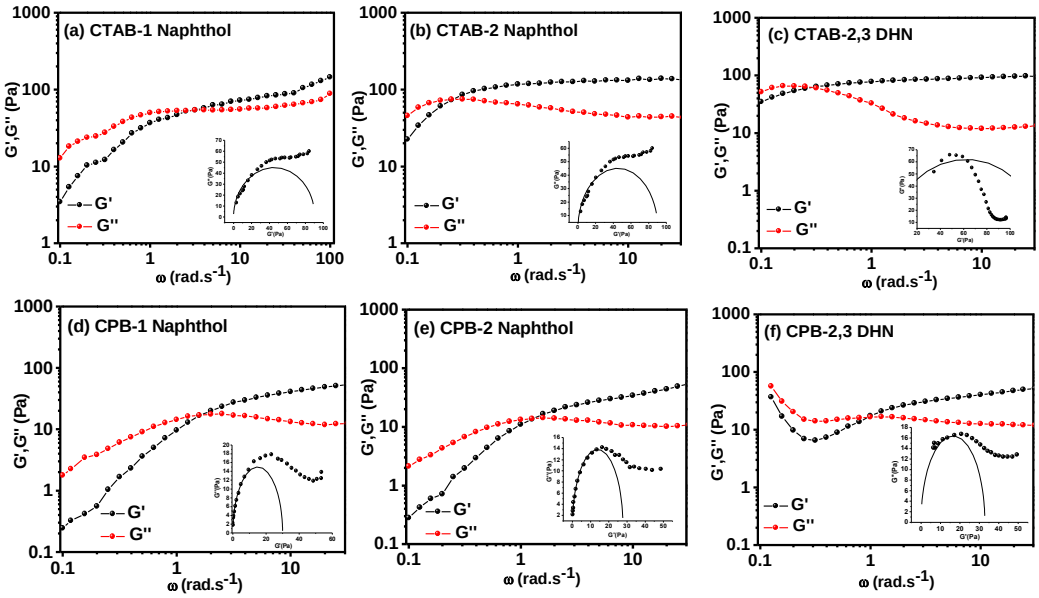

Figure 6. Dynamic viscosity profile of (a) 100 mM CTAB-100 mM 1 Naphthol, (b) 100 mM CTAB-100 mM 2 Naphthol, (c) 100 mM CTAB-100 mM 2,3 DHN, (d)100 mM CPB-100 mM 1 Naphthol, (e) 100 mM CPB-100 mM 2 Naphthol and (f) 100 mM CPB-100 mM 2,3 DHN at 328 K. Insets display the respective Cole-Cole plots.

A higher value of ω_c imply lower relaxation time, τ_R, as $\tau_R = {}^{1}/_{\omega_c}$.[34] The variation of τ_R as function of temperature (Figure 7) shows that the wormlike micellar systems composed of CTAB-additive (2 Naphthol and 2,3 DHN) relaxed relatively slower (or higher values of τ_R) compared to CPB-additive system (2 Naphthol and 2,3 DHN).

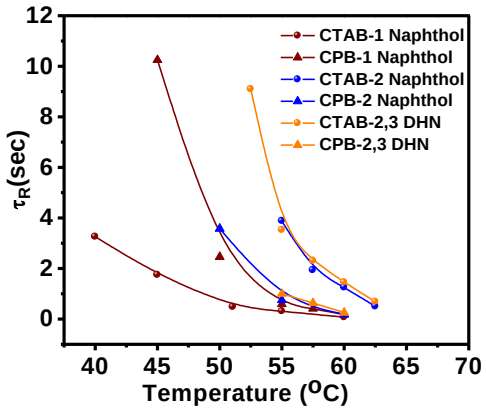

Figure 7. Variation of τ_R with temperature for different surfactant-additive systems.

The network mesh size of the entangled wormlike micelles is characterized by ξ the hydrodynamic correlation length. This length scale can be obtained directly from the plateau modulus G_0: [35]

$$\xi = (\frac{k_B.T}{G_0})^{1/3} \quad (17)$$

ξ is related to the persistence length,l_p, of the micelles and the entanglement length, l_e the average distance along the micelle between two entanglement points in the micellar network as:

$$l_e = \frac{\xi^{1/3}}{l_p^{2/3}} \quad (18)$$

The entanglement length can be determined from measurements of viscoelasticity using:[30]

$$\frac{G_0}{G''_{min}} = \frac{L_{avg,}}{l_e} \quad (19)$$

where $L_{avg,}$ is the average micelle length and G''_{min} is the local minimum of the G'' curve at frequencies above $1/\tau_R$. The ratio $L_{avg,}/l_e$ defines the average number of entanglements per micelle.

Table 3 summarizes the parameters obtained from rheological study of the surfactant-hydrotope systems. It is evident that in all the cases, $\tau_{br} << \tau_{Rep}$, which characterizes all the systems with a single relaxation time i.e., they exhibit Maxwellian behavior in the concerned temperature range.

Table 3 shows that the τ_{Rep} of CTAB-2 Naphthol system varies from ~284 sec to 0.38 sec in temperature range 313-333 K whereas that in case of CPB-2 Naphthol varies within ~976 sec to 3 sec within same temperature range. In the case of CTAB-2,3 DHN system, τ_{Rep} ranges from ~1486 sec to 100 sec for a temperature jump of 5K from 328 K to 333 K whereas under similar conditions, τ_{Rep} for CPB-2,3 DHN system ~47 sec to 3 sec. A higher value of τ_{Rep} is indicative of slower relaxation, which is associated with linearity of the micellear framework,[31] i.e., longer micelles are formed in CTAB-2 Naphthol/2,3 DHN systems compared to CPB-2 Naphthol/2,3 DHN systems while 1 Naphthol shows the preference to form longer micelles with CPB compared to CTAB as evident from the higher values of τ_{Rep} in case of CPB (Table 3). Flow activation energy, E_A, which describes the end-cap energy and the energy required for reversible micellar scission and is regarded as a measure of the "compactness" or "slowness" of the WLM flow has been evaluated as:

$$\tau_R = A.\exp(E_A/R.T) \quad (20)$$

or, $\log \tau_R = \log A + ({}^{E_A}/_{R.T})$ (21)

where A is the pre-exponential factor and is a constant, R is the universal gas constant taken as 8.314 J.mol^{-1}. K^{-1} and T is the temperature.

Table 3. Parameters G''_{min}, $\tau_R, \tau_b, \tau_{rep}, \xi$, L as obtained from rheological data for 100 mM CTAB and 100 mM CPB with 100 mM 1 Naphthol, 100 mM 2 Naphthol and 100 mM 2,3 DHN as additive at different temperatures.

Additive	Temp K	G''_{min} Pa	τ_R s	τ_b s	τ_{rep} s	ξ x 10^6 m	L nm
1 Naphthol				CTAB			
	313	14.18	3.34	0.04	279.32	1.93	340-637
	318	50.78	0.59	0.01	284.11	1.63	158-297
	323	60.33	2.92	0.08	1.44	1.62	138-259
	328	56.82	3.30	0.08	1.55	1.71	127-238
	333	85.28	4.17	0.01	0.38	1.61	102-192
				CPB			
	318	4.63	0.10	0.10	975.86	2.14	766-1437
	323	7.34	0.41	0.05	119.10	2.16	482-903
	328	8.26	1.62	0.02	24.08	2.17	428-804
	330.5	8.36	2.52	0.02	9.92	2.15	435-816
	333	10.84	5.62	0.01	3.24	2.01	421-790
2 Naphthol				CTAB			
	328	43.57	3.88	0.010	1486	1.47	354-664
	330.5	58.61	0.27	0.012	6.08	1.45	202-379
	333	18.63	1.26	0.015	100.3	1.46	637-1195
	335.5	39.76	0.52	0.013	20.9	1.53	259-486
				CPB			
	323	5.09	3.66	0.06	213	2.00	872-1635
	328	6.96	0.77	0.01	47.45	2.01	641-1203
	333	10.43	0.18	0.01	2.82	2.01	427-801
2,3 DHN				CTAB			
	325.5	8.05	9.34	0.13	693.20	1.83	725-1359
	328	11.97	3.48	0.09	121.75	1.66	657-1233
	330.5	13.56	2.29	0.06	82.42	1.63	623-1168
	333	17.70	1.45	0.03	66.71	1.62	487-913
	335.5	23.43	0.67	0.02	28.56	1.88	237-444
				CPB			
	328	12.36	1.05	0.05	22.21	2.02	353-662
	330.5	5.27	0.64	0.13	3.23	2.05	799-1498
	333	17.61	0.26	0.063	1.07	2.29	225-423

Arrhenius' semilog plot of τ_R v/s temperature shows a straight line (Figure 8) implying a single exponential decrease in relaxation time with temperature. This further characterizes the system as Maxwell fluid.[31,36]

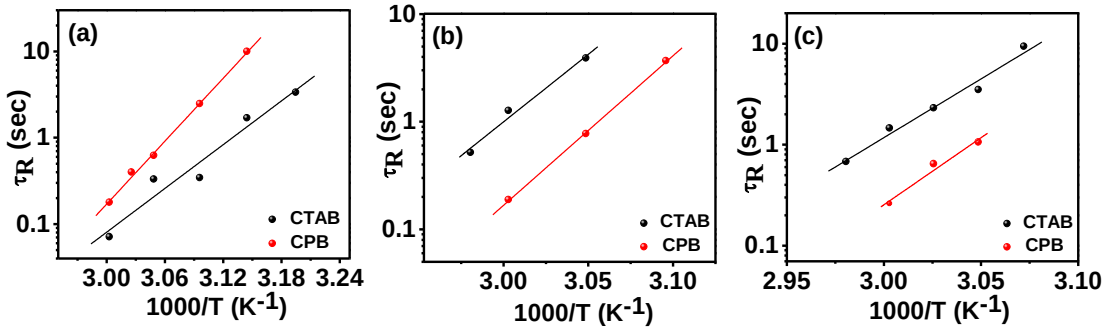

Figure 8. Arrhenius' Semi log plots of τ_R as function of inverse of temperature for 100 mM CTAB and 100 mM CPB in presence of (a) 100 mM 1 Naphthol, (b) 100 mM 2 Naphthol and (c) 100 mM 2,3 DHN for different surfactant systems (100mM ,1:1).

The flow activation energy for all the systems obtained following Equation 21, are summarized in Table 4.

Table 4. Flow Activation energies of different surfactant-additive systems obtained from Arrhenius' semi-log plots.

Flow Activation Energy, E_a (kJ.mole^{-1})			
Surfactant	1 Naphthol	2 Naphthol	2,3 DHN
CTAB	70.26	104.26	96.71
CPB	101.46	115.47	110.38

Results indicate that the wormlike micelles of CPB-additive systems possess a more flow activation energy compared to corresponding CTAB-additive systems implying that more compact micelles are formed in the former. Nevertheless, the study show that the architecture of surfactant head group can fine tune the molecular interaction and determine the specificity of additives towards forming wormlike micelles of desired length scale.

4.0. Conclusion

A synergistic interaction has been observed between the cationic surfactants (viz., CTAB and CPB) and the hydroxy aromatic compounds 1 Naphthol, 2 Naphthol and 2,3 DHN. As a result of reduction in electrostatic repulsion between the surfactant headgroups caused by the π-electrons of naphthalene additives, the cmc's of both

CTAB as well as CPB are lowered in presence of the aromatic compounds, nevertheless CPB displays a greater decrease in cmc compared to CTAB. 1H NMR and 2D NOESY study revealed that the hydroxynaphthalene derivatives intercalate deeper within the CTAB micelles while reside at the palisade layer of CPB micelles. Hydrogen bonding between the OH of the aromatic additives and the interfacial water molecules facilitate favorable orientation of the aromatic compounds to position within the surfactant micelles. 1 Naphthol most efficiently reduces the electrostatic repulsion between the surfactant head groups while 2,3 DHN is found to be least efficient in this respect. Furthermore, morphology transition of the surfactant aggregates from spherical to rod/ellipsoidal (at 25 mM surfactant:additive concentration) is also evident. At higher concentrations, (surfactant:additive >100 mM), the surfactant-additives systems formed thick viscoelastic gel consisting of long wormlike micelles (WLM). While 2 Naphthol and 2,3 DHN form longer micelles with CTAB, in the case of 1 Naphthol, longer micelles are formed with CPB. Moreover, WLM's of CPB are more compact than that of CTAB. This observed difference in rheological behavior probably originates from the difference in headgroup architecture of the surfactants. While strong cation-π interaction between the quaternary ammonium group of CTAB and the π electron cloud of the additives dominate the CTAB-additive systems, the CPB-additive are governed by the consequent π-π stacking between the aromatic pyridinium moiety and the naphthalene ring of the additives. Nevertheless, the study reveals high efficiency of the hydroxyaromatic compound viz., 1 Naphthol, 2 Naphthol and 2,3 DHN as effective triggering agents of morphology transition from spherical to wormlike micelles, under neutral salt-free conditions. The study also highlights the fact that WLM with fascinating rheological properties may be designed by tuning the headgroup architecture of surfactant and the nature of triggering agent under salt-free condition.

References are provided in BIBLIOGRAPHY under "References for Chapter III" (Page 170-172).

Chapter IV

Surface activity and modifying effects of 1 Naphthol, 2 Naphthol and 2,3 Dihydroxynaphthalene on self-assembled nanostructures of 1-Hexadecyl-3-methylimidazolium chloride

1. Introduction

Due to their unique chemical and physical properties and high tunability [1] ionic liquids (ILs) have drawn increasing interest as alternative media in a variety of catalytical, separation and electrochemical methods.[2] The transfer of a compound through an interface is a major part of the extraction process which is controlled by molecules adsorbed at the interface. The presence of surface active ionic liquid (SAIL) aggregates could modulate the efficiency of these processes including partial extraction of the product into micelles. Under certain conditions such as concentration, salinity, temperature, presence of counter ions, etc., the globular micelles may undergo uniaxial growth and form very long and highly flexible aggregates, referred to as ‘‘wormlike’’ or ‘‘threadlike’’ micelles.[3] Due to their cylindrical morphology and high flexibility, wormlike micelles (WLM) have emerged as a novel carrier system that provide larger core volume to load drugs and is, therefore, able to flow readily through capillaries and pores.[4] Since WLM’s have larger drug loading capacity and longer circulation time it may be highly useful and novel strategy for drug delivery to start as WLM’s and later degrade to spherical micelles, which are already known to be extremely useful for therapeutic applications.[5,6] Better prospect of controlled drug release warrants more insight on mechanism and kinetics of such degradability of wormlike micelles.

Study on micelle formation of the surface active ionic liquid, (SAIL) 1-Hexadecyl-3-methylimidazolium chloride, C_{16}-3-MeImCl and the cationic surfactant Cetylpyridinium chloride, C_{16}PyCl in the temperature range 15-75^{0}C, have shown that although aggregation of C_{16}PyCl should have been more favorable than C_{16}-3-MeImCl as C_{16}PyCl is more hydrophobic than the corresponding SAIL, this is not the case.[7] The strong hydrogen-bonding between the counter ion and the relatively acidic hydrogen of the imidazolium ring distinguishes imidazole-based SAILs from other conventional

cationic surfactants. Also, due to presence of asymmetric organic cations, the lattice energy of 1-alkyl-3-methyl-imidazolium [C*n*MIM] salts is reduced which result in low melting point ionic liquids, commonly called room temperature ionic liquid (RTIL) (melting point < 100^0C).[8] Literature shows that the coexistence of incompatible hydrophobic moieties such as fluorocarbon and hydrocarbon chains are a basic requirement but often not sufficient for the formation of the two distinct types of micelles i.e. spherical and WLM in aqueous solutions. On the other hand, synergistic micellization is observed when ionic surfactants are mixed with non-ionic or with oppositely charged surfactants. Both surface and bulk properties of these systems have been studied using different experimental techniques.[9,10,11] Strong synergistic gains in viscoelastic properties of mixtures of anionic and cationic surfactants compared to the parent surfactants have been reported. ILs (especially those with long hydrophobic chains) have been reported to show amphiphilic properties in aqueous solution.[12,13,14] Aromatic hydrotropes like salicylate, tosylate, chlorobenzoate, hydroxynaphthalene carboxylates and nitrobenzoate are reported to induce wormlike micelle formation in cationic surfactant solution. In particular, various hierarchically self-assembled structures such as tubes, ribbons, vesicles and lamellar structures can be fabricated in mixtures of surfactants and hydrotropes.[15] Synergistic effect of aromatic hydrotropes on the solution properties of ammonium gemini surfactants were reported.[16] Recently, highly temperature sensitive wormlike micelle-to-hydrogel and vice-versa transition in the ionic liquid 1-Hexadecyl-3-methylimidazolium chloride, triggered by the aromatic hydrotrope, Sodium salicylate (NaSal), have been reported.[17] It is evident from literature that interaction of aromatic hydrotropes with surfactant yield interesting properties of aggregates which are tunable via external stimuli like temperature, pH etc.[18] However, majority of the reports involve ionic medium and presence of salts, and there are very less reports regarding study of interaction of ionic liquids with non-ionic hydrotropes and on the use of additives in improving the micellization characteristics of ionic liquids. It has also been reported that hydroxy aromatic compound viz., 1 Naphthol and 2 Naphthol interact with the structurally reoriented water molecules on micellar surface of the cationic surfactant CTAB via hydrogen bond formation and induce viscoelasticity in CTAB solution.[19,20] It was observed that 1 Naphthol and 2 Naphthol showed surface active behavior.[20] The surface active property of the aromatic promoters leaves room for understanding of the molecular interactions between the aromatic hydrotropes/additives and the surfactant systems comprising of aromatic

extended conjugated systems especially because the hydroxy aromatic group as well as the imidazolium moiety, both form the fundamental skeleton of two non-essential amino acids viz. tyrosine and tryptophan respectively. Herein further investigation on the effect of the hydroxy aromatic compounds, viz., 1 Naphthol, 2 Naphthol and 2, 3-Dihydroxynaphthalene on the aggregation characteristics of the ionic liquid system namely, 1-Hexadecyl-3-methylimidazolium chloride (C_{16}-3-MeImCl) have been carried out. This ionic liquid has superior individual surface and bulk property compared to its ordinary surfactant analogues viz. Cetylpyridinium bromide (CPB) and CTAB. The pK_a of the additives are > 9.15 and therefore, in aqueous solution of ionic liquids (pH 6.5-7.5), these remain in protonated non-ionic form. In this chapter, the quantitative estimation of the surface parameters of the aromatic compounds: 1 Naphthol, 2 Naphthol and 2,3 Dihydroxynaphthalene has been done and their effect in modifying the aggregation characteristics of the ionic liquid C_{16}-3-MeImCl under salt-free condition has been studied. An interesting aspect of these additives, is their fluorescent nature; which enables them to be used as self-probes. Modification of their spectral properties in presence of the ionic liquid may provide insight of the probe-ionic liquid interaction at the micro-structural level. Interactions in micro-environment of the additives are explored spectroscopically (UV-Visible Spectroscopy, Fluorescence anisotropy and ^{1}H-NMR) and the effect of the additives on aggregate morphology of the ionic liquid micelle are explored. For more specific insight about the binding interactions of the individual additives with the ionic liquid, molecular dynamics calculations using DFT are carried out. Effect of metal salts on viscosity of the SAIL-Additive system have been investigated.

2. Materials and Methods

2.1. Materials

1-Hexadecyl-3-methylimidazolium chloride, was purchased from Across chemicals (USA) and was used as received. 1 and 2 Naphthols (Fluka, Germany) and 2,3-Dihydroxynaphthalene (Fluka, Germany) were further purified by vacuum sublimation followed by crystallization from 1:1 aqueous methanol. Methanol was distilled prior to use. Double distilled water (conductance below 2 μS/cm, pH ~ 6.5-7) was used for all experimental purposes. D_2O was purchased from Aldrich, USA (Purity >99.9%). All conductometric measurements were carried out on Metler Toledo Digital Conductivity

bridge (MC226) using a dip cell with cell constant 1.0 cm^{-1}. Tensiometric studies were done with Krüss GmbH K9 tensiometer following the ring detachment method. Constant temperature was maintained during the experiments with Remi ultra thermostat (CB-700) with precision (± 0.1K).

2.2. Methods

2.2.1. Tensiometry. Tensiometric measurements were performed on Krùss K9 Tensiometer (Germany), based on Du-Nóuy ring detachment method, fitted with Omniiset temperature bath with precision ± 0.1^0C. Before each measurement, the platinum ring was thoroughly cleaned with 1:1 acetone-water solution and heated under oxidizing flame until glowing temperature was attained. After every addition, the experimental solution was stirred for 5 minutes for homogeneity and equilibrated for 10 minutes. For each measurement, three to five subsequent readings were taken for concordance. Standard deviation was < 0.1 $mN.m^{-1}$.

2.2.2. Specific conductivity measurements. The specific conductivity measurements were carried out in Metler Toledo Digital Conductivity bridge (MC226) (accuracy 0.1%) using a dip-type immersion cell with cell constant 1.0 (±0.05) cm^{-1}. 5 min equilibrium time was allotted before each reading. Constant temperature was maintained during the experiments with Remi ultra-thermostat (CB-700) with precision ± 0.1K. The uncertainty of the measurements was ±0.01μS.cm^{-1}.

2.2.3. pH measurements. The pH's of the solutions were measured using Systronics digital pH meter (Model: 335, India), calibrated with standard buffers of pH 4.0 and 9.2. Solutions were equilibrated for 5 min after addition of acid/alkali till a steady pH meter reading was observed.

2.2.4. Fluorescence anisotropy. Steady state fluorescence anisotropy study was carried out in bench top spectrofluorimeter from Photon technologies International (Quantamaster-40) with excitation and emission slit widths fixed at 0.3 nm and 2.0 nm respectively. Steady state anisotropy (r) was determined using the following expressions:[21]

$$r = \frac{I_{VV} - G.I_{VH}}{I_{VV} + 2G.I_{VH}} \text{ and } G = \frac{I_{HH}}{I_{VH}} \quad (1)$$

where I_{VV} and I_{VH} represent the intensities obtained with the excitation polarizer oriented vertically and the emission polarizer oriented vertically and horizontally respectively; I_{HV} and I_{HH} refer to the similar parameters as mentioned above for the horizontal positions of the excitation polarizer.

2.2.5. ^{1}H-NMR. ^{1}H-NMR experiments were performed in Bruker ADVANCE spectrometer operating at 300 MHz frequency at 298 K. Signals are quoted as δ values in ppm using residual protonated solvent signals as internal standard (D_2O: δ 4.79 ppm). Data are reported as chemical shift.

2.2.6. Rheology. The rheological experiments were done using cone-plate geometry with 4^0 truncation angle, with diameter 25 mm and 0.105 mm sample gap in MCR 302 (Anton Paar) equipped with Peltier temperature control system.

Sample Preparation

Since Naphthol(s) and its derivative 2,3-Dihydroxynaphthalene are only sparingly soluble in water, a methanolic solution of higher concentration was initially made. Experimental solutions were prepared routinely by transferring the required volume of solution (in pure methanol) in the experiment vial first, and then the alcohol was evaporated off completely before the addition of aqueous surfactant solution.[20] For rheometry, surfactant was added to the dried additive followed by requisite volume of solvent. Sample concentration for all the systems was 100 mM with 1:1 surfactant: additive mole ratio i.e. concentration of each of the components was 100 mM. The mixture was then stirred at 60^0C for three hours for homogenization and equilibrated for 36 hrs. During measurement, samples were equilibrated for 10 mins at each temperature.[22] For NMR study, respective solutions were made in D_2O and 0.6 mL of the same was used for each measurement.

3. Results and Discussion

3.1. Surface active properties of π-conjugated additives

The variation of surface tension of aqueous solution of the hydroxy aromatic compounds 1 Naphthol, 2 Naphthol and 2,3 Dihydroxynaphthalene (2,3 DHN) is obtained from tensiometric study. It is evident from Figure 1 that the surface tension of water decreases linearly as a function of concentration of 1 Naphthol, 2 Naphthol or 2,3 DHN and reaches a limiting value above critical aggregation concentration (cac)

in each case. The equilibrium surface tension of the additive solutions is 12-15 $mN.m^{-1}$ lower than pure water's which confirms their surface activity. The cac for 1 Naphthol, 2 Naphthol and 2,3 DHN is found to be 4.66 mM, 3.62 mM and 3.06 mM respectively at 303 K.

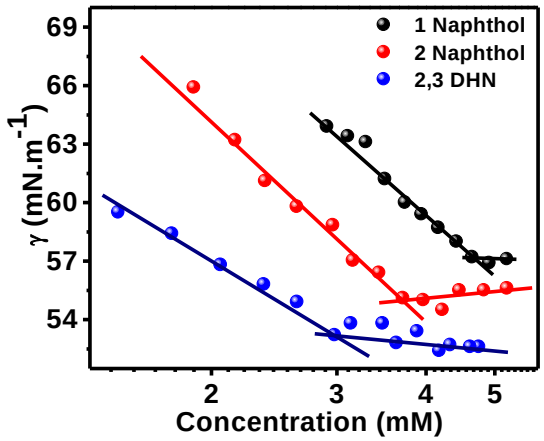

Figure 1. Tensiometric profile of additives (1 Naphthol, 2 Naphthol and 2,3 DHN) in log scale at 303 K.

Table 1 lists the cac values along with the surface tension at cac (γ_{CAC}), the maximum surface excess concentration (Γ_{max}) and the minimum surface area per organic molecule (A_{min}). (Mathematical background of evaluation of surface parameters is provided under section 1.1 of Appendix A).

Table 1. Interfacial parameters of 1 Naphthol, 2 Naphthol and 2,3 DHN in aqueous medium at 303 K

Additive	cac (mM)	$10^3\Pi_{cac}$ ($mN.m^{-1}$)	$10^6\Gamma_{max}$ ($mol.m^{-2}$)	A_{min} ($nm^2.molecule^{-1}$)
1 Naphthol	4.66	17.2	5.64	0.29
2 Naphthol	3.62	19.2	5.93	0.28
2,3 DHN	3.06	21.1	3.02	0.55

Both cac and γ_{cac} values decrease slightly in the order 1 Naphthol > 2 Naphthol > 2,3 DHN, which indicates stronger surface activity and wetting ability at the surface in the opposite order (Table 1). The minimum surface area per molecule (A_{min}) marks the effectiveness of a compound to populate the air-water interface. Higher the value of A_{min}, greater is the tendency to "wet" the surface. A_{min} for 2,3 DHN is found to be 0.55 $nm^2.molecule^{-1}$, almost twice that of 1 and 2 Naphthols, which are almost identical i.e. 0.28 and 0.29 nm^2 $molecule^{-1}$ respectively. The γ_{cac} for 1 Naphthol, 2 Naphthol and 2,3

DHN are respectively 57.02, 55.37 and 52.85 $mM.m^{-1}$. The values indicate in case of 2,3 DHN, the surface activity is the highest while that for 1 Naphthol it is lowest. The maximum surface excess (Γ_{max}) denotes the number of surface active molecules present at the interface in excess of the bulk. Γ_{max} for 2,3 DHN is 3.02 $mol.m^{-2}$ while that of 1 and 2 Naphthol are 5.64 and 5.93 $mol.m^{-2}$ respectively i.e. approximately half the number of dihydroxynaphthalene populate the surface compared to mono hydroxy analogue. This suggests that the 2,3 DHN molecules are arranged in staggered or oblique manner at the water/air interface whereas the 1 and 2 Naphthols may possibly be arranged more or less perpendicularly. While lesser number of 2,3 DHN molecules populate the surface compared to that of Naphthols due to their oblique arrangements, the surface activity vis-a-vis hydrophobic force operating at the surface becomes higher leading to lowering of γ_{cac} value.

3.2. Synergistic improvement of surface and bulk properties of C_{16}-3-MeImCl in presence of Naphthols

The effects of π- conjugated hydroxy aromatic additives 1 Naphthol, 2 Naphthol and 2,3 DHN on the critical micelle concentration, (cmc) of the cationic ionic liquid 1-Hexadecyl-3-methylimidazolium chloride (C_{16}-3-MeImCl) are studied, both by conductivity and surface tension measurements (Figure S1(a) of Appendix A). The cmc of C_{16}-3-MeImCl (0.89 mM) is in agreement with the reported value.[7] The cmc of C_{16}-3-MeImCl decreases significantly as a function of additive (the hydroxy aromatic compounds) concentrations and the systems display strong synergism in their aggregation behavior. The maximum drop in cmc is observed from 0.89 mM to 0.45 mM, 0.52 mM and 0.65 mM in presence of 1 Naphthol, 2 Naphthol and 2,3 DHN respectively inspite of much higher cac of these additives (Figure S1(a) of Appendix A). The observation demonstrates a fairly strong interaction between the additives and the SAIL micelles. From figure S1(b) of Appendix A, it is seen that the CMC decrease with increasing mole fraction of additives up to $\alpha_{Additive}$= 0.5, and increases thereafter. It seems apparent that hydrophobicity of the aromatic ring of the additives is involved in strong interaction with the hydrocarbon tail of SAIL in the micelle. All these additives have similar aromatic architecture for which their effectiveness in reducing the cmc is found to be nearly identical. Earlier, Bergstrom and Eriksson have shown by theoretical calculation based on the theory of regular solution mixtures, that for mixed systems consisting of monovalent ionic surfactant and a non-ionic surfactant, the cmc

vs. composition curve exhibits a skew with maximum shallow at α=0.5 i.e. at equimolar composition, at total surfactant concentration below 0.2 M, wherein the reduced charge density, $S_r >> 1$. S_r dominates the electrostatic free energy per unit charge of the system which arises out of the interaction of additive and surfactant with solvent molecules and amongst themselves.[23] Interestingly, similar nature of curves are obtained in the present mixed systems comprising of C_{16}-3-MeImCl and hydroxy aromatic compounds. It may be argued that the π-conjugated additives, in this case, behave as cosurfactant to lower the cmc of the present systems.

3.3. Interaction Parameters

To quantitatively investigate the interaction between the surface active components viz. 1 Naphthol, 2 Naphthol and 2,3 DHN with the SAIL, C_{16}-3-MeImCl, the interaction parameter (β) and activity coefficients of the respective components in the micellar region is evaluated based on Rubingh's Regular solution theory (RST).[24] The central assumption of RST is that excess entropy of mixing is zero and that the departure from ideal mixing is described by the single interaction parameter, β, which account for the enthalpy of mixing. β, reflects the interaction between the head groups of the surfactant and the additives involved. More negative value of β indicates stronger interaction between the surfactant and the surface active components[25] (Mathematical background of Regular Solution approach is provided under section 1.2 of Appendix A). For components which are non-aggregating in nature, their solubility limit can be taken as the phase-separation point and the regular solution theory can be extended onto them.[26] In cases where the additive is highly water soluble yet non-aggregating in nature the high value of solubility incur a high value of x_1, which predicts an unusually high value of interaction parameter.[27] In the present systems, however, quantitative analysis of the mixture in the usual framework of RST is valid because of the surface active nature of the additives and the observed well defined cac values for each of them. The interaction parameters and activity coefficients of components at different additive mole fraction are, therefore, determined following equation 5 of SI and summarized in Table 2. It is seen that in all the cases, β have negative values at all additive mole fractions ($-2.9 > \beta > -5.7$). While for 1 Naphthol, β increases from -3.45 to -5.73 at mole fraction 0.1 to 0.7; in 2 Naphthol and 2,3 DHN, β reaches minima (highest negative) near a composition~$\alpha_{additive} = 0.5$ there after it decreases (Table 2). This implies that interaction of 1 Naphthol with the micelles of the SAIL is favored with increasing additive

concentration whereas in case of 2 Naphthol and 2,3 DHN, the synergism is highest near equimolar composition of the components.

Table 2. Interaction parameter (β), activity coefficients (f_1 and f_2) of C_{16}-3-MeImCl with 1 Naphthol, 2 Naphthol and 2,3 DHN at 303 K

$\alpha_{Additive}$	1 Naphthol			2 Naphthol			2,3 DHN		
	β_m	f_1	f_2	β_m	f_1	f_2	β_m	f_1	f_2
0.3	-3.45	0.171	0.185	-2.95	0.221	0.236	-2.87	0.222	0.025
0.4	-4.08	0.099	0.168	-3.41	0.139	0.235	-3.21	0.156	0.257
0.5	-5.40	0.033	0.134	-4.23	0.071	0.207	-3.76	0.089	0.258
0.6	-5.44	0.027	0.161	-3.63	0.089	0.295	-3.48	0.095	0.322
0.7	-5.73	0.018	0.176	-3.84	0.065	0.326	-3.69	0.070	0.355

The activity coefficients of the surfactant and the additives are less than unity (Table 2) for all additive compositions, which indicates the deviation from ideal behavior. The behavior seems at par with their ability to lower the cmc of the SAIL. 1 Naphthol is found to lower the cmc to a higher extent compared to 2 Naphthol and 2,3 DHN. This further confirms the strong synergism between the additives and the SAIL micelles.

3.4. Mode of Interaction: Absorption spectroscopy and fluorescence anisotropy study

UV Absorption spectroscopy

To explore the interactions at the molecular level, responsible for the synergism, spectral modifications of the additives viz. 1 Naphthol, 2 Naphthol and 2,3 DHN are studied as a function of SAIL micelle concentration (Figure 2 (a-c)).

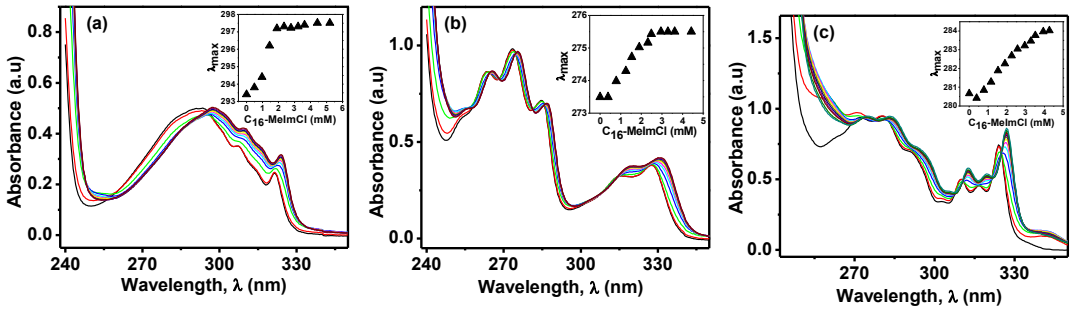

Figure 2 (a) Absorption spectra of 1 Naphthol (0.5 mM) in water at varying concentrations of C_{16}-3-MeImCl at 298 K. [C_{16}-3-MeImCl] : (1) 0.0 (2) 0.49 (3) 0.97 (4) 1.44 (5) 1.90 (6) 2.35 (7) 2.79 (8) 3.22 (9) 3.63 (10) 4.43 (11) 5.21 mM; (b) Absorption spectra of 2 Naphthol (0.5 mM) in water at varying concentrations of C_{16}-3-MeImCl at

25^0C. [C_{16}-3-MeImCl] : (1) 0.0 (2) 0.39 (3) 0.78 (4) 1.16 (5) 1.53 (6) 1.90 (7) 2.26 (8) 2.61 (9) 2.95 (10) 3.29 (11) 3.62 mM; (c) Absorption spectra of 2,3 DHN (0.5 mM) in water at varying concentrations of C_{16}-3-MeImCl at 25^0C. [C_{16}-3-MeImCl] : (1) 0.00 (2) 0.39 (3) 0.78 (4) 1.16 (5) 1.53 (6) 1.90 (7) 2.26 (8) 2.61 (9) 2.95 (10) 3.29 (11) 3.62 (12) 3.94 (13) 4.27 mM.

Aromatic moiety like naphthalene (and its derivatives) has two strongly overlapped bands in the UV-Vis region viz., longitudinally polarized $^1L_a \leftarrow {}^1A$ and transversely polarized, $^1L_b \leftarrow {}^1A$ band.[28] Thus conjugation extended to OH group in transverse direction in 1 Naphthol and that in longitudinal direction in case of 2 Naphthol and 2,3 DHN ought to affect the ^1L_a and ^1L_b bands respectively.[20] Significant red shift in the λ_{max} for all the three additive systems (shown in inset) (Figure 2 (a-c)) is observed in presence of SAIL micelles. The isobestic points indicate equilibria to exist between micelle bound and free additive (probe) molecules (Figure S2 of Appendix A). The red shifts are respectively 4.6 nm for 1 Naphthol with λ_{max} at 293.1 nm, 2.3 nm for 2 Naphthol with λ_{max} at 273nm and 3 nm for 2,3 DHN with λ_{max} at 324nm. This significant red shift in near UV absorbance's in the additives, which arises out of two strongly overlapped π-π^* transitions indicates a lesser π-π^* separation (Figure 2) on addition of SAIL in the post-micellar region (above 1.44 mM in 1 Naphthol, 1.16 mM for 2 Naphthol and 2,3 DHN). Such shift continues to occur till most of the probe molecules are partitioned within the micellar phase at high SAIL-Additive ratio (90:1). The role of Hydrogen bonding in such modification of spectral property is noteworthy. The OH group of the naphthols can act both as proton donor or acceptor in forming intermolecular hydrogen bonds. During hydrogen bond formation of hydroxy group, in which OH act as donor, electron density on the oxygen increases, which is further induced towards the aromatic ring decreasing the π-π^* separation resulting in the observed red shift in the absorption spectra.[20] The results suggest that the considerably polar hydroxyl group of the micelle-embedded additive molecules, protrude out of the micellar interface and engage in hydrogen bond with interfacially located water molecules thereby acting at hydrogen donor. Significant values of binding constants are also observed for C_{16}-3-MeImCl micelles-Additive systems. (Figure S2 of Appendix A). The hydrogen bonds steer the rigidity of re-oriented water structures, and force the additives to position firmly in between the surfactant head-groups thereby screening their positive charge.

Fluorescence anisotropy

Fluorescence anisotropy is an important tool to monitor the changes in microenvironment of the probe in cases involving the structural transition of fluorophores.[29] Since the lifetimes of fluorescence emissions are of similar order as the rate of tumbling of molecules in solution, physical processes like rotational diffusion lead to depolarization of fluorescence and this is a function of solution viscosity and the size and shape of the molecule. 1 Naphthol, 2 Naphthol and 2,3 DHN are already known to be very effective fluorophores[28,30,31] and therefore study of fluorescence anisotropy, would be interesting, in order to understand the microscopic changes in the environment comprising of the SAIL micelles. To ensure complete insertion of the probe molecules within the micelles, the surfactant concentration is varied from 4.7 mM to 100 mM, (much above the cmc of the SAIL) and the concentration of the self-probes viz. 1 Naphthol, 2 Naphthol and 2,3 DHN are fixed at 0.4mM. The excitation wavelength for 1 Naphthol, 2 Naphthol and 2,3 DHN are respectively 323 nm, 324nm and 326 nm while emission for the same are obtained at 465 nm, 478 nm and 351 nm respectively. 1 Naphthol (pK_a 9.34) undergo ultrafast deprotonation in aqueous media due to which the emission intensity of its neutral form (λ = 360 nm) is extremely low.[31] Therefore, anisotropic studies are done considering the anion emission of 1 Naphthol at 465 nm. For similar reason, the most intense peak at 409 nm is considered for 2 Naphthol (pK_a 9.51) whereas that for 2,3 DHN (pK_a 9.10) the single emission band with λ_{max} at 340 nm is considered. The initial anisotropy of the probes in pure aqueous medium is found to be very low and it increases with increase in the SAIL concentration and attains limiting value (Figure 3) (for 2 Naphthol and 2,3 DHN).

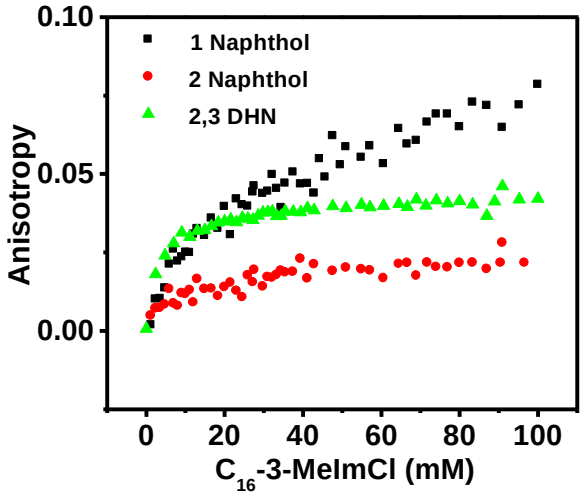

Figure 3. Steady state fluorescence anisotropy of 0.4 mM 1 Naphthol, 2 Naphthol and 2,3 DHN as function of C_{16}-3-MeImCl concentration at 298K.

The increase in anisotropy values reflects an impended rotational diffusion of the fluorophores under high micro viscous environment.[32] Anisotropy-concentration profiles show different degree of polarization for different fluorophores in the SAIL micelles (Figure 3). Anisotropy is highest for 1 Naphthol, it does not exhibit the plateau, while 2 Naphthol and 2,3 DHN reach plateau in anisotropy-concentration profile at high SAIL concentrations. Under the condition, when the probe are encapsulated within the micellar core, no further change in its rotational dynamics is entailed, resulting in near constancy of the anisotropy values. Such situation prevails for 2 Naphthol and 2,3 DHN at SAIL concentration of 20 mM onward, while in case of 1 Naphthol, micellar encapsulation seems to be less favorable and increases with SAIL concentration upto 100 mM i.e. location of the probe in 1 Naphthol, registered stronger hindrance to rotational freedom. However, the scattering of data-points for 2 Naphthol and 2,3 DHN in the anisotropy-concentration profile indicates that unlike 1 Naphthol, the anisotropy of the above probes are not the sole function of encapsulation in the micelles vis-à-vis concentration of SAILs only.

3.5. Improvement in viscous properties of C_{16}-3-MeImCl-Naphthol(s) systems at enhanced concentration.

Upon increasing the concentration of the 1:1 C_{16}-3-MeImCl-Naphthol(s) systems to 100 mM, significant changes in physical properties are observed. The mixture becomes highly viscous and shows recoiling of entrapped air bubbles. Upon equilibrating the

SAIL-Additive mixtures for 24hrs, transparent gel is formed. The gels show arrested flow even after holding upside-down (Figure 4).

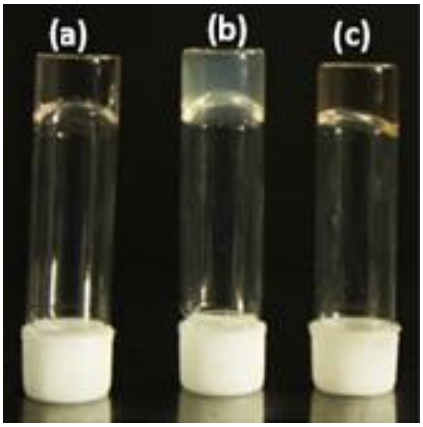

Figure 4. Macroscopic appearance of viscoelastic gels of 100 mM 1:1 solutions of C_{16}-3-MeImCl and (a) 1 Naphthol, (b) 2 Naphthol and (c) 2,3 DHN at 298 K.

The appearance of viscoelasticity suggests the presence of entangled wormlike micelles in the systems.[32,33] In order to understand the changes in physical characteristics, rheological study of the SAIL-Additive gels are carried out. The response of elastic and loss modulus as a function of angular frequency shows that the systems behave like typical viscoelastic fluid with loss modulus (G″) predominating at lower frequencies and elastic or storage modulus (G´) predominating at higher frequencies.[16] A representative plot is shown in Figure 5.

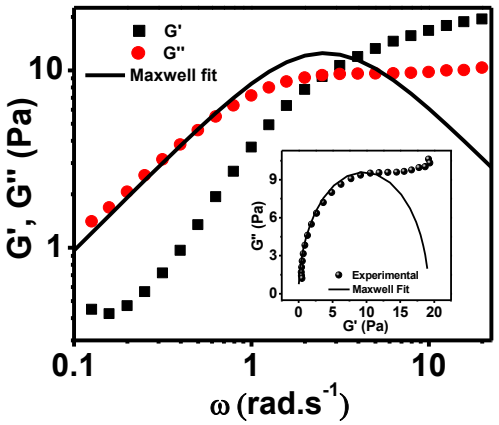

Figure 5. Representative profile of dynamic rheology of C_{16}-3-MeImCl-1 Naphthol system (1:1, 100 mM) as function of angular frequency at 328 K.

Upon increase in temperature, the crossover frequency increases (ω_c) i.e. the frequency at which G´ and G″ intersect (Figure S3 (a-c) of Appendix A). The inverse of ω_c gives the relaxation time (τ_R) which is the time required by the system to regain its equilibrium structure after an external stress is applied. With increase in temperature,

τ_R decreases, implying that the systems adopt faster routes of stress- relaxation. The trend in relaxation time, show that SAIL-Additive composed of 2,3 DHN relaxes much slower followed by 1 Naphthol and 2 Naphthol respectively (Figure S4 of Appendix A).[34] The dynamics of the viscoelastic micellar systems have been most successfully described by Cate's "living polymer model" which is the combination of the reptation model of polymer dynamics and the effect of reversible scission on viscoelastic properties.[35,36,37] According to this model the relaxation of the viscoelastic micelles involves two time scales viz. reptation time (τ_{rep}) corresponding to curvilinear diffusion of a wormlike micellar chain along its own contour and breaking time (τ_b) which is the result of micellar chain scission. When $\tau_b << \tau_{rep}$, there occurs many breakages and recombination before the chain segment relaxes by reptation. The system is then defined by a single stress relaxation time:

$$\tau_R = (\tau_{rep}.\tau_b)^{1/2} \quad (2)$$

and is characterized as a Maxwell Fluid.

For a fluid with near-Maxwell character, the elastic (or storage modulus), G′ and viscous (or loss modulus), G″ are related to angular frequency, ω as:[36]

$$G'(\omega) = G_0\omega^2\tau_R^2/(1+\omega^2\tau_R^2) \quad (3)$$

$$G''(\omega) = G_0\omega\tau_R/(1+\omega^2\tau_R^2) \quad (4)$$

where G_0 is the storage modulus at high frequency, where it exhibits a plateau, also called the plateau modulus. It is proportional to the number density of the entanglement points and hence characterizes the network structure.[37] (More details provided under Section 3.1 of Appendix A) The oscillatory flow spectra of all the SAIL-Additive systems could be fitted to the theoretical curve obtained on basis of Maxwell's model (Figure 5). The semi-circular nature of Cole-Cole plot further proves that the system behaves as Maxwell fluid (Figure 5 inset). Deviation of G″ from Maxwell model at higher ω indicates that the wormlike micelles are in dynamic equilibrium and the process of breaking and recombination takes place rapidly.[38] At this condition, the system adopts faster relaxation time given by Rouse or breathing modes. The characteristic parameters of the wormlike micellar network viz. the hydrodynamic correlation length, ξ, which is a measure of the network mesh size of the entangled

micelles; the persistence length, l_p ; entanglement length, l_e and average micellar length , L are related as:

$$\xi = ({}^{k_B.T}/_{G_0})^{1/3} \quad (5)$$

$$l_e = {}^{\xi^{\frac{5}{3}}}\Big/_{l_p{}^{\frac{2}{3}}} \quad (6)$$

$$\frac{G_0}{G''_{min}} = \frac{L}{l_e} \quad (7)$$

where, k_B is Boltzman constant , T is the temperature, G''_{min} is the local minimum observed in G'' curve at frequency above ω_c.

Assuming near Maxwell behavior for the systems[39] the micellar characteristics of the C_{16}-3-MeImCl-Additive (1:1, 100 mM) systems have been evaluated using the above relations and are presented in Table 3.

Table 3. Parameters G''_{min}, $\tau_R, \tau_b, \tau_{rep}, \xi$, L as obtained from rheological data for C_{16}-3-MeImCl with 1-Naphol, 2 Naphthol and 2,3 DHN as additive at different temperatures.

Temp K	G''_{min} Pa	τ_R s	τ_b s	τ_{rep} s	ξ x 10^6 m	L nm
			1 Naphthol			
318	11.5	4.22	0.16	111.03	2.13	315-473
323	8.46	1.79	0.12	26.67	2.68	217-408
328	10.02	0.38	0.10	1.49	2.82	160-300
333	20.97	0.07	0.02	0.34	2.65	212-397
			2 Naphthol			
318	4.63	4.39	0.395	48.87	3.23	225-422
323	11.74	0.83	0.079	8.67	2.91	123-230
328	24.90	0.28	0.040	1.97	2.98	202-379
330.5	5.71	0.19	0.063	0.60	3.05	224-42
333	1.46	2.01	1.010	3.99	3.49	590-1107
			2,3 DHN			
323	12.46	8.03	0.049	1316.6	1.91	413-774
325.5	15.87	3.35	0.039	285.08	2.01	278-522
328	18.84	2.87	0.040	205.82	2.04	170-319
330.5	20.55	0.76	0.015	37.08	1.91	255-478
333	11.08	0.51	0.099	2.65	2.81	149-280

From the values of τ_b and τ_{rep}, it is clear that $\tau_b \ll \tau_{rep}$, which further testifies the presence of single relaxation mode and hence wormlike micelles, in the systems. The reptation time, in case of C_{16}-3-MeImCl-2,3 DHN system is much higher, varying within 1316.6-2.65 s (approx. 10 order higher) compared to C_{16}-3-MeImCl-1 Naphthol (τ_{rep}=111.03-0.34 s) and C_{16}-3-MeImCl-2 Naphthol (τ_{rep} = 48.87-3.99 s) with temperature (Table 3). Higher the time, slower is the process adopted by the system in order to relax. Results show that the system comprised of C_{16}-3-MeImCl-2,3 DHN undergoes slowest reptation. Slow relaxation is also associated with linearity of the micelles.[35] It can be said that C_{16}-3-MeImCl-2,3 DHN form longer micelles than C_{16}-3-MeImCl-1 Naphthol and C_{16}-3-MeImCl-2 Naphthol systems. From the severe drop in τ_{rep} with temperature in all the C_{16}-3-MeImCl-Additive systems, (Table 3) it is clear that temperature has profound effect on the relaxation mode of the systems. In order to understand the temperature dependence of the wormlike micellar characteristics, oscillatory flow measurements as functions of various forms of stress at different temperatures are studied.The shear dependent flow-curves are extrapolated to zero shear rate to obtain the zero shear viscosity (Figure S5 (a-c) of Appendix A). The samples exhibit a constant viscosity below a critical shear rate above which shear thinning is observed, which corresponds to the non-Newtonian flow behavior typical to wormlike micelle.[37] The critical shear rate, $\gamma_{c,}$ shifts to lower values on increasing the temperature with corresponding increase in zero shear viscosity (η_0). η_0 become maximum at particular temperature specific to the additives (Figure S5 (a-c) of Appendix A). With further increase in temperature, η_0 decreases and the Newtonian region shifts forward i.e. $\gamma_{c,}$ increased.

The molecular origin of the observed changes in viscoelastic behavior is the change in topology of the SAIL aggregates and shape of its micelles due to the presence of the hydroxy aromatic additives. The packing parameter,[26] P for spherical micelles < $^1/_3$ while that for elongated micelles is $^1/_3$ <P<$^1/_2$. P is a dimensionless fundamental parameter, which determines the shape of molecular aggregates. (Details provided under Section 3.2 of Appendix A) At higher concentrations of the SAIL micelles and additives (100 mM, 1:1) the inter-micellar interaction between the components increases to a great extent. Since the local H-bonding network of water at the charged micellar interface differ much from that in the bulk, these water molecules are much

less polar (dielectric constant ~ 30) with restricted mobility.[20] The aromatic ring of the Naphthols and 2,3 DHN embed in between the imidazolium head group of the SAIL micelles and impart strong screening effect on the electrostatic charges of the micellar head groups which reduces the electrostatic double layer around the micelle. The strong hydrogen bonding with the OH group of the naphthol(s) and its derivatives with the interfacial water optimally orients the aromatic π-system of 1 Naphthol, 2 Naphthol and 2,3 DHN perpendicularly for stronger screening of the electrostatic repulsion between the imidazolium headgroups via cation-π interaction.[40] This addition of Naphthol(s)-2,3 DHN into the micelles apparently decreases the effective area of the head groups causing an increase in A_0 and lowers the packing parameter. Thus, the globular micelles flip into cylindrical micelles with lower spontaneous curvature.[41] The WLM's are eventually formed because small cylindrical rods are thermodynamically unstable in aqueous media since their end-cap energy is higher compared to that of the body of the rods. Presence of the long WLM's on entanglement, impart the observed viscoelasticity in the medium. With rise in temperature, the tendency of the additives to get solubilized within the palisade layer of the SAIL micelles increases which further lowers the interfacial curvature of the molecular assembly. This leads to the formation of longer worms with corresponding increase in viscosity (Figure S6 of Appendix A).[42,43,44]

When a linear micelle breaks the energy penalty is compensated by formation of two new end caps. The increased curvature of an end cap which spreads the head groups apart is favored over the concave curvature of a branch point which drives the charged head groups of the surfactants closer together, resulting in formation of branches. The gain in entropy, with temperature, in the branch points is greater than in the end caps, which enables faster and easier route to stress relaxation by sliding of the branches alongside the cylindrical body of the wormlike micelles.[32] These branch points restrict the alignment of micelles when under shear and cause an increase in the critical shear rate while lowering the zero shear viscosity above the critical temperature. The observed critical temperature for the C_{16}-3-MeImCl-Additive systems are: 308 K for 1 Naphthol with η_0 674 Pa.s, 313 K for 2 Naphthol with η_0 211 Pa.s and 318 K for 2,3 DHN with η_0 1819 Pa.s. Tendency of 2,3 DHN to embed within the micellar core is, therefore, higher compared to 1 and 2 Naphthol, which subsequently lead to corresponding highest increase in zero shear viscosity with temperature (Figure S6 of Appendix A).

The flow activation energy, (E_A) describes the end-cap energy required for reversible micellar scission and also, a measure of compactness of the WLM and is related to τ_R and temperature as:[35]

$$\tau_R = A.\exp(^{E_A}/_{R.T}) \quad (8)$$

$$\text{or, } \log \tau_R = \log A + (^{E_A}/_{R.T}) \quad (9)$$

where A is the pre-exponential factor and is a constant, R is the universal gas constant taken as 8.314 J.mol^{-1}. K^{-1} and T is the temperature. E_A is found to be 241.13, 218.20 and 249.61 kJ.mol^{-1} for SAIL WLM in presence of 1 Naphthol, 2 Naphthol and 2,3 DHN respectively (Figure S7 of Appendix A). Above trend of E_A implies that the most compact assembly occurs in case of 2,3 DHN, which causes the "slowest" movement of the worms.

3.6. ^{1}H NMR study: The location of residence of the additive within SAIL micelles

Proton NMR (^{1}H NMR) spectroscopy is an important tool for identifying the time-averaged location of aromatic solubilized species within the surfactant micelles, based on the dependence of chemical shifts of protons in surfactant and aromatic units on the composition of the aqueous phase.[45] The present study is aimed to investigate the effect of addition of the naphthol additives on the protonic environment of C_{16}-3-MeImCl micelles. Figure 6(a) shows the ^{1}H NMR spectra of 10 mM C_{16}-3-MeImCl in D_2O. The concentration is much above the critical micellar concentration of C_{16}-3-MeImCl (0.89 mM), therefore it is assumed that the system consists of micelles of the ionic liquid. The spectra of C_{16}-3-MeImCl is similar to that of 10 mM CTAB.[46,47] Here, the most downfield resonance at ppm 7.36 is due to the aromatic protons of the imidazolium ring (H2, H3 and H4) (Figure 6(a)). The α protons (H5) of the alkyl chain are deshielded due the vicinity of the aromatic ring, and appear at 4.09 ppm. The intense signal at 3.77 ppm corresponds to the N-methyl protons (H1) attached to the imidazolium ring. The relatively less intense resonance at 1.75 ppm is due to the β protons (H6) whereas the γ protons (H7) appear as a hinge at 1.18 ppm. The signals for the intermediate methylene protons (H8-H19) merge together and appear as an intense signal at 1.12 ppm while the terminal methyl group (ω, H20) appear farthest upfield at 0.72 ppm.

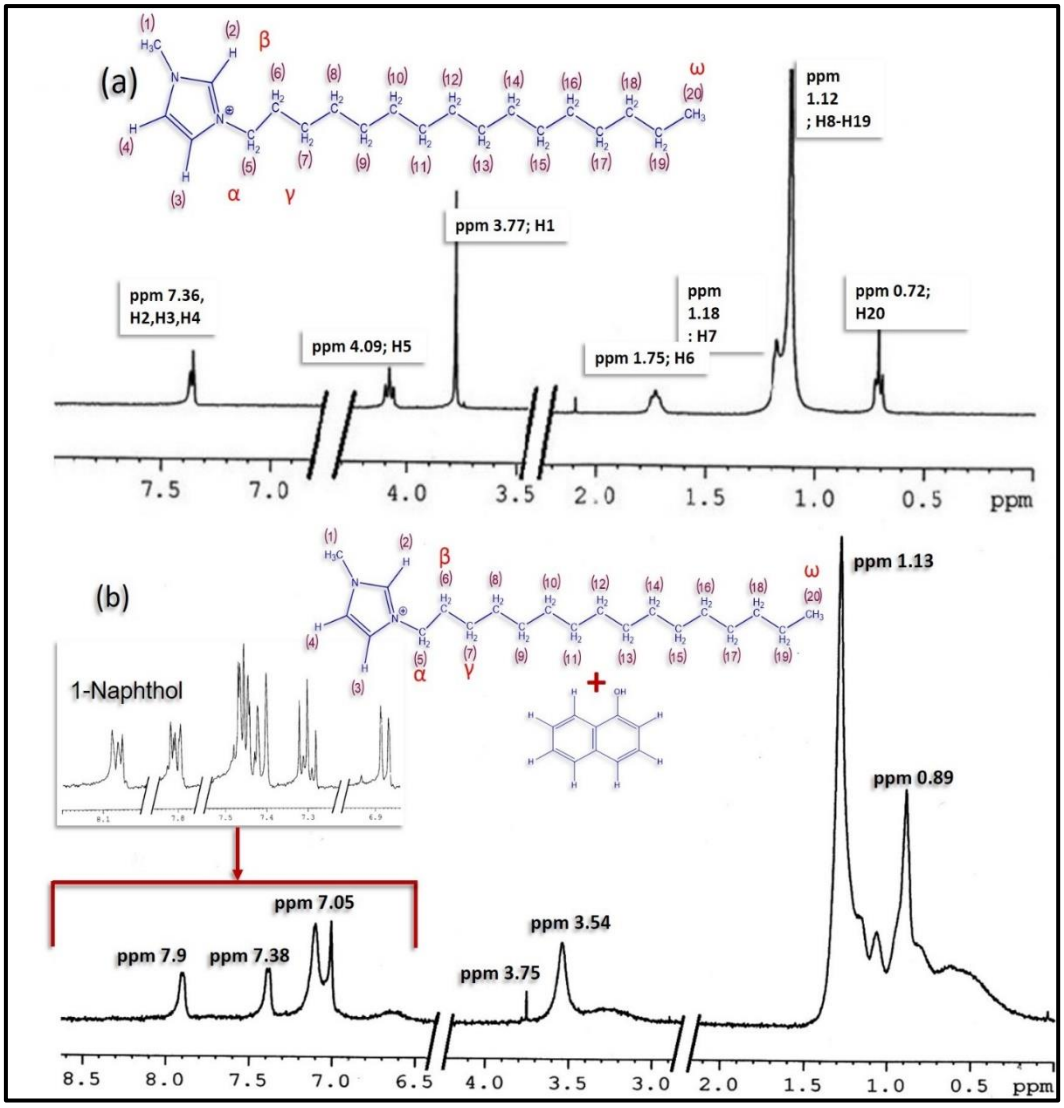

Figure 6 (a) ^{1}H-NMR spectra of 10 mM C_{16}-3-MeImCl in D_2O at 25^{0}C; (b) ^{1}H-NMR spectra of mixture of 10 mM C_{16}-3-MeImCl and 10 mM 1 Naphthol in D_2O at 298 K.

Figure 6 (b) depicts the spectra of the mixture of 10 mM C_{16}-3-MeImCl and 10 mM 1 Naphthol in D_2O with the spectra of 1 Naphthol in D_2O in the inset. The aromatic protons of 1 Naphthols resonate in between 7.10 and 7.76 ppm (Inset) and appear highly split. It is evident that in the mixture, signals due to aromatic protons merge, broaden and appear upfield with three main signals (two singlet and one doublet) at 7.9, 7.38 and 7.05 ppm respectively. The large upfield shift of the resonances indicates that the protons are located in relatively non-polar environment compared to that in water.[19,48] The broadening of the peaks imply restricted motion of the naphthol molecules in the viscoelastic phase on the NMR time scale.[19] The α protons of the ionic liquid resonate highly upfield at 3.54 ppm while the N-methyl protons do not seem affected, resonating at 3.77 ppm.

The chemical shift in the terminal methyl group shows opposite trend, resonating at down field 0.89 ppm. Resonances due to β protons and the intermediate methylene groups merge to a single intense and broad peak at 1.13 ppm. The observed upfield shifts are supposedly induced by ring current of the aromatic ring of the naphthol.[49,50] The large shift of the α and β protons confirms that the aromatic part of the additives are intercalated in the outer micellar part.[46,48] Previously, study of ^{1}H NMR of CTAB micelles (10 mM) have shown that only the protons adjacent to the polar quaternary ammonium head groups of CTAB were affected and shifted upfield in presence of phenols (5 mM) while terminal methyl group and other methylene protons remains unaffected. The aromatic protons of phenols appeared upfield in presence of CTAB and so did the α and β protons of CTAB, hence it was concluded that the phenols reside at the vicinity of the micellar interface without affecting protons beyond γ position of the alkyl chain.[46] In the present study, a downfield shift of the resonance of terminal protons is observed in all the C_{16}-3-MeImCl-Additives systems (Figure 6 (b), Figure S8 (a-b) of Appendix A). The broadening of peak near 1.13 and 0.89 ppm together with the respective upfield and downfield chemical shifts show that both intermediate and terminal protons are perturbed due to the presence of naphthol. This suggests an orientation of the naphthol ring between the alkyl chains such that the ring current affects the terminal protons as well (particularly by those naphthol moieties embedded near endcaps). Due to formation of cylindrical micelles, the alkyl chains of C_{16}-3-MeImCl move apart creating greater space for the spatial distribution of the terminal methyl groups which accounts for the observed downfield shift.[47] This difference in behavior from phenol,[46] is due to the presence of extended conjugation of the extra aromatic ring adding to the hydrophobicity of naphthols (and 2,3 DHN). The hydroxy-naphthalene derivatives have greater hydrophobic length compared to phenol which allows easier partitioning of the same within the alkyl chains. Similar observations were found with 2 Naphthol and 2,3 DHN as well (Figure S8 (a-b) of Appendix A).

3.7. Binding Energy: DFT study

To further understand the differences in electrostatic interactions between the two components of each system viz., the imidazolium head group of C_{16}-3-MeImCl and the naphthalene moiety of the additives, DFT calculations were done using Gaussian 09 package with hybrid functional B3LYP using 6-31G (d, p) basis set.[51] For technical limitation the hydrocarbon chain was truncated beyond C10 (since the electrostatic

interactions considered are primarily between the surfactant head group and the aromatic ring of the additive). The calculated binding energies for the imidazolium moiety and the additive molecules was found to be -10.05 kcal.mol^{-1}, -9.68 kcal.mol^{-1} and -10.31 kcal.mol^{-1} for 1 Naphthol, 2 Naphthol and 2,3 DHN respectively. The values indicate that 2,3 DHN bind to imidazolium head group more strongly followed by 1 Naphthol and 2 Naphthol i.e. the magnitude of electrostatic interaction with the ionic liquid is highest in case of 2,3 DHN and lowest in case of 2 Naphthol. It can be said that due to two hydroxy functionality, 2,3 DHN binds stronger with the head group of the ionic liquid compared to the mono-naphthols. This result corroborates the trend observed in the zero shear viscosity with temperature and the flow activation energy of the systems (Section 3.5). The difference in magnitude arises from the fact that though all the additives have identical aromatic backbone, they differ in the electrostatic surface potential owing to position of the hydroxy functionality, (Figure S9 of Appendix A) which plays major role in stability of the imidazolium-hydroxy aromatic moieties. The present study gives an overview of the extent of interaction between the imidazolium head group and the additive moiety in terms of binding energy.

3.8. Application: Metal ion tolerance of SAIL-π-conjugated additive systems - Improved viscous characteristics in presence of metal ion impurities

Hydraulic fracturing is a method of using pump rate and hydraulic pressure to fracture or crack a subterranean formation in a process for enhancing the recovery of hydrocarbons from the formation. Recently it has been shown that aqueous drilling and treating fluids may be gelled or have their viscosity increased by the use of non-polymeric viscoelastic WLM. These materials are advantageous in many ways over the use of the conventional polymer gelling agents in that they do not leave a filter cake on the formation face, do not coat the proppant or create microgels.[52-56] Since electrostatic interaction plays major role in partitioning Sodium salicylate (NaSal) in cationic micelles, such process is not favorable in absence of electrolyte or high salinity because of charge screening of head groups. Moreover, salicylate forms stable complexes with such metal ions which are present in rock environment.[57] The salicylate moiety acts as an active bidentate donor ligand to form chelates with many heavy and transition metal ions. Its efficiency as the fractured fluid in presence of salinity and the metal salts is thus highly compromised. The Naphthols, (including 2,3 DHN), are a new class of promoters which may act under salt free condition. The study of their effectiveness in

presence of metal ions is, therefore, of considerable interest in order to address the limitation of NaSal as the WLM triggering agent. In this connection, wormlike micellar solutions of C_{16}-3-MeImCl and 1 Naphthol were prepared in presence of metal salts and the viscosities at steady shear rate of 304 sec^{-1}, were measured. All the metal ions are employed as chloride salts, in order to ensure identical effect of anions, if any, on the rheology of the system and also due to the fact that impact of chloride ions on the microstructural transition of surfactant micelles is, in general, small.[58] For the purpose of comparison, similar study is done in the SAIL-NaSal system. The viscosity profiles as a function of metal concentrations are shown in Figure 7.

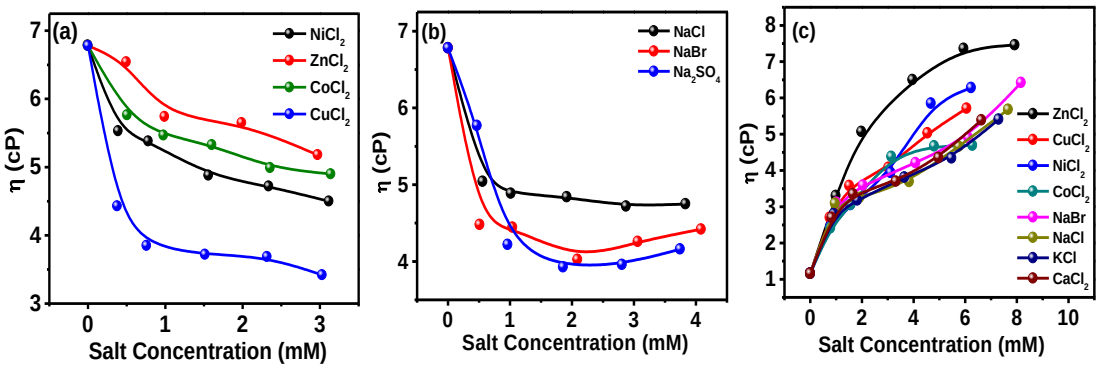

Figure 7 (a) Viscosity of C_{16}-3-MeImCl (5 mM)-NaSal(3.5mM) system as a function of metal ion concentration at 303 K and 304 sec^{-1}. (b) Viscosity of C_{16}-3-MeImCl(5 mM)-NaSal(3.5mM) system as a function of anion concentration at 303 K and 304 sec^{-1}. (c) Viscosity of C_{16}-3-MeImCl-1 Naphthol (1:1, 7.5 mM) system as a function of metal salt concentration at 303 K and 304 sec^{-1} shear rate.

The addition of transition metal salts progressively decreases the viscosity of the SAIL-NaSal system which is indeed significant (Figure 7 (a)). The extent of the lowering of viscosity as a function of metal ion follows the order: $ZnCl_2 < CoCl_2 < NiCl_2 < CuCl_2$. This can be explained in light of degree of complex forming tendency of NaSal with metal ions in aqueous solutions. The trend follows the Mellor and Maley series of stability of metal complexes.[59] The fact that viscosities are highly reduced (maximum reduction in viscosity encountered from ~ 7.0 cP to ~ 3.5 cP, Figure 7 (a)) which also implies that although addition of metal salts increases Cl^- counter ion in the system, counter ion binding, if any, could not ultimately enhance micellar growth. It seems apparent that unavailability of free salicylate ions in presence of metal, for promoting microstructural transition of spherical micelle to WLM becomes key factor in reducing viscosity and augmenting effect, if any, of counter ion condensation is trounced.

The diminishing charge density on the head groups in presence of counter ions reduces the electrostatic interaction between micelles and salicylate ions causing later to remain in the vicinity of the interface only. This further stabilizes the spherical micelles and lowers the viscosity. Therefore, the effect of alkali metal salts is not surprising. Alkali metal salts have been known to induce micellar growth and conspicuous effect of anions on charge screening is reported earlier.[60] The alkali metal ions cannot form complex with salicylate, yet the drop of viscosity as a function of salt concentration is found for all the salts (Figure 7 (b)) in the present study. In the present system, anions lower the viscosity in a trend: $Cl^- < Br^- < SO_4^{2-}$. It seems apparent that same reason is invoked here also. Effect of confiscating salicylate ion by Cl^- prevails over the effect of counter ion binding on sphere-to-rod transition. Recently, in studying the effect of anions on rheology of WLM of Cetyltrimethylammonium salicyalate (CTASal) system, it is also shown that the anions decrease the relaxation time of the systems.[61,62] However, Chloride counter ions of C_{16}-3-MeImCl are reported to participate in hydrogen bonding with the solvent H_2O molecules as well as with the imidazolium head group.[62-65] Therefore, it can be said that the condensation of counter ions from the added alkali metal salts, on the WLM surface following the order $Cl^- < Br^- < SO_4^{2-}$ leads to the corresponding decrease in viscosity.

On the other hand, it is indeed interesting to note that in the present study, the viscosities of C_{16}-3-MeImCl-1 Naphthol system increases considerably with the increase in metal salt concentration. The nature of interaction in this system is probably H-bonding and cation-π interaction along with hydrophobic forces. Therefore, counter ion cannot remove 1 Naphthol from micellar phase. Further, 1 Naphthol, being a non-chelating agent promoter, does not interfere with the metal ions and the linear morphology of the micelles is maintained (Figure 7 (c)). A schematic representation of the possible molecular interactions is given in Scheme 1.

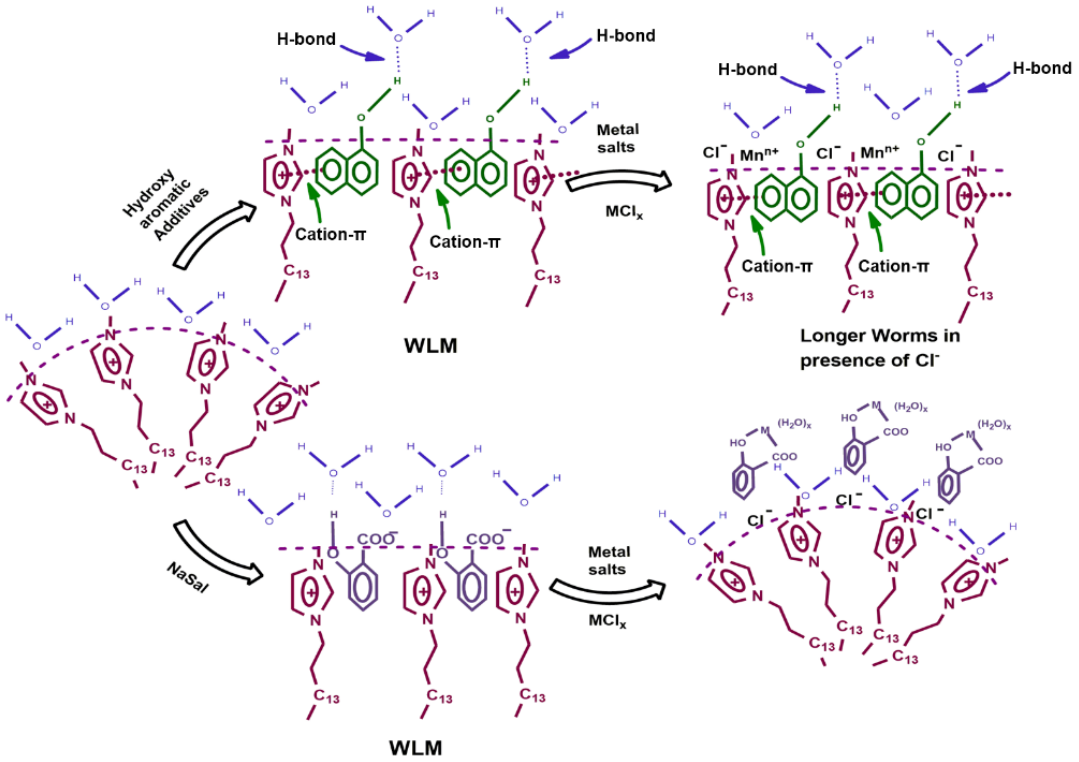

Scheme 1. Schemetic representation of possible microstructural changes in aqueous SAIL-Additive (1 Naphthol) solutions and SAIL-NaSal, on addition of metal salts and the underlying forces.

However the reason underlying the increase in viscosity is not entirely apparent although it can be understood, from the above discussion, that counter ion binding is definitely involved in micellar growth in the present system. Nevertheless, the situation is indeed complex in nature. The effectiveness of counter ion binding is dependent on a number of factors from the tendency of ion-pair formation for alkali metal salt solutions to the ease of formation of aquo-complex formation in transition metals. The observed trend in viscosity enhancement (Figure 7 (c)) is the result of a number of such multiple factors. However, it is clear that, the efficiency of Naphthols as viscoelasiticity inducer is not compromised by the presence of metal impurities and salinity and unlike NaSal it enhances and could be a potential agent to replace NaSal as fractured fluid for oil recovery.

4.0 Conclusion

Strong synergism is observed between the surface active ionic liquid, 1-Hexadecyl-3-methylimidazolium chloride and the π-conjugated additives viz., 1 Naphthol, 2 Naphthol and 2,3-Dihydroxynaphthalene, in improving the surface and bulk properties of the system Significant attractive interaction exist between π-electron clouds of the

additives and charged imidazolium head groups via cation-π interaction. Fluorescence anisotropy study suggests partitioning of the additives within the SAIL micelles while UV-Visible and ^{1}H NMR study support the positioning of the additives at the palisade layer of the micelles and their involvement in hydrogen bonding with interfacial water molecules. The dynamic oscillatory flow measurements confirm the formation of viscoelastic wormlike micelles while flow activation energy supports the efficiency of the π conjugated aromatic additives in triggering wormlike micelles in the order 2 Naphthol <1 Naphthol <2,3-Dihydroxynaphthalene. The viscoelasticity of the SAIL-Additive systems is tuneable by temperature as the systems respond to a critical temperature with highest zero shear viscosity, above which they relax faster forming branched micelles. Results of DFT study show that 2,3 DHN has maximum binding energy followed by 1 Naphthol and 2 Naphthol to the imidazolium moiety. Moreover, the systems are found to be metal tolerant. The viscosity of the present system is found to increase in the presence of metal salts. This observation promises potentiality of the system in enhanced oil recovery as fractured fluids in the presence of metal ion impurities. This study reports, fine-tuning of the temperature sensitive wormlike micelles developed under the salt-free condition which has huge prospects as usage in storage and carriage media of suitable drugs.

References are provided in BIBLIOGRAPHY under "References for Chapter IV" (Page 173-177)

Findings of this chapter has been published in *Colloid Surfaces A.*, **2017**, 516, 262-273.

Chapter V

Solvent induced molecular folding and self-assembled nanostructures of Tyrosine and Tryptophan analogues in aqueous solution

1. Introduction

The environmental concern for the widespread use of a large number of surfactant classes including those of linear alkylbenzene sufonates, alkylphenol ethoxylates and dialkyl quats, leads to legislation in many countries with the aim to gradual phasing out of these materials from commercial and industrial scenario.[1-3] The apprehension is not only due to poor biodegrability under anaerobic conditions concerning the use of anaerobically stabilized sewage sludge as fertilizer in agriculture, but also due to strong inhibitory effects of some of the above surfactant classes on metabolic activity of autotropic ammonia oxidizing bacteria with respect to the nitrogen cycling reaction in soils and water.[4,5] As a result, a trend is quite visible throughout the world to produce more environmentally benign surfactants, although so far only limited success has been achieved to produce the so called green surfactants for industrial purposes at affordable prices. The strategy for preparing environment friendly surfactant molecules could be to start with the biologically active molecules, viz., aminoacids or vegetable oil derivatives.[1,6] The end products of these chemical processes will form the interesting domain of natural surface active biomolecules and create interests not only to chemists and biologists, but also to environmentalists as well.[7-13] These compounds would naturally find a large number of basic and industrial applications too. Since the precursor aminoacid molecules are having biocompatible properties and a large variety of chemical functionalities, the surfactant molecules containing the aminoacids in their molecular architecture would retain the same remarkable properties. Notwithstanding the prevailing situation, the aminoacid based new surfactants would be water soluble, biodegradable, non-toxic, chiral, with little or no adverse impact on soil and aquatic environment.[5-6, 14-16] All these properties ensure their eventual development to cater the need in food, pharmaceutical and cosmetic sectors, which are the major user of various surfactant classes. However, in spite of the promise of optimism that has been raised up in the development of aminoacid based surfactants, volume of industrial production is

still meagre. Further, surprisingly, one of the very important aminoacid class viz., aromatic aminoacids has not been focused for preparing aminoacid based surfactant systems. Therefore, it would indeed be prudent to explore the possibility of surface active properties of long chain derivatives of aromatic aminoacids, especially those of tryptophan and tyrosine, in order to apply these materials as the environment friendly surfactants. This, quite naturally, would not be confined to spherical aggregates and their uses concerning laundry detergent only and rather, the applications of biocompatible and environment-gentle surfactants would be quite diverse. The increasing need for drug delivery systems that improve specificity and activity and at the same time reduce toxicity to ensure maximum treatment safety has led to the development of a great variety of drug vector formation. Since the first reported nonionic surfactants vesicles (ninosomes) at nearly three decade ago, there have been a number of studies on ninosomes as the potential drug carriers, principally focusing on the absence of electrostatic driving force in such systems to create any undesirable secondary interaction interface.[17] The combination of polar aromatic aminoacids and non-polar long chain compounds (esters of tyrosine and tryptophan) might led to the association into vesicles on hydration as a result of existence of a high interfacial tension between water and the hydrocarbon portion of the amphiphile. Therefore, the high promises that are expected to be created for these supramolecular assemblies, if they are formed in aminoacid based systems, would translate into the demand for advanced highly functionalized drug delivery materials having bio-origin.

Another highly challenging fact pertinent to aromatic aminoacid based surfactants, however, prompts also from their biological relevance and strongly functional roles played by aromatic aminoacids in transmembrane proteins at membrane interface. Biological membranes are complex assemblies of lipids and proteins in which phospholipids form the major building blocks. The components of supreme importance in cell membranes are various types of proteins which are associated with lipid bilayer to form functional membranes and perform different important tasks inculcated by the cell. Some crucial of these proteins are either transmembrane proteins, anchored proteins or peripheral proteins. The transmembrane proteins viz., α-helical bundles and β-barrel proteins, localize aromatic aminoacids (especially tyrosine, tryptophan and histidine) at the membrane/water interface where they form functionally significant hydrogen bonds (H-bonds) with interfacial water.[18-23] The discrimination between

nonpolar interior and the polar exterior of the lipid bilayer is made by the transmembrane proteins via the typical hydrophobic and the hydrophilic domains that are present in their molecular architecture. The hydrophobic region which contains a stretch of 20-25 hydrophobic and/or uncharged aminoacids spans the membrane bilayer. The hydrophillic region, on the other hand, are exposed to one or both sides of the membrane, contains hydrophilic aminoacids including aminoacid vesicles. The interplay between hydrophobic and hydrophilic forces in membrane proteins is thus the key to the function and activity of these protein molecules which typically resemble conventional surfactants or amphiphilic molecules in this respect. While amphiphilic behavior of the membrane proteins is indeed significant, it is difficult if not impossible, to study *in situ* because of the inherent complexity of the membrane systems. Long chain alkyl esters of aromatic aminoacids, especially those of tyrosine and tryptophan, could be good models of membrane proteins and a few study on fluorescence behavior of such a model system, viz., tryptophanoctyl ester are reported in literature.[24-29] However, no scientific report of such model systems involving tyrosine or other aromatic amino acids is available. In spite of their importance the surface active property of the model systems have not been reported. Therefore, the initial motivation is to consider the surface activities of long chain esters of tyrosine and tryptophan and to study the behavior of the aromatic π systems at the interface. It is indeed a fact that these materials are not easily available at present, not even from well-known chemical manufacturers. This may be one of the reasons for the lack of interest shown to these model systems. In this chapter, the method of synthesizing octyl esters of tyrosine and tryptophan residues and dodecyl ester of tyrosine and investigation of a detail aspect of the surface activity and related phenomena including their conformations, molecular interactions in aqueous medium, aggregation behavior and the morphology of the self-assembled nano structures of the aggregates are presented.

2. Materials and Methods

2.1. Materials

L-Tyrosinoctyl ester (TYOE), L-Tyrosinedodecyl ester (TYDE) and L-Tryptophanoctyl ester (TROE) were synthesized in our laboratory according to Scheme 1 and Scheme 2 respectively. L-Tyrosine and L-Tryptophan were purchased from HI-Media (India), $SOCl_2$ and n-Dodecanol from Aldrich (USA), n-Octanol from Lancaster

(England). Pyrene was purchased from Fluka (Switzerland) and purified prior to use via column chromatography using Hexane as eluent. Hexane was purchased from SDFCL (India); NaCl, NaOH, Na_2SO_4, for synthesis, were purchased from Merck (India). Purity of all chemicals were greater than 99% and were used as received (except Pyrene). All experiments were done with de-ionised and doubly distilled water with pH 6.5-7 and specific conductance below $2\mu S.cm^{-1}$.

2.2. Methods

2.2.1. Tensiometry. Tensiometric measurements were performed on Krùss K9 Tensiometer (Germany), based on Du-Nóuy ring detachment method, fitted with Omniiset temperature bath with precision ± 0.1^0C. Before each measurement, the platinum ring was thoroughly cleaned with 1:1 acetone-water solution and heated under oxidizing flame until glowing temperature was attained. After every addition, the experimental solution was stirred for 5 minutes for homogeneity and equilibrated for 10 minutes. For each measurement, three to five subsequent readings were taken for concordance. Standard deviation was < 0.1 $mN.m^{-1}$.

2.2.2. pH measurements. The pH's of the solutions were measured using Systronics digital pH meter (Model: 335, India), calibrated with standard buffers of pH 4.0 and 9.2. Solutions were equilibrated for 5 min after addition of alkali till a steady pH meter reading was observed.

2.2.3. **Fluorescence spectroscopy.** Steady state fluorescence emission study was carried out in bench top spectrofluorimeter from Photon Technologies International (Quantamaster-40, USA) with excitation and emission slit widths fixed at 3.0 nm and 2.5 nm respectively. Samples were taken in Hellma quartz cuvette of optical length 1.0 cm.

2.2.4. Nuclear Magnetic Resonance Spectroscopy (NMR). ^{1}H-NMR experiments were performed in Bruker (Germany) ADVANCE spectrometer operating at 300 MHz frequency (for characterisation) and at 400 MHz for 2D ROESY study. Signals are quoted as δ values in ppm using residual protonated solvent signals as internal standard (D_2O: δ 4.79 ppm). Respective solutions were made in D_2O and 0.6 mL of the same was used for each measurement. Data are reported as chemical shift.

2.2.5. High Resolution Transmission Electron Microscopy (HRTEM). HRTEM images were obtained with Jeol JEM 2100 microscope (Japan) operating at accelerating voltage of 200 KV. All images were taken at suitable defocus condition to obtain maximum contrast. A drop of sample solution was added to 200 mesh copper lacey support grid coated with carbon film. Excess sample was manually blotted carefully with Whatman 42 filter paper for 2 s. The grid was dried at 60^0C for 1 hr before experimentation.

2.2.6. Dynamic light scattering (DLS). The dynamic light scattering (DLS) was performed on Zetasizer Nano ZS light scattering apparatus (Malvern Instruments Ltd., UK) with He-Ne laser (632.8 nm, 4 mW) at scattering angle 173^0. The temperature was kept constant at 303 K.

2.3. Synthesis of TYOE and TYDE

To 0.6 mol of n-Alcohol (95 mL n-Octanol; 135 mL n-Dodecanol respectively for TYOE and TYDE) at -5 ^{0} C, 0.055 mol (4 mL) Thionyl chloride was added dropwise and mixture was stirred for 10 min (Scheme 1). To this, 0.05 mol (9 g) of L-Tyrosine was added and the resulting mixture was stirred and refluxed at 95 ^{0} C for 21 hrs under nitrogen atmosphere. The mixture was then allowed to stand at room temperature. The white solid that appeared was washed with diethylether several times (to remove excess n-alkanol) and filtered via vacuum suction. It was then dissolved in water and pH was adjusted to 7 (± 0.2) by dropwise addition of ~ 0.1N NaOH solution. The white cloudy solution was taken in a separating funnel to which ethyl acetate was added and mixture was shaken well and kept to stand overnight. Clear, transparent layer of water and ethyl acetate was obtained.

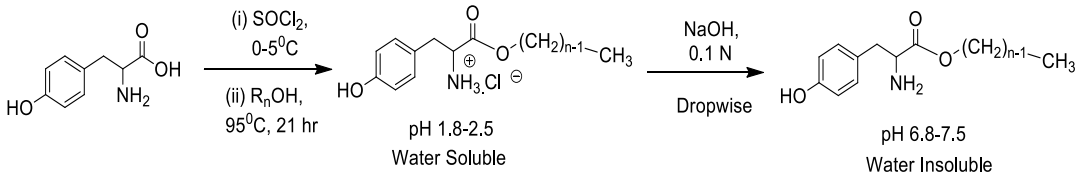

Scheme 1: Synthetic route of L-Tyrosine alkyl ester, n=8 (TYOE), 12 (TYDE)

The organic part of the mixture was collected over Na_2SO_4 and solvent was evaporated in a water bath and product was dried in vacuum pump for 6 hrs.[30] Yellow semisolid product for TYOE (Yield ~72%, 6.5 g) and white crystalline product for TYDE (Yield

~75%, 6.7 g) were respectively obtained and these were characterized using ^{1}H and ^{13}C NMR Spectroscopy.

L-Tyrosine Octyl ester:

^{1}H-NMR (300 MHz, $CDCl_3$): δ (ppm) 7.3 (1H, -OH), 7.01 (d, 2H, 8.4 Hz), 6.69 (dd, 2H, 2.1 Hz), 4.17-4.10 (m, 2H), 3.74-3.66 (m, 1H), 3.2 (broad, $-NH_2$), 3.05 (dd, 1H, 5.1 Hz), 2.94-2.79 (m, 1H), 2.06 (t, 2H), 1.64 (t, 2H), 1.31-1.25 (m, 10H), 0.898 (t, 3H, 6.6 Hz)

^{13}C-NMR (300 MHz, $CDCl_3$): δ (ppm) 174.9, 130.35 (for two C, twice intensity), 127.9, 115.7, 77.45, 77.02, 76.60, 65.43, 55.54, 39.71, 29.18, 28.55, 25.88, 22.62, 14.17, 14.07.

L-Tyrosine Dodecyl ester:

^{1}H-NMR (300 MHz, $CDCl_3$): δ (ppm) 7.2 (s, -OH), 6.99 (d, 2H, 8.4 Hz), 6.66 (d, 2H, 8.4 Hz), 4.12 (t, 2H, 6.6 Hz), 3.71 (q, 1H, 5.1 Hz), 3.03 (broad, $-NH_2$), 3.05 (dd, 1H, 4.8, 5.1 Hz), 2.8 (q, 1H, 7.1 Hz), 1.63 (t, 2H, 6.6 Hz), 1.28 (d, 18H, 5.1 Hz), 0.88 (t, 3H, 6.3 Hz).

^{13}C-NMR (300 MHz, $CDCl_3$): δ (ppm) 174.9, 155.4, 130.34, 127.79, 115.77, 77.46, 77.03, 76.61 65.46, 55.53, 39.71, 31.91, 29.63, 29.58, 29.51, 29.34, 29.24, 28.57, 25.89, 22.68, 14.11.

2.4. Synthesis of TROE

To 63 mL (0.4 mol) n-Octanol maintained at -5^{0}C, 2.2 mL $SOCl_2$ (0.03 mol) was added dropwise and stirred for 30 minutes. Thereafter, 6 g L-Tryptophan (0.03 mol) was added and the mixture was stirred and refluxed at 130^{0}C under nitrogen atmosphere for 21 hrs. The white solid obtained was washed with diethyl ether several times and dried.[31] It was then treated with ethyl acetate and strong NaOH solution was added dropwise to adjust pH to 7.0 (± 0.2)

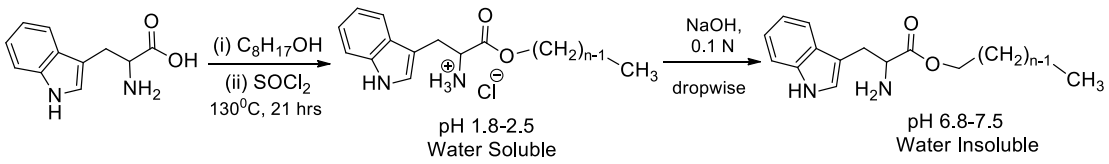

Scheme 2: Synthetic route of L-Tryptophanoctylester (TROE)

The ethyl acetate part was collected over Na_2SO_4 and washed with saturated NaCl solution several times and dried under vacuum for 24 hrs (Scheme 2).[32] The white solid product (TROE) was obtained and characterized using ^{1}H NMR and ^{13}C NMR techniques. Yield of the product was ~92% (8.1 g).

^{1}H-NMR (300 MHz, $CDCl_3$): δ (ppm) 8.2 (s, NH_2), 7.73 (d, 1H, 7.92 Hz), 7.47 (d, 1H, 7.92 Hz), 7.37 (s, 2H), 7.26 (m, 1H), 4.19 (t, 1H, 6.75 Hz), 3.93 (q, 2H, 4.98 Hz), 3.58 (q, 2H, 4.98 Hz), 3.37 (q, 1H, 5.13 Hz), 3.19-3.14 (m, 1H), 1.72 (s, 6H), 1.34 (s, intense, 6H), 0.99 (t, 3H, 6.93 Hz)

^{13}C-NMR (300 MHz, $CDCl_3$): δ (ppm) 171.23, 136.31, 127.46, 123.1, 122.1, 119.46, 118.72, 111.29, 110.92, 65.29, 62.99, 54.91, 31.8, 30.6, 29.4, 29.3, 25.88, 22.66, 14.12.

2.5. Sample preparation

For experiments at low concentration regime (concentration < 5 times critical aggregation concentration (cac)), the aminoacid esters are directly dissolved in water. For experiments at high concentration regimes (concentration > 5 times cac), the samples are dissolved in pure methanol followed by addition of water. The final methanol content in water never exceeded 4%.

3. Results and Discussion

3.1. Molecular modelling of TYOE, TYDE and TROE

Since the geometry of the individual amphiphile molecule determines the packing parameter vis-à-vis morphology of the self-assembled aggregates in aqueous solutions, the structural aspects of TYOE, TYDE and TROE are important and have been studied by density functional theory (DFT) calculations in Gaussian 09 package using the hybrid functional B3LYP and 6-31G as the basis set.[33] According to the above measurements, the most stable conformations of aromatic aminoacid esters are observed as those in which the aromatic moieties are bent/folded towards the hydrocarbon chains at different angles. The optimized conformations of TYOE, TYDE and TROE are shown in Figure 1. The hydrophobic alkyl chain lengths for TYOE, TYDE and TROE as obtained from the DFT calculations are 9.74Å, 14.87 Å and 9.74Å respectively. The respective aromatic planes arise approximately 1.29 Å below the

plane containing the alkyl chain of TYOE and TYDE, and approximately 1.01 Å in case of TROE. The bending angles between the aromatic

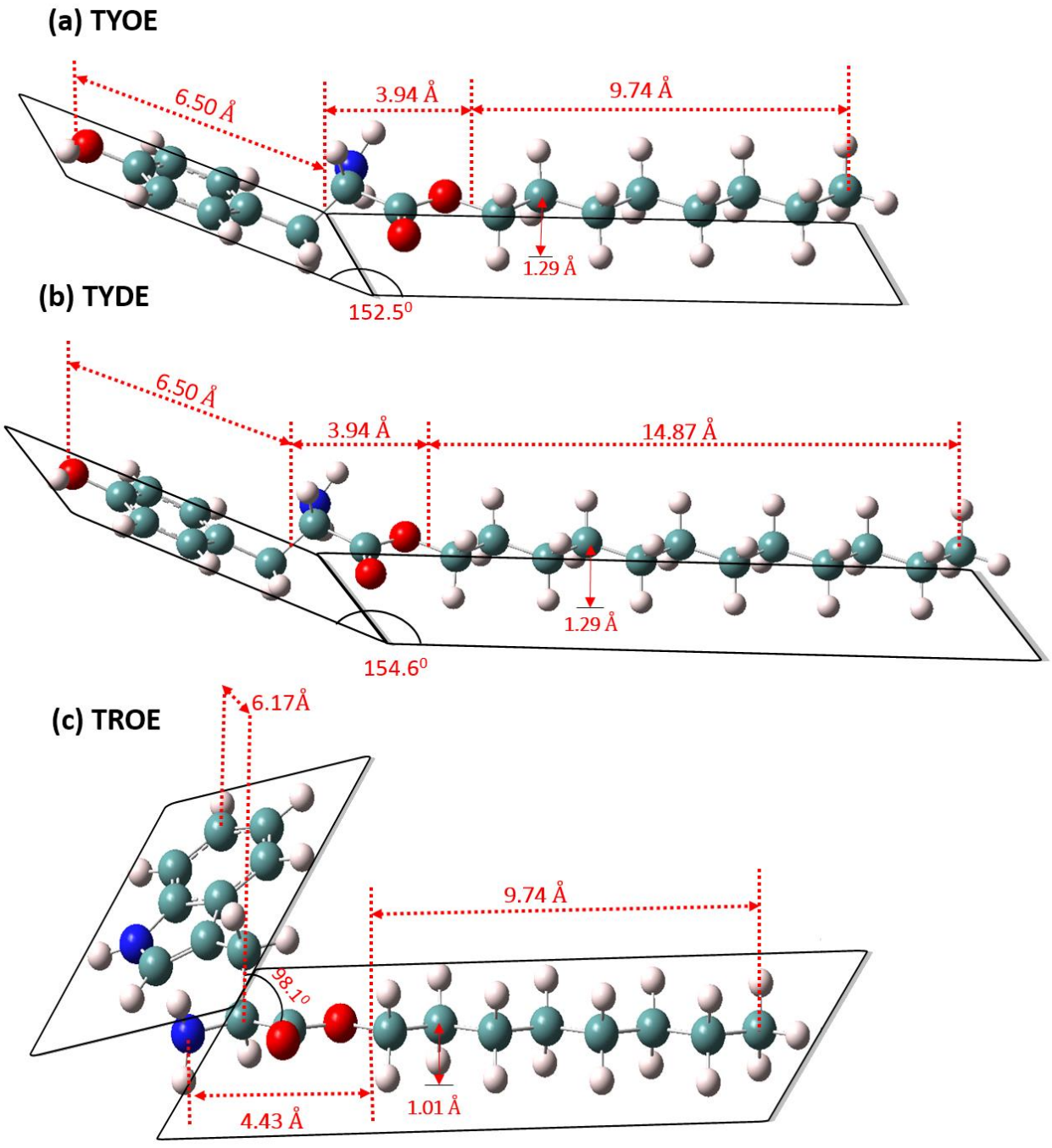

Figure 1. Optimised geometries of (a) TYOE, (b) TYDE, (c) TROE using DFT B3LYP methodology and 6-31G basis set. Color Code: Blue= Nitrogen, Red=Oxygen, Green=Carbon, Grey=Hydrogen

plane and the alkyl chain are 152.5^0, 154.6^0 and 98.1^0 for TYOE, TYDE and TROE respectively. This shows that TYOE and TYDE are comparatively much less aligned (vertically) towards the hydrocarbon skeleton compared to TROE. Single point energy

calculations were done to compute the energetics of the most stable conformation in vacuum. The total thermal internal energy of the most stable conformations i.e., those which display minimum internal energy in vacuum via energy minimization are 280.5 kcal.mol^{-1}, 356.06 kcal.mol^{-1} and 297.55 kcal.mol^{-1} for TYOE, TYDE and TROE respectively. (Theoretical details are provided in Section 1.1 of Appendix B). It is noteworthy that the structural geometry of tryptophan octyl ester was studied previously by molecular mechanics calculation.[28] It has been shown that, in vacuum, the stable conformations were all folded. Extended conformation did occur in water for they were stabilized by electrostatic and Vander Waals interaction between the solvent and TROE molecules. Such interactions are weaker for folded conformations. Nevertheless, there is a difference in potential energy of ~ 5 kcal.mol^{-1} between the extended and folded conformation of TROE in presence of solvent. This again favors the folded conformation.

3.2. Interfacial and bulk properties of TYOE, TYDE and TROE

Measurement of interfacial tension is a reliable and popular tool which provide direct insight into the molecular behaviour of a moiety through careful study of its bulk property. In order to explore the nature of the aminoacid esters, viz., TYOE, TYDE and TROE, in solution, tensiometric study was undertaken. Figure 2 (a-c) shows that the surface tension of water decreases steadily with increasing concentrations of TYOE, TYDE and TROE and reaches a constant value at a critical concentration in each case, like a conventional surfactant. At room temperature, viz., 303 K, sharp break points at 1.81 mM, 1.31 mM and 0.046 mM concentrations of TYOE, TYDE and TROE are observed respectively. The equilibrium surface tension of the solutions at the critical points, (γ_{cac}), are 45.0 mN.m^{-1} for TYOE, 38 mN.m^{-1} for TYDE and 52.5 mN.m^{-1} for TROE. These surface tension values are indeed much lower than that of pure water i.e., 70.8 mN.m^{-1} at 303 K. This result indicates that the aminoacid esters are surface active in nature. The absence of a minimum around the break point confirms the purity of the synthesized ester.[34] Generally, nature of head group and the alkyl chain length of the non-ionic surfactant govern cmc/cac values (cac stands for 'critical aggregation concentration'; the term, in general, is used in this work because of the occasional presence of different types of aggregates together (See Section 3.5)).[35]

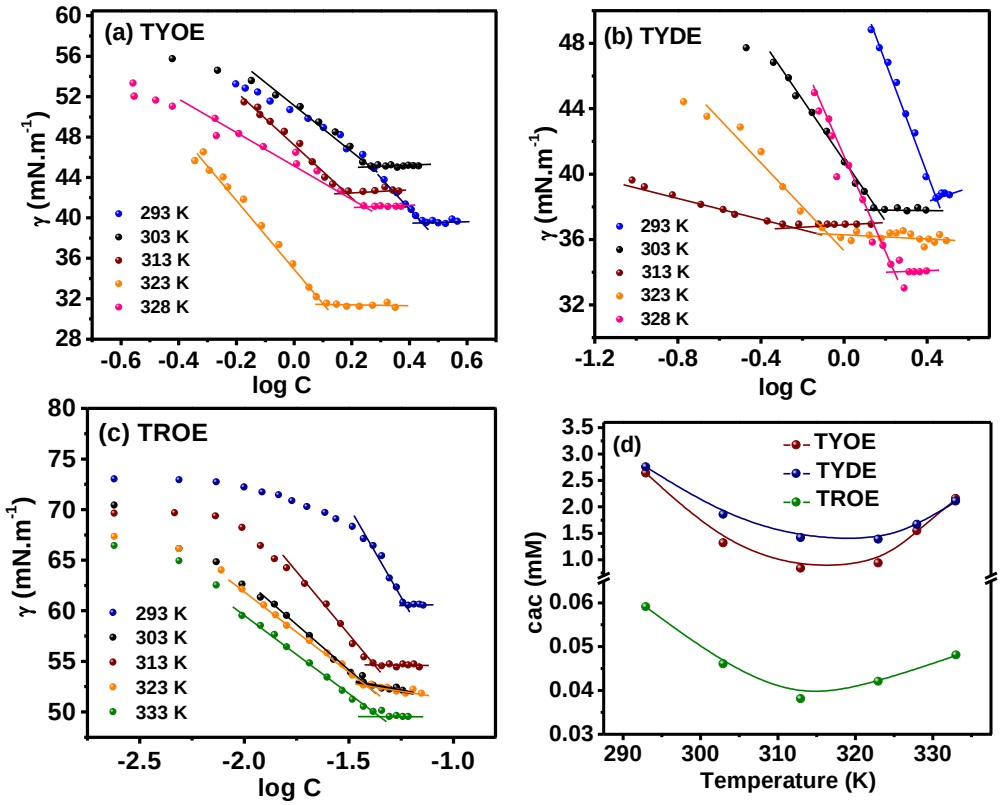

Figure 2. Surface tension profile as function of temperature for (a) TYOE, (b) TYDE, (c) TROE, (d) Variation of cac with temperature for different aminoacid esters.

In the present study, it is observed that the cac values for two tyrosine esters (1.81 mM for octyl and 1.31 mM for dodecyl esters) are not only close to cmc (critical micelle concentration) values normally found for many conventional single tailed surfactants but also follow the well understood trend of synergism as a function of chain length.[36] Tryptophan ester (TROE), however, exhibits surprisingly strong self-assembling tendency in water displaying the cac value of 0.046 mM. The γ_{cac} values for the three aromatic aminoacid esters indicate that none of these amphiphiles packs air-water interface much densely, most probably due to their obliquely bent head group geometry (See also Section 3.4).[37] However, among the three, TYDE molecules are packed most densely while TROE are least densely packed. The pC_{20} values have been determined from the surface tension plots.[38] The pC_{20} is defined as $pC_{20} = - \log C_{20}$, where C_{20} stands for the concentration required to reduce the surface tension of water by 20 $mN.m^{-1}$. The C_{20} is the minimum concentration needed to lead to a saturation of the surface adsorption and thus can be used as the signature for the efficiency of the amphiphile adsorption at the air-water interface. Higher value of pC_{20} imply greater surface active

nature. The pC_{20} values for the present aromatic aminoacid amphiphile systems are found to be 0.05, 0.50 and 1.30 for TYOE, TYDE and TROE respectively. It implies that TROE demonstrates much higher surface activity compared to the tyrosine analogues. The cac of the present systems is a typical weak function of temperature like cmc of the conventional surfactants (Figure 2 (d)).[39] In the present case, it decreases with temperature initially and then increases passing through a shallow minimum. The observed decrease in surface tension is probably caused by orientation of aminoacid esters at the air-water interface. The rapture of hydrogen bonds between the amphiphiles and the water molecules caused by initial rise in temperature, increases the effective hydrophobicity of aminoacid ester molecules, thus favouring its aggregation. The increase in cac at higher temperatures is due to breakdown of the structured "ice-bergs" of water, thus increasing the entropy of aggregation.[40-42] The noted decrease in the equilibrium surface tension values corresponds to higher surface energy with rise in temperature. Other surface parameters underlining the surface behavior of the surface active aminoacid esters in aqueous medium are calculated via Gibbs adsorption equation[43,44] (theoretical background provided under Section 1.2. of Appendix B). and presented in Table 1. The maximum surface excess (Γ_{max}) denotes the number of surface active molecules present at the air-water interface in excess of the bulk. Γ_{max} shows a significant increase of nearly 2.5 times, from 1.96 x 10^{-6} to 4.87 x 10^{-6} $mol.m^{-2}$ in case of TYOE and 2.21 x 10^{-6} to 5.59 x 10^{-6} $mol.m^{-2}$ for TYDE in the temperature range of 323-328 K but in the case of TROE, it decreases from 6.8 x 10^{-6} $mol.m^{-2}$ to 2.6 x 10^{-6} $mol.m^{-2}$ within temperature range of 293-333 K (Table 1). A_{min}, which is the minimum surface area occupied by a molecule at the interface, decreases from 0.85 to 0.46 $nm^2.molecule^{-1}$ for TYOE and 0.75 to 0.46 $nm^2.molecule^{-1}$ for TYDE while increases from 0.24 to 0.66 $nm^2.molecule^{-1}$ for TROE (Table 1). The increase in A_{min} value, in the case on TROE suggests that the molecules are oriented more obliquely at the interface, and explains the decrease in number of excess TROE molecules with temperature. The TYOE and TYDE, on the other hand assume perpendicular orientations and consequently their Γ_{max} is higher.[37] The observation indicates that the head group of the aminoacid ester moieties play a significant role in determining the orientation of the molecules at the interface.

Table 1. Temperature dependence of Critical aggregation concentration (cac), surface parameters viz., surface pressure at cac (Π_{cac}), surface excess, (Γ_{max}), area minimum (A_{min}) of TYOE, TYDE and TROE in aqueous medium

Temperature (K)	cac (mM)	10^3 x Π_{cac} ($mN.m^{-1}$)	10^6 Γ_{max} (mol m^{-2})	A_{min} ($nm^2.molecule^{-1}$)
		TYOE		
293	2.75	33.2	1.96	0.85
303	1.81	26.1	2.55	0.65
313	1.41	26.9	3.45	0.48
323	1.38	36.7	4.87	0.30
328	1.66	25.9	2.55	0.46
		TYDE		
293	2.63	39.6	2.21	0.75
303	1.31	33.4	3.79	0.44
313	0.83	36.9	5.80	0.29
323	0.93	31.8	5.59	0.30
328	1.54	33.1	3.65	0.46
		TROE		
293	0.059	12.6	6.81	0.24
303	0.046	18.3	2.93	0.57
313	0.038	17.8	3.42	0.48
323	0.042	12.8	2.15	0.79
333	0.045	17.7	2.58	0.66

The morphology/phase-transitions of self-assembled aggregates of amphiphilic compounds are dependent on the packing parameter (p),[45]

$$p = v/l.a_0 \ , \qquad (1)$$

where *v* and *l* are the volume and length of the hydrophobic alkyl chain respectively, and a_0 is the area of the hydrophilic head group of the surfactant molecule.

The numerical value of p determines the degree and the extent of morphological transition of the aggregates, formed in surfactant solution. For example, in order to form global micelles, $p \leq 1/3$; for wormlike micelles, $1/3 < p \leq 1/2$; for bilayers, $1/2 < p \leq 1$ and for reverse micelle structures $p > 1$.[46] The effective head group area, $a_{0,}$ of the surfactant molecules, is generally obtained from the variation of the surface tension as a function of concentration[47] and is given by the A_{min} (Table 1). The volume of the

hydrophobic chains, v, can be determined empirically from Tanford's equation as follows-[48]

$$v = 27.4 + 26.9\,n \quad (2)$$

where n is the number of carbon atoms in the chain.

For, n=8 and 12, (for octyl esters of tyrosine and tryptophan and dodecyl ester of tyrosine) v assumes the values of 242.6 $Å^3$ and 350.2 $Å^3$ respectively. Using these values, and the value of A_{min} from Table 1, assuming perpendicular orientation only, p is found to be 0.38 for TYOE, 0.53 for TYDE and 0.43 for TROE. The values indicate that in the case of TYOE, p is slightly above the limit of 0.33 (for micelles), and therefore, is expected to aggregate as nearly spherical micelle as well as ellipsoidal clusters, while both TYDE and TROE would have strong inclination to pack as bilayers or vesicles.[49]

3.2.1. Thermodynamics

The energetics of aggregation and interfacial adsorption have been studied as function of temperature (Table 2) using Gibbs adsorption isotherm[34] and Mass action model [50] of surfactant aggregation respectively. Mathematical details and equations are provided under Section 1.2.1 in Appendix B. The standard free energy of aggregate formation per mole of monomer unit [51] for TYOE, TYDE and TROE in aqueous medium is evaluated based on Mass action model and summarized in Table 2. The high negative ΔG^0_{agg} for TROE aggregation, compared to that for tyrosine analogues, shows that the aggregation process is much favored in the former. The self-assembly of amphiphilic molecules in polar solvents like water generally involves interesting thermodynamic maneuver.

Table 2. Thermodynamic parameters viz., Standard Gibbs free energy change of aggregation (ΔG_{agg}^0), standard enthalpy change of aggregation (ΔH_{agg}^0),standard entropy change of aggregation (ΔS_{agg}^0) and standard free energy change of adsorption (ΔG_{ads}^0) of TYOE, TYDE and TROE in aqueous medium.

Temperature (K)	ΔG_{agg}^0 (kJ.mol^{-1})	ΔH_{agg}^0 (kJ.mol^{-1})	ΔS_{agg}^0 (J.mol^{-1} K^{-1})	ΔG_{ads}^0 (kJ.mol^{-1})
		TYOE		
293	-10.33	+56.56	+228.31	-27.24
303	-12.29	+38.41	+167.31	-22.51
313	-14.48	+16.73	+99.17	-22.27
323	-13.27	-8.56	+14.59	-20.81
328	-13.22	-22.77	-29.11	-23.40
		TYDE		
293	-11.42	+36.19	+162.50	-29.34
303	-12.88	+17.74	+101.08	-21.69
313	-13.55	+0.78	+45.78	-19.91
323	-13.48	-15.65	-6.71	-19.17
328	-14.17	-30.63	-50.17	-23.23
		TROE		
293	-33.51	-9.32	+82.55	-35.36
303	-35.89	-9.05	+88.58	-42.21
313	-36.94	-7.71	+93.38	-42.18
323	-37.85	-6.12	+98.23	-43.94
333	-38.89	-4.31	+103.84	-45.97

On the one hand, the endothermic melting of the ordered solvent cluster due to hydrophobic effect of the amphiphile dominates over the exothermic association of hydrophilic parts leading to positive entropy change. The hydrophilic part, on the other hand, preferentially hydrates in solvent water via hydrogen bond formation with water molecules. Thus a greater enthalpic compensation is brought about compared to that if the hydrophilic parts are interacted among each other leading to electrostatic repulsion between adjacent hydrophobic blocks. The balance between all such forces drives the formation of aggregates of different size, shape and order. Thus, during aggregation, compared to tyrosine analogues, the endothermic melting of ordered water molecules around nonpolar tail of TROE is much greater than the subsequent exothermic assembly of the molecules (Table 2). While hydrophobic and electrostatic interactions

dominate ΔH^0_{agg}, ΔS^0_{agg} is contributed by the transfer of the hydrocarbon chains of the monomers into the aggregate core.[52] Thus temperature favors the decrease of the exothermic repulsion between the tryptophan head groups in TROE. Further, the association of monomers, readjustment of the hydration sphere of the head groups within the aggregates and reorganization of the hydrocarbon chains at the aggregate core increases the overall degrees of freedom of the system causing a net rise in entropy.[53] The linear enthalpy-entropy compensation relationship was observed with compensation temperature, T_c, as 308 K, 313 K and 246 K for TYOE, TYDE and TROE respectively (Figure S1 of Appendix B). Further, the negative values of ΔG^0_{ads} indicate that the phenomenon of interfacial adsorption is also spontaneous in nature. In the case of TYOE and TYDE, ΔG^0_{ads} shows a non-regular trend with temperature while in the case of TROE, the value increases as function of temperature. This shows that temperature favors the process of adsorption in TROE. Furthermore, the more negative values of ΔG^0_{ads} compared to ΔG^0_{agg} for TYOE, TYDE and TROE at all temperatures indicate that the adsorption process in all the aminoacid esters is more spontaneous in comparison to their corresponding aggregation.[44]

3.2.2. Steady state fluorescence emission

Steady state fluorescence emission study was performed in order to verify cac values of the aminoacid aggregates and to ascertain the microenvironment of the molecular aggregates in solution. Figure 3 (a) depicts the variation of fluorescence emission intensity of 2 µM aqueous pyrene solution upon increasing concentration of TYOE (representative plot). Plots for TYDE and TROE are provided in SI (Figure S2 of Appendix B). The lowering of emission intensity signify considerable binding of pyrene to the TYOE molecules. The relative intensities of the vibronic bands, I_1/I_3, of pyrene emission are plotted as function of the concentrations of aminoacid esters (Figure 3 (b)).

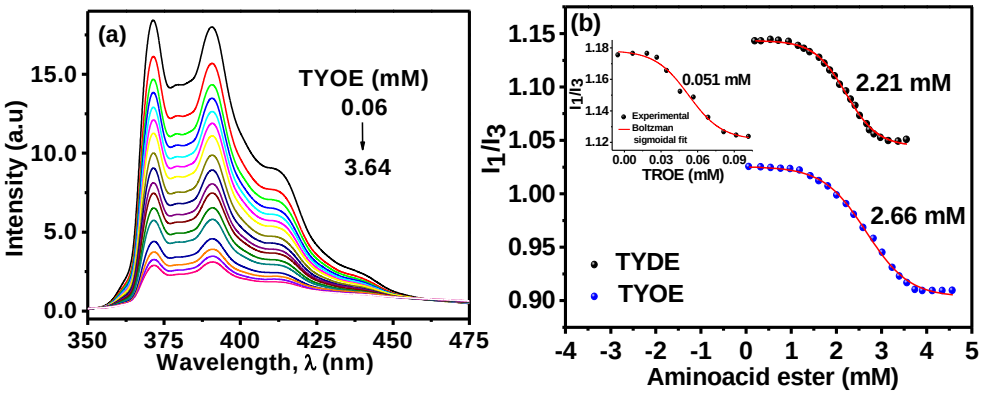

Figure 3. (a) Variation of emission intensity of 2µM aqueous Pyrene as a function of TYOE concentration at 303 K (representative plot), (b) Relative intensities of vibronic band (I_1/I_3) of pyrene fluorescence in aqueous solution of TYOE, TYDE and TROE at 303 K. Solid circles - experimental curve, Dashed line - Boltzmann sigmoidal fit.

A sigmoidal variation is observed in all the three cases (Figure 3(b)). The values were fitted according to Boltzman distribution to obtain the inflexion point, which has been considered as the cac.[54] The cac's obtained by this method are 2.66 mM for TYOE, 2.21 mM for TYDE and 0.051 mM for TROE respectively. These values differ to a considerable extent from those obtained from the surface tension measurement (Table 1). However, such difference of results of the two methods are not uncommon.[6] The I_1/I_3 value, which is shown to be the measure of the polarity of the fluorophore location, ranges from 0.91 to 1.02 in TYOE, 1.04 to 1.14 in TYDE and 1.12 to 1.18 in TROE (Figure 3(b)). The values are consistent with those observed for pyrene in non-polar solvent toluene (1.11) and in non-polar micellar core of traditional anionic surfactant Sodium dodecyl sulfate (1.14).[54] The vibronic bands of the fluorescence emission spectrum of pyrene are highly sensitive to the local polarity; the I_1/I_3 values in micelle-solubilized pyrene increases with solvent polarity.[55] Therefore, it is evident that the pyrene molecules partition into a preferably non-polar location at core of the aggregates. This also corroborates the fact that the lowering of the emission intensity upon increased amphiphile concentration as observed in Figure 3(a), is the signature of partitioning more and more fluorophore into the aggregate core. Further, I_1/I_3 varies in the order TYOE>TYDE>TROE, implying that the aggregate core is more polar in TROE followed by TYDE and least polar in TYOE.

3.2.3. Aggregation Number

The steady-state fluorescence quenching technique was used to determine the aggregation number (N_{agg}) of the aggregates of aminoacid esters. The equilibrium of the aminoacid esters between the aqueous and the self-assembled pseudo-phases follows the Poisson distribution. The following equation is applied to analyze the fluorescence quenching data[56]

$$\ln I = \ln I_0 - \frac{C_Q}{C_a} \quad (3)$$

$$\text{Or, } \ln I = \frac{\ln I_0 - N_{agg.} C_Q}{C_T - cac} \quad (4)$$

where C_Q, C_a, and C_T are the concentrations of quencher, aggregate, and total aminoacid esters, respectively, while I and I_0 are the fluorescence intensities in the presence and absence of the quencher. Figure 4 shows the emission spectra of pyrene in aqueous solutions of the aminoacid esters in the presence of varying quencher concentrations (Cetylpyridinium chloride, CPC). The emission intensity of pyrene decreases with the increase of quencher concentration in all the three aminoacid esters. From the slope of the plots of ln (I/I_0) vs. quencher concentration (Insets of Figure 4(a), (b) and (c)) and the cac values, the N_{agg} is determined by using Equation 4. In order to avoid the possibility of microstructure transition, concentration of amphiphile is kept 4.5 times of cac, whereas higher concentration is usually desirable. However, the results of the quenching experiment suggests that, both pyrene and the quencher, CPC, are partitioned well within the aggregate core under above concentration condition. The shape of the emission spectra of pyrene is modified in presence of CPC; the vibronic structure becomes ill-defined and the spectra is red-shifted due to the interaction of pyrene molecules with the pyridinium head groups of CPC within the aggregates. The aggregation numbers obtained by this method are 35 and 18 respectively for TYOE and TYDE, while that for TROE, N_{agg} could not be determined due to nonlinear nature of the ln (I/I_0) vs. quencher concentration plot (Inset of Figure 4(c)). It seems apparent that the experimental plots (insets of Figure 4 (a) and Figure 4 (b)) for TYOE and TYDE are consistent and yield the values of $N_{agg.}$ Nevertheless, the aggregation numbers are unusually small, especially for TYDE aggregates. Moreover, the deviation of plots of ln (I/I_0) vs. quencher concentration (for TROE), from linearity is undoubtedly indicative of morphology transition of the aggregates at the experimental concentration. It is

therefore tempting to examine the molecular interaction (by 2D NMR) and detail morphology (by HRTEM) at similar and higher concentration regimes of the aminoacid analogues.

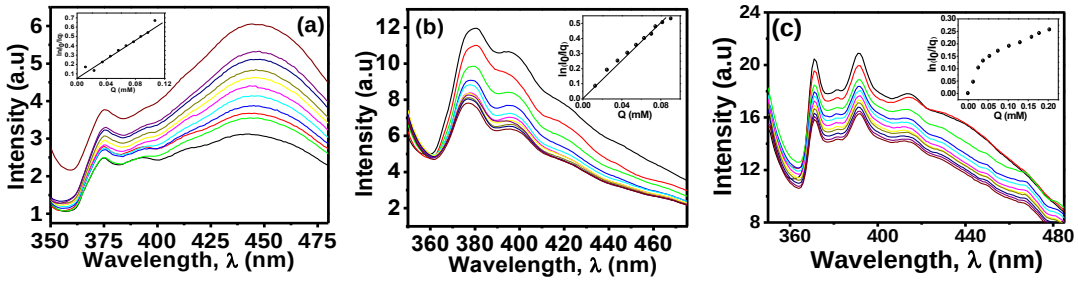

Figure 4. Variation of fluorescence emission spectra of 2µM Pyrene in aqueous solutions of the amino (a) 8.09 mM TYOE, (b) 4.24 mM TYDE, (c) 0.21 mM TROE at 303 K. Insets display linear plots of ln (I/I_0) for 2µM Pyrene in aqueous solutions of the respective aminoacid esters as function of Cetylpyridinium chloride (Q) concentrations.

3.4. Molecular interactions: 2D NMR (Concentration > 5 fold cac)

Nuclear magnetic resonance (NMR) spectroscopy is a powerful and reliable tool for the investigation of molecular aggregates.[57] The NMR techniques have been successfully utilized in determining parameters like size, shape, degree of association, structure etc. of various self-assemblies.[58-61] Rotating frame Nuclear Overhauser effect spectroscopy (ROESY) is one of the 2D NMR techniques which correlates signals arising via dipolar interaction from protons that are close in space (<5Å). The intensity of cross peaks of ROESY spectra reflects the extent of magnetization transfer between the nuclei and is proportional to the internuclei distance.[62] Herein, 2D ROESY spectroscopic analysis is utilized to study the microstructure of the aminoacid esters, viz., TYOE and TROE in solution (D_2O). The chemical representation and proton numbering of TYOE and TROE are shown in Scheme 3.

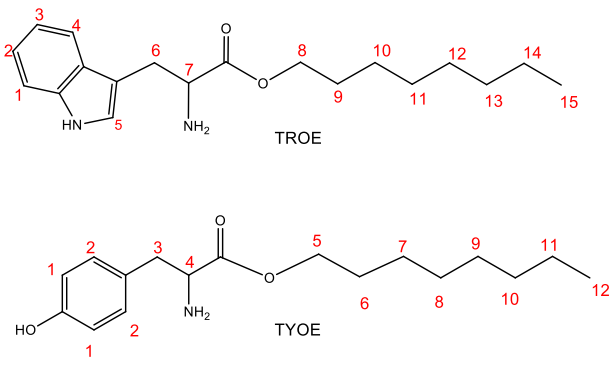

Scheme 3. Chemical representation and proton numbering of TROE and TYOE

The presence of key cross peaks in the ROESY spectra of TYOE and TROE (Figure 5) suggests that strong interaction occurs between various protons of the respective molecules. In Figure 5(a), the intense cross peaks 3/4-15 and 1/2-15 correlate the aromatic protons of the indole ring of tryptophan moiety with the terminal alkyl protons.

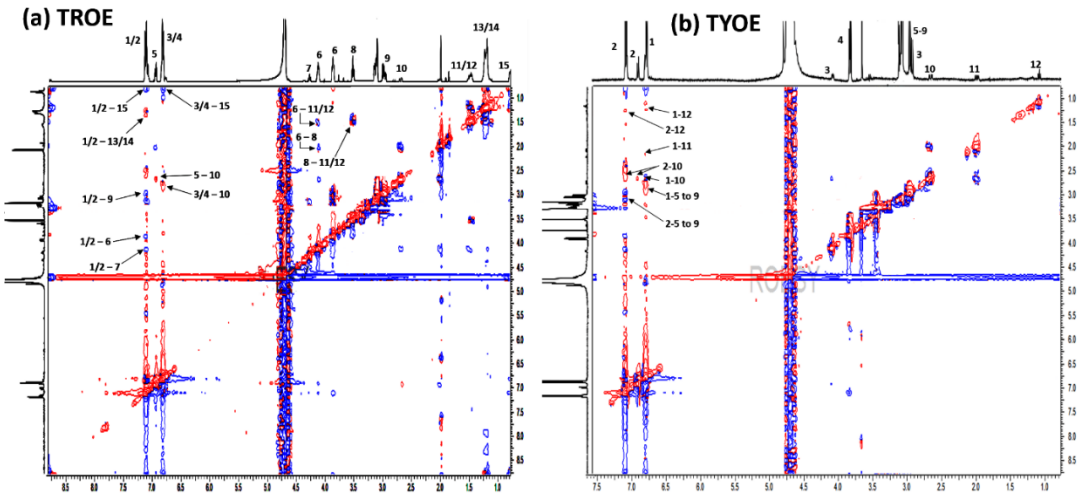

Figure 5. 2D ^{1}H-^{1}H ROESY spectra of (a) TROE (0.5 mM), (b) TYOE (7.2 mM) in D_2O at 303K.

Cross peaks viz., 1/2 -13/14, 3/4-10 and 1/2-9 are observed between the aromatic protons and the intermediate aliphatic protons of the octyl chain of TROE. These correlations suggest that the aromatic face of the TROE molecule containing the benzene ring of the indole moiety lie in close proximity of the aliphatic protons of the alkyl chain of TROE, including the terminal methyl protons. The optimized geometries of aminoacid esters (Section 3.1) in vacuum especially that of TROE, also showed that aromatic ring remains folded. Previously, theoretical studies using molecular mechanics calculations,[28] have shown that an extended conformation of TROE molecule is energetically unfavorable and that TROE molecule exist as folded conformer in vacuum as well as in water box, with the amino and carboxylate groups located at one end creating a polar extremity. Similar conformation of TROE is observed herein from the ROESY spectrum. The interaction of aromatic protons with terminal methyl group further suggests that the aliphatic chain tend to bend towards the aromatic ring exhibiting a folded structure. Strong hydrophobic interactions between the aromatic ring and the aliphatic chain might be the driving force behind the “bending inwards” of the terminal alkyl protons and the observed cross-peaks in ROESY spectrum. This conformation of TROE may be stabilized by the favorable vander Waal

interaction and possible hydrogen bonding between the solvent water molecules and the polar amino and carboxyl groups of TROE, which lie at the micellar interface. Furthermore, the two H6 protons exists in two magnetically non-equivalent environment. One is closer to the polar amino group and appear downfield at δ 4.2 ppm while other is oriented away from the amino group and appear relatively upfield at δ 3.9 ppm (Figure S3 (a) of Appendix B). In ROESY spectrum, a correlation between the more downfield H6 proton is observed with H8 and H11/H12 proton of the alkyl chain. Moreover, several other weak cross peaks viz., 1/2-6, 1/2-7 and 5-10 are also observed correlating the aromatic protons with the protons at the polar end of the head group. These interactions, suggests that molecular interactions may also occur between two adjacent TROE molecules.

In the case of TYOE, two fascinating aspects were observed. Firstly, in spite of consisting of two types of magnetically non-equivalent aromatic protons viz., H1 and H2 (Figure 5(b)), the ^{1}H NMR spectra displayed low intensity resonance signals for a third type aromatic proton at δ 7.00 ppm (Figure S3 (b)). This indicates that some of the H2 protons may be hydrogen-bonded to the amino group in its vicinity. The 2D ROESY spectrum reveals that this hydrogen-bonded proton interacts with H10 of the aliphatic chain giving rise to cross peak at 6.99-2.75. A very weak correlation peak is observed between the aromatic H1 proton and the terminal methyl protons viz., H12. This shows that the aliphatic chain terminal is located away from the proximity of the aromatic ring contrary to that observed in TROE. Secondly, unlike commonly observed for aliphatic proton resonances and as observed in the spectra of TYOE in non-polar solvent $CDCl_3$ where it appears at δ 1.33 ppm (Figure S3 (a) of Appendix B), the chain protons H5-H9 appears highly downfield in D_2O and merges into a single peak observed at 3.16 ppm (Figure S3 (b) of Appendix B). No intense peak at the non-polar end suggesting otherwise is evident. The observation indicates that the chain protons of TYOE experiences unusually high polar environment in aqueous medium compared to TROE. Intense cross-peaks correlating these protons viz., H5-H9 with the aromatic non-bonded H2 proton is observed. It seems likely that in TYOE, the aromatic moiety bends inwards the carbonyl group along with the ester–oxygen facing the interface.[63] Due to incorporation of rigidity in structure owing to the hydrogen bonding, the aromatic group remain less closely packed compared to TROE. The highly polar environment experienced by H5-H9 in TYOE may be explained by the close proximity

of the $–NH_2$ group in the vicinity, as well as the presence of larger number of the polar solvent molecules compared to TROE.

On basis of the 2D NMR observation, a probable structure of TROE and TYOE as present within the aggregates and the intra-molecular interaction between different protons is shown in Scheme 4.

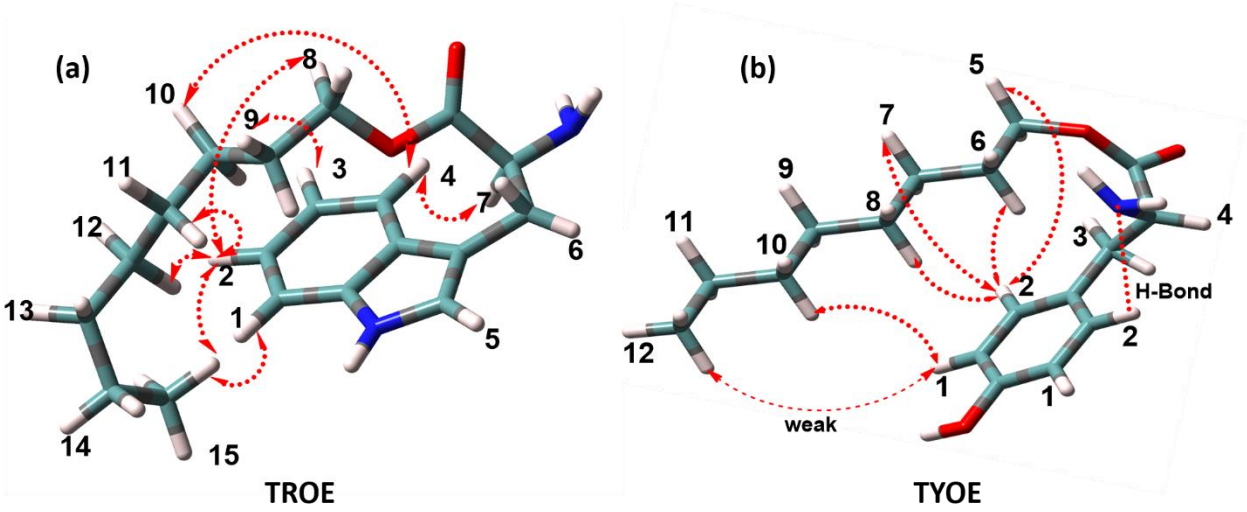

Scheme 4. Key ^1H-^1H intra-molecular ROESY (⟷) correlations in (a) TROE and (b) TYOE. Color code: Blue= Nitrogen, Red=Oxygen, Green=Carbon, Grey=Hydrogen

3.5. Morphology of aggregates: HRTEM and DLS (Concentration >5 fold cac)

The aggregate morphology of the aminoacid esters were visualized using High Resolution Transmission Electron Microscopy (HRTEM)[6] (Figure 6). To ensure complete aggregation and microstructure transformation, aqueous solutions of the aminoacid esters were prepared with concentrations 5-10 times of their respective cac. The TEM micrographs show presence of aggregates of different sizes having diverse microstructural features. In TYOE, spherical micelles of size 5-10 nm (representative indication by red square) and small spherical vesicles of size 20-30 nm (representative indication by red arrow) are observed to pack together in form of ellipsoid domains (Figure 6 (a)).

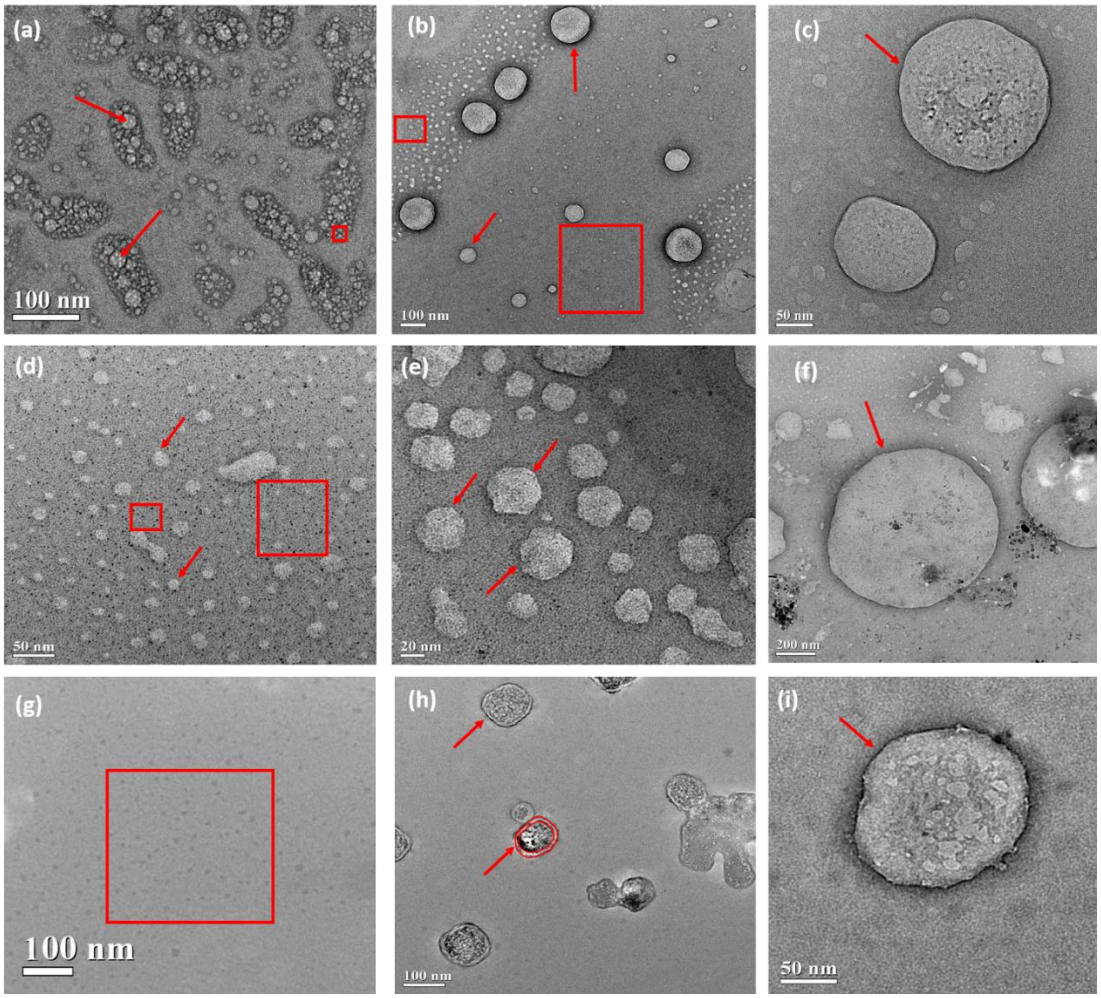

Figure 6. HRTEM micrographs of (a-c) 7.2 mM TYOE in aqueous medium in different fields of view: (a) shows the clusters of vesicular aggregates, (b) Boxes highlight dispersed micellar aggregates, size < 10nm. Arrows indicate presence of large vesicles of diameter >50 nm. (c) Presence of giant spherical vesicles of diameter ~200 nm; (d-f) 9.0 mM TYDE in different fields of view: (d) presence of aggregates of micellar dimension (arrows and boxes), (e) Mesosize aggregates with regular hollow internal structures (Trigonal dodecahedron/icosahedron?), (h) Giant vesicle of diameter ~200nm (g-i) 0.5 mM TROE in different fields of view: (g) uniformly distributed micellar aggregates, (h) vesicles with distinct bilayer membrane of thickness ~5-7 nm of predominantly square geometry, Hollow concentric circles indicate bilayer thickness. (i) Large spherical vesicle of diameter ~ 150 nm.

Furthermore, the vesicles form stacked-up structures, as is evident from their overlapped contour (indicated by red arrow).[64,65] Absence of well-defined membrane around the periphery of the large ellipsoidal assembly suggests that the formation of this cluster is driven by solvophobic repulsive interactions between the micelles or vesicles and the solvent molecules. It may also be seen that large spherical vesicles, of average diameter of ~100 nm are present alongside the smaller micellar aggregates which are dispersed throughout the field of view (Figure 6 (b)). Larger vesicles of diameter > 200 nm are also present (Figure 6 (c)). Similar co-existence of small micelles (size <8 nm) and vesicles (diameter 20-25 nm) is evident in TYDE (Figure 6 (d)) as well. Closer inspection of HRTEM picture of TYDE aggregates reveals the presence of mesosize aggregates with regular hollow internal structures, which look like trigonal dodecahedron/icosahedron geometry (Figure 6 (e)). The aggregates in TYDE are spheroidal and have diameter ~10-20 nm. These are comparatively more homogeneously distributed (Figure 6 (d)) than TYOE. Besides, there are large number of smaller aggregates of micellar dimension (black dots), evenly distributed within the field of view (Figure 6). However, giant spherical vesicles (diameter ~200 nm) similar to that in TYOE are also observed in TYDE (Figure 6 (f)). In TROE, micellar aggregates of size <10 nm are found dispersed in the medium (Figure 6 (g) indicated by red square), while larger vesicles of average dimension ~60-80 nm, having cubic geometry (indicated by red arrow) are found to co-exist (Figure 6 (h)). Giant vesicles similar to those in TYOE and TYDE are also observed in another field of view (Figure 6 (i)). The membrane bilayer thickness observed in larger vesicles of TYOE, which are relatively less abundant than the smaller ones, is about ~4-6 nm. The TROE consisted of large vesicles with well-defined bilayer boundaries. The bilayer membrane thickness of TROE was ~8-10 nm. The vesicles of TROE are sparsely distributed compared to TYOE and TYDE, and this may be due to much lower concentration of TROE (0.5 mM) compared to TYOE (7.2 mM) and TYDE (9 mM) of the experimental samples.

The presence of the large vesicular aggregates in TYOE, TYDE and TROE was also examined using the dynamic light scattering measurements (DLS), at 303 K (Figure 7). For better understanding, the sample concentrations were kept identical to that used during HRTEM measurement. It is evident that giant aggregates of size 200 nm – 600 nm are present in all the three aminoacid esters. The average hydrodynamic diameter (d_h), of TYOE, TYDE and TROE are obtained as 451 nm, 353 nm and 540 nm

respectively. The results confirm the aggregation of the aminoacid esters into giant vesicles.

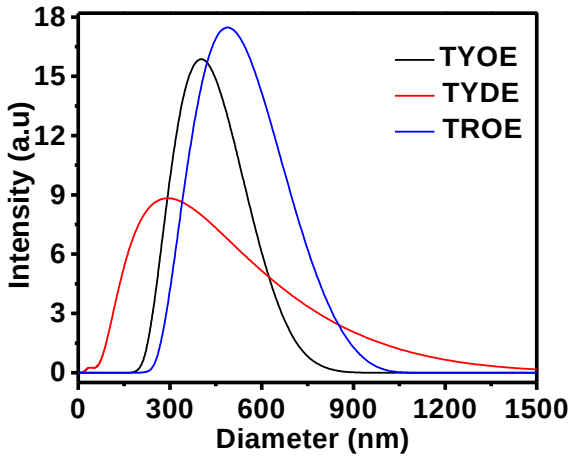

Figure 7. Size distribution of aggregates in aqueous solutions of 7.2 mM TYOE, 9.0 mM TYDE and 0.5 mM TROE as obtained from DLS measurement at 303 K.

Unlike conventional single tailed surfactant systems, TYOE, TYDE and TROE aggregates display rich morphologies as observed from HRTEM study in the absence of any promoter/additive. The key difference of aromatic aminoacid esters from the conventional surfactants is that unlike the later, aminoacid esters contain blocks of hydrophobic and hydrophilic moieties in their molecular structures. This molecular picture is similar to that one witnesses in block copolymer amphiphiles, the self-assembled aggregates of which have attracted wide interests due to creation of a plethora of morphologies.[17,65,66] For these systems which contain multiple number of hydrophobic and hydrophilic blocks, the morphologies are determined by the curvature created in the assembly via relative volume of such water insoluble and water soluble domains. The balance between the hydrophobic and hydrophilic interactions give rise to an optimum surface area (a_0) of hydrophobic block at the interface between hydrophobic and hydrophilic domains. This area, together with the length and volume of hydrophobic block contributes to the packing parameter. In the present amphiphilic systems, viz., TYOE, TYDE and TROE, containing hydrophobic and hydrophilic blocks in the molecule, the geometries and degree of order of the aggregate nanostructures depends on the amphiphile concentration as well as the volume ratio of the water insoluble and water soluble blocks – 'the insoluble soluble ratio (ISR)'.[66,67] As a result, at low concentration, due to the soluble domain compatibility with the solvent, the system may be soluble. On the other hand, at the cac or higher

concentrations, the molecules containing multiple number of blocks self-assemble to form either dispersed isotropic globular phase or larger aggregates with higher order morphology. From the length of hydrophobic and hydrophilic domains for TYOE, TYDE and TROE, as determined by DFT calculations (Figure 1), the corresponding ISR values for these amphiphiles are found to be 4.12, 5.42 and 3.93 respectively (assuming identical cross-sectional area). It may, therefore, be presumed that the surface activity of the above systems would be in the order TYDE > TYOE > TROE, unless major structural discrimination is encountered by them in presence of polar solvent.

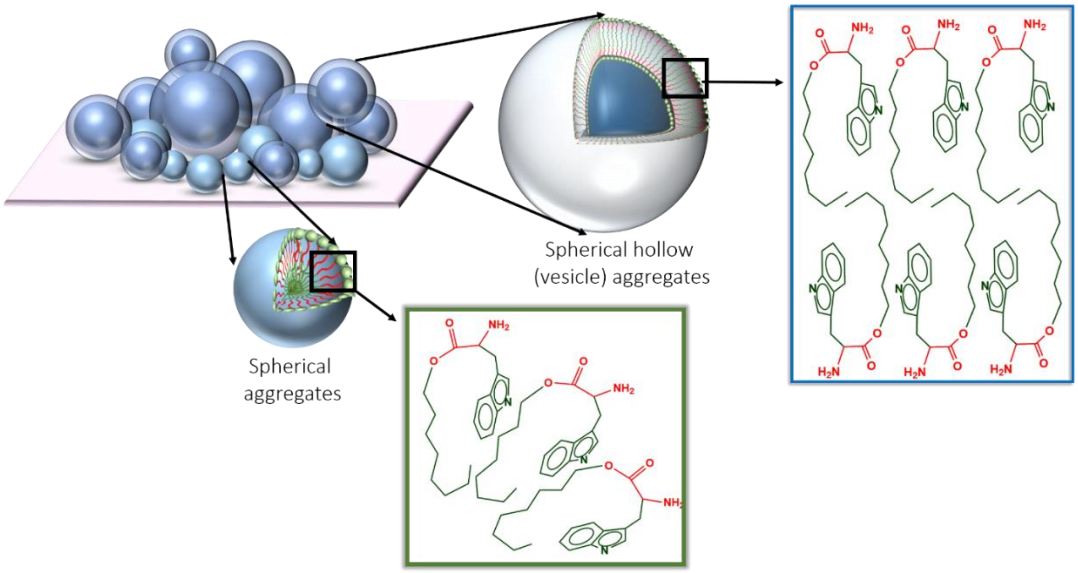

Scheme 5. Schematic representation of possible morphology and orientation of L-Tryptophanoctyl ester molecules in bilayer and micelles.

However, due to segregated structure in presence of solvent, present system deviate from above trend. Therefore, instead of kinetically trapped non equilibrium structures of small vesicles formed by conventional double tailed surfactants with inverted cone/truncated cone like molecular form, thermodynamically stable vesicles and bilayers are formed in present amphiphile systems due to their intrinsic polydispersity. Such polydispersity leads to selective segregation of hydrophobic blocks to the inside of vesicles, whereas hydrophilic blocks segregates to the outside. The preferred curvature of the bilayer is stabilized in this way. The effect is enhanced in smaller vesicles since the tendency to segregate would be greater as interfacial curvature is increased. The various morphologies that are observed in the present systems are primarily a result of inherent molecular curvature of these and how this influences the packing of the amphiphiles in the assemblies. A schematic representation of possible

morphology and orientation of the molecules in bilayer and micelles is shown in Scheme 5. The vesicles which are formed in the present aminoacid ester based amphiphile systems are found to be stable (examined up to 10 days and found stable in terms of size). The conformation of individual aminoacid ester molecule as observed by DFT computation is modified in aqueous aggregates. As is revealed from 2D NMR study, these molecules are further folded in the aggregates due to the interplay between hydrophobic and hydrophilic forces including H-bonding between the polar groups present in the hydrophilic blocks with the water molecules at the interface. Therefore, the driving force of the self-assembly formation is the hydrophobic and hydrophilic interactions along with the non-covalent interactions including H-bonding. The thermodynamic maneuver (enthalpy and entropy) plays a vital role just like the aggregation process as involved in block copolymers and common surfactants in polar solvents. Hydrogen bond formation in aqueous amphiphilic systems have attracted much attention recently, both experimentally and theoretically, because it has been proved of crucial importance on the structural and dynamic properties of self-assembled nanostructural motifs.[67] The array of intramolecular and intermolecular interactions among the blocks within TYOE, TYDE and TROE assemblies in water generates the sophisticated structures. These interactions for the formation and stability of rich morphologies also undoubtedly includes H-bonding network that is formed among interfacially located hydrophilic blocks as well. The difference between the molecular packing predicted from Israelachvili's approach[46] (Section 3.1) and that observed in solvent is, therefore, due to the molecular folding induced by the solvent. In presence of solvent, the aminoacid esters, with the folded aromatic ring behave as the pseudo-double tailed surfactants with truncated cone geometries and the hydrophilic blocks oriented towards the interface act as the "head groups". Such orientation is favored due to strong hydrogen bonding of the polar head groups with the solvent water molecules.[67] Therefore, due to molecular folding in presence of water vis-à-vis segregation of hydrophobic and hydrophilic blocks, the conventional approach of the calculation of packing parameter and the prediction of aggregation morphology in terms of individual molecular geometry is not valid, and hence, does not follow in the present study.[68]

4. Conclusion

Molecular geometries of the models for membrane proteins, viz., TYOE, TYDE and TROE, as determined via energy minimization by DFT calculations, exhibit partial

bending of the aromatic ring (phenol or indole respectively) towards hydrocarbon chain of the molecules. Occurrence of a hydrophilic block (consisting of ethereal oxygen, carbonyl and the amine groups) between two strongly hydrophobic blocks (consisting of phenol/indole ring and the hydrocarbon chain respectively) in the molecular architectures and the obliquely bend molecular geometry leads to form a distinctive amphiphilic system that unveil strong surface active properties in aqueous solutions. The 2D NMR in D_2O reveals that the unique molecular geometry of these tyrosine and tryptophan analogues facilitate strong segregation domain of the two hydrophobic blocks to form within the same molecule and this leads to further folding of the molecules via non-covalent interactions including hydrogen bonding. The display of rich morphology of the exclusive aggregates, as has been witnessed in the present systems, is not only rare for single chain amphiphiles, the biocompatibility of the aromatic aminoacid esters make them highly potential contender for drug delivery vehicle and drug vectors as well. The demonstration of chemically segregated domains with exceptional chemistries and topographies, leading to the formation of bilayer and membrane motifs commands fundamental features of cell membranes and may have important relevance in biotechnology. Further, it points out to the fact that membrane proteins are not just integral dopants in the membrane system but very much set its role as the building blocks of the cell membrane and may act as the stabilizer of the membrane structure as well.

References are provided in BIBLIOGRAPHY under "References for Chapter V" (Page 178-183)

Findings of this chapter has been published in *Langmuir*, **2017**, 33, 6581-6594.

Chapter VI

Interaction of tyrosine analogues with quaternary ammonium head group at micelle/water interface and their influence on aggregation characteristics of cationic micelles

1. Introduction

Most cellular membranes are complex assemblies of different lipids and proteins in which phospholipids are the major building blocks. Phosphatidylcholine (lecithin) is usually the most abundant phospholipid in animals and plants. It is a neutral or zwitterionic phospholipid (with quaternary ammonium cation and phosphate anion) over a range of pH. Membranes are thin, fluidic and highly flexible in nature with low bending modulus and permits selective passage of materials from and into the cells as well as allow lateral flow of membrane components in itself.[1] A number of different types of proteins also form an integral part of the cell membrane. These functional protein molecules are bound to the cell membrane through different mechanism and perform various tasks. Some of these crucial proteins are either *transmembrane proteins* which extend across the lipid bilayer or intercellular *anchored proteins* that do not span the membrane but are covalently attached to the inner surface by fatty acids or phospholipids. *Peripheral proteins* are weakly bound to the membrane surface by non-covalent interactions with other membrane proteins but most of the proteins of the plasma membrane that are exposed to cell surface are covalently linked to some sugar molecules.[2-5] The transmembrane proteins, viz., α-helical bundles and β-barrel proteins, localize aromatic aminoacids (especially, tyrosine, tryptophan and histidine) at the membrane/water interface where they form functionally significant H-bonds with interfacial water. The prevalent understanding is that these residues help the anchoring of membrane proteins to the biological membranes via interaction with the lipid head groups. In membrane proteins, these residues have been demonstrated to orient themselves to face the lipid head groups and are part of the so called 'aromatic belt'.[6-9] A highly significant non-covalent interaction, which is believed to occur abundantly in biological systems is cation-π interactions, the weak attractive interactions that exist between cationic species and π-electron cloud of aromatic ring.[10-13] However, the relevance of this interaction in biological structures has been recognized only in recent

years. While the majority of x-ray crystal structure analysis reveals cation-π interaction as one of the main forces that stabilizes protein folding and protein complexes with small molecules, most of the above findings are the results achieved through indirect experiments. Therefore, investigation aimed at individual interactions by other lead techniques are of extreme importance for better understanding of the forces in complex biological organizations.[14-16] Furthermore, neurotransmitters transmit signals across a chemical synapse from one neuron (nerve cell) to another target neuron where the synapse binds specific receptor in the membrane. It is understood that almost all the neurotransmitters contain a cationic center and a common strategy for biological recognition of cation is the cation-π interaction. The nicotinic acetylcholine receptor is the example of ligand-gated ion channel.[17,18] A number of aromatic aminoacids have been identified as contributing to the agonist binding site, suggesting that cation-π interaction is involved in binding the quaternary amino group of the agonist, acetylcholine. Therefore, it is imperative to say that studies on the interaction of aromatic aminoacids with such cationic species as quaternary ammonium group at the membrane/water interface is of particular importance. But, surprisingly, report of such a fundamental study is lacking in the literature. In view of the inherent complexity of the biomembrane systems, use of suitable models for the aromatic aminoacid residues of such proteins would indeed be helpful. In spite of the importance, very few model systems have been developed that could help understand the behavior of aromatic aminoacids viz., tyrosine and tryptophan residues in the membrane. Tyrosine and tryptophan octyl esters are recognized as the important models for the membrane bound aromatic residues.[19-24] It is interesting to note that fluorescence properties of long chain esters of tryptophan (L-Tryptophanoctyl ester), incorporated in model membrane of surfactant micelles, have been shown to be similar to that of tryptophan residue of transmembrane proteins. In the previous chapter, it has been shown that occurrence of hydrophilic and hydrophobic blocks in octyl and dodecyl esters of tyrosine as well as in octyl ester of tryptophan, leads to molecular bending of these aromatic systems in aqueous solutions and eventually fascinating high order morphology of the exclusive aggregates are formed.[25] These self-assembled systems also exhibit high promise toward application as bio-inspired drug carriers.

It will be interesting to pay attention as well, in this context, to the shape of biological membrane and the mechanism of its tuning in various vital processes like cell fusion

and fission. Biological membranes exhibit various function-related shapes, and the mechanism by which these shapes are created is largely unclear. It is generally believed that the changes of membrane topology is produced as a result of a complex interplay between membrane proteins, lipids and certain physical forces. Therefore, it is also tempting to explore whether the aromatic amino acid residues of transmembrane proteins can have any role to play in controlling shape transition of the membranes near head group of phosphatidylcholine.

2. Materials and Methods

2.1. Materials

L-Tyrosineoctyl ester (TYOE) and L-Tyrosine dodecyl ester (TYDE) were synthesized in our laboratory following the procedure published previously.[3] CTAB was purchased from Fluka (Switzerland). D_2O for NMR study was purchased from Aldrich (USA). Purity of all the chemicals were greater than 99.5% and were used as received. All experiments were done with de-ionised and doubly distilled water with pH 6.5-7 and specific conductance below $2\mu S.cm^{-1}$.

2.2. Methods

2.2.1. Tensiometry. Tensiometric measurements were performed on Krùss K9 Tensiometer (Germany), based on Du-Nóuy ring detachment method, fitted with Omniiset temperature bath with precision ± 0.1^0C. Before each measurement, the platinum ring was thoroughly cleaned with 1:1 acetone-water solution and heated under oxidizing flame until glowing temperature was attained. After every addition, the experimental solution was stirred for 5 minutes for homogeneity and equilibrated for 10 minutes. For each measurement, three to five subsequent readings were taken for concordance. Standard deviation was < 0.1 $mN.m^{-1}$.

2.2.2. pH measurements. The pH of the solutions were measured using Systronics digital pH meter (Model: 335, India), calibrated with standard buffers of pH 4.0 and 9.2. Solutions were equilibrated for 5 min after addition of acid/alkali till a steady pH meter reading was observed.

2.2.3. UV-Vis Spectroscopy. UV-Vis study was carried on Jasco V 530 Spectrophotometer fitted with a tungsten filament. A matched pair of glass cuvette of

optical length 1 cm was used for control and sample solutions. The solutions were allowed to equilibrate for 10 minutes before each measurement.

2.2.4. Fluorescence spectroscopy. Steady state fluorescence emission study was carried out in bench top spectrofluorimeter from Photon Technologies International (Quantamaster-40, USA) with excitation and emission slit widths fixed at 3.0 nm and 2.5 nm respectively. Steady state anisotropy (r) was determined using the following expressions[26]

$$r = \frac{I_{VV} - GI_{VH}}{I_{VV} + 2GI_{VH}} \text{ and } G = I_{HH}/I_{HV} \quad \text{(i)}$$

where I_{VV} and I_{VH} represent the intensities obtained with the excitation polarizer oriented vertically and the emission polarizer oriented vertically and horizontally respectively; I_{HV} and I_{HH} refer to the similar parameters as mentioned above for the horizontal positions of the excitation polarizer. The anisotropy values were averaged over an integration time of 60 seconds. Samples were taken in Hellma quartz cuvette of optical length 1.0 cm.

2.2.5. Nuclear Magnetic Resonance Spectroscopy (NMR). ^{1}H NMR experiments were performed in Bruker (Germany) ADVANCE spectrometer operating at 400 MHz. Signals are quoted as δ values in ppm using residual protonated solvent signals as internal standard (D_2O: δ 4.79 ppm). Respective solutions were made in D_2O and 0.6 mL of the same was used for each measurement. Data are reported as chemical shift. 2D Nuclear Overhauser effect spectroscopy (NOESY) spectra was studied using Brucker standard software acquisition program noesyphpr in phase-sensitive mode using 5 mm BBO probe. An acquisition time of 0.085 sec and relaxation delay of 2 sec was used between the scans. The mixing time was 300 milisec. A total number of 2048 complex point were collected. Number of 16 scans were undertaken.

2.2.6. Small Angle Neutron Scattering (SANS). The SANS measurements were carried out using small angle neutron scattering diffractometer at the Dhruva reactor, Bhabha Atomic Research Centre, Trombay, India. The diffractometer uses a beryllium oxide filtered beam with a mean wavelength (λ) of 5.2 Å. The angular distribution of the scattered neutrons is recorded using a one-dimensional (1D) position-sensitive detector (PSD). The accessible wave vector transfer ($Q = 4\pi \sin\theta/\lambda$, where 2θ is the scattering angle) range of the diffractometer is 0.017-0.35 Å^{-1}. The PSD allows

simultaneous recording of data over the full Q. The samples were held in a quartz sample holder of 0.5 cm thickness. The measured SANS data have been corrected and normalized to absolute unit (as cross-section per unit volume), using standard procedures.

2.2.7. Cryogenic Transmission Electron Microscopy (Cryo-TEM). Samples for Cryo-TEM were prepared in controlled environment vitrification system (CEVS). A drop of sample solution was added to 300 mesh copper support grid coated with carbon film. Excess sample was blotted carefully. For vitrification, the TEM grids were plunged rapidly in liquid ethane at -183^{0}C, and stored in liquid nitrogen. The Cryo-TEM images were obtained with Hitachi H-7650 microscope (Japan) operating at accelerating voltage of 120 kV.

2.2.8. Rheology. The rheological experiments were done using cone-plate geometry with 4^0 truncation angle, with diameter 25 mm and sample gap of 0.105 mm sample gap in MCR 302 rheometer (Anton Paar, Germany) equipped with Peltier temperature control system. The samples were initially stirred at 60^{0}C for three hours for homogenization and equilibrated for 72 hrs. During measurement, samples were equilibrated for 10 mins at each temperature.[27]

2.3. Analysis of SANS data

For a system of monodispersed interacting particles, the differential scattering cross-section per unit volume ($d\Sigma/d\Omega$) may be expressed as a function of scattering vector Q as:

$$\frac{d\Sigma}{d\Omega} = n\,(\rho_m - \rho_s)^2\, V^2\, [\langle F(Q)^2\rangle + \langle F(Q)\rangle^2 (S(Q)-1)] + B \qquad (1)$$

where n is the number density of micelles, ρ_m and ρ_s are the scattering length densities of the micelle and the solvent, respectively, and V is the volume of the micelle. F(Q) denotes the single-particle form factor which is the characteristic of specific size and the shape of the scatterer, and S(Q) denotes the interparticle structure factor. B is a constant, which represents the incoherent scattering background. The F(Q) is calculated by treating the micelles as prolate ellipsoids, using the equations:[28]

$$\langle F(q)^2\rangle = \int_0^1 [F(q,\mu)]^2\, d\mu \qquad (2)$$

$$\langle F(q)\rangle^2 = \int_0^1 [F(q,\mu)\, d\mu]^2 \quad (3)$$

$$F(q,\mu) = \frac{3(\sin x - x\cos x)}{x^3} \quad (4)$$

$$x = q[a^2\mu^2 + b^2(1-\mu^2)} \quad (5)$$

where a and b are the semimajor and semiminor axes of an ellipsoidal micelle, respectively, and μ is the cosine of the angle between the directions of a and the wave vector transfer Q. The interparticle structure factor S(Q) identifies the correlation between the centers of different micelles, and it is the Fourier transform of the radial distribution function g(r) for the mass centers of the micelle. S(Q) is calculated using expressions derived by Hayter and Penfold from the Ornstein-Zernike equation and using the rescaled mean spherical approximation.[29] To simplify the calculation of S(Q), the micelle is assumed to be a rigid equivalent sphere of radius $\sigma = (ab^2)^{1/3}$ interacting through a screened Coulomb potential.

3. Results and Discussion

3.1. Surface properties of CTAB-TYOE/TYDE mixtures

The cac and other physico-chemical properties of TYOE and TYDE are reported in Chapter V.[25] In the present chapter, the surface and other related properties of TYOE and TYDE, in presence of CTAB is examined. On the one hand, the cmc values of CTAB decrease significantly as a function of TYOE or TYDE concentrations and the system display significant improvement of surface and bulk properties. On the other hand, the values of γ_{cmc} of the system (in the composition regime of x_1= 0 to x_1=1) are much lower than that of pure CTAB (x_1=1) or TYOE/TYDE (x_2=0). The pC_{20} (negative logarithm of surfactant concentration pure required to reduce the surface tension of water by 20 units at the temperature of measurement) values of the mixed systems are found to be much higher than that of CTAB.

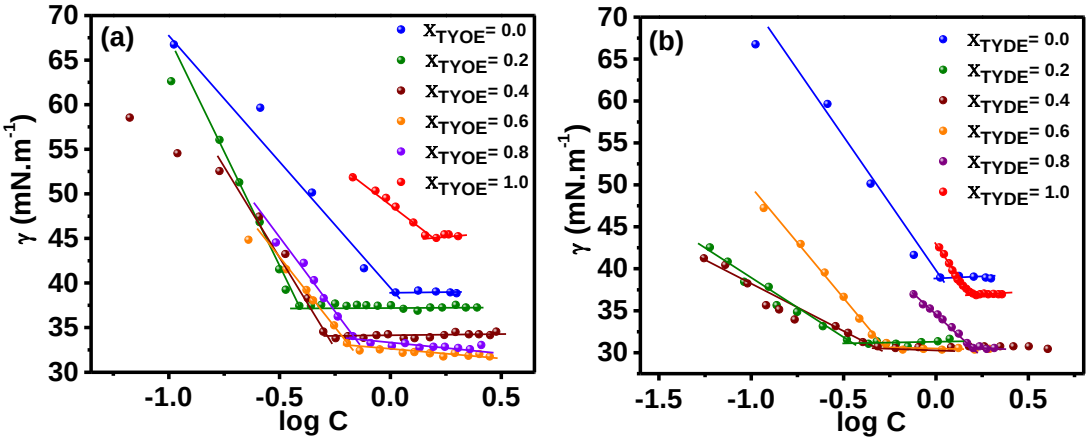

Figure 1. Variation of surface tension of CTAB in presence of (a) TYOE, (b) TYDE, as function of mole fraction at 303 K. C denotes the concentration of CTAB within the mixed systems.

Since the cac value of TYOE (cac = 1.81 mM) and TYDE (cac = 1.31 mM) is much higher than that of CTAB (cmc = 0.9 mM), the cmc of mixed system gives a minima at the aminoacid ester composition of x_1 = 0.2 for both TYOE and TYDE and predictably consistent value of 0.9 mM ($x_{TYOE/TYDE}$ = 0.0) and 1.49 mM (at x_{TYOE} = 1) and 1.45 mM (at x_{TYDE} = 1) for octyl and dodecyl esters of tyrosine respectively. The strong synergism in surface properties as observed at x_{TYOE} and x_{TYDE} of 0.2, is attributed to the electrostatic interaction between the π-electron face of tyrosine ester with quaternary ammonia groups of CTAB. This interaction stabilizes ester-CTAB pairs as the pseudo double tailed surfactant systems, resulting in the stronger hydrophobic interactions in the mixed micelle core and lowers cmc of the system. The CTAB-TYOE/TYDE systems may, therefore, be assumed to behave as mixed surfactant solution.[30] The nature of mixing may be evaluated on basis of Clint's approach. For any mixed component system, the cac is related to individual component as:[31]

$$\frac{1}{cac_{mix}} = \sum_{i=1}^{n} \frac{x_i}{f_{i.}cac_i} \tag{6}$$

where cac_i and cac_{mix} are the cac of the i^{th} component and the mixed surfactant system respectively, x_i and f_i are the mole fractions and activity coefficients of the respective i^{th} component in the mixed aggregate. For ideal mixing, f_i = 1, and Equation 6 may be applied to the present systems as:

$$\frac{1}{cac_{ideal}} = \frac{x_1}{cac_1} + \frac{(1-x_1)}{cac_2} \tag{7}$$

where 1 denotes CTAB and 2 denotes the respective aminoacid esters.

The cac_{ideal} for the mixed systems have been calculated and presented in Table 1. It is evident that the cac of the mixed system deviate significantly from the cac_{ideal}, which reveals that the interaction between the CTAB and the aminoacid ester molecules is non-ideal in nature. The much lower values of cac, along with the tendency of TYOE and TYDE to lower the interfacial tension of CTAB indicates that both TYOE and TYDE molecules synergistically interact with CTAB and modify the aggregation characteristics of CTAB micelles.[32,33] For more insight on the modification of interfacial property of CTAB in presence of TYOE and TYDE, surface parameters viz., equilibrium surface pressure, Π_{cac}, the total surface excess (Γ_{max}^{tot}) and the minimum surface area per molecule (A_{min}^{tot}) of the CTAB-aminoacid ester mixed systems are evaluated (Table 1). Increase in Π_{cac} of CTAB from 32.1 $mN.m^{-1}$,[34] (at $\chi_{TYOE/TYDE} = 0$) to 38.8 $mN.m^{-1}$ at χ_{TYOE} = 0.6 (Table 1) and to 40.9 $mN.m^{-1}$ at χ_{TYDE} = 0.6 indicates enhanced efficiency of surface tension reduction in the mixed surfactant system at these compositions compared to pure CTAB.[35] The A_{min}^{tot}, which is the minimum surface area occupied by a surfactant component at the air-water interface, have been calculated using Gibbs adsorption isotherm (Table 1).[36] The lower A_{min}^{tot} in CTAB-TYOE system, at $\chi_{TYOE=}$0.2 and 0.4, *viz.,* 0.2 and 0.4 nm^2/molecule respectively compared to the individual components, i.e., 0.24 nm^2/molecule for CTAB and 0.49 nm^2/molecule for TYOE, suggest that the mutual repulsion between the surfactant head groups is reduced at these compositions and the components pack closer at the interface.[30] Interestingly, the CTAB-TYDE systems exhibit higher values of A_{min}^{tot} compared to individual surfactants at all compositions (Table 1) indicating much higher hydrophobicity.[35]

3.2. CTAB -TYOE/TYDE interaction

The interaction parameter β, as defined by the regular solution theory, is useful in characterizing the nature and degree of interaction between two nonhomogeneous amphiphile molecules in solution. The β value explains the interaction between the head groups of surfactants. Interestingly, it does not include the interaction between hydrocarbon chains of the amphiphiles when the lengths of the chain are different. The interaction parameter β is determined by measuring cmc of the mixtures of CTAB with aromatic aminoacid esters. The degree of head group interaction in the mixed aggregate systems is measured by calculating β from the equation derived from Rubingh's[37]

theory of non-ideal mixing (Equation 2 in Appendix C). The values of the interaction parameter as determined for the present system is listed in Table 1.

Table 1. Critical aggregation concentration (cac), cac_{ideal}, i.e., cac predicted using Clint's equation; surface parameters viz., equilibrium surface tension (γ_{cac}), surface pressure at cac (Π_{cac}), maximum surface excess concentration (Γ_{max}), minimum surface area per monomer (A_{min}); interaction parameter (β), activity coefficient of CTAB (f_1) and aminoacid esters (f_2) as a function of mole fraction of TYOE and TYDE respectively, in aqueous medium at 303 K

X_{TYOE}	cac_{ideal} (mM)	cac (mM)	γ_{cac} (mN.m^{-1})	Π_{cac} (mN.m-1)	$10^6\ \Gamma_{max}$ (mol.m^{-2})	A_{min} (nm^2 /molecule)	β	f_1	f_2
				TYOE					
0.0	-	0.89	39.1	32.1	6.98	0.24	-	-	-
0.2	0.99	0.36	37.5	33.7	9.08	0.18	-5.26	0.045	0.116
0.4	1.12	0.53	34.1	37.1	8.27	0.20	-3.24	0.126	0.312
0.6	1.28	0.70	32.4	38.8	5.71	0.29	-2.36	0.183	0.515
0.8	1.49	0.72	33.1	38.1	6.09	0.27	-3.01	0.086	0.573
1.0	-	1.81	45.1	26.1	3.38	0.49	-	-	-
X_{TYDE}				TYDE					
0.0	-	0.89	39.1	32.1	6.98	0.24	-	-	-
0.2	0.95	0.38	30.9	40.3	2.54	0.65	-4.47	0.067	0.169
0.4	1.02	0.50	30.4	40.8	2.53	0.65	-2.83	0.147	0.397
0.6	1.10	0.55	30.3	40.9	4.91	0.34	-2.63	0.136	0.532
0.8	1.19	1.29	30.4	40.8	3.55	0.47	-1.71	0.262	0.684
1.0	-	1.31	37.8	33.4	5.29	0.31	-	-	-

A number of interesting features are apparent. The β values for all compositions of binary mixtures are negative, indicating more attractive interaction to exist in the mixed micelles compared to the self-assembly of the individual amphiphile. According to the regular solution theory, the β parameter should be independent of composition. Indeed, the β parameter values in the present study lie within close range of (2.91-2.56) and (2.31-2.09) for CTAB-TYOE and CTAB-TYDE respectively in the composition (x) regimes of x_1 =0.4 - 0.8. At low and high x, the β is more negative due to self-assemblies of the CTAB and aminoacid esters respectively rather than mixed micelle formation. It is also interesting to mention that the average value of β ($x_1 \rightarrow$ 0.4 - 0.8) for CTAB-TYOE and CTAB-TYDE mixtures are found to be -2.72 and -2.35 respectively. This indicates that the interaction between quaternary ammonia head groups of CTAB with aromatic aminoacid esters is stronger in TYOE compared to TYDE, although the TYDE molecules contains longer hydrocarbon chain in its molecular framework. This result is indeed surprising and needs to be examined carefully by means of subsequent experiments.

3.3. UV-Vis absorption and study of micropolarity.

UV-Vis absorption spectra of 0.2 mM aqueous TYOE exhibit a red shift of about 3 nm with $\lambda_{max,}$ varying from 274 nm to 277 nm, upon addition of CTAB (Figure 2). Aromatic compounds, in general, exhibit two strongly overlapped bands in the near UV region, viz., longitudinally polarized $^1L_a \leftarrow {}^1A$ and the transversely polarized $^1L_b \leftarrow {}^1A$ band.[38] Distinct isobestic points at 297 nm, 270 nm and 246 nm are observed in the spectra for sub micellar concentration regime, indicating that the interaction between the aromatic aminoacid and the quaternary ammonium ion head groups to occur even at the water/air interface, prior to self-assembly formation of CTAB in aqueous solution. The absorbance-concentration profile at the $\lambda_{max,}$ exhibits linear variation with a break point close to cmc. This shows that the interaction of amino acid esters with CTAB molecules is fairly strong and the aromatic esters are embedded rather strongly once the micelles of CTAB are formed above the cmc. The energy associated with this apparently small shift in the λ_{max} is found to be nearly 1.13 kcal.mol^{-1}. It is interesting to note that in a theoretical study, the energy involved in cation-π interaction in solvent separated quaternary ammonia-benzene system in aqueous media has been shown to be 1.67 kcal.mol^{-1}. The folded molecular geometry of TYOE molecules are probably embedded in the CTAB micelles with the hydrophilic block consisting of ethereal oxygen, amine

and carbonyls groups protruded toward the interfacial water and the aromatic face of TYOE molecule is arranged near the quaternary ammonium head group. Presence of isobestic points, both in pre and post micellar regions (shown in Figure 3) indicates that interaction between CTAB headgroups and aromatic moieties of esters takes place at the solution interface (pre micellar regime) as well as in the bulk (post micellar regime).

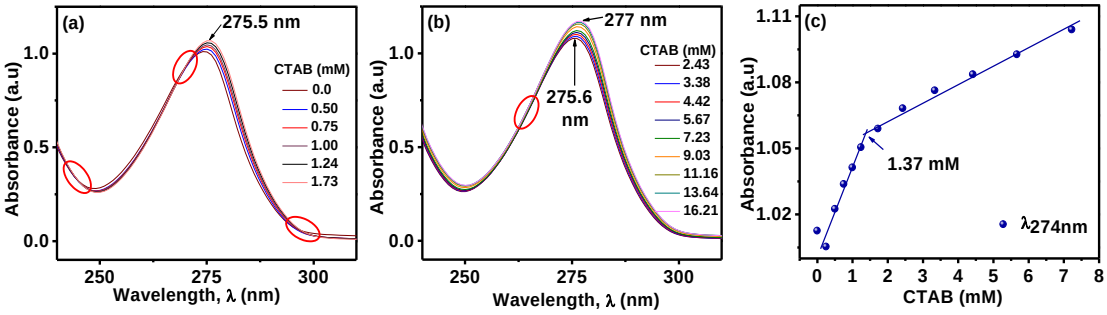

Figure 2 (a) Effect of addition of CTAB in the pre-micellar regime on absorption spectra of 0.2 mM aqueous TYOE at 303 K, (b) Effect of addition of CTAB in the post-micellar regime on absorption spectra of 0.2 mM aqueous TYOE at 303 K, (c) Variation of absorption intensity of 0.2 mM TYOE at 274 nm with CTAB concentration at 303 K.

In the case of 0.2 mM TYDE, the intensity at absorption at λ_{max} 277 nm (initially decreases (upto 1.27 mM which is slightly above the cmc of CTAB, i.e. 0.9 mM) (Figure 3 (a)) and increases thereafter (Figure 3 (b)) in the post-micellar region. An isobestic point is observed at 265 nm. A red shift of 1 nm was observed in the post-micellar region, where absorption maxima varies from 277 nm to 278 nm.

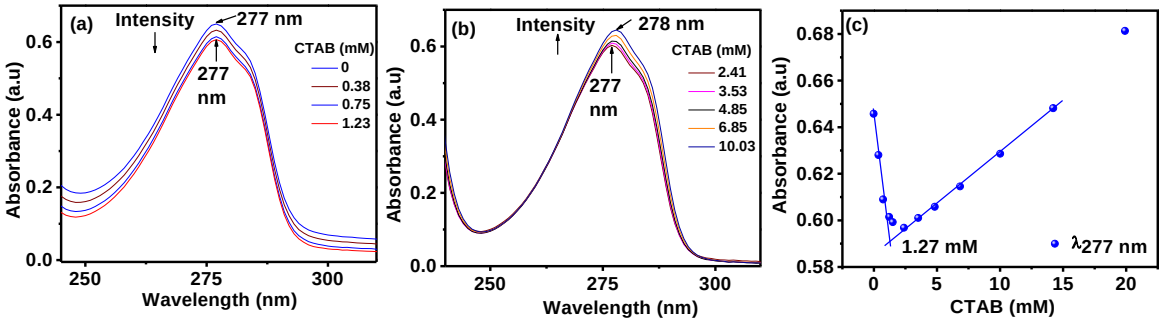

Figure 3 (a, b) Effect of addition of CTAB on absorption spectra of 0.2 mM aqueous TYDE at 303 K, (c) Variation of absorption intensity of 0.2 mM TYDE at 274 nm and 276 nm with CTAB concentration at 303 K.

The contrasting result may originate from the rigidity of folded geometry of TYDE molecule, the aromatic group of which flips upward due to a slight obliquely tilted alkyl

chain inside the micelle core via stronger force of hydrophobic interactions. As a result, the phenol group of TYDE localizes to little deeper in bulk water, diminishing the interaction with the head group.

An important aspect of tyrosine is its pH dependent dissociation of the phenolic OH proton in aqueous solution. Study of the micropolarity of the charged interface could also provide a better understanding of the exact nature of the location of the OH groups at the vicinity of CTAB micelles. Any changes in surface potential and polarity at the charged interface would be reflected in the acid-base equilibrium of the dissociation of the hydroxyl protons.[39,40] Therefore, determination of the pKa values and its changes could provide vital information about the underlying interaction phenomenon occurring within the CTAB-aminoacid ester systems. Assuming the dissociation of the hydroxyl proton of the tyrosine moiety as:[41]

$$R - OH + H_2O = RO^- + H_3O^+$$

where $R - OH$, RO^-, H_3O^+ are the deprotonated, protonated (neutral) form of the phenolic OH group of the aminoacid esters, viz., TYOE and TYDE, and the hydrated proton respectively. Change in UV spectra as a function of bulk aqueous pH provide the apparent pKa values using Handerson-Hanselbach equation-

$$pK_a = pH - log[\frac{RO^-}{ROH}] \quad (8)$$

The quantity $[\frac{RO^-}{ROH}]$ is determined as $\frac{[A-A_{ROH}]}{A_{OH^--A}}$ where *A*, A_{ROH}, A_{OH^-} are absorbances of the aminoacid esters at experimental, low and high pH's respectively. The pK_a^{obs} may be separated into electrostatic and non-electrostatic components respectively as follows:

$$pK_a^{obs} = pK_a^0 - \frac{e.\psi_0}{2.303kT} \quad (9)$$

where pK_a^0 is the apparent pK_a^{obs} in absence of any surface potential i.e., at . ψ_0 = zero. Comparing the pK_a^0 values of the aminoacid esters in aqueous CTAB micellar media to the pK_a in aqueous-organic mixtures viz., 1,4-Dioxane – water mixtures, will provide the necessary information about the acid-base equilibria at the micellar interface. Defining apparent pK_a in aqueous-organic solvent mixtures, pK_a^m, as:

$$pK_a^m = B + logU_H^0 - \log\left[\frac{RO^-}{ROH}\right] - \log\left[\frac{\gamma_{OH^-}^m}{\gamma_{ROH}^m}\right] \quad (10)$$

where γ^m term denotes the respective activity coefficients, B is the pH meter reading and $logU_H^0$ is the associated correction factor. The pK_a^0 values relate to an interfacial phenomenon whereas the pH measured is that of the bulk solution. Therefore, while comparing between the pK_a in 1,4-Dioxane-water mixture and pK_a^0 in the micellar systems, the primary medium effect on the proton, ${}_m\gamma_{H^+}$, needs to be considered, i.e., pK_a^0 should be compared with pK_a^i rather than pK_a^m, where i stand for interface. These are related as:

$$pK_a^i = pK_a^m + {}_m\gamma_{H^+} \quad (11)$$

Usually, the mean primary medium effect on HCl, ${}_m\gamma_{\pm}$ approximately gives ${}_m\gamma_{H^+}$. The values of ${}_m\gamma_{\pm}$ and U_H^0 are adopted from works of Drummond and co-workers.[39,40] In determining the pK_a^0 values for aminoacid esters in the CTAB micelles, a surface potential of ±141mV is assigned to CTAB.[40] Comparing ΔpK_a^0 of micellar surface and ΔpK_a^i in 1,4-dioxane-water mixtures, the effective dielectric constant, D_{eff} , of the medium at the location of the dissociable proton is found out. The evaluation of the effective dielectric constant considers the underlying assumptions are- (i) both the protonated and the deprotonated forms of the aminoacid esters are quantitatively partitioned within the micellar phase at high CTAB-aminoacid ester ratio, and (ii) since the concentration of the aminoacid esters is low, the activity coefficients terms $\frac{\gamma_{OH^-}^m}{\gamma_{ROH}^m}$ can be neglected such that ΔpK_a^0 can be compared to ΔpK_a^i in different solvent media. The results of pH metric titrations are summarized in Table 2. (UV Absorptions plots as function of pH are provided in Figure S1of SI). The pK_a^w of the phenolic –OH of the tyrosinate moiety in TYOE and TYDE in aqueous media at 298 K was found to be 9.05 and 9.25 respectively for TYOE and TYDE which is close to that of L-Tyrosine in aqueous media (pK_a^w 9.35).[42] The D_{eff} decreases only very slightly on increasing CTAB concentration from 50 mM to 100 mM. Previous study based on solvatochromic visible absorption maxima on CTAB micelles show that the D_{eff} at the micellar interface is around 28-33. In a similar study of CTAB micelles, the D_{eff} in presence of 1 Naphthol was found to vary within 49-51 for 50 mM and 100 mM CTAB.[43] It was concluded that the hydroxy group of 1 Naphthol were directed away from the micellar

surface and resided at a more polar environment. Present study shows that the D_{eff} for TYOE ranges within 40.8 to 40.2 while that for TYDE ranges from 56.9 to 57.9 for 50 mM and 100 mM CTAB respectively (Table 2) which is much higher than that at the CTAB micellar interface. Therefore, it may be said that both TYOE and TYDE locate in such a manner that their OH groups are directed away from the micellar interface, and towards the bulk of the aqueous solvent which is highly polar (D_e of water = 78). Moreover, compared to TYOE, the phenolic OH in TYDE reside further away from CTAB micellar interface, while the phenolic ring of TYOE is located relatively nearer to the CTAB micelles. One of the reasons behind this orientation may be the higher hydrophobic character of TYDE compared to TYOE due to its longer hydrophobic alkyl chain. Nevertheless, this study explains the less interaction of the TYDE molecules with CTAB micelles as observed from SANS study (discussed later).

Table 2: Results of pH titration of 0.2mM TYOE and 0.2 mM TYDE in aqueous solution and aqueous CTAB solutions at 298 K.

CTAB Concentration (mM)	pK_a^w	pK_a^{obs}	ΔpK_a^{obs}	pK_a^0	ΔpK_a^0	D_{eff}
			TYOE			
50 mM	9.055	9.82	2.12	12.20	4.5	40.8
100 mM		10.02	2.31	12.34	4.69	40.2
			TYDE			
50 mM	9.25	10.08	4.6	12.46	3.21	57.9
100 mM		10.53	5.05	12.91	3.66	56.9

3.4. Fluorescence depolarization and steady state emission study.

The degree of depolarization of fluorescence emission of a fluorophore is an index of rotational diffusion during the lifetime of its excited state. Any alterations in microstructure of fluorophore is reflected in the micro viscosity of the probes and hence in their anisotropy values. Therefore this technique is widely employed in exploring the structural modifications of micro heterogeneous systems.[44] As the tyrosine moiety in TYOE and TYDE, are fluorescent active species,[42] fluorescence steady state anisotropy study was done to gain further insight on change in microenvironment of the TYOE and TYDE molecules in presence of the CTAB micelles. Figure 4 shows the variation

of fluorescence anisotropy of 5μM aqueous TYOE and TYDE solutions as function of CTAB concentration at 303 K.

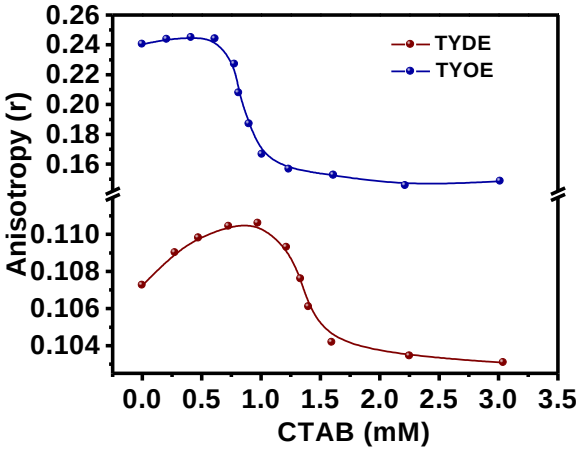

Figure 4. Variation of steady state fluorescence anisotropy of 5 μM aqueous TYOE and 5 μM aqueous TYDE as function of CTAB concentration at 303 K.

It is evident that, the initial anisotropy value (r_0) of TYDE in aqueous solution i.e., 0.24, is much higher compared to TYOE i.e., 0.11. Higher r_0 value imply greater rotational restriction experienced by TYDE in solution. This may arise due to tighter packing of the longer alkyl chains in TYDE compared to TYOE. Figure 4 shows that on increasing CTAB concentration, the anisotropy increases up to a certain point after which, the value diminishes progressively. This critical concentration limit is found to be 1.01 mM in TYOE and 0.66 mM, in TYDE. In both the cases, it corresponds to a concentration near to the cmc of CTAB (0.89 mM). This shows that the aminoacid ester molecules, which act as fluorescent probes, bind with the CTAB monomers till micellization occurs. The cationic micelles consist of a nearly water-free hydrophobic micellar core with polar head groups forming the palisade layer. As CTAB is present in large excess (probe: CTAB~1:120, at cmc) it may be assumed that at cmc, all the probe molecules are bound to the CTAB micelles. Further addition of CTAB increases the number of micelles in solution. The constant population of probes is therefore now redistributed within the enhanced number of micelles and hence we observe the decrease in anisotropy values. The fluorescence emission spectra of 5 μM TYOE and 5 μM TYDE in presence of the CTAB micelles are shown in Figure 5. Upon excitation at the wavelength of maximum absorption, the neutral form of tyrosine emits near 303 nm while the tyrosinate form emits near 340 nm.[42] The emission intensity increases on addition of the CTAB in both TYOE and TYDE (Figure 5 (a), (b)). Insets show that

there exists a break in the intensity vs concentration plots, at 1.05 mM in TYOE and at 0.99 mM in TYDE, which corresponds to the respective cmc of CTAB. This observation corroborates the trend observed in anisotropic behavior of the aminoacid esters. The relative intensities of the neutral (I_N) and tyrosinate (I_T) form depend upon the surrounding medium i.e., in presence of proton acceptor, the tyrosinate band is expected to predominate whereas the neutral form will dominate when no proton acceptor is present in the immediate vicinity.[42]

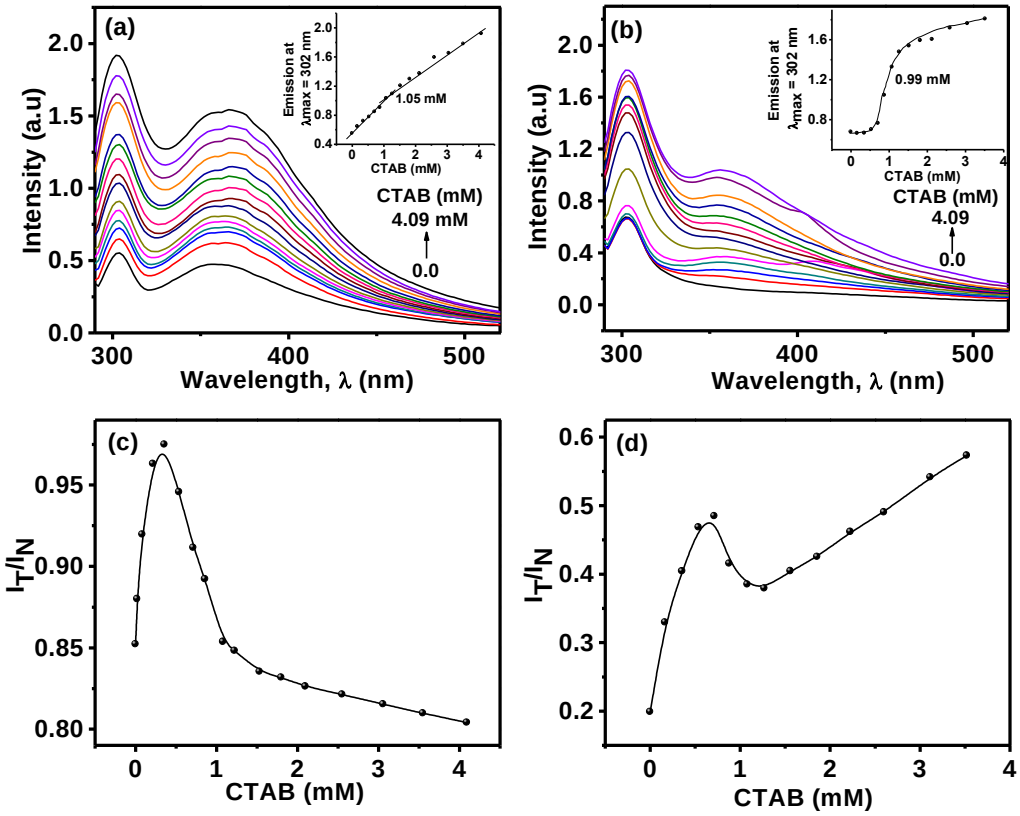

Figure 5. Modification of steady state fluorescence emission spectra of (a) 5µM aqueous TYOE (b) 5µM aqueous TYDE, as function of CTAB concentration at 303 K. Insets display emission at λ_{max} (neutral) as function of respective concentration, Plots of ratio of anionic (I_T i.e tyrosinate emission) to neutral (I_N) emission or, (I_T/I_N) as function of CTAB concentration of (c) 5µM aqueous TYOE and (d) 5µM aqueous TYDE, at 303 K.

Greater inherent positive charge imply higher concentration of hydroxyl ions in immediate vicinity which may act as proton acceptor.[45] The initial linear increase in the ratio of I_T/I_N in both TYOE and TYDE show that proton transfer from the phenolic hydroxy group of tyrosine moiety is facilitated as concentration of micelles increase (Figure 5 (c), (d)). The decrease thereafter indicate that the neutral form in present in excess and that the micelles do not act effectively as proton acceptor.

3.5.1. ^{1}H NMR Study

^{1}H NMR Study is an important tool for identifying the time-averaged location of aromatic solubilized species within surfactant micelles, based on the dependence of chemical shifts of protons in surfactant and aromatic units, on the composition of the aqueous phase. In order to investigate on the relative arrangement of the model aminoacid molecules, viz., TYOE and TYDE with the CTAB molecules in the mixed systems, ^{1}H NMR spectra of the mixture were recorded in aqueous medium (D_2O). The molecular structure and proton numbering of CTAB, TYOE and TYDE are given in Scheme 1.

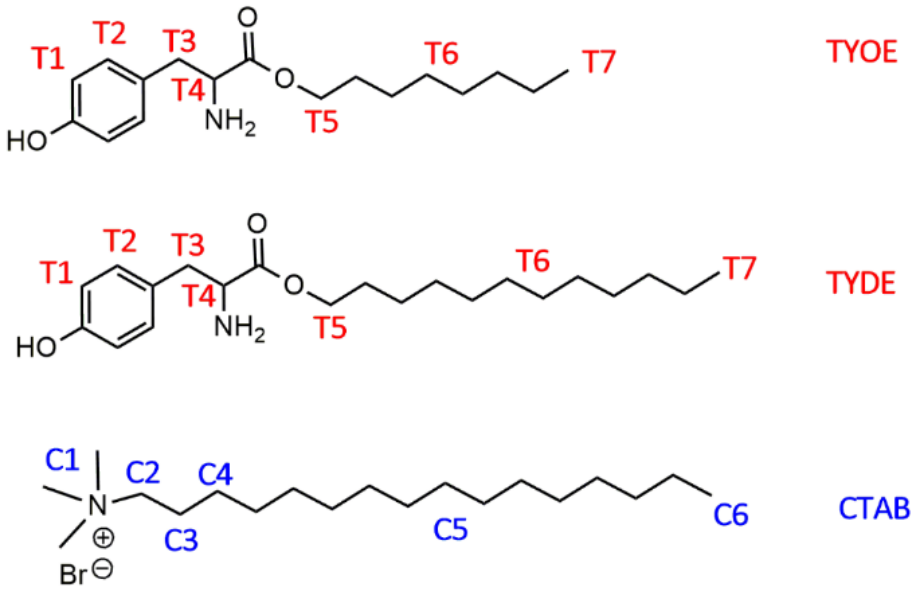

Scheme 1. Schematic presentation of structures and proton numbering of TYOE, TYDE and CTAB.

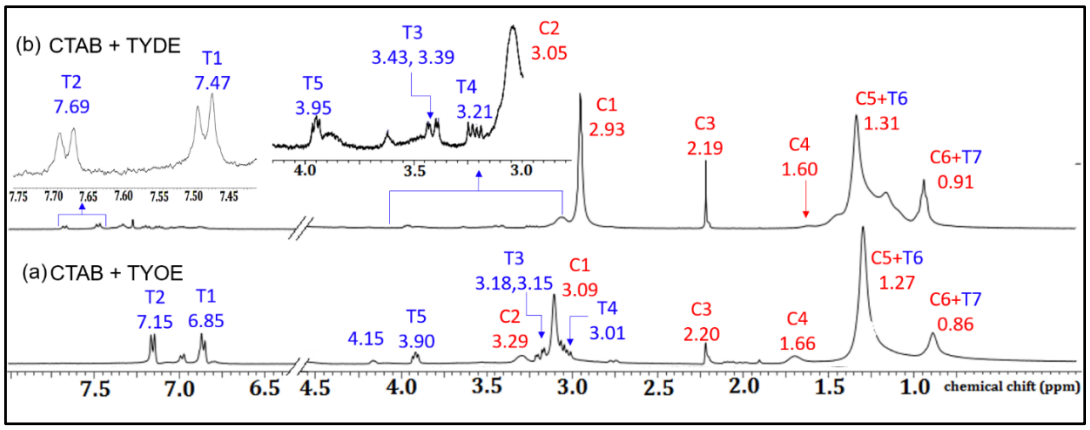

Figure 6. Comparative ^{1}H NMR spectra of (a) CTAB (10 mM)-TYOE (5 mM) and (b) CTAB (10 mM)-TYDE (5 mM) mixed systems in D_2O at 303 K.

The ^{1}H NMR spectra of CTAB (10 mM)-TYOE and CTAB (10 mM)-TYDE (5 mM) mixed systems in D_2O at 303 K is presented in Figure 6. The key resonances are highlighted in the figure. The terminal methyl protons of TYOE resonate at 1.17 ppm in D_2O,[25] whereas, in presence of CTAB, only a single peak at 0.86 ppm corresponding to the resonances of terminal methyl protons of both CTAB (C6) and TYOE (T7) is observed (Figure 6 (a)). This imply that T7 and C6 protons experience similar environment in the CTAB-TYOE mixed system. This shows that the T7 protons of the aromatic amino acid ester experiences considerably more non-polar environment compared to that of which is considerably non polar compared to that of its own self-assembled aggregates. Moreover, in absence of CTAB, the chain protons of TYOE appeared considerably downfield[25] at 3.16 ppm, whereas in presence of CTAB, these signals merged with that of CTAB chain protons and resonates at 1.27 ppm. This further indicates greater hydrophobic environment to exist around the chain protons of TYOE (T6) in presence of CTAB. It has been reported, both experimentally and theoretically, that in aqueous solution, the TYOE moiety prefer folded conformation with the NH_2 and the carbonyl groups oriented toward interfacial water while the aromatic ring and the alky chain are embedded towards the aggregate core.[25,23] 2D NMR analysis of TYOE in aqueous medium further revealed that the alkyl chain of TYOE “bend inwards” due to which the terminal protons of TYOE reside near the aromatic face of the same resulting in a polar environment around the terminal and chain protons of TYOE. Therefore, it may be said that, in presence of CTAB, the orientation of TYOE is modified such that alkyl chain remains in a straight conformation similar to CTAB alkyl chain wherein hydrophobic non polar micro environment is experienced by the alkyl and terminal protons of both the moieties. This conformation of TYOE may be

driven by the mutual strong hydrophobic interactions between the alkyl chain protons of TYOE and CTAB.

Now, let us turn to dodecyl ester of tyrosine, i.e., TYDE. It is evident that the aromatic protons of TYDE in CTAB-TYDE (Figure 6 (b)) system appear relatively downfield compared to TYOE (Figure 6 (a)) which indicates that the T1 and T2 protons of TYDE experience a greater de-shielding of magnetic resonance as compared to the same in TYOE i.e., TYDE aromatic protons reside at more polar environment compared to TYOE. The more polar environment might be due to the interfacial water molecules present around T2 and T1 of TYDE, which is protruded towards the interfacial water, as also indicated from the micro polarity study. Resonance for T3 and T4 protons in CTAB-TYDE system appear significantly downfield compared to CTAB-TYOE suggesting that these protons experience relatively more polar environment like T1 and T2, compared to the same in CTAB-TYOE system. On the other hand, C1 and C2 appear upfield. This observation supports the idea that the CTAB head group are localized near non-polar region, in between the alkyl chains of TYDE monomers. It shows that indeed the TYDE molecule remain "pushed outward" such that the aromatic part is indicates that aromatic part of the TYDE molecules projected out of the micellar interface and remains close to the interfacial water. Consequently, T1, T2, T3 and T4 protons of TYDE molecules are located towards the bulk water and therefore, the signal for T5 proton in CTAB-TYDE system appear at slight downfield compared to CTAB-TYOE system because in the former it remains at the proximity of the CTAB headgroups. The relatively downfield chemical shifts of the intermediate chain protons and the terminal protons in TYDE may be due to the greater spatial distribution of the alkyl chains as result of formation of longer cylindrical micelles.[32, 46]

This observation is rather surprising, because TYDE with longer chain, is expected to be embedded more deep inside CTAB micelles compared to TYOE. However, the similar results is observed in thermodynamic and spectroscopic measurements as well, indicates that it may be connected with folded and rigid geometry of the aromatic esters. It may be argued that as the longer alkyl chain of TYDE experiences stronger hydrophobic interaction with CTAB micelles compared to TYOE, the alkyl chain of the former favors entrenchment deeper inside the CTAB micelle, and due to its rather folded geometry the aromatic moiety flips towards interfacial water, over ridding the

weak attractive force via cation-π interaction at the headgroups. The TYDE molecules are now more tilted obliquely as shown in Scheme 2.

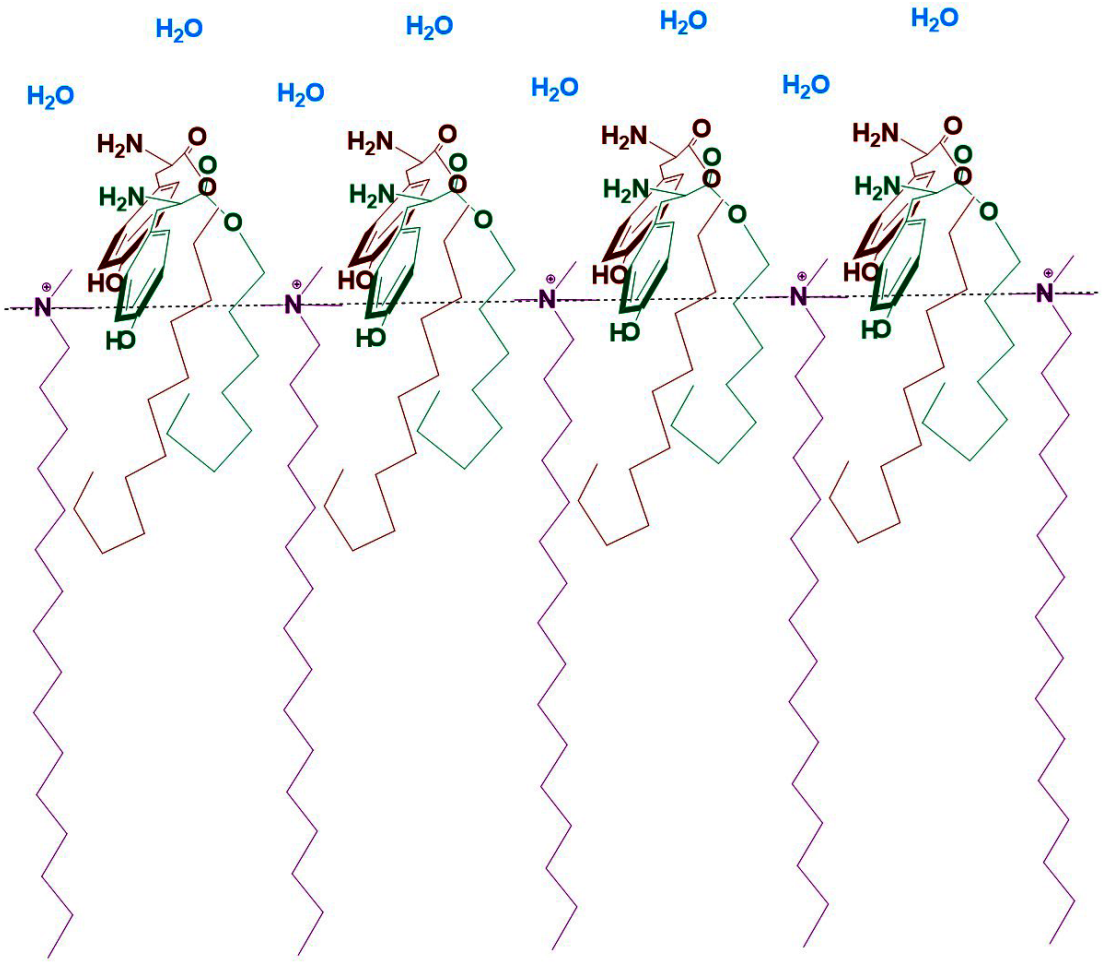

Scheme 2. Possible orientation of TYOE and TYDE w.r.t. CTAB molecules at the micelle/water interface of the wormlike micelles.

3.5.2. NOESY Study

Nuclear Overhauser effect spectroscopy (NOESY) is a 2D NMR technique based on correlation of signals arising via dipolar interaction from the protons that are located close in space (<5Å). The intensity of cross peaks of NOESY spectra is a measure of the extent of magnetization transfer between the proton nuclei and is proportional to the internuclei distance.[47] The NOESY spectra of CTAB (10 mM) and TYOE (5 mM) system, is recorded at 303 K (Figure 7). The intense key cross-peaks, T2-C1 and T1-C1 (Figure 7), correlating the aromatic protons T2 and T1 with the NMe protons of CTAB show that the benzene ring of TYOE is located in the vicinity of the quaternary ammonium head of CTAB (<5 Å). The folded geometry of TYOE favors hydrophilic

blocks consisting of amine, carbonyl and the ethereal oxygen to localize near interfacial water and the aromatic face near quaternary ammonium head groups. This orientation allows an effective cation-π interaction to take place. The key cross-peaks T2-C6+T7, T1-C6+T7 and T2-C5+T6, T1-C5+T6, which are observed in the present system, correlate the aromatic protons with the terminal and the hydrocarbon chain protons, of CTAB and TYOE respectively. Intense cross peak C1-C5+T6, correlating the NMe protons of CTAB with the alkyl chain protons of CTAB as well as TYOE are also observed. These cross peaks are particularly interesting because they suggest that both the aromatic system of TYOE and the quaternary ammonium head group of CTAB are present within the proximity of the chain protons of both CTAB and TYOE. Similar cross peaks were observed in the CTAB (10 mM)-TYDE (5 mM) system as well. Molecular folding is indeed possible in both TYOE and TYDE due to the presence of hydrophobic and hydrophilic blocks in the molecule, such folding is not possible in CTAB molecules. However, keeping in view the transition of morphology from spherical to rod like/wormlike micelles under the present concentration condition of CTAB and TYOE, above spectroscopic observation could be justified if we consider the end-cap region of the rods rather than spherical micelles or body of the rods. A revisit of the geometry of the end-caps is, therefore, necessary to find the explanation of above observation. Further discussion on the geometry of end-caps of rod/worm like micelles is presented in section 3.8 of this report.

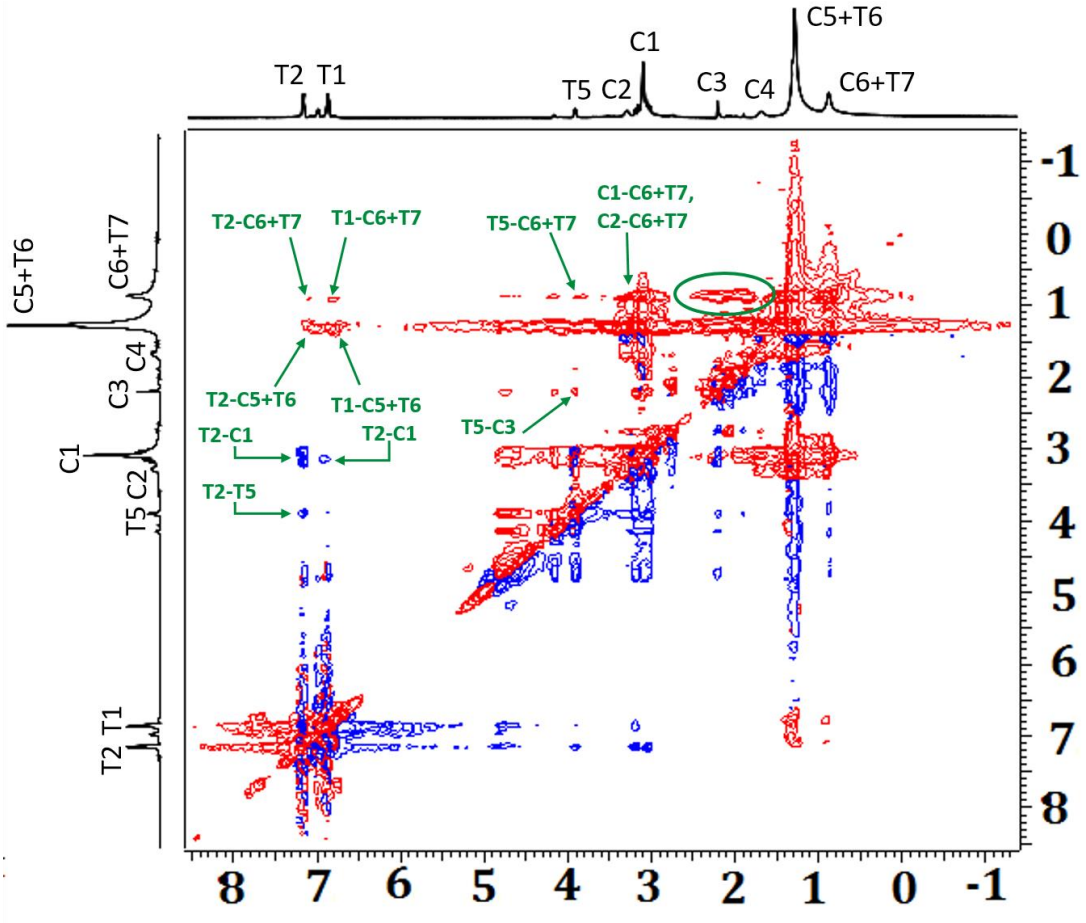

Figure 7. 2D NOESY spectrum of 10mM CTAB and 5mM TYOE in D_2O at 303 K

3.6. Cryo-TEM study

For direct visualization of the CTAB-aminoacid aggregates, Cryo-TEM images of CTAB-TYDE systems were obtained (Figure 8). Figure 8 (a) shows the presence of abundant small spheroidal micelles along with the elongated micelles at 100 mM CTAB and 40 mM TYDE concentration. When concentration was increased to 60 mM, long worm-like micelles developed (Figure 8 (b)). The elongated micelles create a network of entangles thread-like structure due to which the viscosity as well as the elasticity of the system increases. The presence of very few micellar ends implies that the micelles are probably at their longest form.[48] At further higher concentration of TYDE, viz., 75 mM, breakdown of the network occurs and system forms prominent vesicles (Figure 8 (c)). The cryo-TEM images provide inevitable support to the observation of change in micro-structure of CTAB in under the influence of the aminoacid analogues.

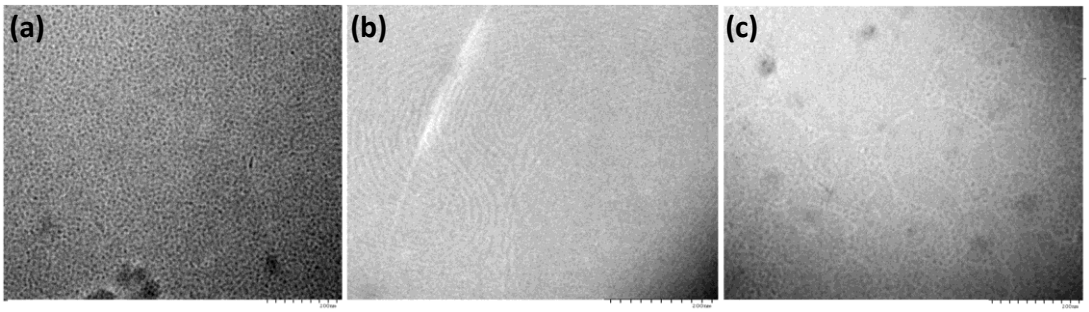

Figure 8. Cryo-TEM micrographs of aggregates of (a) 100 mM CTAB -40 mM TYDE, (b) 100 mM CTAB-60 mM TYOE, and (c) 100 mM CTAB-75 mM TYDE.

3.7. Small angle neutron scattering (SANS) study.

Information regarding structural polymorphism of self-assembled aggregates in solution may be obtained from SANS spectroscopy, in a non-invasive manner.[49] In a SANS experiment, the experimental sample is subjected to a beam of neutrons and the scattered intensities at different directions are measured. As the neutrons are scattered by the nuclei of the atoms, large scattering contrast can be achieved in deuterated solvents compared to protonated solvents as deuterons and protons differ largely in their respective neutron scattering capacities. The microstructural modification of CTAB micelles in presence of the aminoacid ester systems were studied with the help of SANS spectroscopy.

Figure 9 (a) shows the SANS spectra of (100 Mm) CTAB-(40 mM) TYOE and (100 mM) CTAB-(40 mM) TYDE mixed systems at 303 K. Measurements were taken with Q range of 0.017 to 0.358 $Å^{-1}$. SANS distribution for both the CTAB-TYOE and CTAB-TYDE systems display a rise in the low Q region whereas the intensity at high q region is independent of the nature of the aminoacid ester. For CTAB-TYOE system, a broad peak is evident at intermediate Q region, which becomes sharper in the case of CTAB-TYDE system. This peak arises due to the corresponding correlation peak in the interparticle structure factor, S(Q), which generally occurs at $Q \approx \frac{2\pi}{d}$, where d is the average distance between the aggregates present in the sample. Appearance of the correlation peak at nearly identical Q for both CTAB-TYOE and CTAB-TYDE systems suggest that the aggregate density in both the systems is nearly equal.[49] The well-defined and sharp nature of the correlation peak in CTAB-TYDE system indicates that electrostatic repulsion is predominant within the aggregates in this system. The broadening of the correlation peak in the case CTAB-TYOE system imply effectively

reduced interparticle repulsion within the aggregates.[50] A slope of -1 in the low Q region for all the SANS spectra is indictive of the presence of rodlike or elongated aggrregates in the system (Figure 9).[51,52] The experimental data was fitted with the theoretical curves (solid line) obtained on basis on Heyter and Penfold's approach of analysis considering the micelles as prolate ellipsoids.[53] It is evident that this model of micelles fits very well to the experimental data (Figure 9 (a)) confirming the presence of cylindrical or rod-like micellar aggregates within the systems. The increase in intensity of the low Q region in the case of CTAB-TYDE system further indicate growth in micellar size.[54] The observation reveals that the aminoacid esters are efficient in screening the electrostatic repulsive interaction between the quaternary ammonium head groups of the CTAB micelles, which results in one dimensional micellar growth forming elongated micelles.[50,51,55,56]

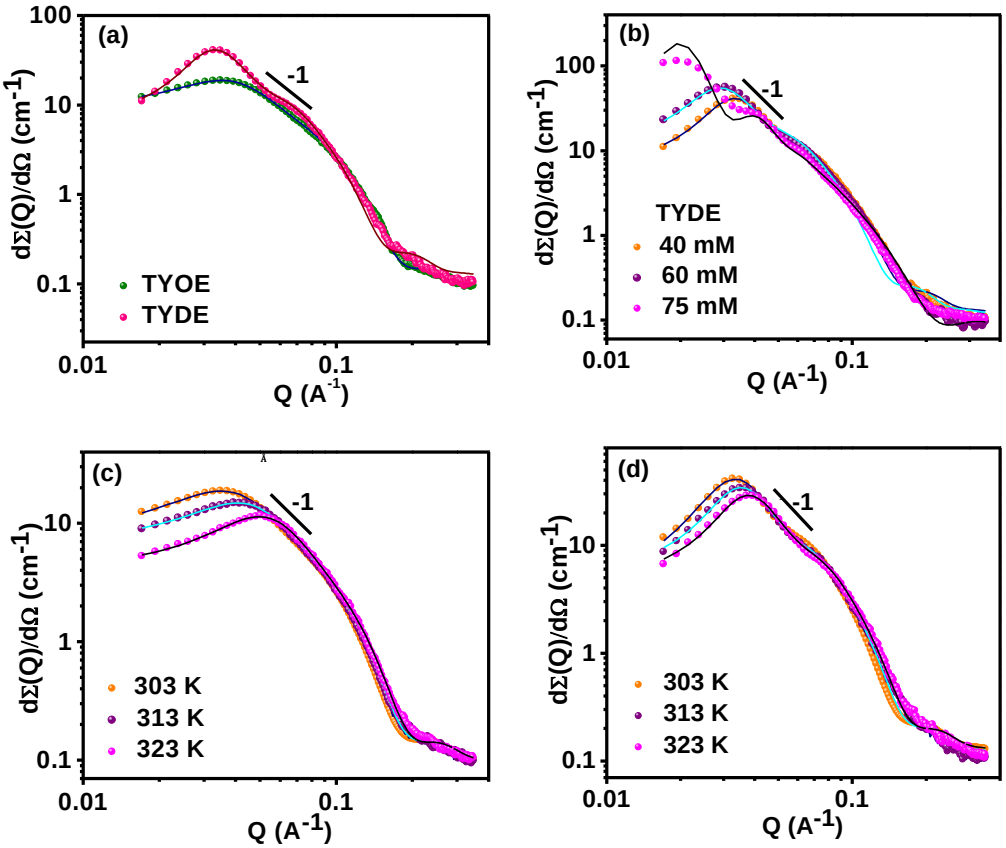

Figure 9. (a) SANS distribution of CTAB (100 mM)-TYOE (40 mM) and CTAB (100 mM)-TYDE (40 mM) systems at 303 K, (b) SANS profile of CTAB (100 mM)-TYDE system as function of TYDE concentration at 303 K, (c) Effect of temperature on CTAB (100 mM)-TYOE (40 mM) system, and (d) Effect of temperature on CTAB (100 mM)-TYDE (40 mM) system. Solid circles represent experimental curve, solid lines represent theoretical fit for prolate ellipsoid micelle model.

This observation is highly significant as it exemplifies the role of the tyrosine analogues, which are abundantly present in transmembrane proteins, in modifying the surface curvature of the lipid membranes which largely consists of phosphocholine derivatives having quaternary ammonium head groups similar to CTAB. SANS study of CTAB-TYDE system as function of TYDE concentration (at constant CTAB concentration of 100 mM) show that longer micelles form at 60 mM TYDE compared to 40 mM concentration as evident from the increase in correlation peak intensity in the SANS profile (Figure 9 (b)). At TYDE concentration of 75 mM, the spectra deviates from the prolate ellipsoidal model fit, implying a major structural change at this composition. The effect of temperature on 100 mM-40 mM CTAB-aminoacid composition is studied (Figure 9 (c), (d)). With rise in temperature, the intensity of the correlation peak increases with shifting of Q_{max} to higher Q values. The shift in Q_{max} suggests a decrease in correlation length, ξ, given by $\xi = 2\pi/Q_{max}$[57] i.e., with rise in temperature, the micellar length decreases, for both the systems while the radius of the micelles remains constant as indicated by the overlapping intensities in the high Q region. As evident, the effect is more prominent in CTAB-TYOE system compared to CTAB-TYDE system. Table 3 quantitatively summarizes the dimensions of the CTAB-aminoacid ester assemblies obtained from SANS treatment at various conditions. It may be seen that the semi major axis, a, is 4-5 times the semi-minor axis, b, in all the systems at all temperature and compositions, which confirms the cylindrical shape of the aggregates throughout. Micelles formed with TYDE as additive are nearly 40% longer than that formed in presence of TYOE (Table 3) at all temperatures. Increasing concentration of TYDE in CTAB-TYDE system from 40 to 60 mM causes an increase of ~ 20 - 40 nm in the micellar length. Increasing temperature from 303 K to 323 K decrease the micellar length by approximately 25% in each case.

Table 3. Dimension of wormlike micelles of CTAB with additives as a function of concentration and temperature obtained from SANS study.

CTAB=100mM						
Temperature (K)	TYDE 40 mM		TYDE 60 mM		TYOE 40 mM	
	Semi Major Axis (Å)	Semi Minor Axis (Å)	Semi Major Axis (Å)	Semi Minor Axis (Å)	Semi Major Axis (Å)	Semi Minor Axis (Å)
303	126.29	26.869	148.21	29.739	94.23	22.693
313	108.51	25.421	143.17	26.92	79.127	21.784
323	99.852	24.079	109.05	25.36	70.992	20.839

The SANS study corroborates the synergistic interplay between the CTAB and the aminoacid ester molecules, as observed from the study of interfacial property study, at much higher concentrations. The differences in the micellar lengths and extent of electrostatic interaction of the additives with CTAB head group arises primarily due to the difference in their molecular architecture. While both TYOE and TYDE contain identical head group, viz., the phenol ring of tyrosine moiety, the longer alkyl chain length of TYDE, viz., 12 carbon units, confers higher hydrophobicity to it compared to TYOE with 8 carbon units. Secondly, the spatial orientation of the additives and their location w.r.t CTAB monomers as well as the micelles is also likely to influence the interaction behavior of the aminoacid esters with the CTAB molecules.

3.8. End-caps and end-cap geometry

Morphology transition of cationic micelles from sphere to rod like micelles and subsequent transition to wormlike micelle via charge screening is a well studied process. Formation of rod/wormlike micelle in the present system, consisting of CTAB and TYOE or TYDE, is understood from the observation of non-Newtonian nature of flow and subsequent SANS and TEM studies. The transition from spherical to rod like micelles by tuning the surface curvature via charge screening involves topological defects at the end-caps. Such end-cap region with different curvature compared to main cylindrical body incur an added energetic penalty. This thermodynamically unfavorable situation leads to long wormlike micelles instead of large number of small rods. Therefore, among the other factors, the contour length of WLM becomes a function of end-cap energy as well. A mean field theory of the growth process of WLM for either

neutral or strongly screened system predicts the average contour length to be function of volume fraction ϕ, temperature and the end-cap energy E_C with two hemispherical end-cap model as given in the following relation:[58-60]

$$L \sim \phi^{\frac{1}{2}} \exp[{}^{E_C}/_{k_B.T}] \quad (12)$$

where k_B is the Boltzman constant.

On the other hand, a molecular level self-consistent field analysis of very long cylindrical micelles supports the idea of swollen end-caps with respect to the cylindrical part.[61] This dumbell shaped model is, however, energetically not favorable on two counts. First, in such a case, the diameter of the spheres of the dumbell shaped part be longer than twice the straight chain length of the surfactant molecule and second, the dumbell-shaped micelles contains energetically unfavorable negative curvature at the neck. Present discussion on the end-cap geometry of cylindrical micelles of CTAB is, therefore, confined to hemispherical end-caps with the possibility of perturbation on geometry due to the presence of TYOE/TYDE in the system (e.g. flat end caps).

In addition to the 2D NMR results, as shown in section 3.5.2, some further observation is also worth mentioning here. The cross peaks viz., C1-C6+T7 and C2-C6+T7 are observed and they correlate the quaternary ammonium protons of CTAB with the terminal protons of both CTAB and TYOE. C2 interacts with T7 quite obviously because of the folded structure of TYOE but interaction of C2 with C6 of the same CTAB molecule is ruled out because complete folding of CTAB molecule would lead to instability of the rod as mentioned above. Moreover, cross peaks corresponding to correlation between C3, C4 and the terminal methyl protons of CTAB are observed (indicated by elliptical symbols in Figure 7). This further indicates that the cross peaks arise from interactions of the protons from the two sets of CTAB molecules, residing at different environments. First, the NMe protons of CTAB (C1) are located close to the aromatic protons, viz., T1, T2 of TYOE facilitating cation-π interaction to take place. This orientation results in the observed cross peaks between the NMe and C1 protons with aromatic protons of TYOE. Second, from the CTAB protons residing at the end caps adjacent to the body of the rod-like micelles which exhibit the interaction between the C2, C3 protons of one CTAB molecule with the intermediate (C5) as well

as terminal protons of the other (C6) at the flat part of the cap (Figure 8 (interaction shown by elliptical symbol))

1D SCF (Self-consistent field; concentration gradient in one direction) study shows that the end-cap energy of very long wormlike micelles is nearly 2.8 k_BT per cap, which is equivalent to ~1.67 kCal.mol^{-1}.[59] Interestingly, this energy is of the order of cation-π interaction (~1.13 kCal.mol^{-1}) of the present system.

Further, lowering of the curvature of the end-caps via embedding of TYOE/TYDE in the end-cap region, just like the body of the cylinder by hydrophobic force and cation-π interaction, cannot be ruled out. Under this situation, the end-cap would suffer a perturbation on its geometry and a somewhat flat caps with positive curvature at the junction with the cylindrical body would result (Scheme 3) The CTAB and TYOE/TYDE molecules at the flat part of the cap would, therefore, direct toward the body in somewhat parallel orientation, whereas the alkyl chains of CTAB molecules of the junctions tend to converge towards the core of the micelles. The junctions with positive curvature do not accommodate TYOE/TYDE molecules and, therefore, no screening of CTAB head groups results. The molecular interactions which are present in the micelles and manifested in 2D NMR spectra are not only due to the molecules present in the cylindrical body but also for the molecules at the end-caps (shown by elliptical symbol in Scheme 3)

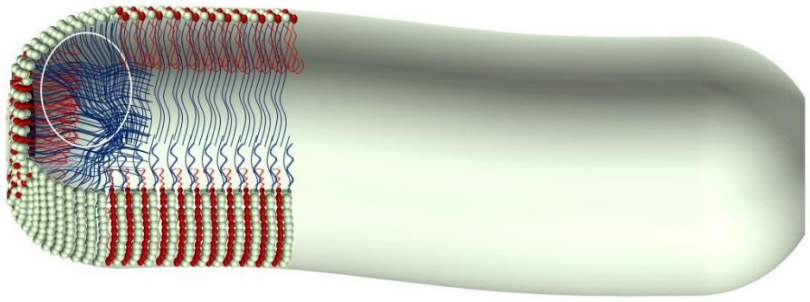

Scheme 3. Cylindrical/Worm-like micelle with flat end-caps (unusual molecular Interactions are shown by elliptical symbol

3.9. Characteristic study of rheological behavior of the CTAB-amino acid ester systems

The formation of worm-like or elongated micelles in CTAB triggered by the tyrosine analogues highly interesting, more so, because the elongated aggregates impart

viscoelastic property to the biomimetic model membrane system thereby modifying its bulk property to a huge extent. It was, therefore, tempting to study the bulk rheological property of the CTAB-aminoacid ester systems to explore its potentiality further. The concentration of CTAB (75 mM) and aminoacid esters (37 mM) i.e., at $\chi_{TYOE/TYDE}$= 0.33 was chosen as it is an intermediate between the compositions 100 mM CTAB-40 mM aminoacid ester, where $\chi_{TYOE/TYDE}$= 0.28 and CTAB (100 mM)- aminoacid ester (60 mM), where $\chi_{TYOE/TYDE}$= 0.37. The shear viscosity profile of CTAB-TYOE and CTAB-TYDE systems studied as function of temperature, show that the systems exhibit Non-Newtonian behavior at different temperature ranges (Figure 10). The shear thinning at higher shear rates may be considered as another evidence regarding presence of worm-like micelles within the system.[62]

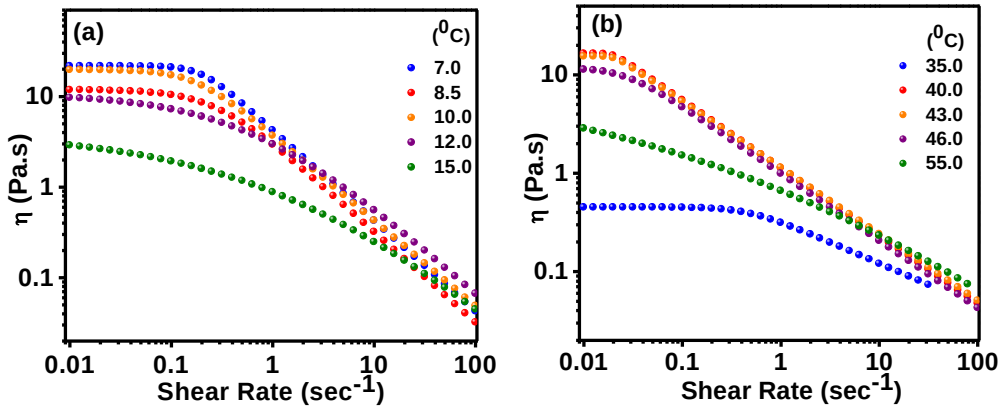

Figure 10. Shear viscosity profiles of (a) CTAB (75 mM)-TYOE (37 mM) system and (b) CTAB (75 mM)-TYDE (37 mM) system as function of temperature.

While in the case of CTAB-TYOE, the linear viscoelastic regime appeared between temperatures 7^0C and 15^0C (Figure 10 (a)), in the case of CTAB-TYDE system, the temperature range was as high as 35^0C-55^0C (Figure 10 (b)). This difference in the non-Newtonian behavior could not be explained in straightforward manner and requires more attention, which may be undertaken in a separate study. The response of the viscoelastic moduli of these model systems were examined as function of angular frequency within the observed respective viscoelastic range (Figure 11). It is evident that at shorter time scale, or high ω, elastic behavior is displayed by the samples, with storage or elastic modulus, G′, dominating over the viscous or the loss modulus, G″ (Figure 10 (a), (b)). At longer time scale, or lower ω, an opposite trend is observed, i.e., G″> G′. The dominant relaxation time,τ_R, for these CTAB-aminoacid ester systems is

estimated as $\frac{1}{\omega_C}$, where ω_C denotes the cross-over angular frequency, where G′ = G″. The observation demonstrates that the CTAB-aminoacid mixed systems behave as "living polymers" which exist in dynamic equilibrium where the micelles undergo constant breakage and recombination to form a transient network.[63] The viscoelastic response of the CTAB-TYOE and CTAB-TYDE systems is in good agreement with Maxwell's mechanical model which may be used in describing the dynamic rheological property of the present systems.[32,64]

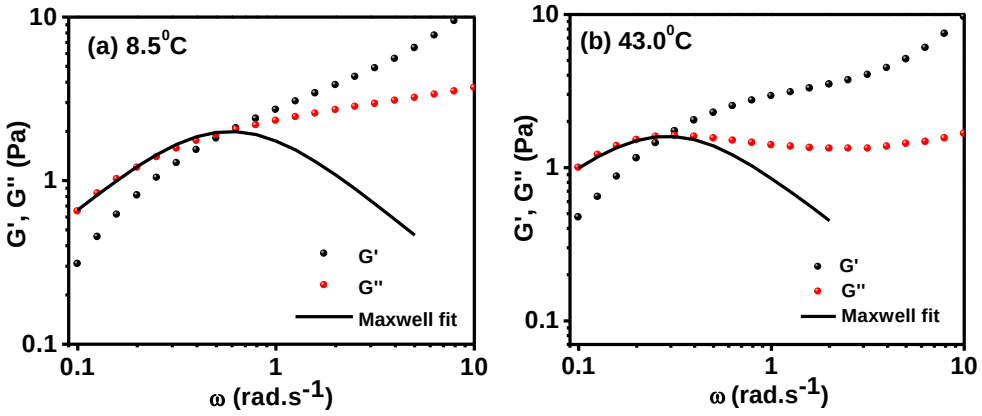

Figure 11. Representative plot of frequency sweep curves of (a) CTAB (75 mM)-TYOE (37 mM) at 8.5^{0}C, (b) CTAB (75 mM)-TYDE (37 mM) at 43.0^{0}C.

According to this model, the G′and G″ are given as-

$$G'(\omega) = G_0\omega^2\tau_R^2/(1+\omega^2\tau_R^2) \quad (12)$$

$$G''(\omega) = G_0\omega\tau_R/(1+\omega^2\tau_R^2) \quad (13)$$

where G_0 is the storage modulus at high frequency.

The oscillatory flow spectra are fitted to the theoretical curve obtained from Maxwell model (solid line in Figure 11 (a), (b)). At lower ω, the systems exhibit well-defined Maxell behavior, however at higher ω, much deviation is apparent. This deviation is caused by presence of faster modes of stress relaxation, like "Rouse or breathing modes".[55,56,48,62] From the lower values of ω_C, for CTAB-TYDE systems compared to that in CTAB-TYOE (Figure S2 of Appendix C), it may be said that the former system adopts slower reptation mode of relaxation. Slower relaxation modes may also be associated with linearity of the worm-like micelles. From the lower values of ω_C, for CTAB-TYDE systems compared to that in CTAB-TYOE (Figure S2 of Appendix C),

it may be said that the former system adopts slower reptation mode of relaxation. Slower relaxation modes may also be associated with linearity of the worm-like micelles.[65]

4. Conclusion

Synergistic improvement of the interfacial properties of the aqueous mixtures of CTAB with L-Tyrosineoctyl ester or L-Tyrosinedodecyl ester stems from cation-π interaction between quaternary ammonium head group of CTAB and π-electron cloud of aromatic aminoacid, in addition to usual non-covalent forces present in the system. The hydrophobic and hydrophilic blocks present in the molecular architecture of tyrosine analogues lead to highly folded geometry, which makes headway for unusual flipping of the molecule in the event of slight perturbation on the delicate balance of prevailing driving forces resulting in contrasting effects pertaining to hydrophobicity and micropolarity. Micellar morphology transition from cylindrical to rod/wormlike micelles via charge screening of the headgroups by π-electrons of aromatic aminoacid is indeed interesting in view of the abundance of zwitterionic phosphatidylcholine in bio-membranes and the ubiquitous feature of transmembrane proteins to localize tyrosine and tryptophan at the interface. Since the interplay between lipids and proteins is the key to how cells control membrane shape during many vital events including cellular fission, fusion and virus entry, the observed tuning of micellar surface curvature by tyrosine analogues is thought provoking and opens up avenue for new physical chemistry research on a vital biological phenomena. The end-cap geometry of the cylindrical/wormlike micelles formed via charge screening of the cationic micelles is discussed and found to be flat-cap in shape for the first time.

References are provided in BIBLIOGRAPHY under “References for Chapter VI” (Page 184-189).

Chapter VII

Interaction of a tryptophan analogue with quaternary ammonium head group at micelle/water interface and its influence on aggregation characteristics of cationic micelles

1. Introduction

The integral membrane proteins show a surprising preference for the aromatic amino acids tyrosine (Tyr) and tryptophan (Trp) residues in their transmembrane domains especially in region where lipid density is highest. Statistical analyses of distribution patterns of the amino acids show that all major classes of the membrane proteins i.e., the single as well as multi-span, α-helix bundle as well as the β-barrel type, are found to have pronounced enrichment of Tyr and Trp (and not phenylalanine) at their transmembrane domains.[1-3] Especially, the Trp residues show remarkable involvement in the ion channel activity of the peptide gramicidin and in the control of its structure and function.[4-7] Moreover, Trp also show site preference at the agonist site of the nicotinic Acetylcholine receptors (nAChR) which are responsible for transmission of electric signals from one neuron to another through nerve synapse.[8] As many as six to eight aromatic residues and all of the Trp and Tyr residues are known to accumulate at the agonist bonding site of nAChR and mediate binding to the cationic agonist Acetylcholine via cation-π interaction.[8] The importance of Trp in maintenance of the structure and functionality of membrane proteins is exemplified by the fact that removal of this residue results in degeneration or complete loss of the protein functionality in some cases.[9] Although Trp is the principal source of intrinsic fluorescence of most of the proteins, optical spectroscopic study on multitryptophan proteins is often complicated due to the complex nature of the fluorescence process and also due to the heterogeneity in parameters like quantum yield, arising from the different environmental sensitivity of the individual Trp residues. Tryptophan octyl ester (TROE) has been acknowledged as an important model for this purpose. Studies on of TROE incorporated into model membranes and membrane-mimetic systems are available in literature and have shown to be similar to that of membrane-bound tryptophans.[10-13] However, such investigations are restricted to study the of fluorescence characteristics only. It has been reported in chapter V that the TROE

molecules undergo solvent induced molecular folding, just like its tyrosine counterpart and reveal unusual aggregation characteristics and surface active nature in aqueous medium retaining the folded geometry in self-assembled nanostructure.[14] TROE molecules form bilayers and large unilamellar vesicles (LUV) in aqueous medium, which is rather unique for a short chain single tailed amphiphilic molecule.[14] Due to its strong surface active behavior and amphiphilic nature, the long chain ester may behave as the bioactive surfactants as well. [5]

In connection with development of models related to biomembranes, it is essential to use simple systems, which can mimic the important and essential physico-chemical features of the membrane architecture, and simultaneously, devoid of much of the complexities of natural membranes. Surfactant micelles serve as valuable substitutes for membranes for the study of solubilized membrane proteins and amphiphilic or hydrophobic peptides.[15,16] In this regard, the micelles of cetyltrimethylammonium bromide (CTAB) is of significant relevance due to the similarity of its molecular structure with phosphatidylcholine,[17] which is the most abundant phospholipid present in plant and animal membranes. Furthermore, biological membranes exhibit various function-related shapes, and the mechanism by which these shapes are created is largely unclear. It is generally believed that the changes of membrane topology is produced as a result of a complex interplay between membrane proteins, lipids and certain physical forces. Therefore, it is also tempting to explore whether the aromatic amino acid residues of transmembrane proteins can have any role to play in controlling shape transition of the membranes. In this connection, the study of interaction between the CTAB micelles and TROE seem highly interesting in relation to fundamental understanding of the complex interactions involved at the membrane interface. In this chapter, tensiometric and spectroscopic techniques, Density functional theory (DFT) and high resolution transmission electronic microscopic (HRTEM) imaging have been employed to study the interaction of CTAB micelles with TROE.

It may be emphasized here that in this work the ability and efficiency of aromatic aminoacid ester (viz., TROE) to tune micellar surface curvature has been probed via the ease of micellar shape transition from spherical to cylindrical micelles, triggered by the aminoacid ester. Due to thermodynamic requirement, the cylindrical or rod like micelles once formed, grow very long and impart strong viscoelasticity in the solution

which often display unusual rheology. It is also interesting to note that solution containing spherical micelles or small rods around normal cmc show Newtonian flow characteristics whereas wormlike micelles at relatively higher concentration often shows non-Newtonian property. Therefore, the whole study of the present chapter is divided into two parts, viz., (i) Newtonian flow regime and (ii) non-Newtonian flow regime.

2. Materials and Methods

2.1. Materials

L-Tryptophanoctyl ester (TROE) were synthesized in our laboratory according to previous scheme.[5] CTAB was purchased from Fluka (Switzerland). D_2O for NMR study was purchased from Aldrich, USA (Purity >99.9%). Purity of the chemicals were greater than 99.5% and were used as received. All experiments were done with de-ionised and doubly distilled water with pH 6.5-7 and specific conductance below $2\mu S.cm^{-1}$.

2.2. Methods

2.2.1. Tensiometry. Tensiometric measurements were performed on Krùss K9 Tensiometer (Germany), based on Du-Nóuy ring detachment method, fitted with Omniiset temperature bath with precision ± 0.1^0C. Before each measurement, the platinum ring was thoroughly cleaned with 1:1 acetone-water solution and heated under oxidizing flame until glowing temperature was attained. After every addition, the experimental solution was stirred for 5 minutes for homogeneity and equilibrated for 10 minutes. For each measurement, three to five subsequent readings were taken for concordance. Standard deviation was < 0.1 $mN.m^{-1}$.

2.2.2. pH measurements. The pH of the solutions were measured using Systronics digital pH meter (Model: 335, India), calibrated with standard buffers of pH 4.0 and 9.2. Solutions were equilibrated for 5 min after addition of acid/alkali till a steady pH meter reading was observed.

2.2.3. Fluorescence spectroscopy. Steady state fluorescence emission study was carried out in bench top spectrofluorimeter from Photon Technologies International (Quantamaster-40, USA) with excitation and emission slit widths fixed at 3.0 nm and

2.5 nm respectively. Samples were taken in Hellma quartz cuvette of optical length 1.0 cm.

2.2.4. Nuclear Magnetic Resonance Spectroscopy (NMR). ^{1}H-NMR experiments were performed in Bruker (Germany) ADVANCE spectrometer operating at 300 MHz frequency (for characterization) and at 600.13 MHz for 2D Rotating frame nuclear overhauser spectroscopy (ROESY) study. Signals are quoted as δ values in ppm using residual protonated solvent signals as internal standard (D_2O: δ 4.79 ppm). Respective solutions were made in D_2O and 0.6 mL of the same was used for each measurement. Data are reported as chemical shift. 2D ROESY spectra was studied using Brucker standard software acquisition program roesytp in phase-sensitive mode using 5 mm BBO probe. An acquisition time of 0.12 sec and relaxation delay of 2 sec was used between the scans. A total number of 2048 complex point were collected.

2.2.5. High Resolution Transmission Electron Microscopy (HRTEM). HRTEM images were obtained with Jeol JEM 2100 microscope (Japan) operating at accelerating voltage of 200 KV. All images were taken at suitable defocus condition to obtain maximum contrast. A drop of sample solution was added to 200 mesh copper lacey support grid coated with carbon film. Excess sample was manually blotted carefully with Whatman 42 filter paper for 2 s. The grid was dried at 60^0C for 1 hr before experimentation.

2.2.6. Rheology. The rheological experiments were done using cone-plate geometry with 4^0 truncation angle, with diameter 25 mm and 0.105 mm sample gap in MCR 302 (Anton Paar, Germany) equipped with Peltier temperature control system. The samples were initially stirred at 60^0C for three hours for homogenization and equilibrated for 72 hrs. During measurement, samples were equilibrated for 10 mins at each temperature.[9]

3. Results and Discussion

Newtonian flow regime

3.1. Modification of interfacial and bulk properties of CTAB in aqueous medium as triggered by TROE

Figure 1 shows the variation of surface tension, γ, as function of various mole fractions of TROE. The surface tension, γ, decreases with increase in the concentration of CTAB-TYOE mixture before reaching a critical aggregation concentration, after which a

nearly constant value is obtained. On further increasing the concentration of TYOE, i.e. at χ_{TROE} 0.6, the mixture became cloudy and formed a suspension of TYOE in CTAB. Therefore, the study was restricted to χ_{TROE} 0.5 composition. The equilibrium surface tension of the mixed systems are 8-10 mN.s^{-1} lower than that of CTAB (Figure 1). This suggests that the surface-activity of CTAB is enhanced in presence of TROE. The CMC (critical micelle concentration) of CTAB viz., 0.89 mM[20] decreases gradually with increasing mole fraction of TROE and becomes 0.14 mM at χ_{TROE} 0.5. This indicates that, with the increase in TROE concentration, the electrostatic repulsion between the quaternary ammonium heads of CTAB molecules is greatly reduced which results in strong synergism lowering the cmc values via electrostatic stabilization of the micelles' polar shell.[11]

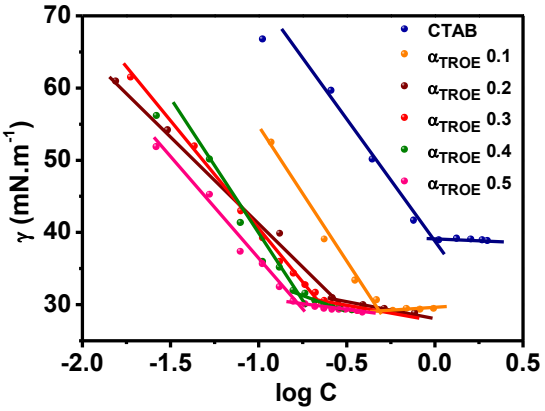

Figure 1. Surface tension as a function of total concentration of CTAB-TROE mixed system at different composition at 303 K

The surface excess concentration (Γ_{max}^{total}) for the CTAB-TROE systems at the air/water interface was calculated using Gibbs' equation[12] (Theoretical details are provided under Section 1.1 under Appendix D)-

$$\Gamma_{max}^{tot} = \frac{1}{2.303RT} lim_{C \to cmc}\left[\frac{d\Pi}{d\log C}\right] \quad (1)$$

where, Π is the surface pressure, [$\Pi = \gamma_0 - \gamma$; γ_0 is the surface tension of water, γ denotes the surface tension of surfactant solution], C is the total surfactant concentration, T and R are the absolute temperature and universal gas constant (8.314 J.mol^{-1}. K^{-1}) respectively.

Table 1 presents the surface parameters of CTAB-TROE mixtures at different compositions. The Π_{cmc}, which is a measure of efficiency of surface tension reduction,[13]

increases from 32.40 $mN.m^{-1}$ for pure CTAB to 41.22 $mN.m^{-1}$ at χ_{TROE} = 0.2 followed by a small decrease to 40.82 at χ_{TROE} = 0.3 , above which it becomes constant. The increase in surface pressure denotes improved efficiency of the mixed system in reducing the interfacial tension. The trend indicates that beyond α_{TROE} of 0.3, addition of TROE causes no further improvement in surface activity of the system. The maximum surface excess (Γ_{max}^{tot}) which denotes the number of surface active molecules present at the air-water interface in excess of the bulk, shows an initial decrease from 6.6 x 10^{-6} $mol.m^{-2}$ in pure CTAB to 4.2 x 10^{-6} $mol.m^{-2}$ at χ_{TROE} of 0.2 suggesting that a smaller number of molecules now populate the surface. The abrupt rise in Γ_{max}^{tot} to 6.4 x 10^{-6} $mol.m^{-2}$ χ_{TROE} of 0.3 indicates the possibility of conformational changes of the molecules at this composition. This is corroborated by the trend in the A_{min}^{tot} values as well. A_{min}^{tot} is the minimum surface area occupied by a molecule at the interface. A_{min}^{tot} increase in presence of TROE (0.395 $nm^2.molecule^{-1}$ at χ_{TROE} 0.2) compared to pure CTAB (0.249 $nm^2.molecule^{-1}$) and shows a sudden decrease at χ_{TROE} of 0.3 (0.258 $nm^2.molecule^{-1}$). The observation suggests that the molecules are arranged in more oblique manner at χ_{TROE} < 0.3.[5,11] At χ_{TROE} of 0.3, the molecular packing density changes; decrease in average surface area of the molecules together with increase in surface excess suggests a more perpendicular arrangement of molecules at the air-solution surface at this composition and above. The interaction parameter, β, which explains the interaction between the head groups of surfactants were calculated on basis of Rubingh's regular solution theory (RST)[18] and presented in Table 1.

Table 1. Interfacial parameters of CTAB-TROE system at different mole fraction of TROE in aqueous medium at 303 K

α_{TROE}	CMC (mM)	Π_{CMC} ($mN.m^{-1}$)	$10^6\Gamma_{max}^{tot}$ ($mol.m^{-2}$)	A_{min}^{tot} ($nm^2.molecule^{-1}$)	β	f_1	f_1
0	0.78	32.40	6.649	0.249	-	-	-
0.1	0.47	39.42	4.814	0.344	-2.27	0.261	0.395
0.2	0.30	41.22	4.205	0.395	-3.25	0.099	0.338
0.3	0.26	40.82	6.412	0.258	-3.34	0.078	0.450
0.4	0.19	40.72	5.910	0.281	-4.36	0.031	0.399
0.5	0.14	40.9	4.993	0.332	-5.21	0.014	0.384

The negative nature of interaction parameter, further confirms the attractive nature of the interaction to exist between CTAB and TROE molecules. Activity coefficient values (f_1 and f_2) are, less than unity, implying non-ideal mixing behavior of the components.

3.2. Steady state fluorescence emission study

Depending on pH, TROE may exist in protonated or unprotonated form. The pK_a of the amino functionality of TROE in water is ~9.7.[19] Therefore, it may be assumed that under experimental conditions, (pH 7.2-7.5) the emission arises solely from the neutral form. The effect of CTAB on the steady state emission spectra of 0.2 mM TROE in aqueous medium at 25^0C is shown in Figure 2. TROE was excited at λ_{exc} =278 nm which is also the λ_{max} of UV absorption spectra (Figure S1 of Appendix D). In absence of CTAB, the maximum emission occurred at 350 nm. The intensity at λ_{em} decreased gradually upon addition of CTAB up to a concentration of 0.39 mM without any change in λ_{em}. Above 0.39 mM, there is a steady rise in intensity where the λ_{em} shifted to 342 nm in 1.68 mM CTAB showing a prominent blue shift of 8 nm. The fluorescence activity of TROE is caused by the indole moiety which is highly sensitive to the polarity of its micro-environment.[20] Above blue shift in emission maxima indicates an increase in non-polar nature of the site of localization of tryptophan moiety of TROE with increasing CTAB concentration.[4] This is consistent with the transfer of indole of TROE from polar bulk aqueous phase to a less polar micellar phase. The intensification in fluorescence emission begins at concentration 0.49 mM which is much lower than the cmc of CTAB in water (cmc_{CTAB} =0.89 mM in water.[15] This suggests that binding of TROE with the CTAB molecules begins at considerably low concentrations of CTAB and that the aggregation of CTAB is much favored in presence of TROE. This is corroborated by conductivity and tensiometric studies as discussed previously (Section 3.1). The initial decrease in emission intensity might have occurred due to the binding of TROE units with the CTAB monomers in the premicellar regime.

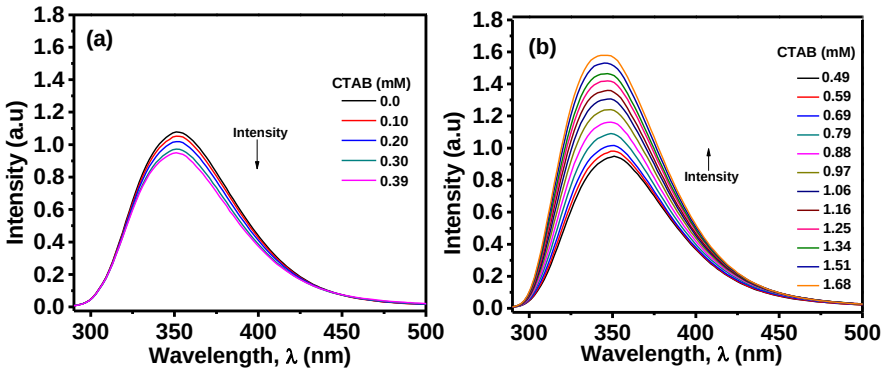

Figure 2 (a) Fluorescence emission spectra of 0.2 mM TROE as function of CTAB concentration up to 0.39 mM (b) Fluorescence emission spectra of 0.2 mM TROE as function of CTAB concentration >0.49, at 298 K.

3.3. Molecular interactions (non-Newtonian flow regime)

3.3.1. ^{1}H NMR Study

NMR spectroscopy is a non-invasive tool to study the microenvironment of a system.[16] The characteristics of self-assembled aggregates viz., shape, size, degree of ionization etc., have been successfully studied using NMR spectroscopic technique.[7,21] As the ^{1}H signals from surfactants, in general, are sensitive to the polarity of the solutions, any microstructural changes in CTAB induced by the TROE molecule would be reflected in the respective ^{1}H NMR spectra of the CTAB molecule. Therefore, the nature of the interaction of CTAB and TROE have been studied by ^{1}H NMR spectroscopy. Current literature concerning the formation and characterization of wormlike micelles being quite large compared to molecular level chemistries, we have emphasized on the molecular interaction among the components of the complex fluids as well. The NMR spectroscopic study, therefore, involves a system containing 14 mM CTAB and 6 mM TROE where viscoelasticity is visibly apparent. The 1D ^{1}H NMR spectra of 14 mM CTAB and 6 mM TROE in D_2O is shown in Figure 1. The molecular structure and proton numbering of CTAB and TROE are given in the inset (Scheme 1).

The ^{1}H NMR spectra of CTAB is known and available in literature.[22] The methyl protons of CTAB head group resonates at 3.2 ppm, the γ, β and α protons appear at 1.43, 1.83 and 3.43 ppm in D_2O respectively. The alkyl chain protons appear as an intense peak at 1.35 ppm and the terminal protons correspond to a singlet, resonating furthest upfield at 0.93 ppm.[22] Addition of TROE induces several changes in the

protonic environment of CTAB (Figure 3 (a)). The methyl protons of the quaternary ammonium head group (C1) now resonates significantly upfield at 2.94 ppm. The β protons (C2) also experience a prominent shielding effect and resonate upfield at 3.07 ppm. The signal for γ protons appear at 1.43 ppm indicating that these protons are unaffected by the presence

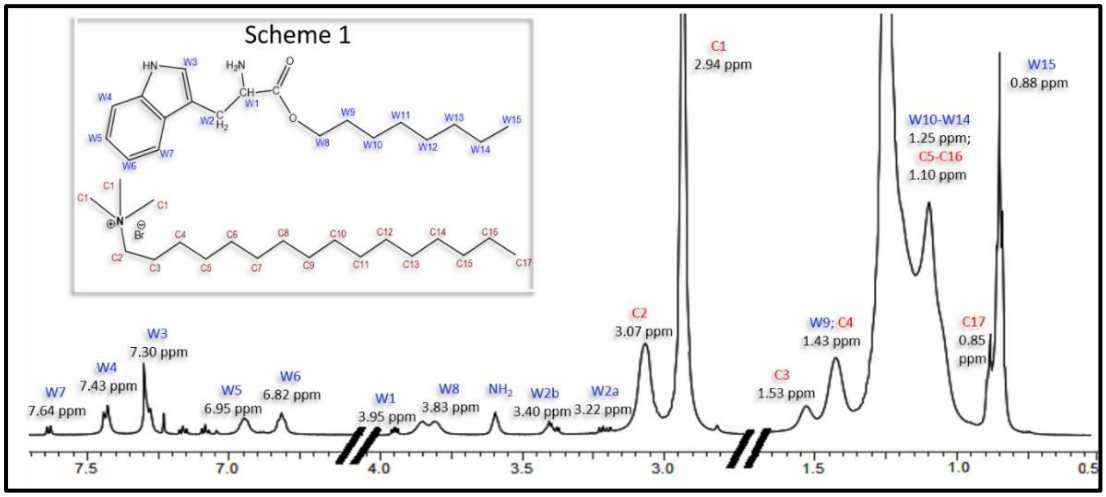

Figure 3 (a) ^{1}H NMR spectra of mixture of 14 mM CTAB and 6 mM TROE in D_2O at 298 K.

of TROE in the system. Two intense signals corresponding to resonances of aliphatic protons of both TROE and CTAB, are observed at 1.10 and 1.25 ppm respectively. As the intensity of signal at 1.25 ppm is much higher than that at 1.10 ppm, it may be argued that 1.25 ppm corresponds to the hydrocarbon chain of CTAB (since it contains greater number of protons viz. 24 aliphatic protons for CTAB compared to 10 protons for TROE) while that at 1.10 ppm belongs to TROE respectively i.e. slight shielding effect of the aliphatic chain is evident. Precise assignment of the terminal proton resonances cannot be done since the corresponding signal from both CTAB and TROE appear as merged and overlapped peak at 0.88 ppm. The large chemical shift values of the head group and adjacent protons indicates strong interaction with the TROE moiety. The upfield nature of the shifts show that the surfactant molecule is in relatively non-polar environment in presence of TROE. Significant perturbation is experienced by protons in the following order: α proton, Δδ 0.36 ppm ($\Delta\delta = \delta_{CTAB}-\delta_{MIX}$); β protons, Δδ 0.30 ppm; head group protons, Δδ 0.26 ppm; alkyl protons: Δδ 0.10 ppm and terminal protons: Δδ 0.05 ppm. This shows that the protons in close proximity with the surfactant head group are more strongly influenced by TROE compared to that of hydrocarbon chain or the terminal protons. In previous studies, the location of aromatic additive,

viz., phenol, within the CTAB micelles was identified by ^{1}H NMR technique.[23,24] The ring induced upfield shift in ^{1}H NMR peaks of quaternary ammonium protons of 10 mM CTAB in presence of 5 mM phenol, was taken as evidence in favor of intercalation of aromatic moiety at the outer micellar surface.[23] In the present study similar shielding effect on the CTAB protons have been observed. The shielding effects is extended to the adjacent methylene protons (C2 and C3) as well. It is, therefore, suggested that the phenolic moiety of TROE intercalates between the CTAB molecules at the micellar interface and penetrates deep within the palisade layer, due to which the α (C2) and β (C3) protons experience a significant upfield perturbation. This disrupts the hydration of quaternary ammonium head group creating relatively more non-polar environment for the head group and the methylene groups, and is reflected in the upfield chemical shift.[22] The insertion of octyl chain of TROE increases the hydrophobicity of the micellar core which is further evident in the small but significant upfield resonance signals for the chain protons and terminal methyl protons of CTAB. The hydrophobic association between the hydrocarbon chains of both micelles and the TROE along with the interaction of the aromatic ring with the cationic head group of CTAB are the major driving forces which stabilize the system and eventually decreases the surface curvature of CTAB micelles via screening of head group charges and leads to the formation of wormlike micelles.

3.3.2. 2D ROESY

In order to understand the internuclei distances and the molecular conformation of CTAB and TROE in the CTAB-TROE mixture, two dimensional (2D) rotating frame nuclear overhauser effect spectroscopy (ROESY) was carried out. The key cross-peaks in ROESY experiment reflect the extent of magnetization transfer between the nuclei and proximity of the associated proton pairs. ROESY spectra provide vital information regarding the spatial orientation and conformation of the molecule in the system.[5,16]

Figure 3 (b) shows the 2D ROESY spectrum of 14mM CTAB in presence of 6mM TROE in D_2O.

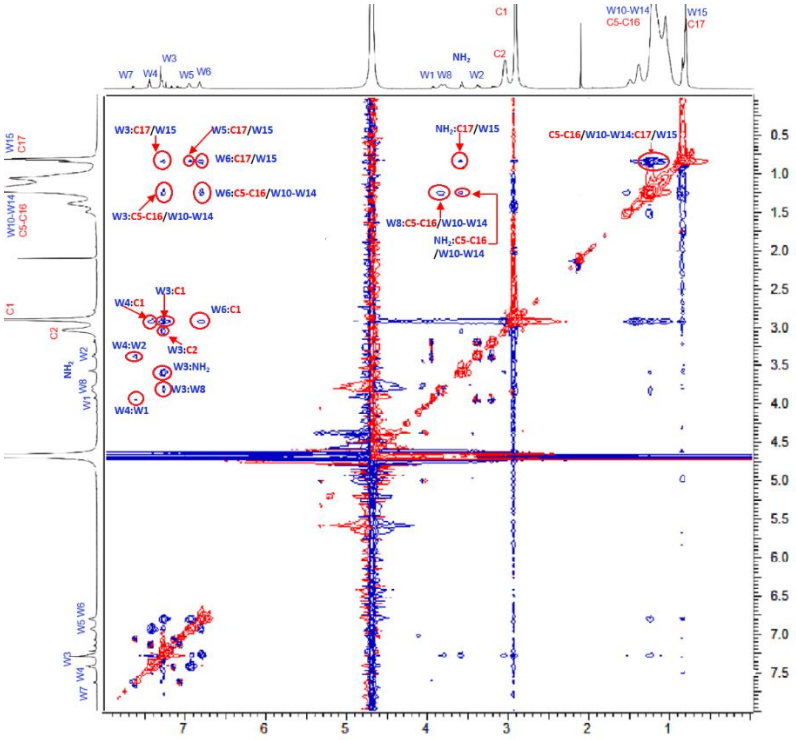

Figure 3 (b) 2D ROESY spectrum of mixture of 14 mM CTAB and 6 mM TROE in D_2O at 298 K.

The presence of ROESY cross-peaks indicates that the interacting proton pairs reside within a proximity of 5 Å.[11] Several cross-peaks are observed indicating intra- and inter-molecular interactions between the CTAB and the TROE. Intense cross-peaks W3:C1, W4:C1 and W6:C1 signify substantial interaction of the NMe group of CTAB with the aromatic part of TROE. Further, it suggests that the aromatic part of TROE reside very close to the CTAB head group i.e. at the micellar interface. No cross-peaks linking the aromatic part to the further methylene protons viz. C3 or C4 have been observed. This further emphasized that indeed the aromatic π-system of TROE is in close proximity of the head group only and does not extend further down the palisade layer. Moreover, the cross-peak W3:C2 shows interaction of the α protons (C2) of CTAB with aromatic part proton W3 while no signal connecting C2 with any of the protons on benzene ring of TROE is observed. This implies that the TROE is intercalated through the micellar interface with the five membered ring oriented downward and the six membered ring towards the interface. Proximity of hydrocarbon chains of CTAB and terminal methyl group of TROE is evident from the cross-peak C5-C16:W15/C17. Another significant cross-peak viz., W8:C5-C16, is obtained and suggests the proximity of W8 (first methylene proton of the hydrocarbon chain) of TROE with the aliphatic chain of CTAB. This provides considerable evidence that the

TROE molecule is flanked between the CTAB molecules as the protons from both the hydrocarbon chains interact strongly with each other, while the cationic head group of the surfactant interact with the aromatic head of TROE. However, the presence of the key cross-peaks W3:C17/W15, W5:C17/W15, W6:C17/W15 is rather interesting. These signify that the aromatic protons W3, W5 and W6 interact with the terminal protons C17/W15 as well. W3 and W6 protons of TROE also interact with the aliphatic carbon chain of CTAB i.e. C5-C16 as indicated by the corresponding cross-peak viz. W3:C5-C16 and W6:C5-C16. The presence of these cross-peaks indicate that CTAB and TROE exist in more than one conformation. Such interaction between the aromatic protons of TROE and terminal/aliphatic protons is possible if the aliphatic methylene groups of CTAB come in close proximity (>5 Å) with the aromatic part of TROE.

The rheological behavior of the CTAB-TROE mixture at same composition but at higher concentration (140:60 mM) showed the presence of well-defined worm-like micelles in the system. It is likely that even at lower concentration i.e. 14:6 mM (CTAB:TROE); the system consists of rod-like micelles although the micellar density may be much less. The shielding of electrostatic charge of the quaternary ammonium head groups of CTAB caused by the flanked TROE moiety drives the surfactant head groups to come closer reducing the surface curvature as already mentioned in section 3.1.[11,25] Thus parallel orientation of the two moieties constitute the "cylindrical body" of the rod/worm-like micelles. The end-caps, however, have different geometry (detailed in chapter VI). The key cross peaks indicating the interaction between the CTAB head group protons and the terminal alkyl protons suggest that the long hydrocarbon chain of CTAB might remain in the vicinity of the quaternary ammonium head group. Therefore, it is obvious that the above interactions have been originated from the CTAB and TROE molecules from some other environment rather than cylindrical body of the micelles. The geometry of the end-caps of rod/wormlike micelles for CTAB-TYOE and CTAB-TYDE is shown to be flat end-caps and not hemispherical due to the presence of considerable cation-π interaction in the cap regions (Chapter VI). Similar end-cap geometry for the present system indeed explain the observed ROESY results. This further suggests that under the present concentration condition of CTAB and TROE, the rod or cylindrical micelles are not very long and the number density of these micelles and the end-caps are quite high. The ROESY cross-

peaks corresponding to these interactions are quite intense suggesting that considerably large fraction of molecules remain in this orientation.

Non-Newtonian flow regime

3.5. Rheological behavior of the wormlike micelles

The dilute solutions of CTAB-TROE, showed an increase in viscosity with TROE concentration and the viscosity was maximum at χ_{TROE} 0.3. At this concentration, i.e. CTAB (14 mM)-TROE (6 mM), the solution showed recoiling of entrapped air bubbles. Upon increasing the concentration ten times, i.e. at 140 mM CTAB and 60 mM TROE, the solution became viscous enough to support its own weight when the vial was held upside down. This motivated us to study its dynamic rheological behavior which is a very sensitive nanostructure probe in complex fluids. Figure 4 shows the dynamic stress sweep to determine the linear viscoelastic regime of the CTAB-TROE gels at two different temperatures.

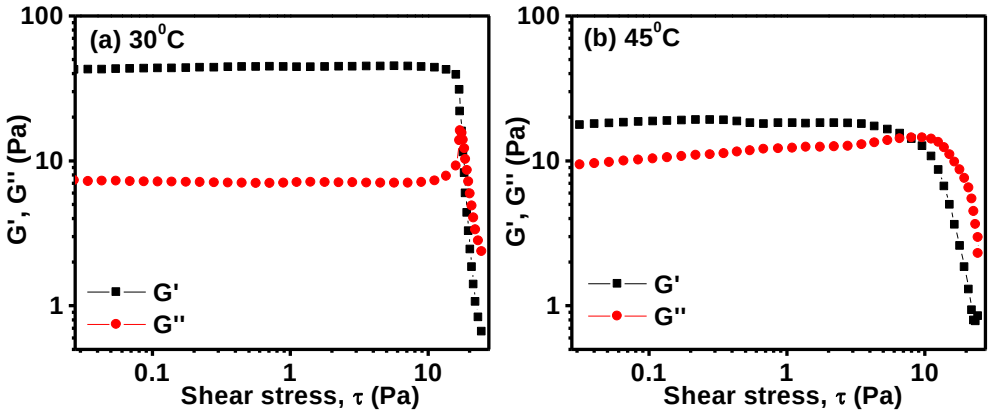

Figure 4. Dynamic shear stress sweep of CTAB-TROE mixed system at χ_{TROE} 0.3 and total concentration of 200 mM at (a) 30^{0}C and (b) 45^{0}C.

Both elastic (G′) and loss modulus (G″) are independent of the applied stress upto 10 Pa. This shows that the system has viscoelastic nature.[11] The storage modulus is greater than the loss modulus at both temperatures and this shows that the system is predominantly elastic within the Newtonian flow regime. At increased temperature of 45^{0}C, the drop of elastic modulus, G′, from ~ 45 Pa to ~ 20 Pa at 30^{0}C and increase in viscous modulus G″, from ~ 0.7 Pa to ~1 Pa at 30^{0}C show that the temperature has profound effect on the micro-structural arrangement of the molecules. The plots G′ and

G″ as a function of shear frequency for the CTAB (140 mM)-TROE (60 mM) mixture at different temperature are shown in Figure 5.

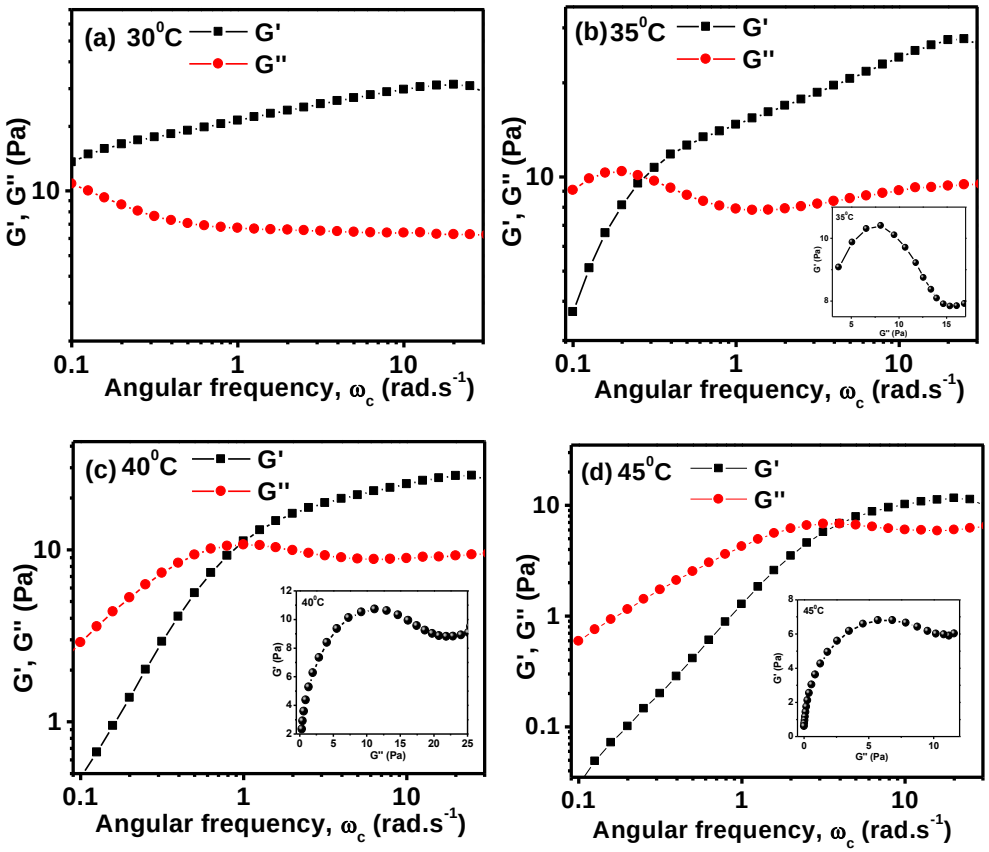

Figure 5. Variation of storage modulus. G′ and viscous modulus, G″ with angular frequency, ω of CTAB-TROE mixed system at $\alpha_{TROE\ 0.3}$ and total concentration 200 mM at (A) 30^{0}C, (B) 35^{0}C, (C) 40^{0}C, (D) 45^{0}C. Inset display corresponding Cole-Cole plot (G′ *vs* G″) of the systems.

At a lower frequency regime, both the elastic modulus G′ and the viscous modulus G″ increased with increasing frequency; G″ was slightly greater than G′ and overlapped at the frequency (ω_c) for 35^{0}C, 40^{0}C and 45^{0}C. ω_c for 30^{0}C was not observed within the inspected range. However, at higher frequency, G′ was greater than G″ indicating predominance of the elastic response, whereas G″ slightly decreased initially and then increased. Similar rheological behavior have been observed in samples reported earlier.[26] This phenomenon is in good agreement with Maxwell's mechanical model[27] which can be used to describe the dynamic rheological behavior of a viscoelastic micellar solution. According to this model, the parameters are related as per following equations:

$$G'(\omega) = G_0\omega^2\tau_R^2/(1+\omega^2\tau_R^2) \quad (1)$$

$$G''(\omega) = G_0 \omega \tau_R / (1 + \omega^2 \tau_R^2) \quad (2)$$

$$\tau_R = {}^{1}/_{\omega_c} \quad (3)$$

$$G_0 = 2G_c \quad (4)$$

where τ_R is the relaxation time with a value of ${}^{1}/_{\omega_c}$. At a certain temperature, G_0, or the plateau modulus, (the constant value of G´ at higher frequencies) is a measure of the degree of entanglement, whereas the relaxation time, τ_R gives information regarding the average micellar length.

G´ dominates G″ over a wide range of frequencies (above ω 0. 3 rad s^{-1}). As can be seen from Figure 5, with increase in temperature, the relaxation time decreases following an exponential trend in decay i.e. from 3.65 s at 35^0C to 0.23 s at 45^0C. This further shows that relaxation of stress, which mainly occur by reptation and breakage in viscoelastic solutions,[27] is dependent on temperature. The semicircular shape of the Cole–Cole plots (plots of G″ as a function of G´) corresponding to the oscillatory measurements shows how well the rheological data fit with the Maxwell model, which is expressed by Equation (5)-

$$G''^2 + \left(G' - \frac{G_0}{2}\right)^2 = \left(\frac{G_0}{2}\right)^2 \quad (5)$$

As shown in Figure 5 (insets), the Cole-Cole plots are in good agreement with the semicircular behavior at low frequencies and this proves the presence of wormlike micelles. G″ deviate at high frequencies indicating that the worm-like micelles are in dynamic equilibrium and the process of breaking and recombination of the micellar chains takes place rapidly while the system relaxes faster via Rouse or breathing modes.[28] Figure 6 show the steady rheological measurements in aqueous CTAB (140 mM)-TROE (60 mM) mixture solution, demonstrating the variation of steady shear viscosity (η) as a function of shear rate at different temperatures.

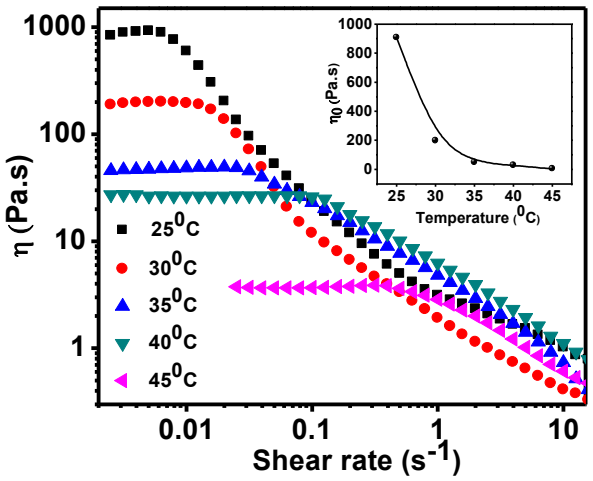

Figure 6. Variation of shear viscosity, η, of the CTAB-TROE mixed system at χ_{TROE} 0.3 and total concentration 200 of mM with temperature.

The system exhibits shear-thinning behavior with a Newtonian plateau which varies from about 1000 Pa.s at 25^{0}C to 4 Pa.s at 45^{0}C at lower shear rates; while at higher shear rates, a notable decrease in viscosity is observed. This is caused by the alignment of the wormlike chains under the direction of flow.[29] The critical shear rate ($\dot{\gamma}$) (the shear rate at which shear thinning starts) increases by 2 orders of magnitude when temperature is raised from 25^{0}C to 45^{0}C. From the inset of Figure 6, it can be seen that the viscosity of the system decreases exponentially with increase in temperature. The exponential decay of both viscosity and the relaxation time, is in accordance with Arrhenius equation for Maxwell fluids:[25]

$$\tau_R = A.\exp(^{E_A}/_{R.T}) \quad (6)$$

$$\eta_0 = G_0 A.\exp(^{E_A}/_{R.T}) \quad (7)$$

where A is the pre-exponential factor and is a constant, R is the universal gas constant taken as 8.314 J.mol^{-1}. K^{-1} and T is the temperature. From the slope of the plot of $\log \tau_R$ vs 1/T, (Figure 7) the flow activation energy was found out to be 91.47 kJ.mol^{-1}. The plot of $\log \eta_0$ vs 1/T have identical slope which further confirms the Maxwellian nature of worm-like micelles.

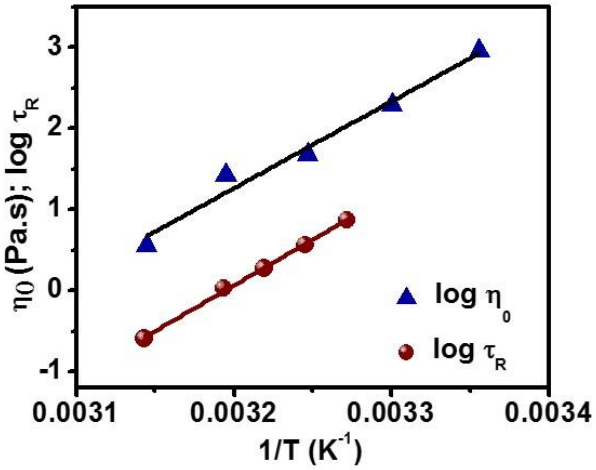

Figure 7. Plot of $\log \tau_R$ *vs* 1/T and $\log \eta_0$ vs 1/T (Arrheius' Semilog plots) of CTAB (140 mM)-TROE (60 mM) solution.

3.6. HRTEM and DFT study

For better understanding and quantitative estimation of energy involved in the cation-π interaction in the present system, DFT calculations using the hybrid functional UB3LYP and basis set 6-31G were performed in Gaussian 09 package[30] with CTA^+-TROE molecules in absence of solvent. The associated binding energy was found to be -48.14 $kJ.mol^{-1}$ (or -11.10 $kcal.mol^{-1}$). This is consistent with the order of magnitude of binding energy observed between the ammonium head group and aromatic systems viz., benzene, acetylcholine etc.[31,32] under similar conditions. It is further confirmed that the observed binding energy is due to strong cation- π interaction between the moieties. This observation in the present system, therefore, suggests that the synergistic nature of the interaction between CTA^+ and TROE is primarily driven by the strong cation- π interaction between the aromatic π electron cloud of tryptophan moiety and the positively charged ammonium head group of CTAB. The electrostatic surface potentials at 0.001 $e.Bohr^{-3}$ isodensity surface have been calculated and presented in Figure 8.

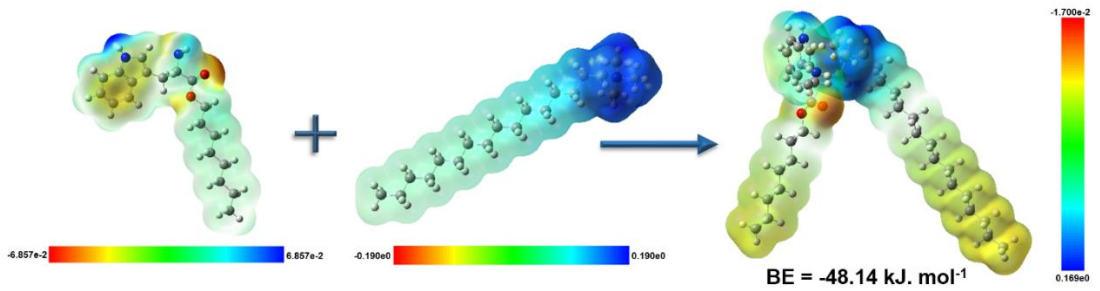

Figure 8. B3LYP/6-31G electrostatic surface potentials, in Hartrees, at 0.001 e. Bohr^{-3} isodensity surface of TROE, CTA$^+$ and CTA$^+$- TROE system.

A large difference in electrostatic surface potentials at the head group of individual TROE and CTA$^+$ moiety is evident which gives rise to the observed strong cation-π interaction between the same.

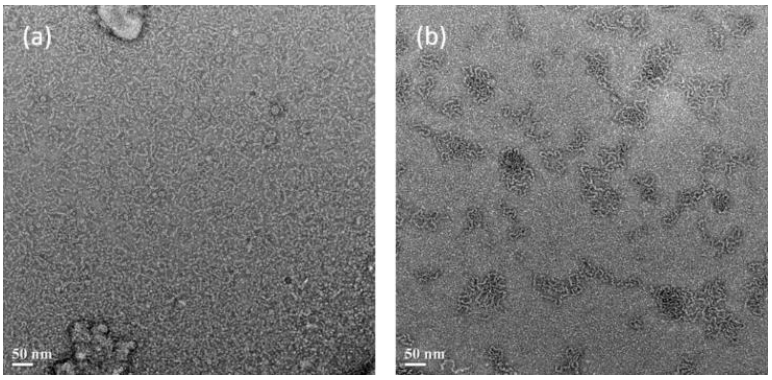

Figure 9. HRTEM micrographs of 10 mM CTAB and 6 mM TROE at different fields of view at 298 K.

The aggregates of CTAB-TROE system are visualized using HRTEM. The TEM micrographs distinctively show the presence of both linear (Figure 9 (a)) as well as highly entangled (Figure 9 (b)) worm like micelles in the system. This also gives direct evidence of the efficient transition of spherical aggregates of CTAB to wormlike cylindrical micelles, triggered by the aminoacid ester.

4. Conclusion

Study of interfacial property reveals that surface activity of CTAB is highly enhanced in presence of TROE. Calculation of interaction parameter provide support in favor of non-ideal mixing of the CTAB and TROE molecules, yielding negative magnitude of β, which shows that this interaction is attractive and synergistic in nature. Fluorescent behavior of TROE reveals progressive binding of TROE molecules to CTAB. NMR

spectroscopy provided considerable evidence of strong cation-π interaction to take place between the quaternary ammonium head groups of CTAB and the electron rich π conjugated indole face of TROE. The CTAB-TROE system showed marked change in their physical property at increased concentration. Highly viscoelastic gels comprised of linear as well as wormlike micelles were observed via HR TEM microscopy. The study demonstrates high efficiency of TROE, which is an important model representing membrane bound tryptophan residues, in tuning the morphology of CTAB micelles. The system mimics the microenvironment of lipid membranes through cation-π interaction as well as hydrogen bond. As the above morphology transition is mediated via tryptophan residues, it opens up an interesting avenue to examine through careful monitoring of the external parameters, whether such process can selectively modify the local bending of membrane curvature at the tryptophan-rich sites, and to understand the structural change at the membrane interface induced in vital biological processes including cellular fission, fusion or viral entry through cell membrane.

References are provided in BIBLIOGRAPHY under “References for Chapter VII” (Page 190-192)

BIBLIOGRAPHY

References for Chapter I

1. Fuhrhop, J.-H.; Koning, J., *Membranes and Molecular Assemblies: The Synkinetic Approach*. The Royal Society of Chemistry: Cambridge, p X001-X004.
2. Platz, G., J. H. Clint: Surfactant Aggregation, Blackie Publishing Group, Glasgow, London, 1992, ISBN In *Berichte der Bunsengesellschaft für physikalische Chemie*, Wiley-VCH Verlag GmbH & Co. KGaA: 1992; Vol. 96, pp 742-742.
3. Lasic, D. D., *Liposomes : from physics to applications*. Elsevier: Amsterdam ; New York 1993; p xviii.
4. Kunitake, T., Synthetic Bilayer Membranes: Molecular Design, Self-Organization, and Application. *Angewandte Chemie International Edition in English* **1992,** *31* (6), 709-726.
5. Mortara, R. A.; Quina, F. H.; Chaimovich, H., Formation of closed vesicles from a simple phosphate diester. Preparation and some properties of vesicles of dihexadecyl phosphate. *Biochemical and Biophysical Research Communications* **1978,** *81* (4), 1080-1086.
6. Hoffmann, H.; Kalus, J.; Thurn, H., Small angle neutron scattering measurements on micellar solutions of perfluor detergents. *Colloid and Polymer Science* **1983,** *261* (12), 1043-1049.
7. Kunitake, T.; Okahata, Y.; Tamaki, K.; Kumamaru, F.; Takayanagi, M., formation of the bilayer membrane from a series of quaternary ammonium salts. *Chemistry Letters* **1977,** *6* (4), 387-390.
8. Nagarajan, R., Molecular Packing Parameter and Surfactant Self-Assembly: The Neglected Role of the Surfactant Tail. *Langmuir* **2002,** *18* (1), 31-38.
9. Kunitake, T.; Okahata, Y., A totally synthetic bilayer membrane. *Journal of the American Chemical Society* **1977,** *99* (11), 3860-3861.
10. Feitosa, E.; Brown, W., Fragment and Vesicle Structures in Sonicated Dispersions of Dioctadecyldimethylammonium Bromide. *Langmuir* **1997,** *13* (18), 4810-4816.
11. Benatti, C. R.; Tiera, M. J.; Feitosa, E.; Olofsson, G., Phase behavior of synthetic amphiphile vesicles investigated by calorimetry and fluorescence methods1Presented at the IUPAC International Symposium on Calorimetry and Chemical Thermodynamics, April 5–9, 1998, Campinas, Brazil.1. *Thermochimica Acta* **1999,** *328* (1), 137-142.
12. Benatti, C. R.; Feitosa, E.; Fernandez, R. M.; Lamy-Freund, M. T., Structural and thermal characterization of dioctadecyldimethylammonium bromide dispersions by spin labels. *Chemistry and Physics of Lipids* **2001,** *111* (2), 93-104.
13. Feitosa, E.; Barreleiro, P. C. A.; Olofsson, G., Phase transition in dioctadecyldimethylammonium bromide and chloride vesicles prepared by different methods. *Chemistry and Physics of Lipids* **2000,** *105* (2), 201-213.

14. Bhattacharya, S.; Dileep, P. V., Membrane-Forming Properties of Cationic Lipids Bearing Oxyethylene-Based Linkages. *The Journal of Physical Chemistry B* **2003,** *107* (16), 3719-3725.

15. Berr, S. S.; Caponetti, E.; Johnson, J. S.; Jones, R. R. M.; Magid, L. J., Small-angle neutron scattering from hexadecyltrimethylammonium bromide micelles in aqueous solutions. *The Journal of Physical Chemistry* **1986,** *90* (22), 5766-5770.

16. Berr, S. S.; Coleman, M. J.; Jones, R. R. M.; Johnson, J. S., Small-angle neutron scattering study of the structural effects of substitution of tetramethylammonium for sodium as the counterion in dodecyl sulfate micelles. *The Journal of Physical Chemistry* **1986,** *90* (24), 6492-6499.

17. Berr, S. S., Solvent isotope effects on alkytrimethylammonium bromide micelles as a function of alkyl chain length. *The Journal of Physical Chemistry* **1987,** *91* (18), 4760-4765.

18. Turro, N. J.; Grätzel, M.; Braun, A. M., Photophysical and Photochemical Processes in Micellar Systems. *Angewandte Chemie International Edition in English* **1980,** *19* (9), 675-696.

19. Zana, R., Surfactant solutions: new methods of investigation. M. Dekker: New York, 1987.

20. Mukherjee, P.; Mysels, K. J., *Critical micelle concentrations of aqueous surfactant systems. NSRDS-NBS 36*. Wiley Subscription Services, Inc., A Wiley Company: Washington, DC, 1971; Vol. 61, p 319-319.

21. Fenske, B.; Maurer, N.; Cullis, P. R., Encapsulation of weakly-basic drugs, antisense oligonucleotides and plasmid DNA within large unilamellar vesicles for drug delivery applications,. In *In Liposomes: a practical approach, ,* 2nd ed.; Torchilin, V.; Weissig, V., Eds. Oxford University Press: Oxford, 2003; pp 167-191.

22. Taylor, K. M. G.; J., F., Liposomes in drug delivery. Patel, H. M., Ed. Harwood Academic Publishers: Switzerland, 1993; Vol. 2, pp 95-109.

23. Paleos, C. M.; Sideratou, Z.; Tsiourvas, D., Molecular Recognition of Complementary Liposomes in Modeling Cell–Cell Recognition. *ChemBioChem* **2001,** *2* (5), 305-310.

24. Voskuhl, J.; Ravoo, B. J., Molecular recognition of bilayer vesicles. *Chemical Society Reviews* **2009,** *38* (2), 495-505.

25. van Swaay, D.; deMello, A., Microfluidic methods for forming liposomes. *Lab on a Chip* **2013,** *13* (5), 752-767.

26. Lin, Z.; Cai, J. J.; Scriven, L. E.; Davis, H. T., Spherical-to-Wormlike Micelle Transition in CTAB Solutions. *The Journal of Physical Chemistry* **1994,** *98* (23), 5984-5993.

27. Zheng, Y.; Lin, Z.; Zakin, J. L.; Talmon, Y.; Davis, H. T.; Scriven, L. E., Cryo-TEM Imaging the Flow-Induced Transition from Vesicles to Threadlike Micelles. *The Journal of Physical Chemistry B* **2000,** *104* (22), 5263-5271.

28. Manohar, C.; Rao, U. R. K.; Valaulikar, B. S.; Lyer, R. M., On the origin of viscoelasticity in micellar solutions of cetyltrimethylammonium bromide and sodium salicylate. *Journal of the Chemical Society, Chemical Communications* **1986,** (5), 379-381.

29. Hassan, P. A.; Valaulikar, B. S.; Manohar, C.; Kern, F.; Bourdieu, L.; Candau, S. J., Vesicle to Micelle Transition: Rheological Investigations. *Langmuir* **1996,** *12* (18), 4350-4357.

30. Davies, T. S.; Ketner, A. M.; Raghavan, S. R., Self-Assembly of Surfactant Vesicles that Transform into Viscoelastic Wormlike Micelles upon Heating. *Journal of the American Chemical Society* **2006,** *128* (20), 6669-6675.

31. Zhang, L.; Eisenberg, A., Multiple Morphologies of "Crew-Cut" Aggregates of Polystyrene-b-poly(acrylic acid) Block Copolymers. *Science* **1995,** *268* (5218), 1728.

32. Blanazs, A.; Armes, S. P.; Ryan, A. J., Self-Assembled Block Copolymer Aggregates: From Micelles to Vesicles and their Biological Applications. *Macromolecular Rapid Communications* **2009,** *30* (4-5), 267-277.

33. Antonietti, M.; Förster, S., Vesicles and Liposomes: A Self-Assembly Principle Beyond Lipids. *Advanced Materials* **2003,** *15* (16), 1323-1333.

34. Discher, D. E.; Eisenberg, A., Polymer Vesicles. *Science* **2002,** *297* (5583), 967.

35. Hamley, I. W., Nanoshells and nanotubes from block copolymers. *Soft Matter* **2005,** *1* (1), 36-43.

36. Kita-Tokarczyk, K.; Grumelard, J.; Haefele, T.; Meier, W., Block copolymer vesicles—using concepts from polymer chemistry to mimic biomembranes. *Polymer* **2005,** *46* (11), 3540-3563.

37. Smart, T.; Lomas, H.; Massignani, M.; Flores-Merino, M. V.; Perez, L. R.; Battaglia, G., Block copolymer nanostructures. *Nano Today* **2008,** *3* (3), 38-46.

38. Ahmed, F.; Pakunlu, R. I.; Srinivas, G.; Brannan, A.; Bates, F.; Klein, M. L.; Minko, T.; Discher, D. E., Shrinkage of a Rapidly Growing Tumor by Drug-Loaded Polymersomes: pH-Triggered Release through Copolymer Degradation. *Molecular Pharmaceutics* **2006,** *3* (3), 340-350.

39. Pang, Z.; Lu, W.; Gao, H.; Hu, K.; Chen, J.; Zhang, C.; Gao, X.; Jiang, X.; Zhu, C., Preparation and brain delivery property of biodegradable polymersomes conjugated with OX26. *Journal of Controlled Release* **2008,** *128* (2), 120-127.

40. Lomas, H.; Canton, I.; MacNeil, S.; Du, J.; Armes, S. P.; Ryan, A. J.; Lewis, A. L.; Battaglia, G., Biomimetic pH Sensitive Polymersomes for Efficient DNA Encapsulation and Delivery. *Advanced Materials* **2007,** *19* (23), 4238-4243.

41. Lomas, H.; Massignani, M.; Abdullah, K. A.; Canton, I.; Lo Presti, C.; MacNeil, S.; Du, J.; Blanazs, A.; Madsen, J.; Armes, S. P.; Lewis, A. L.; Battaglia, G., Non-cytotoxic polymer vesicles for rapid and efficient intracellular delivery. *Faraday Discussions* **2008,** *139* (0), 143-159.

42. Axthelm, F.; Casse, O.; Koppenol, W. H.; Nauser, T.; Meier, W.; Palivan, C. G., Antioxidant Nanoreactor Based on Superoxide Dismutase Encapsulated in

Superoxide-Permeable Vesicles. *The Journal of Physical Chemistry B* **2008,** *112* (28), 8211-8217.

43. Broz, P.; Driamov, S.; Ziegler, J.; Ben-Haim, N.; Marsch, S.; Meier, W.; Hunziker, P., Toward Intelligent Nanosize Bioreactors: A pH-Switchable, Channel-Equipped, Functional Polymer Nanocontainer. *Nano Letters* **2006,** *6* (10), 2349-2353.

44. Ben-Haim, N.; Broz, P.; Marsch, S.; Meier, W.; Hunziker, P., Cell-Specific Integration of Artificial Organelles Based on Functionalized Polymer Vesicles. *Nano Letters* **2008,** *8* (5), 1368-1373.

45. Walker, L. M., Rheology and structure of worm-like micelles. *Current Opinion in Colloid & Interface Science* **2001,** *6* (5), 451-456.

46. Cates, M. E., Reptation of living polymers: dynamics of entangled polymers in the presence of reversible chain-scission reactions. *Macromolecules* **1987,** *20* (9), 2289-2296.

47. Cates, M. E.; Candau, S. J., Statics and dynamics of worm-like surfactant micelles. *Journal of Physics: Condensed Matter* **1990,** *2* (33), 6869.

48. Candau, S. J.; Khatory, A.; Lequeux, F.; Kern, F., Rheological behaviour of wormlike micelles : effect of salt content. *J. Phys. IV France* **1993,** *03* (C1), C1-197-C1-209.

49. Candau, S. J.; Hirsch, E.; Zana, R., Light scattering investigations of the behavior of semidilute aqueous micellar solutions of cetyltrimethylammonium bromide: Analogy with semidilute polymer solutions. *Journal of Colloid and Interface Science* **1985,** *105* (2), 521-528.

50. Cates, M. E., Nonlinear viscoelasticity of wormlike micelles (and other reversibly breakable polymers). *The Journal of Physical Chemistry* **1990,** *94* (1), 371-375.

51. Magid, L. J., The Surfactant−Polyelectrolyte Analogy. *The Journal of Physical Chemistry B* **1998,** *102* (21), 4064-4074.

52. Rose, G. D.; Teot, A. S., Viscoelastic Surfactants. In *Structure and Flow in Surfactant Solutions*, American Chemical Society: 1994; Vol. 578, pp 352-369.

53. Zakin Jacques, L.; Lu, B.; Bewersdorff, H.-W., Surfactant Drag Reduction. In *Reviews in Chemical Engineering*, 1998; Vol. 14, p 253.

54. Lin, Z.; Zakin, J. L.; Zheng, Y.; Davis, H. T.; Scriven, L. E.; Talmon, Y., Comparison of the effects of dimethyl and dichloro benzoate counterions on drag reduction, rheological behaviors, and microstructures of a cationic surfactant. *Journal of Rheology* **2001,** *45* (4), 963-981.

55. Zhang, Y.; Qi, Y.; Zakin, J. L., Headgroup effect on drag reduction and rheological properties of micellar solutions of quaternary ammonium surfactants. *Rheologica Acta* **2005,** *45* (1), 42-58.

56. Drappier, J.; Divoux, T.; Amarouchene, Y.; Bertrand, F.; Rodts, S.; Cadot, O.; Meunier, J.; Daniel, B., Turbulent drag reduction by surfactants. *EPL (Europhysics Letters)* **2006,** *74* (2), 362.

57. Samuel, M. M.; Dismuke, K. I.; Card, R. J.; Brown, J. E.; England, K. W., Methods of fracturing subterranean formations. Google Patents: 2001.

58. Yang, J., Viscoelastic wormlike micelles and their applications. *Current Opinion in Colloid & Interface Science* **2002,** *7* (5), 276-281.

59. Wittmer, J. P.; van der Schoot, P.; Milchev, A.; Barrat, J. L., Dynamical Monte Carlo study of equilibrium polymers. II. The role of rings. *The Journal of Chemical Physics* **2000,** *113* (16), 6992-7005.

60. Padding, J. T.; Boek, E. S.; Briels, W. J., Rheology of wormlike micellar fluids from Brownian and molecular dynamics simulations. *Journal of Physics: Condensed Matter* **2005,** *17* (45), S3347.

61. Andreev, V. A.; Victorov, A. I., Molecular Thermodynamics for Micellar Branching in Solutions of Ionic Surfactants. *Langmuir* **2006,** *22* (20), 8298-8310.

62. Dreiss, C. A., Wormlike micelles: where do we stand? Recent developments, linear rheology and scattering techniques. *Soft Matter* **2007,** *3* (8), 956-970.

63. Bylund, G., Rheology. In *Dairy processing handbook*, Tetra Pak Processing Systems Lund, Sweden, 1995; pp 37-44.

64. de Gennes, P. G., *Scaling Concepts in Polymer Physics*. Cornell University Press: 1979.

65. Khatory, A.; Lequeux, F.; Kern, F.; Candau, S. J., Linear and nonlinear viscoelasticity of semidilute solutions of wormlike micelles at high salt content. *Langmuir* **1993,** *9* (6), 1456-1464.

66. Granek, R.; Cates, M. E., Stress relaxation in living polymers: Results from a Poisson renewal model. *The Journal of Chemical Physics* **1992,** *96* (6), 4758-4767.

67. Larson, R. G., The structure and rheology of complex fluids. **1999**.

68. Aniansson, E. A. G.; Wall, S. N.; Almgren, M.; Hoffmann, H.; Kielmann, I.; Ulbricht, W.; Zana, R.; Lang, J.; Tondre, C., Theory of the kinetics of micellar equilibria and quantitative interpretation of chemical relaxation studies of micellar solutions of ionic surfactants. *The Journal of Physical Chemistry* **1976,** *80* (9), 905-922.

69. Candau, S. J.; Hirsch, E.; Zana, R.; Adam, M., Network properties of semidilute aqueous KBr solutions of cetyltrimethylammonium bromide. *Journal of Colloid and Interface Science* **1988,** *122* (2), 430-440.

70. Gelbart, W. M.; Ben-Shaul, A.; Roux, D., *Micelles, Membranes, Microemulsions, and Monolayers*. 1 ed.; Springer-Verlag New York: New York, 1994; p XVI, 608.

71. Israelachvili, J. N., *Intermolecular and Surface Forces*. Academic Press: Santa Barbara, 1992; p 704.

72. Cates, M. E., Dynamics of living polymers and flexible surfactant micelles : scaling laws for dilution. *J. Phys. France* **1988,** *49* (9), 1593-1600.

73. Safran, S. A.; Pincus, P. A.; Cates, M. E.; MacKintosh, F. C., Growth of charged micelles. *J. Phys. France* **1990,** *51* (6), 503-510.

74. MacKintosh, F. C.; Safran, S. A.; Pincus, P. A., Self-Assembly of Linear Aggregates: the Effect of Electrostatics on Growth. *EPL (Europhysics Letters)* **1990,** *12* (8), 697.

75. Reiss-Husson, F.; Luzzati, V., The Structure of the Micellar Solutions of Some Amphiphilic Compounds in Pure Water as Determined by Absolute Small-Angle X-Ray Scattering Techniques. *The Journal of Physical Chemistry* **1964,** *68* (12), 3504-3511.

76. Ekwall, P.; Mandell, L.; Solyom, P., The aqueous cetyl trimethylammonium bromide solutions. *Journal of Colloid and Interface Science* **1971,** *35* (4), 519-528.

77. Fontell, K.; Khan, A.; Lindström, B.; Maciejewska, D.; Puang-Ngern, S., Phase equilibria and structures in ternary systems of a cationic surfactant (C16 TABr or (C16 TA)2SO4), alcohol, and water. *Colloid and Polymer Science* **1991,** *269* (7), 727-742.

78. Porte, G.; Poggi, Y.; Appell, J.; Maret, G., Large micelles in concentrated solutions. The second critical micellar concentration. *The Journal of Physical Chemistry* **1984,** *88* (23), 5713-5720.

79. Lequeux, F.; Candau, S. J., Dynamical Properties of Wormlike Micelles. In *Structure and Flow in Surfactant Solutions*, American Chemical Society: 1994; Vol. 578, pp 51-62.

80. Candau, S. J.; Merikhi, F.; Waton, G.; Lemarechal, P., Temperature-jump study of elongated micelles of cetyltrimethylammonium bromide. *J. Phys. France* **1990,** *51* (10), 977-989.

81. Debye, P.; Anacker, E. W., Micelle Shape from Dissymmetry Measurements. *The Journal of Physical Chemistry* **1951,** *55* (5), 644-655.

82. Quirion, F.; Magid, L. J., Growth and counterion binding of cetyltrimethylammonium bromide aggregates at 25.degree.C: a neutron and light scattering study. *The Journal of Physical Chemistry* **1986,** *90* (21), 5435-5441.

83. Candau, S. J.; Hirsch, E.; Zana, R., New aspects of the behaviour of alkyltrimethylammonium bromide micelles : light scattering and viscosimetric studies. *J. Phys. France* **1984,** *45* (7), 1263-1270.

84. Arleth, L.; Bergström, M.; Pedersen, J. S., Small-Angle Neutron Scattering Study of the Growth Behavior, Flexibility, and Intermicellar Interactions of Wormlike SDS Micelles in NaBr Aqueous Solutions. *Langmuir* **2002,** *18* (14), 5343-5353.

85. Emerson, M. F.; Holtzer, A., On the ionic strength dependence of micelle number. II. *The Journal of Physical Chemistry* **1967,** *71* (6), 1898-1907.

86. Mazer, N. A.; Benedek, G. B.; Carey, M. C., An investigation of the micellar phase of sodium dodecyl sulfate in aqueous sodium chloride solutions using quasielastic light scattering spectroscopy. *The Journal of Physical Chemistry* **1976,** *80* (10), 1075-1085.

87. Young, C. Y.; Missel, P. J.; Mazer, N. A.; Benedek, G. B.; Carey, M. C., Deduction of micellar shape from angular dissymmetry measurements of light scattered from aqueous sodium dodecyl sulfate solutions at high sodium chloride concentrations. *The Journal of Physical Chemistry* **1978,** *82* (12), 1375-1378.

88. Missel, P. J.; Mazer, N. A.; Benedek, G. B.; Carey, M. C., Influence of chain length on the sphere-to-rod transition in alkyl sulfate micelles. *The Journal of Physical Chemistry* **1983,** *87* (7), 1264-1277.

89. Missel, P. J.; Mazer, N. A.; Benedek, G. B.; Young, C. Y.; Carey, M. C., Thermodynamic analysis of the growth of sodium dodecyl sulfate micelles. *The Journal of Physical Chemistry* **1980,** *84* (9), 1044-1057.

90. Magid, L. J.; Li, Z.; Butler, P. D., Flexibility of Elongated Sodium Dodecyl Sulfate Micelles in Aqueous Sodium Chloride: A Small-Angle Neutron Scattering Study. *Langmuir* **2000,** *16* (26), 10028-10036.

91. Mu, J.-H.; Li, G.-Z.; Jia, X.-L.; Wang, H.-X.; Zhang, G.-Y., Rheological Properties and Microstructures of Anionic Micellar Solutions in the Presence of Different Inorganic Salts. *The Journal of Physical Chemistry B* **2002,** *106* (44), 11685-11693.

92. Mu, J.-H.; Li, G.-Z.; Wang, Z.-W., Effect of surfactant concentration on the formation and viscoelasticity of anionic wormlike micelle by the methods of rheology and freeze-fracture TEM. *Rheologica Acta* **2002,** *41* (6), 493-499.

93. Lawson, K. D.; Flautt, T. J., Magnetically oriented lyotropic luquid crystalline phases. *Journal of the American Chemical Society* **1967,** *89* (21), 5489-5491.

94. Yu, L. J.; Saupe, A., Observation of a Biaxial Nematic Phase in Potassium Laurate-1-Decanol-Water Mixtures. *Physical Review Letters* **1980,** *45* (12), 1000-1003.

95. Hendrikx, Y.; Charvolin, J., Structural relations between lyotropic phases in the vicinity of the nematic phases. *J. Phys. France* **1981,** *42* (10), 1427-1440.

96. Hendrikx, V.; Charvolin, J.; Rawiso, M.; Liebert, L.; Holmes, M. C., Anisotropic aggregates of amphiphilic molecules in lyotropic nematic phases. *The Journal of Physical Chemistry* **1983,** *87* (20), 3991-3999.

97. Amaral, L. Q.; Helene, M. E. M., Nematic domain in the sodium lauryl sulfate/water/decanol system. *The Journal of Physical Chemistry* **1988,** *92* (21), 6094-6098.

98. Quist, P. O.; Halle, B.; Furó, I., Micelle size and order in lyotropic nematic phases from nuclear spin relaxation. *The Journal of Chemical Physics* **1992,** *96* (5), 3875-3891.

99. Thiele, T.; Berret, J. F.; Müller, S.; Schmidt, C., Rheology and NMR Measurements of Sodium Dodecyl Sulphate/Decanol/Water Nematics. In *Progress and Trends in Rheology V: Proceedings of the Fifth European Rheology Conference Portorož, Slovenia, September 6–11, 1998*, Emri, I., Ed. Steinkopff: Heidelberg, 1998; pp 537-538.

100. Porte, G.; Gomati, R.; El Haitamy, O.; Appell, J.; Marignan, J., Morphological transformations of the primary surfactant structures in brine-rich mixtures of ternary systems (surfactant/alcohol/brine). *The Journal of Physical Chemistry* **1986,** *90* (22), 5746-5751.

101. Gomati, R.; Appell, J.; Bassereau, P.; Marignan, J.; Porte, G., Influence of the nature of the counterion and of hexanol on the phase behavior of the dilute ternary

systems: cetylpyridinium bromide or chloride-hexanol-brine. *The Journal of Physical Chemistry* **1987,** *91* (24), 6203-6210.

102. Porte, G.; Marignan, J.; Bassereau, P.; May, R., Shape transformations of the aggregates in dilute surfactant solutions : a small-angle neutron scattering study. *J. Phys. France* **1988,** *49* (3), 511-519.

103. Marignan, J.; Appell, J.; Bassereau, P.; Porte, G.; May, R. P., Local structures of the surfactant aggregates in dilute solutions deduced from small angle neutron scattering patterns. *J. Phys. France* **1989,** *50* (24), 3553-3566.

104. Nastishin, Y. A., Brine-Rich Corner of the Phase Diagram of the Ternary System Cetylpyridinium Chloride−Hexanol−Brine. *Langmuir* **1996,** *12* (21), 5011-5015.

105. Bijma, K.; Blandamer, M. J.; Engberts, J. B. F. N., Effect of Counterions and Headgroup Hydrophobicity on Properties of Micelles Formed by Alkylpyridinium Surfactants. 2. Microcalorimetry. *Langmuir* **1998,** *14* (1), 79-83.

106. Bijma, K.; Engberts, J. B. F. N., Effect of Counterions on Properties of Micelles Formed by Alkylpyridinium Surfactants. 1. Conductometry and 1H-NMR Chemical Shifts. *Langmuir* **1997,** *13* (18), 4843-4849.

107. Clausen, T. M.; Vinson, P. K.; Minter, J. R.; Davis, H. T.; Talmon, Y.; Miller, W. G., Viscoelastic micellar solutions: microscopy and rheology. *The Journal of Physical Chemistry* **1992,** *96* (1), 474-484.

108. Harwigsson, I.; Soederman, O.; Regev, O., Diffusion and Cryo Transmission Electron Microscopy Studies of Bicontinuous "Micellar" Solutions. *Langmuir* **1994,** *10* (12), 4731-4734.

109. Hoffmann, H.; Platz, G.; Rehage, H.; Schorr, W., The Influence of Counter-Ion Concentration on the Aggregation Behaviour of Viscoelastic Detergents. *Berichte der Bunsengesellschaft für physikalische Chemie* **1981,** *85* (10), 877-882.

110. Hoffmann, H.; Platz, G.; Rehage, H.; Schorr, W.; Ulbricht, W., Viskoelastische Tensidlösungen. *Berichte der Bunsengesellschaft für physikalische Chemie* **1981,** *85* (4), 255-266.

111. Hyde, A. J.; Johnstone, D. W. M., The effect of organic additives on paraffin chain electrolyte solutions. VI. Light scattering measurements on viscoelastic solubilized solutions of methyl naphthalene in aqueous hexadecyl trimethyl ammonium bromide. *Journal of Colloid and Interface Science* **1975,** *53* (3), 349-357.

112. Imae, T., Light scattering of spinnable, viscoelastic solutions of hexadecyltrimethylammonium salicylate. *The Journal of Physical Chemistry* **1990,** *94* (15), 5953-5959.

113. Larsen, J. W.; Magid, L. J.; Payton, V., A highly specific effect or organic solutes at low concentration on the structure of ctab micelles. *Tetrahedron Letters* **1973,** *14* (29), 2663-2666.

114. Makhloufi, R.; Hirsch, E.; Candau, S. J.; Binana-Limbele, W.; Zana, R., Fluorescence quenching and elastic and quasi-elastic light scattering studies of elongated micelles in solutions of cetyltrimethylammonium chloride in the presence of sodium salicylate. *The Journal of Physical Chemistry* **1989,** *93* (24), 8095-8101.

115. Nash, T., The interaction of some naphthalene derivatives with a cationic soap below the critical micelle concentration. *Journal of Colloid Science* **1958,** *13* (2), 134-139.

116. Rehage, H.; Hoffmann, H., Viscoelastic surfactant solutions: model systems for rheological research. *Molecular Physics* **1991,** *74* (5), 933-973.

117. Shikata, T.; Hirata, H.; Kotaka, T., Micelle formation of detergent molecules in aqueous media: viscoelastic properties of aqueous cetyltrimethylammonium bromide solutions. *Langmuir* **1987,** *3* (6), 1081-1086.

118. Shikata, T.; Hirata, H.; Takatori, E.; Osaki, K., Nonlinear viscoelastic behavior of aqueous detergent solutions. *Journal of Non-Newtonian Fluid Mechanics* **1988,** *28* (2), 171-182.

119. Ulmius, J.; Wennerstroem, H.; Johansson, L. B. A.; Lindblom, G.; Gravsholt, S., Viscoelasticity in surfactant solutions. Characteristics of the micellar aggregates and the formation of periodic colloidal structures. *The Journal of Physical Chemistry* **1979,** *83* (17), 2232-2236.

120. Underwood, A. L.; Anacker, E. W., Organic counterions and micellar parameters: methyl-, chloro-, and phenyl-substituted acetates. *Journal of Colloid and Interface Science* **1984,** *100* (1), 128-135.

121. Göbel, S.; Hiltrop, K., Influence of organic counterions on the structure of lyotropic mesophases. In *Trends in Colloid and Interface Science V*, Corti, M.; Mallamace, F., Eds. Steinkopff: Heidelberg, 1991; pp 241-242.

122. Fischer, P.; Rehage, H.; Grüning, B., Rheological Properties of Dimeric Acid Betaine Solutions. *Tenside Surf. Det.* **1994,** *31*, 99-108.

123. Fischer, P.; Rehage, H.; Grüning, B., Linear Flow Properties of Dimer Acid Betaine Solutions with and without Changed Ionic Strength. *The Journal of Physical Chemistry B* **2002,** *106* (42), 11041-11046.

124. von Wandruszka, R., Reactions and Synthesis in Surfactant Systems. Surfactant Science Series. Volume 100 Edited by John Texter (Strider Research Corporation, Rochester, NY). Marcel Dekker: New York, Basel. 2001. xii + 909 pp. $250.00. ISBN: 0-8247-0255-7. *Journal of the American Chemical Society* **2002,** *124* (6), 1126-1127.

125. Buhler, E.; Mendes, E.; Boltenhagen, P.; Munch, J. P.; Zana, R.; Candau, S. J., Phase Behavior of Aqueous Solutions of a Dimeric Surfactant. *Langmuir* **1997,** *13* (12), 3096-3102.

126. Oda, R.; Panizza, P.; Schmutz, M.; Lequeux, F., Direct Evidence of the Shear-Induced Structure of Wormlike Micelles: Gemini Surfactant 12−2−12. *Langmuir* **1997,** *13* (24), 6407-6412.

127. Oda, R.; Huc, I.; Homo, J.-C.; Heinrich, B.; Schmutz, M.; Candau, S., Elongated Aggregates Formed by Cationic Gemini Surfactants. *Langmuir* **1999,** *15* (7), 2384-2390.

128. In, M.; Warr, G. G.; Zana, R., Dynamics of Branched Threadlike Micelles. *Physical Review Letters* **1999,** *83* (11), 2278-2281.

129. Oelschlaeger, C.; Buhler, E.; Waton, G.; Candau, S. J., Synergistic effects in mixed wormlike micelles of dimeric and single-chain cationic surfactants at high ionic strength. *The European Physical Journal E* **2003,** *11* (1), 7-20.

130. In, M.; Aguerre-Chariol, O.; Zana, R., Closed-Looped Micelles in Surfactant Tetramer Solutions. *The Journal of Physical Chemistry B* **1999,** *103* (37), 7747-7750.

131. Bergström, M.; Pedersen, J. S., Formation of Tablet-Shaped and Ribbonlike Micelles in Mixtures of an Anionic and a Cationic Surfactant. *Langmuir* **1999,** *15* (7), 2250-2253.

132. Yin, H.; Mao, M.; Huang, J.; Fu, H., Two-Phase Region in the DTAB/SL Mixed Surfactant System. *Langmuir* **2002,** *18* (24), 9198-9203.

133. Kaler, E. W.; Herrington, K. L.; Murthy, A. K.; Zasadzinski, J. A. N., Phase behavior and structures of mixtures of anionic and cationic surfactants. *The Journal of Physical Chemistry* **1992,** *96* (16), 6698-6707.

134. Koehler, R. D.; Raghavan, S. R.; Kaler, E. W., Microstructure and Dynamics of Wormlike Micellar Solutions Formed by Mixing Cationic and Anionic Surfactants. *The Journal of Physical Chemistry B* **2000,** *104* (47), 11035-11044.

135. Won, Y.-Y.; Davis, H. T.; Bates, F. S., Giant Wormlike Rubber Micelles. *Science* **1999,** *283* (5404), 960-963.

136. Won, Y.-Y.; Paso, K.; Davis, H. T.; Bates, F. S., Comparison of Original and Cross-linked Wormlike Micelles of Poly(ethylene oxide-b-butadiene) in Water: Rheological Properties and Effects of Poly(ethylene oxide) Addition. *The Journal of Physical Chemistry B* **2001,** *105* (35), 8302-8311.

137. Hamley, I. W.; Pedersen, J. S.; Booth, C.; Nace, V. M., A Small-Angle Neutron Scattering Study of Spherical and Wormlike Micelles Formed by Poly(oxyethylene)-Based Diblock Copolymers. *Langmuir* **2001,** *17* (20), 6386-6388.

138. Bernheim-Groswasser, A.; Wachtel, E.; Talmon, Y., Micellar Growth, Network Formation, and Criticality in Aqueous Solutions of the Nonionic Surfactant C12E5. *Langmuir* **2000,** *16* (9), 4131-4140.

139. Imanishi, K.; Einaga, Y., Wormlike Micelles of Polyoxyethylene Alkyl Ether Mixtures C10E5 + C14E5 and C14E5 + C14E7: Hydrophobic and Hydrophilic Chain Length Dependence of the Micellar Characteristics. *The Journal of Physical Chemistry B* **2007,** *111* (1), 62-73.

140. Jerke, G.; Pedersen, J. S.; Egelhaaf, S. U.; Schurtenberger, P., Flexibility of Charged and Uncharged Polymer-like Micelles. *Langmuir* **1998,** *14* (21), 6013-6024.

141. Jerke, G.; Pedersen, J. S.; Egelhaaf, S. U.; Schurtenberger, P., Static structure factor of polymerlike micelles: Overall dimension, flexibility, and local properties of lecithin reverse micelles in deuterated isooctane. *Physical Review E* **1997,** *56* (5), 5772-5788.

142. Arleth, L.; Bauer, R.; Øgendal, L. H.; Egelhaaf, S. U.; Schurtenberger, P.; Pedersen, J. S., Growth Behavior of Mixed Wormlike Micelles: a Small-Angle

Scattering Study of the Lecithin−Bile Salt System. *Langmuir* **2003,** *19* (10), 4096-4104.

143. Tung, S.-H.; Huang, Y.-E.; Raghavan, S. R., A New Reverse Wormlike Micellar System: Mixtures of Bile Salt and Lecithin in Organic Liquids. *Journal of the American Chemical Society* **2006,** *128* (17), 5751-5756.

144. Shumilina, E. V.; Khromova, Y. L.; Shchipunov, Y. A., The effect of lysophosphatidylcholine and phosphatidylglycerol on lecithin polymer-like micelles. *Colloid Journal* **2006,** *68* (2), 241-247.

145. Zhang, J.; Wang, L.-Q.; Wang, H.; Tu, K., Micellization Phenomena of Amphiphilic Block Copolymers Based on Methoxy Poly(ethylene glycol) and Either Crystalline or Amorphous Poly(caprolactone-b-lactide). *Biomacromolecules* **2006,** *7* (9), 2492-2500.

146. Dong, C.-M.; Chaikof, E. L., Self-assembled nanostructures of a biomimetic glycopolymer–polypeptide triblock copolymer. *Colloid and Polymer Science* **2005,** *283* (12), 1366-1370.

147. Hoeben, F. J. M.; Jonkheijm, P.; Meijer, E. W.; Schenning, A. P. H. J., About Supramolecular Assemblies of π-Conjugated Systems. *Chemical Reviews* **2005,** *105* (4), 1491-1546.

148. Guldi, D. M.; Zerbetto, F.; Georgakilas, V.; Prato, M., Ordering Fullerene Materials at Nanometer Dimensions. *Accounts of Chemical Research* **2005,** *38* (1), 38-43.

149. Yoosaf, K.; Belbakra, A.; Armaroli, N.; Llanes-Pallas, A.; Bonifazi, D., Engineering spherical nanostructures through hydrogen bonds. *Chemical Communications* **2009,** (20), 2830-2832.

150. Cui, S.; Liu, H.; Gan, L.; Li, Y.; Zhu, D., Fabrication of Low-Dimension Nanostructures Based on Organic Conjugated Molecules. *Advanced Materials* **2008,** *20* (15), 2918-2925.

151. Chaghi, R.; de Ménorval, L.-C.; Charnay, C.; Derrien, G.; Zajac, J., Interactions of phenol with cationic micelles of hexadecyltrimethylammonium bromide studied by titration calorimetry, conductimetry, and 1H NMR in the range of low additive and surfactant concentrations. *Journal of Colloid and Interface Science* **2008,** *326* (1), 227-234.

152. Mata, J. P.; Aswal, V. K.; Hassan, P. A.; Bahadur, P., A phenol-induced structural transition in aqueous cetyltrimethylammonium bromide solution. *Journal of Colloid and Interface Science* **2006,** *299* (2), 910-915.

153. Xu, K.; Ren, H.-q.; Zeng, G.-m.; Ding, L.-l.; Huang, J.-h., Investigation of interaction between phenol and cetylpyridinium chloride micelle in the absence and in the presence of electrolyte by 1H NMR spectroscopy. *Colloids and Surfaces A: Physicochemical and Engineering Aspects* **2010,** *356* (1), 150-155.

154. Lin, Y.; Qiao, Y.; Yan, Y.; Huang, J., Thermo-responsive viscoelastic wormlike micelle to elastic hydrogel transition in dual-component systems. *Soft Matter* **2009,** *5* (16), 3047-3053.

155. You, Q.; Zhang, Y.; Wang, H.; Fan, H.; Guo, J.; Li, M., The Formation of pH-Sensitive Wormlike Micelles in Ionic Liquids Driven by the Binding Ability of Anthranilic Acid. *International Journal of Molecular Sciences* **2015,** *16* (12), 26096.

156. Umeasiegbu, C. D.; Balakotaiah, V.; Krishnamoorti, R., pH-Induced Re-entrant Microstructural Transitions in Cationic Surfactant–Hydrotrope Mixtures. *Langmuir* **2016,** *32* (3), 655-663.

157. Saha, S. K.; Jha, M.; Ali, M.; Chakraborty, A.; Bit, G.; Das, S. K., Micellar Shape Transition under Dilute Salt-Free Conditions: Promotion and Self-Fluorescence Monitoring of Stimuli-Responsive Viscoelasticity by 1- and 2-Naphthols. *The Journal of Physical Chemistry B* **2008,** *112* (15), 4642-4647.

158. Ali, M.; Jha, M.; Das, S. K.; Saha, S. K., Hydrogen-Bond-Induced Microstructural Transition of Ionic Micelles in the Presence of Neutral Naphthols: pH Dependent Morphology and Location of Surface Activity. *The Journal of Physical Chemistry B* **2009,** *113* (47), 15563-15571.

159. Shintani, M.; Matsuo, Y.; Sakuraba, S.; Matubayasi, N., Interaction of naphthalene derivatives with lipids in membranes studied by the 1H-nuclear Overhauser effect and molecular dynamics simulation. *Physical Chemistry Chemical Physics* **2012,** *14* (40), 14049-14060.

160. Singh, G.; Singh, G.; Kang, T. S., Micellization Behavior of Surface Active Ionic Liquids Having Aromatic Counterions in Aqueous Media. *The Journal of Physical Chemistry B* **2016,** *120* (6), 1092-1105.

161. Sheldon, R., Catalytic reactions in ionic liquids. *Chemical Communications* **2001,** (23), 2399-2407.

162. Sheldon, R. A.; Lau, R. M.; Sorgedrager, M. J.; van Rantwijk, F.; Seddon, K. R., Biocatalysis in ionic liquids. *Green Chemistry* **2002,** *4* (2), 147-151.

163. Wasserscheid, P.; Hal, R. v.; Bosmann, A., 1-n-Butyl-3-methylimidazolium ([bmim]) octylsulfate-an even 'greener' ionic liquid. *Green Chemistry* **2002,** *4* (4), 400-404.

164. Baker, G. A.; Pandey, S.; Pandey, S.; Baker, S. N., A new class of cationic surfactants inspired by N-alkyl-N-methyl pyrrolidinium ionic liquids. *Analyst* **2004,** *129* (10), 890-892.

165. Ranu, B. C.; Banerjee, S., Ionic Liquid as Catalyst and Reaction Medium. The Dramatic Influence of a Task-Specific Ionic Liquid, [bmIm]OH, in Michael Addition of Active Methylene Compounds to Conjugated Ketones, Carboxylic Esters, and Nitriles. *Organic Letters* **2005,** *7* (14), 3049-3052.

166. Cooper, E. R.; Andrews, C. D.; Wheatley, P. S.; Webb, P. B.; Wormald, P.; Morris, R. E., Ionic liquids and eutectic mixtures as solvent and template in synthesis of zeolite analogues. *Nature* **2004,** *430* (7003), 1012-1016.

167. Kuang, D.; Brezesinski, T.; Smarsly, B., Hierarchical Porous Silica Materials with a Trimodal Pore System Using Surfactant Templates. *Journal of the American Chemical Society* **2004,** *126* (34), 10534-10535.

168. Endres, F.; Bukowski, M.; Hempelmann, R.; Natter, H., Electrodeposition of Nanocrystalline Metals and Alloys from Ionic Liquids. *Angewandte Chemie International Edition* **2003,** *42* (29), 3428-3430.

169. Huddleston, J. G.; Willauer, H. D.; Swatloski, R. P.; Visser, A. E.; Rogers, R. D., Room temperature ionic liquids as novel media for 'clean' liquid-liquid extraction. *Chemical Communications* **1998,** (16), 1765-1766.

170. Anouti, M.; Jones, J.; Boisset, A.; Jacquemin, J.; Caillon-Caravanier, M.; Lemordant, D., Aggregation behavior in water of new imidazolium and pyrrolidinium alkycarboxylates protic ionic liquids. *Journal of Colloid and Interface Science* **2009,** *340* (1), 104-111.

171. Visser, A. E.; Swatloski, R. P.; Reichert, W. M.; Mayton, R.; Sheff, S.; Wierzbicki, A.; Davis, J. H.; Rogers, R. D., Task-Specific Ionic Liquids Incorporating Novel Cations for the Coordination and Extraction of Hg2+ and Cd2+: Synthesis, Characterization, and Extraction Studies. *Environmental Science & Technology* **2002,** *36* (11), 2523-2529.

172. Stepnowski, P.; Nichthauser, J.; Mrozik, W.; Buszewski, B., Usefulness of π...π aromatic interactions in the selective separation and analysis of imidazolium and pyridinium ionic liquid cations. *Analytical and Bioanalytical Chemistry* **2006,** *385* (8), 1483-1491.

173. Holbrey, J. D.; Reichert, W. M.; Nieuwenhuyzen, M.; Sheppard, O.; Hardacre, C.; Rogers, R. D., Liquid clathrate formation in ionic liquid-aromatic mixtures. *Chemical Communications* **2003,** (4), 476-477.

174. Abe, M.; Uchiyama, H.; Yamaguchi, T.; Suzuki, T.; Ogino, K.; Scamehorn, J. F.; Christian, S. D., Micelle formation of pure nonionic surfactants and their mixtures. *Langmuir* **1992,** *8* (9), 2147-2151.

175. Park, J. W.; Bak, C. S.; Labes, M. M., Effects of molecular complexing on the properties of binary nematic liquid crystal mixtures. *Journal of the American Chemical Society* **1975,** *97* (15), 4398-4400.

176. Bowers, J.; Butts, C. P.; Martin, P. J.; Vergara-Gutierrez, M. C.; Heenan, R. K., Aggregation Behavior of Aqueous Solutions of Ionic Liquids. *Langmuir* **2004,** *20* (6), 2191-2198.

177. Vanyúr, R.; Biczók, L.; Miskolczy, Z., Micelle formation of 1-alkyl-3-methylimidazolium bromide ionic liquids in aqueous solution. *Colloids and Surfaces A: Physicochemical and Engineering Aspects* **2007,** *299* (1), 256-261.

178. Wang, X.; Liu, J.; Yu, L.; Jiao, J.; Wang, R.; Sun, L., Surface adsorption and micelle formation of imidazolium-based zwitterionic surface active ionic liquids in aqueous solution. *Journal of Colloid and Interface Science* **2013,** *391*, 103-110.

179. Cheng, N.; Yu, P.; Wang, T.; Sheng, X.; Bi, Y.; Gong, Y.; Yu, L., Self-Aggregation of New Alkylcarboxylate-Based Anionic Surface Active Ionic Liquids: Experimental and Theoretical Investigations. *The Journal of Physical Chemistry B* **2014,** *118* (10), 2758-2768.

180. Bi, Y.; Wei, H.; Hu, Q.; Xu, W.; Gong, Y.; Yu, L., Wormlike Micelles with Photoresponsive Viscoelastic Behavior Formed by Surface Active Ionic

Liquid/Azobenzene Derivative Mixed Solution. *Langmuir* **2015,** *31* (13), 3789-3798.

181. Łuczak, J.; Hupka, J.; Thöming, J.; Jungnickel, C., Self-organization of imidazolium ionic liquids in aqueous solution. *Colloids and Surfaces A: Physicochemical and Engineering Aspects* **2008,** *329* (3), 125-133.

182. Wang, A.; Shi, W.; Huang, J.; Yan, Y., Adaptive soft molecular self-assemblies. *Soft Matter* **2016,** *12* (2), 337-357.

183. Li, Y.; Holmberg, K.; Bordes, R., Micellization of true amphoteric surfactants. *Journal of Colloid and Interface Science* **2013,** *411*, 47-52.

184. Yoshimura, T.; Sakato, A.; Tsuchiya, K.; Ohkubo, T.; Sakai, H.; Abe, M.; Esumi, K., Adsorption and aggregation properties of amino acid-based N-alkyl cysteine monomeric and N,N′-dialkyl cystine gemini surfactants. *Journal of Colloid and Interface Science* **2007,** *308* (2), 466-473.

185. Trivedi, T. J.; Rao, K. S.; Singh, T.; Mandal, S. K.; Sutradhar, N.; Panda, A. B.; Kumar, A., Task-Specific, Biodegradable Amino Acid Ionic Liquid Surfactants. *ChemSusChem* **2011,** *4* (5), 604-608.

186. Moosmann, B.; Behl, C., Cytoprotective antioxidant function of tyrosine and tryptophan residues in transmembrane proteins. *European Journal of Biochemistry* **2000,** *267* (18), 5687-5692.

187. Heijne, G. V., Membrane Proteins: From Sequence to Structure. *Annual Review of Biophysics and Biomolecular Structure* **1994,** *23* (1), 167-192.

188. Landolt-Marticorena, C.; Williams, K. A.; Deber, C. M.; Reithmeier, R. A. F., Non-random Distribution of Amino Acids in the Transmembrane Segments of Human Type I Single Span Membrane Proteins. *Journal of Molecular Biology* **1993,** *229* (3), 602-608.

189. Jones, D. T.; Taylor, W. R.; Thornton, J. M., A Model Recognition Approach to the Prediction of All-Helical Membrane Protein Structure and Topology. *Biochemistry* **1994,** *33* (10), 3038-3049.

References for Chapter II

1. Dreiss, C. A., Wormlike micelles: where do we stand? Recent developments, linear rheology and scattering techniques. *Soft Matter* **2007,** *3* (8), 956-970.

2. Bowers, J.; Butts, C. P.; Martin, P. J.; Vergara-Gutierrez, M. C.; Heenan, R. K., Aggregation Behavior of Aqueous Solutions of Ionic Liquids. *Langmuir* **2004,** *20* (6), 2191-2198.

3. Catalano, V. J.; Etogo, A. O., Preparation of Au(I), Ag(I), and Pd(II) N-Heterocyclic Carbene Complexes Utilizing a Methylpyridyl-Substituted NHC Ligand. Formation of a Luminescent Coordination Polymer. *Inorganic Chemistry* **2007,** *46* (14), 5608-5615.

4. Organ, M. G.; Avola, S.; Dubovyk, I.; Hadei, N.; Kantchev, E. A. B.; O'Brien, C. J.; Valente, C., A User-Friendly, All-Purpose Pd–NHC (NHC=N-Heterocyclic Carbene) Precatalyst for the Negishi Reaction: A Step Towards a Universal Cross-Coupling Catalyst. *Chemistry – A European Journal* **2006,** *12* (18), 4749-4755.

5. Preethi, N.; Shinohara, H.; Nishide, H., Reversible oxygen-binding and facilitated oxygen transport in membranes of polyvinylimidazole complexed with cobalt-phthalocyanine. *Reactive and Functional Polymers* **2006,** *66* (8), 851-855.

6. Samantaray, M. K.; Katiyar, V.; Pang, K.; Nanavati, H.; Ghosh, P., Silver N-heterocyclic carbene complexes as initiators for bulk ring-opening polymerization (ROP) of l-lactides. *Journal of Organometallic Chemistry* **2007,** *692* (8), 1672-1682.

7. Le Poul, N.; Campion, M.; Douziech, B.; Rondelez, Y.; Le Clainche, L.; Reinaud, O.; Le Mest, Y., Monocopper Center Embedded in a Biomimetic Cavity: From Supramolecular Control of Copper Coordination to Redox Regulation. *Journal of the American Chemical Society* **2007,** *129* (28), 8801-8810.

8. Moosmann, B.; Behl, C., Cytoprotective antioxidant function of tyrosine and tryptophan residues in transmembrane proteins. *European Journal of Biochemistry* **2000,** *267* (18), 5687-5692.

References for Chapter III

1. Tung, S.H.; Huang, Y.E.; Raghavan, S. R., Contrasting Effects of Temperature on the Rheology of Normal and Reverse Wormlike Micelles. *Langmuir* **2007,** *23* (2), 372-376.

2. Koshy, P.; Aswal, V. K.; Venkatesh, M.; Hassan, P. A., Unusual Scaling in the Rheology of Branched Wormlike Micelles Formed by Cetyltrimethylammonium Bromide and Sodium Oleate. *The Journal of Physical Chemistry B* **2011,** *115* (37), 10817-10825.

3. Hayter, J. B.; Penfold, J., An analytic structure factor for macroion solutions. *Molecular Physics* **1981,** *42* (1), 109-118.

4. Chaghi, R.; de Ménorval, L.-C.; Charnay, C.; Derrien, G.; Zajac, J., Interactions of phenol with cationic micelles of hexadecyltrimethylammonium bromide studied by titration calorimetry, conductimetry, and 1H NMR in the range of low additive and surfactant concentrations. *Journal of Colloid and Interface Science* **2008,** *326* (1), 227-234.

5. Xu, K.; Ren, H.-q.; Zeng, G.-m.; Ding, L.-l.; Huang, J.-h., Investigation of interaction between phenol and cetylpyridinium chloride micelle in the absence and in the presence of electrolyte by 1H NMR spectroscopy. *Colloids and Surfaces A: Physicochemical and Engineering Aspects* **2010,** *356* (1), 150-155.

6. Alexander Ross, J. B.; Laws, W. R.; Rousslang, K. W.; Wyssbrod, H. R., Tyrosine Fluorescence and Phosphorescence from Proteins and Polypeptides. In *Topics in Fluorescence Spectroscopy*, Lakowicz, J. R., Ed. Springer US: Boston, MA, 2002; pp 1-64.

7. Rubingh, D. N., Mixed micelle solutions. In *Solution chemistry of surfactants*, Springer: 1979; pp 337-354.

8. Bergström, M.; Eriksson, J. C., A Theoretical Analysis of Synergistic Effects in Mixed Surfactant Systems. *Langmuir* **2000,** *16* (18), 7173-7181.

9. Khan, I. A.; Khanam, A. J.; Khan, Z. A.; Kabir ud, D., Mixing Behavior of Anionic Hydrotropes with Cationic Gemini Surfactants. *Journal of Chemical & Engineering Data* **2010,** *55* (11), 4775-4779.

10. Holland, P. M.; Rubingh, D. N., Mixed Surfactant Systems. In *Mixed Surfactant Systems*, American Chemical Society: 1992; Vol. 501, pp 2-30.

11. Rosen, M. J., Molecular Interactions and Synergism in Mixtures of Two Surfactants. In *Surfactants and Interfacial Phenomena*, John Wiley & Sons, Inc.: 2004; pp 379-414.

12. Ali, M.; Jha, M.; Das, S. K.; Saha, S. K., Hydrogen-Bond-Induced Microstructural Transition of Ionic Micelles in the Presence of Neutral Naphthols: pH Dependent Morphology and Location of Surface Activity. *The Journal of Physical Chemistry B* **2009,** *113* (47), 15563-15571.

13. Saha, S. K.; Jha, M.; Ali, M.; Chakraborty, A.; Bit, G.; Das, S. K., Micellar Shape Transition under Dilute Salt-Free Conditions: Promotion and Self-Fluorescence Monitoring of Stimuli-Responsive Viscoelasticity by 1- and 2-Naphthols. *The Journal of Physical Chemistry B* **2008,** *112* (15), 4642-4647.

14. Suratkar, V.; Mahapatra, S., Solubilization Site of Organic Perfume Molecules in Sodium Dodecyl Sulfate Micelles: New Insights from Proton NMR Studies. *Journal of Colloid and Interface Science* **2000,** *225* (1), 32-38.

15. Kim, B.-J.; Im, S.-S.; Oh, S.-G., Investigation on the Solubilization Locus of Aniline-HCl Salt in SDS Micelles with 1H NMR Spectroscopy. *Langmuir* **2001,** *17* (2), 565-566.

16. Sabatino, P.; Szczygiel, A.; Sinnaeve, D.; Hakimhashemi, M.; Saveyn, H.; Martins, J. C.; Van der Meeren, P., NMR study of the influence of pH on phenol sorption in cationic CTAB micellar solutions. *Colloids and Surfaces A: Physicochemical and Engineering Aspects* **2010,** *370* (1), 42-48.

17. Kaur, G.; Chiappisi, L.; Prévost, S.; Schweins, R.; Gradzielski, M.; Mehta, S. K., Probing the Microstructure of Nonionic Microemulsions with Ethyl Oleate by Viscosity, ROESY, DLS, SANS, and Cyclic Voltammetry. *Langmuir* **2012,** *28* (29), 10640-10652.

18. Umeasiegbu, C. D.; Balakotaiah, V.; Krishnamoorti, R., pH-Induced Re-entrant Microstructural Transitions in Cationic Surfactant–Hydrotrope Mixtures. *Langmuir* **2016,** *32* (3), 655-663.

19. Dougherty, D. A., The Cation−π Interaction. *Accounts of Chemical Research* **2013,** *46* (4), 885-893.

20. Saenger, W., Principles of Nucleic Acid Structure. In *Springer Advanced Texts in Chemistry*, Cantor, C. R., Ed. New York, 1984; pp 116-158.

21. Burley, S. K.; Petsko, G. A., Weakly Polar Interactions In Proteins. *Advances in Protein Chemistry* **1988,** *39*, 125-189.

22. Desiraju, G. R.; Gavezzotti, A., From molecular to crystal structure; polynuclear aromatic hydrocarbons. *Journal of the Chemical Society, Chemical Communications* **1989,** (10), 621-623.

23. Hunter, C. A.; Sanders, J. K. M., The nature of .pi.-.pi. interactions. *Journal of the American Chemical Society* **1990,** *112* (14), 5525-5534.

24. Muehldorf, A. V.; Van Engen, D.; Warner, J. C.; Hamilton, A. D., Aromatic-aromatic interactions in molecular recognition: a family of artificial receptors for thymine that shows both face-to-face and edge-to-face orientations. *Journal of the American Chemical Society* **1988,** *110* (19), 6561-6562.

25. Israelachvili, J. N.; Mitchell, D. J.; Ninham, B. W., Theory of self-assembly of hydrocarbon amphiphiles into micelles and bilayers. *Journal of the Chemical Society, Faraday Transactions 2: Molecular and Chemical Physics* **1976,** *72* (0), 1525-1568.

26. Raghavan, S. R.; Fritz, G.; Kaler, E. W., Wormlike Micelles Formed by Synergistic Self-Assembly in Mixtures of Anionic and Cationic Surfactants. *Langmuir* **2002,** *18* (10), 3797-3803.

27. Hoque, J.; Kumar, P.; Aswal, V. K.; Haldar, J., Aggregation Properties of Amide Bearing Cleavable Gemini Surfactants by Small Angle Neutron Scattering and Conductivity Studies. *The Journal of Physical Chemistry B* **2012,** *116* (32), 9718-9726.

28. Haldar, J.; Aswal, V. K.; Goyal, P. S.; Bhattacharya, S., Aggregation Properties of Novel Cationic Surfactants with Multiple Pyridinium Headgroups. Small-Angle Neutron Scattering and Conductivity Studies. *The Journal of Physical Chemistry B* **2004,** *108* (31), 11406-11411.

29. Dreiss, C. A., Wormlike micelles: where do we stand? Recent developments, linear rheology and scattering techniques. *Soft Matter* **2007,** *3* (8), 956-970.

30. Grenek, R.; Cates, M. E., Stress relaxation in living polymers: Results from a Poisson renewal model. *The Journal of Chemical Physics* **1992,** *96* (6), 4758-4767.

31. Cates, M. E.; Candau, S. J., Statics and dynamics of worm-like surfactant micelles. *Journal of Physics: Condensed Matter* **1990,** *2* (33), 6869.

32. Parker, A.; Fieber, W., Viscoelasticity of anionic wormlike micelles: effects of ionic strength and small hydrophobic molecules. *Soft Matter* **2013,** *9* (4), 1203-1213.

33. Shrestha, R. G.; Abezgauz, L.; Danino, D.; Sakai, K.; Sakai, H.; Abe, M., Structure and Dynamics of Poly(oxyethylene) Cholesteryl Ether Wormlike Micelles: Rheometry, SAXS, and Cryo-TEM Studies. *Langmuir* **2011,** *27* (21), 12877-12883.

34. Chakraborty, G.; Paulchowdhury, M.; Bardhan, S.; Saha, S. K., Surface activity and modifying effects of 1-Naphthol, 2-Naphthol and 2,3-Dihydroxynaphthalene on self-assembled nanostructures of 1-Hexadecyl-3-methylimidazolium chloride. *Colloids and Surfaces A: Physicochemical and Engineering Aspects* **2017,** *516*, 262-273.

35. Khatory, A.; Lequeux, F.; Kern, F.; Candau, S. J., Linear and nonlinear viscoelasticity of semidilute solutions of wormlike micelles at high salt content. *Langmuir* **1993,** *9* (6), 1456-1464.

36. Raghavan, S. R.; Kaler, E. W., Highly Viscoelastic Wormlike Micellar Solutions Formed by Cationic Surfactants with Long Unsaturated Tails. *Langmuir* **2001,** *17* (2), 300-306.

References for Chapter IV

1. Freemantle, M., Designer Solvents. *Chemical & Engineering News Archive* **1998,** *76* (13), 32-37.
2. Sheldon, R., Catalytic reactions in ionic liquids. *Chemical Communications* **2001,** (23), 2399-2407.
3. Rehage, H.; Hoffmann, H., Rheological properties of viscoelastic surfactant systems. *The Journal of Physical Chemistry* **1988,** *92* (16), 4712-4719.
4. Younghoon, K.; Paul, D.; David, A. C.; Dennis, E. D., Polymeric worm micelles as nano-carriers for drug delivery. *Nanotechnology* **2005,** *16* (7), S484.
5. Christian, D. A.; Cai, S.; Garbuzenko, O. B.; Harada, T.; Zajac, A. L.; Minko, T.; Discher, D. E., Flexible Filaments for in Vivo Imaging and Delivery: Persistent Circulation of Filomicelles Opens the Dosage Window for Sustained Tumor Shrinkage. *Molecular Pharmaceutics* **2009,** *6* (5), 1343-1352.
6. Kataoka, K.; Harada, A.; Nagasaki, Y., Block copolymer micelles for drug delivery: design, characterization and biological significance. *Advanced Drug Delivery Reviews* **2001,** *47* (1), 113-131.
7. Galgano, P. D.; El Seoud, O. A., Micellar properties of surface active ionic liquids: A comparison of 1-hexadecyl-3-methylimidazolium chloride with structurally related cationic surfactants. *Journal of Colloid and Interface Science* **2010,** *345* (1), 1-11.
8. Modaressi, A.; Sifaoui, H.; Mielcarz, M.; Domańska, U.; Rogalski, M., Influence of the molecular structure on the aggregation of imidazolium ionic liquids in aqueous solutions. *Colloids and Surfaces A: Physicochemical and Engineering Aspects* **2007,** *302* (1), 181-185.
9. Asakawa, T.; Hisamatsu, H.; Miyagishi, S., Experimental Verification of Demixing Micelles Composed of Fluorocarbon and Hydrocarbon Surfactants via the Fluorescence-Quenching Method. *Langmuir* **1996,** *12* (5), 1204-1207.
10. Clapperton, R. M.; Ottewill, R. H.; Ingram, B. T., A study of fluorocarbon-hydrocarbon surface active agent mixtures by NMR spectroscopy. *Langmuir* **1994,** *10* (1), 51-56.
11. Ben Ghoulam, M.; Moatadid, N.; Graciaa, A.; Marion, G.; Lachaise, J., Hydrocarbon/Fluorocarbon Mixed Micelle Diagram from Surface Tensiometry. *Langmuir* **1996,** *12* (21), 5048-5051.
12. Raghavan, S. R.; Fritz, G.; Kaler, E. W., Wormlike Micelles Formed by Synergistic Self-Assembly in Mixtures of Anionic and Cationic Surfactants. *Langmuir* **2002,** *18* (10), 3797-3803.
13. Kaler, E. W.; Herrington, K. L.; Murthy, A. K.; Zasadzinski, J. A. N., Phase behavior and structures of mixtures of anionic and cationic surfactants. *The Journal of Physical Chemistry* **1992,** *96* (16), 6698-6707.

14. Koehler, R. D.; Raghavan, S. R.; Kaler, E. W., Microstructure and Dynamics of Wormlike Micellar Solutions Formed by Mixing Cationic and Anionic Surfactants. *The Journal of Physical Chemistry B* **2000,** *104* (47), 11035-11044.

15. Gräbner, D.; Zhai, L.; Talmon, Y.; Schmidt, J.; Freiberger, N.; Glatter, O.; Herzog, B.; Hoffmann, H., Phase Behavior of Aqueous Mixtures of 2-Phenylbenzimidazole-5-sulfonic Acid and Cetyltrimethylammonium Bromide: Hydrogels, Vesicles, Tubules, and Ribbons. *The Journal of Physical Chemistry B* **2008,** *112* (10), 2901-2908.

16. Wattebled, L.; Laschewsky, A., Effects of Organic Salt Additives on the Behavior of Dimeric ("Gemini") Surfactants in Aqueous Solution. *Langmuir* **2007,** *23* (20), 10044-10052.

17. Lin, Y.; Qiao, Y.; Yan, Y.; Huang, J., Thermo-responsive viscoelastic wormlike micelle to elastic hydrogel transition in dual-component systems. *Soft Matter* **2009,** *5* (16), 3047-3053.

18. You, Q.; Zhang, Y.; Wang, H.; Fan, H.; Guo, J.; Li, M., The Formation of pH-Sensitive Wormlike Micelles in Ionic Liquids Driven by the Binding Ability of Anthranilic Acid. *International Journal of Molecular Sciences* **2015,** *16* (12).

19. Saha, S. K.; Jha, M.; Ali, M.; Chakraborty, A.; Bit, G.; Das, S. K., Micellar Shape Transition under Dilute Salt-Free Conditions: Promotion and Self-Fluorescence Monitoring of Stimuli-Responsive Viscoelasticity by 1- and 2 Naphthols. *The Journal of Physical Chemistry B* **2008,** *112* (15), 4642-4647.

20. Ali, M.; Jha, M.; Das, S. K.; Saha, S. K., Hydrogen-Bond-Induced Microstructural Transition of Ionic Micelles in the Presence of Neutral Naphthols: pH Dependent Morphology and Location of Surface Activity. *The Journal of Physical Chemistry B* **2009,** *113* (47), 15563-15571.

21. Lackowicz, J., Fluorescence anisotropy. In *Principles of Fluorescence Spectroscopy*, Springer: 2006; pp 353–381.

22. Tung, S.-H.; Huang, Y.-E.; Raghavan, S. R., Contrasting Effects of Temperature on the Rheology of Normal and Reverse Wormlike Micelles. *Langmuir* **2007,** *23* (2), 372-376.

23. Bergström, M.; Eriksson, J. C., A Theoretical Analysis of Synergistic Effects in Mixed Surfactant Systems. *Langmuir* **2000,** *16* (18), 7173-7181.

24. Rubingh, D. N., Mixed micelle solutions. In *Solution chemistry of surfactants*, Springer: 1979; pp 337-354.

25. Rosen, M. J., Molecular Interactions and Synergism in Mixtures of Two Surfactants. In *Surfactants and Interfacial Phenomena*, John Wiley & Sons, Inc.: 2004; pp 379-414.

26. Platz, G., J. H. Clint: Surfactant Aggregation, Blackie Publishing Group, Glasgow, London, *Berichte der Bunsengesellschaft für physikalische Chemie* **1992,** *96* (5), 742.

27. Khan, I. A.; Khanam, A. J.; Khan, Z. A.; Kabir ud, D., Mixing Behavior of Anionic Hydrotropes with Cationic Gemini Surfactants. *Journal of Chemical & Engineering Data* **2010,** *55* (11), 4775-4779.

28. Lackowicz, J. R., *Principles of Fluorescence Spectroscopy*. 3 ed.; Springer US: 2006.

29. Laws, W. R.; Brand, L., Analysis of two-state excited-state reactions. The fluorescence decay of 2 Naphthol. *The Journal of Physical Chemistry* **1979,** *83* (7), 795-802.

30. Erkki, S.; Ilkka, H. Fluorescence spectroscopy assay means with fluorescent chelate of a lanthanide,.

31. Mandal, D.; Pal, S. K.; Bhattacharyya, K., Excited-State Proton Transfer of 1 Naphthol in Micelles. *The Journal of Physical Chemistry A* **1998,** *102* (48), 9710-9714.

32. Grenek, R.; Cates, M. E., Stress relaxation in living polymers: Results from a Poisson renewal model. *The Journal of Chemical Physics* **1992,** *96* (6), 4758-4767.

33. Sabadini, E.; Ungarato, R. F. S.; Miranda, P. B., The Elasticity of Soap Bubbles Containing Wormlike Micelles. *Langmuir* **2014,** *30* (3), 727-732.

34. Parker, A.; Fieber, W., Viscoelasticity of anionic wormlike micelles: effects of ionic strength and small hydrophobic molecules. *Soft Matter* **2013,** *9* (4), 1203-1213.

35. Cates, M. E.; Candau, S. J., Statics and dynamics of worm-like surfactant micelles. *Journal of Physics: Condensed Matter* **1990,** *2* (33), 6869.

36. Lopez-Diaz, D.; Castillo, R., The Wormlike Micellar Solution made of a Zwitterionic Surfactant (TDPS), an Anionic Surfactant (SDS), and Brine in the Semidilute Regime. *The Journal of Physical Chemistry B* **2010,** *114* (27), 8917-8925.

37. Shrestha, R. G.; Abezgauz, L.; Danino, D.; Sakai, K.; Sakai, H.; Abe, M., Structure and Dynamics of Poly(oxyethylene) Cholesteryl Ether Wormlike Micelles: Rheometry, SAXS, and Cryo-TEM Studies. *Langmuir* **2011,** *27* (21), 12877-12883.

38. Kern, F.; Lequeux, F.; Zana, R.; Candau, S. J., Dynamic Properties of Salt-Free Viscoelastic Micellar Solutions. *Langmuir* **1994,** *10* (6), 1714-1723.

39. Cates, M. E., Reptation of living polymers: dynamics of entangled polymers in the presence of reversible chain-scission reactions. *Macromolecules* **1987,** *20* (9), 2289-2296.

40. Umeasiegbu, C. D.; Balakotaiah, V.; Krishnamoorti, R., pH-Induced Re-entrant Microstructural Transitions in Cationic Surfactant–Hydrotrope Mixtures. *Langmuir* **2016,** *32* (3), 655-663.

41. Dreiss, C. A., Wormlike micelles: where do we stand? Recent developments, linear rheology and scattering techniques. *Soft Matter* **2007,** *3* (8), 956-970.

42. In, M.; Warr, G. G.; Zana, R., Dynamics of Branched Threadlike Micelles. *Physical Review Letters* **1999,** *83* (11), 2278-2281.

43. Hassan, P. A.; Raghavan, S. R.; Kaler, E. W., Microstructural Changes in SDS Micelles Induced by Hydrotropic Salt. *Langmuir* **2002,** *18* (7), 2543-2548.

44. Gråsjö, J.; Andersson, E.; Forsberg, J.; Aziz, E. F.; Brena, B.; Johansson, C.; Nordgren, J.; Duda, L.; Andersson, J.; Hennies, F.; Rubensson, J.-E.; Hansson, P., Electronic Structure of Water Molecules Confined in a Micelle Lattice. *The Journal of Physical Chemistry B* **2009,** *113* (24), 8201-8205.

45. Bernardez, L. A., Investigation on the locus of solubilization of polycyclic aromatic hydrocarbons in non-ionic surfactant micelles with 1H NMR spectroscopy. *Colloids and Surfaces A: Physicochemical and Engineering Aspects* **2008,** *324* (1), 71-78.

46. Sabatino, P.; Szczygiel, A.; Sinnaeve, D.; Hakimhashemi, M.; Saveyn, H.; Martins, J. C.; Van der Meeren, P., NMR study of the influence of pH on phenol sorption in cationic CTAB micellar solutions. *Colloids and Surfaces A: Physicochemical and Engineering Aspects* **2010,** *370* (1), 42-48.

47. Chaghi, R.; de Ménorval, L.-C.; Charnay, C.; Derrien, G.; Zajac, J., Interactions of phenol with cationic micelles of hexadecyltrimethylammonium bromide studied by titration calorimetry, conductimetry, and 1H NMR in the range of low additive and surfactant concentrations. *Journal of Colloid and Interface Science* **2008,** *326* (1), 227-234.

48. Rao, U. R. K.; Manohar, C.; Valaulikar, B. S.; Iyer, R. M., Micellar chain model for the origin of the visoelasticity in dilute surfactant solutions. *The Journal of Physical Chemistry* **1987,** *91* (12), 3286-3291.

49. Mata, J. P.; Aswal, V. K.; Hassan, P. A.; Bahadur, P., A phenol-induced structural transition in aqueous cetyltrimethylammonium bromide solution. *Journal of Colloid and Interface Science* **2006,** *299* (2), 910-915.

50. Xu, K.; Ren, H.-q.; Zeng, G.-m.; Ding, L.-l.; Huang, J.-h., Investigation of interaction between phenol and cetylpyridinium chloride micelle in the absence and in the presence of electrolyte by 1H NMR spectroscopy. *Colloids and Surfaces A: Physicochemical and Engineering Aspects* **2010,** *356* (1), 150-155.

51. Frisch, M. J. T., G. W.; Schlegel, H. B.; Scuseria, G. E.; Robb, M. A.; Cheeseman, J. R.; Scalmani, G.; Barone, V.; Mennucci, B.; Petersson, G. A.; Nakatsuji, H.; Caricato, M.; Li, X.; Hratchian, H. P.; Izmaylov, A. F.; Bloino, J.; Zheng, G.; Sonnenberg, J. L.; Hada, M.; Ehara, M.; Toyota, K.; Fukuda, R.; Hasegawa, J.; Ishida, M.; Nakajima, T.; Honda, Y.; Kitao, O.; Nakai, H.; Vreven, T.; Montgomery Jr, J. A.; Peralta, J. E.; Ogliaro, F.; Bearpark, M.; Heyd, J. J.; Brothers, E.; Kudin, K. N.; Staroverov, V. N.; Kobayashi, R.; Normand, J.; Raghavachari, K.; Rendell, A.; Burant, J. C.; Iyengar, S. S.; Tomasi, J.; Cossi, M.; Rega, N.; Millam, J. M.; Klene, M.; Knox, J. E.; Cross, J. B.; Bakken, V.; Adamo, C.; Jaramillo, J.; Gomperts, R.; Stratmann, R. E.; Yazyev, O.; Austin, A. J.; Cammi, R.; Pomelli, C.; Ochterski, J. W.; Martin, R. L.; Morokuma, K.; Zakrzewski, V. G.; Voth, G. A.; Salvador, P.; Dannenberg, J. J.; Dapprich, S.; Daniels, A. D.; Farkas, O.; Foresman, J. B.; Ortiz, J. V.; Cioslowski, J.; Fox, D. J. *Gaussian 09*, Gaussian, Inc: Wallingford CT, 2009.

52. Yang, J., Viscoelastic wormlike micelles and their applications. *Current Opinion in Colloid & Interface Science* **2002,** *7* (5), 276-281.

53. Wever, D. A. Z.; Picchioni, F.; Broekhuis, A. A., Polymers for enhanced oil recovery: A paradigm for structure–property relationship in aqueous solution. *Progress in Polymer Science* **2011,** *36* (11), 1558-1628.

54. Abidin, A. Z.; Puspasari, T.; Nugroho, W. A., Polymers for Enhanced Oil Recovery Technology. *Procedia Chemistry* **2012,** *4*, 11-16.

55. Hourdet, D.; Ducouret, G.; Varghese, S.; Badiger, M. V.; Wadgaonkar, P. P., Thermodynamic behavior of hydrophobically modified polyacrylamide containing random distribution of hydrophobes: Experimental and theoretical investigations. *Polymer* **2013,** *54* (11), 2676-2689.

56. Zhao, Z.; Liu, T.; Luo, P.; Li, Y.; Liu, J.; Cheng, J.; Yu, Y., Performance and field implementation of a new fracturing fluid consisting of hydrophobically associating polyacrylamide and anionic surfactant. In *Journal of Polymer Engineering*, 2016; Vol. 36, p 13.

57. Egorov, V. M.; Djigailo, D. I.; Momotenko, D. S.; Chernyshov, D. V.; Torocheshnikova, I. I.; Smirnova, S. V.; Pletnev, I. V., Task-specific ionic liquid trioctylmethylammonium salicylate as extraction solvent for transition metal ions. *Talanta* **2010,** *80* (3), 1177-1182.

58. Abezgauz, L.; Kuperkar, K.; Hassan, P. A.; Ramon, O.; Bahadur, P.; Danino, D., Effect of Hofmeister anions on micellization and micellar growth of the surfactant cetylpyridinium chloride. *Journal of Colloid and Interface Science* **2010,** *342* (1), 83-92.

59. Mellor, D. P.; Maley, L., Order of Stability of Metal Complexes. *Nature* **1948,** *161*, 436-437.

60. Flores, S. C.; Kherb, J.; Konelick, N.; Chen, X.; Cremer, P. S., The Effects of Hofmeister Cations at Negatively Charged Hydrophilic Surfaces. *The Journal of Physical Chemistry C* **2012,** *116* (9), 5730-5734.

61. Alkschbirs, M. I.; Percebom, A. M.; Loh, W.; Westfahl, H.; Cardoso, M. B.; Sabadini, E., Effects of some anions of the Hofmeister series on the rheology of cetyltrimethylammonium-salicylate wormlike micelles. *Colloids and Surfaces A: Physicochemical and Engineering Aspects* **2015,** *470*, 1-7.

62. Angelico, R.; Amin, S.; Monduzzi, M.; Murgia, S.; Olsson, U.; Palazzo, G., Impact of branching on the viscoelasticity of wormlike reverse micelles. *Soft Matter* **2012,** *8* (42), 10941-10949.

63. Cammarata, L.; Kazarian, S. G.; Salter, P. A.; Welton, T., Molecular states of water in room temperature ionic liquids. *Physical Chemistry Chemical Physics* **2001,** *3* (23), 5192-5200.

64. Downard, A.; Earle, M. J.; Hardacre, C.; McMath, S. E. J.; Nieuwenhuyzen, M.; Teat, S. J., Structural Studies of Crystalline 1-Alkyl-3-Methylimidazolium Chloride Salts. *Chemistry of Materials* **2004,** *16* (1), 43-48.

65. Zhang, G.; Chen, X.; Zhao, Y.; Xie, Y.; Qiu, H., Effects of Alcohols and Counterions on the Phase Behavior of 1-Octyl-3-methylimidazolium Chloride Aqueous Solution. *The Journal of Physical Chemistry B* **2007,** *111* (40), 11708-11713.

References for Chapter V

1. Bordes, R.; Holmberg, K., Amino acid-based surfactants – do they deserve more attention? *Advances in Colloid and Interface Science* **2015,** *222*, 79-91.

2. Infante, M. R.; Clapes, P.; Perez, L.; Pinazo, A.; Moran, M. D. C., Amino Acid-based surfactants In *Novel Surfactants: Application and Biodegradibility*, Holmberg, K., Ed. CRC Press: 2003; pp 193-216.

3. Pérez, L.; Pinazo, A.; Pons, R.; Infante, M., Gemini surfactants from natural amino acids. *Advances in Colloid and Interface Science* **2014,** *205*, 134-155.

4. Angelidaki, I.; Toräng, L.; Waul, C. M.; Schmidt, J. E., Anaerobic bioprocessing of sewage sludge, focusing on degradation of linear alkylbenzene sulfonates (LAS). *Water Science and Technology* **2004,** *49* (10), 115-122.

5. Brandt, K. K.; Hesselso/e, M.; Roslev, P.; Henriksen, K.; So/rensen, J., Toxic Effects of Linear Alkylbenzene Sulfonate on Metabolic Activity, Growth Rate, and Microcolony Formation ofNitrosomonas and Nitrosospira Strains. *Applied and Environmental Microbiology* **2001,** *67* (6), 2489-2498.

6. Srinivasa Rao, K.; Singh, T.; Trivedi, T. J.; Kumar, A., Aggregation Behavior of Amino Acid Ionic Liquid Surfactants in Aqueous Media. *The Journal of Physical Chemistry B* **2011,** *115* (47), 13847-13853.

7. Jiao, Y.; Li, W.-L.; Xu, J.-F.; Wang, G.; Li, J.; Wang, Z.; Zhang, X., A Supramolecularly Activated Radical Cation for Accelerated Catalytic Oxidation. *Angewandte Chemie International Edition* **2016,** *55* (31), 8933-8937.

8. Liu, K.; Xing, R.; Zou, Q.; Ma, G.; Möhwald, H.; Yan, X., Simple Peptide-Tuned Self-Assembly of Photosensitizers towards Anticancer Photodynamic Therapy. *Angewandte Chemie International Edition* **2016,** *55* (9), 3036-3039.

9. Shao, J.; Wen, C.; Xuan, M.; Zhang, H.; Frueh, J.; Wan, M.; Gao, L.; He, Q., Polyelectrolyte multilayer-cushioned fluid lipid bilayers: a parachute model. *Physical Chemistry Chemical Physics* **2017,** *19* (3), 2008-2016.

10. Shao, J.; Xuan, M.; Dai, L.; Si, T.; Li, J.; He, Q., Near-Infrared-Activated Nanocalorifiers in Microcapsules: Vapor Bubble Generation for In Vivo Enhanced Cancer Therapy. *Angewandte Chemie International Edition* **2015,** *54* (43), 12782-12787.

11. Wang, J.; Shen, G.; Ma, K.; Jiao, T.; Liu, K.; Yan, X., Dipeptide concave nanospheres based on interfacially controlled self-assembly: from crescent to solid. *Physical Chemistry Chemical Physics* **2016,** *18* (45), 30926-30930.

12. Xu, W.; Song, Q.; Xu, J.-F.; Serpe, M. J.; Zhang, X., Supramolecular Hydrogels Fabricated from Supramonomers: A Novel Wound Dressing Material. *ACS Applied Materials & Interfaces* **2017,** *9* (13), 11368-11372.

13. Zou, Q.; Abbas, M.; Zhao, L.; Li, S.; Shen, G.; Yan, X., Biological Photothermal Nanodots Based on Self-Assembly of Peptide–Porphyrin Conjugates for

Antitumor Therapy. *Journal of the American Chemical Society* **2017,** *139* (5), 1921-1927.

14. Miyagishi, S.; Nishida, M., Influence of chirality on micelle formation of sodium N-acylalanates and sodium N-lauroylvalinates. *Journal of Colloid and Interface Science* **1978,** *65* (2), 380-386.

15. Takehara, M.; Yoshimura, I.; Yoshida, R., Surface-active N-acylglutamate: IV. Physicochemical properties of triethanolamine long chain N-acylglutamates. *Journal of the American Oil Chemists Society* **1974,** *51* (9), 419-423.

16. Ohta, A.; Nakashima, S.; Matsuyanagi, H.; Asakawa, T.; Miyagishi, S., Krafft temperature and enthalpy of solution of N-acyl amino acid surfactants and their racemic modifications: effect of the counter ion. *Colloid and Polymer Science* **2003,** *282* (2), 162-169.

17. Roy, A.; Kundu, N.; Banik, D.; Sarkar, N., Comparative Fluorescence Resonance Energy-Transfer Study in Pluronic Triblock Copolymer Micelle and Niosome Composed of Biological Component Cholesterol: An Investigation of Effect of Cholesterol and Sucrose on the FRET Parameters. *The Journal of Physical Chemistry B* **2016,** *120* (1), 131-142.

18. Kelkar, D. A.; Chattopadhyay, A., The gramicidin ion channel: A model membrane protein. *Biochimica et Biophysica Acta (BBA) - Biomembranes* **2007,** *1768* (9), 2011-2025.

19. Yau, W.-M.; Wimley, W. C.; Gawrisch, K.; White, S. H., The Preference of Tryptophan for Membrane Interfaces. *Biochemistry* **1998,** *37* (42), 14713-14718.

20. Levine, Z. A.; Venable, R. M.; Watson, M. C.; Lerner, M. G.; Shea, J.-E.; Pastor, R. W.; Brown, F. L. H., Determination of Biomembrane Bending Moduli in Fully Atomistic Simulations. *Journal of the American Chemical Society* **2014,** *136* (39), 13582-13585.

21. Sainz, B.; Rausch, J. M.; Gallaher, W. R.; Garry, R. F.; Wimley, W. C., The Aromatic Domain of the Coronavirus Class I Viral Fusion Protein Induces Membrane Permeabilization: Putative Role during Viral Entry. *Biochemistry* **2005,** *44* (3), 947-958.

22. McMahon, H. T.; Gallop, J. L., Membrane curvature and mechanisms of dynamic cell membrane remodelling. *Nature* **2005,** *438* (7068), 590-596.

23. Kollmitzer, B.; Heftberger, P.; Rappolt, M.; Pabst, G., Monolayer spontaneous curvature of raft-forming membrane lipids. *Soft Matter* **2013,** *9* (45), 10877-10884.

24. Sengupta, B.; Sengupta, P. K., Influence of Reverse Micellar Environments on the Fluorescence Emission Properties of Tryptophan Octyl Ester. *Biochemical and Biophysical Research Communications* **2000,** *277* (1), 13-19.

25. Chattopadhyay, A.; Mukherjee, S.; Rukmini, R.; Rawat, S. S.; Sudha, S., Ionization, partitioning, and dynamics of tryptophan octyl ester: implications for membrane-bound tryptophan residues. *Biophysical Journal* **1997,** *73* (2), 839-849.

26. Chattopadhyay, A.; Arora, A.; Kelkar, D. A., Dynamics of a membrane-bound tryptophan analog in environments of varying hydration: a fluorescence approach. *European Biophysics Journal* **2005,** *35* (1), 62.

27. Arora-Sharawat, A.; Chattopadhyay, A., Effect of structural transition of the host assembly on dynamics of a membrane-bound tryptophan analogue. *Biophysical Chemistry* **2007,** *129* (2), 172-180.

28. de Foresta, B.; Gallay, J.; Sopkova, J.; Champeil, P.; Vincent, M., Tryptophan Octyl Ester in Detergent Micelles of Dodecylmaltoside: Fluorescence Properties and Quenching by Brominated Detergent Analogs. *Biophysical Journal* **1999,** *77* (6), 3071-3084.

29. Tortech, L.; Jaxel, C.; Vincent, M.; Gallay, J.; de Foresta, B., The polar headgroup of the detergent governs the accessibility to water of tryptophan octyl ester in host micelles. *Biochimica et Biophysica Acta (BBA) - Biomembranes* **2001,** *1514* (1), 76-86.

30. Yang, Y.; Zhou, Y.; Ge, J.; Wang, Y.; Chen, X., Synthesis, characterization and infrared emissivity property of optically active polyurethane derived from tyrosine. *Polymer* **2011,** *52* (17), 3745-3751.

31. Ley, J. P.; Bertram, H.-J., Synthesis of Lipophilic Clovamide Derivatives and Their Antioxidative Potential against Lipid Peroxidation. *Journal of Agricultural and Food Chemistry* **2003,** *51* (16), 4596-4602.

32. Hassani, M.; Cai, W.; Holley, D. C.; Lineswala, J. P.; Maharjan, B. R.; Ebrahimian, G. R.; Seradj, H.; Stocksdale, M. G.; Mohammadi, F.; Marvin, C. C.; Gerdes, J. M.; Beall, H. D.; Behforouz, M., Novel Lavendamycin Analogues as Antitumor Agents: Synthesis, in Vitro Cytotoxicity, Structure−Metabolism, and Computational Molecular Modeling Studies with NAD(P)H:Quinone Oxidoreductase 1. *Journal of Medicinal Chemistry* **2005,** *48* (24), 7733-7749.

33. Frisch, M. J. T., G. W.; Schlegel, H. B.; Scuseria, G. E.; Robb, M. A.; Cheeseman, J. R.; Scalmani, G.; Barone, V.; Mennucci, B.; Petersson, G. A.; Nakatsuji, H.; Caricato, M.; Li, X.; Hratchian, H. P.; Izmaylov, A. F.; Bloino, J.; Zheng, G.; Sonnenberg, J. L.; Hada, M.; Ehara, M.; Toyota, K.; Fukuda, R.; Hasegawa, J.; Ishida, M.; Nakajima, T.; Honda, Y.; Kitao, O.; Nakai, H.; Vreven, T.; Montgomery Jr, J. A.; Peralta, J. E.; Ogliaro, F.; Bearpark, M.; Heyd, J. J.; Brothers, E.; Kudin, K. N.; Staroverov, V. N.; Kobayashi, R.; Normand, J.; Raghavachari, K.; Rendell, A.; Burant, J. C.; Iyengar, S. S.; Tomasi, J.; Cossi, M.; Rega, N.; Millam, J. M.; Klene, M.; Knox, J. E.; Cross, J. B.; Bakken, V.; Adamo, C.; Jaramillo, J.; Gomperts, R.; Stratmann, R. E.; Yazyev, O.; Austin, A. J.; Cammi, R.; Pomelli, C.; Ochterski, J. W.; Martin, R. L.; Morokuma, K.; Zakrzewski, V. G.; Voth, G. A.; Salvador, P.; Dannenberg, J. J.; Dapprich, S.; Daniels, A. D.; Farkas, O.; Foresman, J. B.; Ortiz, J. V.; Cioslowski, J.; Fox, D. J. *Gaussian 09*, Gaussian, Inc: Wallingford CT, 2009.

34. Clint, J. H., Mixed-micelle formation. In *Surfactant Aggregation*, Springer Netherlands: Dordrecht, 1992; pp 130-146.

35. Huibers, P. D. T.; Lobanov, V. S.; Katritzky, A. R.; Shah, D. O.; Karelson, M., Prediction of Critical Micelle Concentration Using a Quantitative Structure−Property Relationship Approach. 1. Nonionic Surfactants. *Langmuir* **1996,** *12* (6), 1462-1470.

36. Okano, L. T.; Seoud, O. A. E.; Halstead, T. K., A proton NMR study on aggregation of cationic surfactants in water: effects of the structure of the headgroup. *Colloid and Polymer Science* **1997,** *275* (2), 138-145.

37. Chakraborty, G.; Paulchowdhury, M.; Bardhan, S.; Saha, S. K., Surface activity and modifying effects of 1-Naphthol, 2-Naphthol and 2,3-Dihydroxynaphthalene on self-assembled nanostructures of 1-Hexadecyl-3-methylimidazolium chloride. *Colloids and Surfaces A: Physicochemical and Engineering Aspects* **2017,** *516*, 262-273.

38. Dong, B.; Li, N.; Zheng, L.; Yu, L.; Inoue, T., Surface Adsorption and Micelle Formation of Surface Active Ionic Liquids in Aqueous Solution. *Langmuir* **2007,** *23* (8), 4178-4182.

39. Chen, L.-J.; Lin, S.-Y.; Huang, C.-C., Effect of Hydrophobic Chain Length of Surfactants on Enthalpy−Entropy Compensation of Micellization. *The Journal of Physical Chemistry B* **1998,** *102* (22), 4350-4356.

40. Galamba, N., Water's Structure around Hydrophobic Solutes and the Iceberg Model. *The Journal of Physical Chemistry B* **2013,** *117* (7), 2153-2159.

41. Graziano, G., Comment on "Water's Structure around Hydrophobic Solutes and the Iceberg Model". *The Journal of Physical Chemistry B* **2014,** *118* (9), 2598-2599.

42. Shinoda, K.; Kobayashi, M.; Yamaguchi, N., Effect of "Iceberg" formation of water on the enthalpy and entropy of solution of paraffin chain compounds: the effect of temperature on the critical micelle concentration of lithium perfluorooctane sulfonate. *The Journal of Physical Chemistry* **1987,** *91* (20), 5292-5294.

43. Sarmoria, C.; Puvvada, S.; Blankschtein, D., Prediction of critical micelle concentrations of nonideal binary surfactant mixtures. *Langmuir* **1992,** *8* (11), 2690-2697.

44. Ghosh, S.; Das Burman, A.; De, G. C.; Das, A. R., Interfacial and Self-Aggregation of Binary Mixtures of Anionic and Nonionic Amphiphiles in Aqueous Medium. *The Journal of Physical Chemistry B* **2011,** *115* (38), 11098-11112.

45. Anacker, E. W., The hydrophobic effect: Formation of micelles and biological membranes. *Journal of Colloid and Interface Science* **1975,** *50* (3), 615.

46. Israelachvili, J. N.; Mitchell, D. J.; Ninham, B. W., Theory of self-assembly of hydrocarbon amphiphiles into micelles and bilayers. *Journal of the Chemical Society, Faraday Transactions 2: Molecular and Chemical Physics* **1976,** *72* (0), 1525-1568.

47. Xu, W.; Wang, T.; Cheng, N.; Hu, Q.; Bi, Y.; Gong, Y.; Yu, L., Experimental and DFT Studies on the Aggregation Behavior of Imidazolium-Based Surface-Active Ionic Liquids with Aromatic Counterions in Aqueous Solution. *Langmuir* **2015,** *31* (4), 1272-1282.

48. Tanford, C., Micelle shape and size. *The Journal of Physical Chemistry* **1972,** *76* (21), 3020-3024.

49. Oliver, R. C.; Lipfert, J.; Fox, D. A.; Lo, R. H.; Doniach, S.; Columbus, L., Dependence of Micelle Size and Shape on Detergent Alkyl Chain Length and Head Group. *PLOS ONE* **2013,** *8* (5), e62488.

50. Moroi, Y., Mass action model of micelle formation: Its application to sodium dodecyl sulfate solution. *Journal of Colloid and Interface Science* **1988,** *122* (2), 308-314.

51. Chatterjee, A.; Moulik, S. P.; Sanyal, S. K.; Mishra, B. K.; Puri, P. M., Thermodynamics of Micelle Formation of Ionic Surfactants: A Critical Assessment for Sodium Dodecyl Sulfate, Cetyl Pyridinium Chloride and Dioctyl Sulfosuccinate (Na Salt) by Microcalorimetric, Conductometric, and Tensiometric Measurements. *The Journal of Physical Chemistry B* **2001,** *105* (51), 12823-12831.

52. Galgano, P. D.; El Seoud, O. A., Micellar properties of surface active ionic liquids: A comparison of 1-hexadecyl-3-methylimidazolium chloride with structurally related cationic surfactants. *Journal of Colloid and Interface Science* **2010,** *345* (1), 1-11.

53. Das, S.; Naskar, B.; Ghosh, S., Influence of temperature and organic solvents (isopropanol and 1,4-dioxane) on the micellization of cationic gemini surfactant (14-4-14). *Soft Matter* **2014,** *10* (16), 2863-2875.

54. Kalyanasundaram, K.; Thomas, J. K., Environmental effects on vibronic band intensities in pyrene monomer fluorescence and their application in studies of micellar systems. *Journal of the American Chemical Society* **1977,** *99* (7), 2039-2044.

55. Mehta, S. K.; Bhasin, K. K.; Kumar, A.; Dham, S., Micellar behavior of dodecyldimethylethyl ammonium bromide and dodecyltrimethylammonium chloride in aqueous media in the presence of diclofenac sodium. *Colloids and Surfaces A: Physicochemical and Engineering Aspects* **2006,** *278* (1), 17-25.

56. Turro, N. J.; Yekta, A., Luminescent probes for detergent solutions. A simple procedure for determination of the mean aggregation number of micelles. *Journal of the American Chemical Society* **1978,** *100* (18), 5951-5952.

57. Kaur, G.; Chiappisi, L.; Prévost, S.; Schweins, R.; Gradzielski, M.; Mehta, S. K., Probing the Microstructure of Nonionic Microemulsions with Ethyl Oleate by Viscosity, ROESY, DLS, SANS, and Cyclic Voltammetry. *Langmuir* **2012,** *28* (29), 10640-10652.

58. Fraenkel, Y.; Gershoni, J. M.; Navon, G., Acetylcholine interactions with tryptophan-184 of the α-subunit of the nicotinic acetylcholine receptor revealed by transferred nuclear Overhauser effect. *FEBS Letters* **1991,** *291* (2), 225-228.

59. Kreke, P. J.; Magid, L. J.; Gee, J. C., 1H and 13C NMR Studies of Mixed Counterion, Cetyltrimethylammonium Bromide/Cetyltrimethylammonium Dichlorobenzoate, Surfactant Solutions: The Intercalation of Aromatic Counterions. *Langmuir* **1996,** *12* (3), 699-705.

60. Jiang, Z.; Jia, K.; Liu, X.; Dong, J.; Li, X., Multiple Responsive Fluids Based on Vesicle to Wormlike Micelle Transitions by Single-Tailed Pyrrolidone Surfactants. *Langmuir* **2015,** *31* (43), 11760-11768.

61. Ali, M.; Jha, M.; Das, S. K.; Saha, S. K., Hydrogen-Bond-Induced Microstructural Transition of Ionic Micelles in the Presence of Neutral Naphthols: pH Dependent Morphology and Location of Surface Activity. *The Journal of Physical Chemistry B* **2009,** *113* (47), 15563-15571.

62. Wangsakan, A.; McClements, D. J.; Chinachoti, P.; Charles Dickinson, L., Two-dimensional rotating-frame Overhauser spectroscopy (ROESY) and 13C NMR study of the interactions between maltodextrin and an anionic surfactant. *Carbohydrate Research* **2004,** *339* (6), 1105-1111.

63. Lavoie, S.; Gauthier, C.; Mshvildadze, V.; Legault, J.; Roger, B.; Pichette, A., DFT Calculations and ROESY NMR Data for the Diastereochemical Characterization of Cytotoxic Tetraterpenoids from the Oleoresin of Abies balsamea. *Journal of Natural Products* **2015,** *78* (12), 2896-2907.

64. Liu, Q.; Chen, S.; Chen, J.; Du, J., An Asymmetrical Polymer Vesicle Strategy for Significantly Improving T1 MRI Sensitivity and Cancer-Targeted Drug Delivery. *Macromolecules* **2015,** *48* (3), 739-749.

65. Mai, Y.; Eisenberg, A., Self-assembly of block copolymers. *Chemical Society Reviews* **2012,** *41* (18), 5969-5985.

66. Smart, T.; Lomas, H.; Massignani, M.; Flores-Merino, M. V.; Perez, L. R.; Battaglia, G., Block copolymer nanostructures. *Nano Today* **2008,** *3* (3), 38-46.

67. Singh, P. C.; Inoue, K.-i.; Nihonyanagi, S.; Yamaguchi, S.; Tahara, T., Femtosecond Hydrogen Bond Dynamics of Bulk-like and Bound Water at Positively and Negatively Charged Lipid Interfaces Revealed by 2D HD-VSFG Spectroscopy. *Angewandte Chemie International Edition* **2016,** *55* (36), 10621-10625.

68. Nagarajan, R., Molecular Packing Parameter and Surfactant Self-Assembly: The Neglected Role of the Surfactant Tail. *Langmuir* **2002,** *18* (1), 31-38.

References for Chapter VI

1. Levine, Z. A.; Venable, R. M.; Watson, M. C.; Lerner, M. G.; Shea, J.-E.; Pastor, R. W.; Brown, F. L. H., Determination of Biomembrane Bending Moduli in Fully Atomistic Simulations. *Journal of the American Chemical Society* **2014,** *136* (39), 13582-13585.

2. Yau, W.-M.; Wimley, W. C.; Gawrisch, K.; White, S. H., The Preference of Tryptophan for Membrane Interfaces. *Biochemistry* **1998,** *37* (42), 14713-14718.

3. Sainz, B.; Rausch, J. M.; Gallaher, W. R.; Garry, R. F.; Wimley, W. C., The Aromatic Domain of the Coronavirus Class I Viral Fusion Protein Induces Membrane Permeabilization: Putative Role during Viral Entry. *Biochemistry* **2005,** *44* (3), 947-958.

4. McMahon, H. T.; Gallop, J. L., Membrane curvature and mechanisms of dynamic cell membrane remodelling. *Nature* **2005,** *438* (7068), 590-596.

5. Kollmitzer, B.; Heftberger, P.; Rappolt, M.; Pabst, G., Monolayer spontaneous curvature of raft-forming membrane lipids. *Soft Matter* **2013,** *9* (45), 10877-10884.

6. Moosmann, B.; Behl, C., Cytoprotective antioxidant function of tyrosine and tryptophan residues in transmembrane proteins. *European Journal of Biochemistry* **2000,** *267* (18), 5687-5692.

7. Heijne, G. V., Membrane Proteins: From Sequence to Structure. *Annual Review of Biophysics and Biomolecular Structure* **1994,** *23* (1), 167-192.

8. Landolt-Marticorena, C.; Williams, K. A.; Deber, C. M.; Reithmeier, R. A. F., Non-random Distribution of Amino Acids in the Transmembrane Segments of Human Type I Single Span Membrane Proteins. *Journal of Molecular Biology* **1993,** *229* (3), 602-608.

9. Jones, D. T.; Taylor, W. R.; Thornton, J. M., A Model Recognition Approach to the Prediction of All-Helical Membrane Protein Structure and Topology. *Biochemistry* **1994,** *33* (10), 3038-3049.

10. Gao, J.; Chou, L. W.; Auerbach, A., The nature of cation-pi binding: interactions between tetramethylammonium ion and benzene in aqueous solution. *Biophysical Journal* **1993,** *65* (1), 43-47.

11. Dougherty, D. A., Cation-π Interactions in Chemistry and Biology: A New View of Benzene, Phe, Tyr, and Trp. *Science* **1996,** *271* (5246), 163-168.

12. MECOZZI, S.; WEST JR., A. P.; Dougherty, D. A., Cation-π interactions in aromatics of biological and medicinal interest: Electrostatic potential surfaces as a useful qualitative guide *Proc. Natl. Acad. Sci.* **1996,** *93* (20), 10566-10571.

13. Dougherty, D. A., The Cation−π Interaction. *Accounts of Chemical Research* **2013,** *46* (4), 885-893.

14. Shepodd, T. J.; Petti, M. A.; Dougherty, D. A., Molecular recognition in aqueous media: donor-acceptor and ion-dipole interactions produce tight binding for highly soluble guests. *Journal of the American Chemical Society* **1988,** *110* (6), 1983-1985.

15. Perutz, M. F.; Fermi, G.; Abraham, D. J.; Poyart, C.; Bursaux, E., Hemoglobin as a receptor of drugs and peptides: x-ray studies of the stereochemistry of binding. *Journal of the American Chemical Society* **1986,** *108* (5), 1064-1078.

16. Levitt, M.; Perutz, M. F., Aromatic rings act as hydrogen bond acceptors. *Journal of Molecular Biology* **1988,** *201* (4), 751-754.

17. Nowak, M.; Kearney, P.; Sampson; Saks, M.; Labarca, C.; Silverman, S.; Zhong, W.; Thorson, J.; Abelson, J.; Davidson, N.; et, a., Nicotinic receptor binding site probed with unnatural amino acid incorporation in intact cells. *Science* **1995,** *268* (5209), 439-442.

18. Zhong, W.; Gallivan, J. P.; Zhang, Y.; Li, L.; Lester, H. A.; Dougherty, D. A., From ab initio quantum mechanics to molecular neurobiology: A cation–π binding site in the nicotinic receptor. *Proceedings of the National Academy of Sciences* **1998,** *95* (21), 12088-12093.

19. Sengupta, B.; Sengupta, P. K., Influence of Reverse Micellar Environments on the Fluorescence Emission Properties of Tryptophan Octyl Ester. *Biochemical and Biophysical Research Communications* **2000,** *277* (1), 13-19.

20. Chattopadhyay, A.; Mukherjee, S.; Rukmini, R.; Rawat, S. S.; Sudha, S., Ionization, partitioning, and dynamics of tryptophan octyl ester: implications for membrane-bound tryptophan residues. *Biophysical Journal 73* (2), 839-849.

21. Chattopadhyay, A.; Arora, A.; Kelkar, D. A., Dynamics of a membrane-bound tryptophan analog in environments of varying hydration: a fluorescence approach. *European Biophysics Journal* **2005,** *35* (1), 62.

22. Arora-Sharawat, A.; Chattopadhyay, A., Effect of structural transition of the host assembly on dynamics of a membrane-bound tryptophan analogue. *Biophysical Chemistry* **2007,** *129* (2), 172-180.

23. de Foresta, B.; Gallay, J.; Sopkova, J.; Champeil, P.; Vincent, M., Tryptophan Octyl Ester in Detergent Micelles of Dodecylmaltoside: Fluorescence Properties and Quenching by Brominated Detergent Analogs. *Biophysical Journal 77* (6), 3071-3084.

24. Tortech, L.; Jaxel, C.; Vincent, M.; Gallay, J.; de Foresta, B., The polar headgroup of the detergent governs the accessibility to water of tryptophan octyl ester in host micelles. *Biochimica et Biophysica Acta (BBA) - Biomembranes* **2001,** *1514* (1), 76-86.

25. Chakraborty, G.; Chowdhury, M. P.; Saha, S. K., Solvent-Induced Molecular Folding and Self-Assembled Nanostructures of Tyrosine and Tryptophan Analogues in Aqueous Solution: Fascinating Morphology of High Order. *Langmuir* **2017,** *33* (26), 6581-6594.

26. Lackowicz, J., Fluorescence anisotropy. In *Principles of Fluorescence Spectroscopy*, Springer: 2006; pp 353–381.

27. Tung, S.-H.; Huang, Y.-E.; Raghavan, S. R., Contrasting Effects of Temperature on the Rheology of Normal and Reverse Wormlike Micelles. *Langmuir* **2007,** *23* (2), 372-376.

28. Koshy, P.; Aswal, V. K.; Venkatesh, M.; Hassan, P. A., Unusual Scaling in the Rheology of Branched Wormlike Micelles Formed by Cetyltrimethylammonium Bromide and Sodium Oleate. *The Journal of Physical Chemistry B* **2011,** *115* (37), 10817-10825.

29. Hayter, J. B.; Penfold, J., An analytic structure factor for macroion solutions. *Molecular Physics* **1981,** *42* (1), 109-118.

30. Ghosh, S.; Das Burman, A.; De, G. C.; Das, A. R., Interfacial and Self-Aggregation of Binary Mixtures of Anionic and Nonionic Amphiphiles in Aqueous Medium. *The Journal of Physical Chemistry B* **2011,** *115* (38), 11098-11112.

31. Sarmoria, C.; Puvvada, S.; Blankschtein, D., Prediction of critical micelle concentrations of nonideal binary surfactant mixtures. *Langmuir* **1992,** *8* (11), 2690-2697.

32. Chakraborty, G.; Paulchowdhury, M.; Bardhan, S.; Saha, S. K., Surface activity and modifying effects of 1-Naphthol, 2-Naphthol and 2,3-Dihydroxynaphthalene on self-assembled nanostructures of 1-Hexadecyl-3-methylimidazolium chloride. *Colloids and Surfaces A: Physicochemical and Engineering Aspects* **2017,** *516*, 262-273.

33. Chakraborty, T.; Ghosh, S.; Moulik, S. P., Micellization and Related Behavior of Binary and Ternary Surfactant Mixtures in Aqueous Medium: Cetyl Pyridinium Chloride (CPC), Cetyl Trimethyl Ammonium Bromide (CTAB), and Polyoxyethylene (10) Cetyl Ether (Brij-56) Derived System. *The Journal of Physical Chemistry B* **2005,** *109* (31), 14813-14823.

34. Swanson-Vethamuthu, M.; Almgren, M.; Hansson, P.; Zhao, J., Surface Tension Studies of Cetyltrimethylammonium Bromide−Bile Salt Association. *Langmuir* **1996,** *12* (9), 2186-2189.

35. Srinivasa Rao, K.; Singh, T.; Trivedi, T. J.; Kumar, A., Aggregation Behavior of Amino Acid Ionic Liquid Surfactants in Aqueous Media. *The Journal of Physical Chemistry B* **2011,** *115* (47), 13847-13853.

36. Jaycock, M. J.; Parfitt, G. D., Chemistry of Interfaces, M. J. Jaycock and G. D. Parfitt. Halstead Press, John Wiley and Sons, New York, 1981. 279 pp. $90. Paul Becher, Wilmington. *Journal of Dispersion Science and Technology* **1982,** *3* (4), 467-468.

37. Rubingh, D. N., Mixed micelle solutions. In *Solution chemistry of surfactants*, Springer: 1979; pp 337-354.

38. Alexander Ross, J. B.; Laws, W. R.; Rousslang, K. W.; Wyssbrod, H. R., Tyrosine Fluorescence and Phosphorescence from Proteins and Polypeptides. In *Topics in Fluorescence Spectroscopy*, Lakowicz, J. R., Ed. Springer US: Boston, MA, 2002; pp 1-64.

39. Drummond, C. J.; Grieser, F.; Healy, T. W., Acid-base equilibria in aqueous micellar solutions. Part 1.-'Simple' weak acids and bases. *Journal of the Chemical Society, Faraday Transactions 1: Physical Chemistry in Condensed Phases* **1989,** *85* (3), 521-535.

40. Drummond, C. J.; Grieser, F.; Healy, T. W., Acid-base equilibria in aqueous micellar solutions. Part 2.-Sulphonephthalein indicators. *Journal of the Chemical Society, Faraday Transactions 1: Physical Chemistry in Condensed Phases* **1989,** *85* (3), 537-550.

41. Rayner, D. M.; Krajcarski, D. T.; Szabo, A. G., Excited state acid–base equilibrium of tyrosine. *Canadian Journal of Chemistry* **1978,** *56* (9), 1238-1245.

42. Dunn, B.; Zink, J. I., Optical properties of sol-gel glasses doped with organic molecules. *Journal of Materials Chemistry* **1991,** *1* (6), 903-913.

43. Ali, M.; Jha, M.; Das, S. K.; Saha, S. K., Hydrogen-Bond-Induced Microstructural Transition of Ionic Micelles in the Presence of Neutral Naphthols: pH Dependent Morphology and Location of Surface Activity. *The Journal of Physical Chemistry B* **2009,** *113* (47), 15563-15571.

44. Lackowicz, J. R., *Principles of Fluorescence Spectroscopy*. 3 ed.; Springer US: 2006.

45. Sujatha, J.; Mishra, A. K., Phase Transitions in Phospholipid Vesicles: Excited State Prototropism of 1-Naphthol as a Novel Probe Concept. *Langmuir* **1998,** *14* (9), 2256-2262.

46. Chaghi, R.; de Ménorval, L.-C.; Charnay, C.; Derrien, G.; Zajac, J., Interactions of phenol with cationic micelles of hexadecyltrimethylammonium bromide studied by titration calorimetry, conductimetry, and 1H NMR in the range of low additive and surfactant concentrations. *Journal of Colloid and Interface Science* **2008,** *326* (1), 227-234.

47. Kaur, G.; Chiappisi, L.; Prévost, S.; Schweins, R.; Gradzielski, M.; Mehta, S. K., Probing the Microstructure of Nonionic Microemulsions with Ethyl Oleate by Viscosity, ROESY, DLS, SANS, and Cyclic Voltammetry. *Langmuir* **2012,** *28* (29), 10640-10652.

48. Shrestha, R. G.; Abezgauz, L.; Danino, D.; Sakai, K.; Sakai, H.; Abe, M., Structure and Dynamics of Poly(oxyethylene) Cholesteryl Ether Wormlike Micelles: Rheometry, SAXS, and Cryo-TEM Studies. *Langmuir* **2011,** *27* (21), 12877-12883.

49. Hoque, J.; Kumar, P.; Aswal, V. K.; Haldar, J., Aggregation Properties of Amide Bearing Cleavable Gemini Surfactants by Small Angle Neutron Scattering and

Conductivity Studies. *The Journal of Physical Chemistry B* **2012,** *116* (32), 9718-9726.

50. Aswal, V. K.; Goyal, P. S.; Thiyagarajan, P., Small-Angle Neutron-Scattering and Viscosity Studies of CTAB/NaSal Viscoelastic Micellar Solutions. *The Journal of Physical Chemistry B* **1998,** *102* (14), 2469-2473.

51. Aswal, V. K.; Goyal, P. S., Mixed micelles of alkyltrimethylammonium halides a small-angle neutron-scattering study. *Physica B: Condensed Matter* **1998,** *245* (1), 73-80.

52. Zemb, T.; Lindner, P., *Neutron, X-rays and Light. Scattering Methods Applied to Soft Condensed Matter*.

53. Hayter, J. B.; Penfold, J., Determination of micelle structure and charge by neutron small-angle scattering. *Colloid and Polymer Science* **1983,** *261* (12), 1022-1030.

54. Kalur, G. C.; Frounfelker, B. D.; Cipriano, B. H.; Norman, A. I.; Raghavan, S. R., Viscosity Increase with Temperature in Cationic Surfactant Solutions Due to the Growth of Wormlike Micelles. *Langmuir* **2005,** *21* (24), 10998-11004.

55. Raghavan, S. R.; Fritz, G.; Kaler, E. W., Wormlike Micelles Formed by Synergistic Self-Assembly in Mixtures of Anionic and Cationic Surfactants. *Langmuir* **2002,** *18* (10), 3797-3803.

56. Dreiss, C. A., Wormlike micelles: where do we stand? Recent developments, linear rheology and scattering techniques. *Soft Matter* **2007,** *3* (8), 956-970.

57. Chen, S. H.; Sheu, E. Y.; Kalus, J.; Hoffman, H., Small-angle neutron scattering investigation of correlations in charged macromolecular and supramolecular solutions. *Journal of Applied Crystallography* **1988,** *21* (6), 751-769.

58. Mukerjee, P., Size distribution of small and large micelles. Multiple equilibrium analysis. *The Journal of Physical Chemistry* **1972,** *76* (4), 565-570.

59. Majhi, P. R.; Dubin, P. L.; Feng, X.; Guo, X.; Leermakers, F. A. M.; Tribet, C., Coexistence of Spheres and Rods in Micellar Solution of Dodecyldimethylamine Oxide. *The Journal of Physical Chemistry B* **2004,** *108* (19), 5980-5988.

60. Eriksson, J. C.; Ljunggren, S., Model calculations on the transitions between surfactant aggregates of different shapes. *Langmuir* **1990,** *6* (5), 895-904.

61. Raghavan, S. R.; Feng, Y., Chapter 2 Wormlike Micelles: Solutions, Gels, or Both? In *Wormlike Micelles: Advances in Systems, Characterisation and Applications*, The Royal Society of Chemistry: 2017; pp 9-30.

62. Shrestha, R. G.; Shrestha, L. K.; Aramaki, K., Formation of wormlike micelle in a mixed amino-acid based anionic surfactant and cationic surfactant systems. *Journal of Colloid and Interface Science* **2007,** *311* (1), 276-284.

63. Cates, M. E., Reptation of living polymers: dynamics of entangled polymers in the presence of reversible chain-scission reactions. *Macromolecules* **1987,** *20* (9), 2289-2296.

64. Grenek, R.; Cates, M. E., Stress relaxation in living polymers: Results from a Poisson renewal model. *The Journal of Chemical Physics* **1992,** *96* (6), 4758-4767.

65. Cates, M. E.; Candau, S. J., Statics and dynamics of worm-like surfactant micelles. *Journal of Physics: Condensed Matter* **1990,** *2* (33), 6869.

References for Chapter VII

1. Jones, D. T.; Taylor, W. R.; Thornton, J. M., A Model Recognition Approach to the Prediction of All-Helical Membrane Protein Structure and Topology. *Biochemistry* **1994,** *33* (10), 3038-3049.

2. Landolt-Marticorena, C.; Williams, K. A.; Deber, C. M.; Reithmeier, R. A. F., Non-random Distribution of Amino Acids in the Transmembrane Segments of Human Type I Single Span Membrane Proteins. *Journal of Molecular Biology* **1993,** *229* (3), 602-608.

3. Ketchem, R. R.; Hu, W.; Cross, T. A., High-resolution conformation of gramicidin A in a lipid bilayer by solid-state NMR. *Science* **1993,** *261* (5127), 1457.

4. Chattopadhyay, A.; Arora, A.; Kelkar, D. A., Dynamics of a membrane-bound tryptophan analog in environments of varying hydration: a fluorescence approach. *European Biophysics Journal* **2005,** *35* (1), 62.

5. Chakraborty, G.; Chowdhury, M. P.; Saha, S. K., Solvent-Induced Molecular Folding and Self-Assembled Nanostructures of Tyrosine and Tryptophan Analogues in Aqueous Solution: Fascinating Morphology of High Order. *Langmuir* **2017,** *33* (26), 6581-6594.

6. Tortech, L.; Jaxel, C.; Vincent, M.; Gallay, J.; de Foresta, B., The polar headgroup of the detergent governs the accessibility to water of tryptophan octyl ester in host micelles. *Biochimica et Biophysica Acta (BBA) - Biomembranes* **2001,** *1514* (1), 76-86.

7. Jiang, Z.; Jia, K.; Liu, X.; Dong, J.; Li, X., Multiple Responsive Fluids Based on Vesicle to Wormlike Micelle Transitions by Single-Tailed Pyrrolidone Surfactants. *Langmuir* **2015,** *31* (43), 11760-11768.

8. Sengupta, B.; Sengupta, P. K., Influence of Reverse Micellar Environments on the Fluorescence Emission Properties of Tryptophan Octyl Ester. *Biochemical and Biophysical Research Communications* **2000,** *277* (1), 13-19.

9. Tung, S.-H.; Huang, Y.-E.; Raghavan, S. R., Contrasting Effects of Temperature on the Rheology of Normal and Reverse Wormlike Micelles. *Langmuir* **2007,** *23* (2), 372-376.

10. Ekwall, P.; Mandell, L.; Solyom, P., The aqueous cetyl trimethylammonium bromide solutions. *Journal of Colloid and Interface Science* **1971,** *35* (4), 519-528.

11. Chakraborty, G.; Paulchowdhury, M.; Bardhan, S.; Saha, S. K., Surface activity and modifying effects of 1-Naphthol, 2-Naphthol and 2,3-Dihydroxynaphthalene on self-assembled nanostructures of 1-Hexadecyl-3-methylimidazolium chloride. *Colloids and Surfaces A: Physicochemical and Engineering Aspects* **2017,** *516*, 262-273.

12. Findenegg, G. H., D. K. Chattoraj and K. S. Birdi: Adsorption and the Gibbs Surface Excess. Plenum Press, New York and London 1984, 471 Seiten, Preis: $

59.50. *Berichte der Bunsengesellschaft für physikalische Chemie* **1985,** *89* (11), 1250-1250.

13. Xu, W.; Wang, T.; Cheng, N.; Hu, Q.; Bi, Y.; Gong, Y.; Yu, L., Experimental and DFT Studies on the Aggregation Behavior of Imidazolium-Based Surface-Active Ionic Liquids with Aromatic Counterions in Aqueous Solution. *Langmuir* **2015,** *31* (4), 1272-1282.

14. Kreke, P. J.; Magid, L. J.; Gee, J. C., 1H and 13C NMR Studies of Mixed Counterion, Cetyltrimethylammonium Bromide/Cetyltrimethylammonium Dichlorobenzoate, Surfactant Solutions: The Intercalation of Aromatic Counterions. *Langmuir* **1996,** *12* (3), 699-705.

15. Zana, R.; Lévy, H.; Danino, D.; Talmon, Y.; Kwetkat, K., Mixed Micellization of Cetyltrimethylammonium Bromide and an Anionic Dimeric (Gemini) Surfactant in Aqueous Solution. *Langmuir* **1997,** *13* (3), 402-408.

16. Kaur, G.; Chiappisi, L.; Prévost, S.; Schweins, R.; Gradzielski, M.; Mehta, S. K., Probing the Microstructure of Nonionic Microemulsions with Ethyl Oleate by Viscosity, ROESY, DLS, SANS, and Cyclic Voltammetry. *Langmuir* **2012,** *28* (29), 10640-10652.

17. Fraenkel, Y.; Gershoni, J. M.; Navon, G., Acetylcholine interactions with tryptophan-184 of the α-subunit of the nicotinic acetylcholine receptor revealed by transferred nuclear Overhauser effect. *FEBS Letters* **1991,** *291* (2), 225-228.

18. Rubingh, D. N., Mixed micelle solutions. In *Solution chemistry of surfactants*, Springer: 1979; pp 337-354.

19. Chattopadhyay, A.; Mukherjee, S.; Rukmini, R.; Rawat, S. S.; Sudha, S., Ionization, partitioning, and dynamics of tryptophan octyl ester: implications for membrane-bound tryptophan residues. *Biophysical Journal 73* (2), 839-849.

20. de Foresta, B.; Gallay, J.; Sopkova, J.; Champeil, P.; Vincent, M., Tryptophan Octyl Ester in Detergent Micelles of Dodecylmaltoside: Fluorescence Properties and Quenching by Brominated Detergent Analogs. *Biophysical Journal 77* (6), 3071-3084.

21. Ali, M.; Jha, M.; Das, S. K.; Saha, S. K., Hydrogen-Bond-Induced Microstructural Transition of Ionic Micelles in the Presence of Neutral Naphthols: pH Dependent Morphology and Location of Surface Activity. *The Journal of Physical Chemistry B* **2009,** *113* (47), 15563-15571.

22. Sabatino, P.; Szczygiel, A.; Sinnaeve, D.; Hakimhashemi, M.; Saveyn, H.; Martins, J. C.; Van der Meeren, P., NMR study of the influence of pH on phenol sorption in cationic CTAB micellar solutions. *Colloids and Surfaces A: Physicochemical and Engineering Aspects* **2010,** *370* (1–3), 42-48.

23. Chaghi, R.; de Ménorval, L.-C.; Charnay, C.; Derrien, G.; Zajac, J., Interactions of phenol with cationic micelles of hexadecyltrimethylammonium bromide studied by titration calorimetry, conductimetry, and 1H NMR in the range of low additive

and surfactant concentrations. *Journal of Colloid and Interface Science* **2008,** *326* (1), 227-234.

24. Mata, J. P.; Aswal, V. K.; Hassan, P. A.; Bahadur, P., A phenol-induced structural transition in aqueous cetyltrimethylammonium bromide solution. *Journal of Colloid and Interface Science* **2006,** *299* (2), 910-915.

25. Raghavan, S. R.; Kaler, E. W., Highly Viscoelastic Wormlike Micellar Solutions Formed by Cationic Surfactants with Long Unsaturated Tails. *Langmuir* **2001,** *17* (2), 300-306.

26. Dreiss, C. A., Wormlike micelles: where do we stand? Recent developments, linear rheology and scattering techniques. *Soft Matter* **2007,** *3* (8), 956-970.

27. Cates, M. E.; Candau, S. J., Statics and dynamics of worm-like surfactant micelles. *Journal of Physics: Condensed Matter* **1990,** *2* (33), 6869.

28. Kern, F.; Lequeux, F.; Zana, R.; Candau, S. J., Dynamic Properties of Salt-Free Viscoelastic Micellar Solutions. *Langmuir* **1994,** *10* (6), 1714-1723.

29. Chu, Z.; Feng, Y., Thermo-switchable surfactant gel. *Chemical Communications* **2011,** *47* (25), 7191-7193.

30. Frisch, M. J. T., G. W.; Schlegel, H. B.; Scuseria, G. E.; Robb, M. A.; Cheeseman, J. R.; Scalmani, G.; Barone, V.; Mennucci, B.; Petersson, G. A.; Nakatsuji, H.; Caricato, M.; Li, X.; Hratchian, H. P.; Izmaylov, A. F.; Bloino, J.; Zheng, G.; Sonnenberg, J. L.; Hada, M.; Ehara, M.; Toyota, K.; Fukuda, R.; Hasegawa, J.; Ishida, M.; Nakajima, T.; Honda, Y.; Kitao, O.; Nakai, H.; Vreven, T.; Montgomery Jr, J. A.; Peralta, J. E.; Ogliaro, F.; Bearpark, M.; Heyd, J. J.; Brothers, E.; Kudin, K. N.; Staroverov, V. N.; Kobayashi, R.; Normand, J.; Raghavachari, K.; Rendell, A.; Burant, J. C.; Iyengar, S. S.; Tomasi, J.; Cossi, M.; Rega, N.; Millam, J. M.; Klene, M.; Knox, J. E.; Cross, J. B.; Bakken, V.; Adamo, C.; Jaramillo, J.; Gomperts, R.; Stratmann, R. E.; Yazyev, O.; Austin, A. J.; Cammi, R.; Pomelli, C.; Ochterski, J. W.; Martin, R. L.; Morokuma, K.; Zakrzewski, V. G.; Voth, G. A.; Salvador, P.; Dannenberg, J. J.; Dapprich, S.; Daniels, A. D.; Farkas, O.; Foresman, J. B.; Ortiz, J. V.; Cioslowski, J.; Fox, D. J. *Gaussian 09*, Gaussian, Inc: Wallingford CT, 2009.

31. Dougherty, D. A., Cation-π Interactions in Chemistry and Biology: A New View of Benzene, Phe, Tyr, and Trp. *Science* **1996,** *271* (5246), 163-168.

32. Dougherty, D. A., The Cation−π Interaction. *Accounts of Chemical Research* **2013,** *46* (4), 885-893.

INDEX

M

N

P

R

S

T

U

V

Z

Colloids and Surfaces A: Physicochem. Eng. Aspects 516 (2017) 262–273

Contents lists available at ScienceDirect

Colloids and Surfaces A: Physicochemical and Engineering Aspects

journal homepage: www.elsevier.com/locate/colsurfa

Surface activity and modifying effects of 1-Naphthol, 2-Naphthol and 2,3-Dihydroxynaphthalene on self-assembled nanostructures of 1-Hexadecyl-3-methylimidazolium chloride

Gulmi Chakraborty, Madhurima Paulchowdhury, Soumik Bardhan, Swapan K. Saha *

Department of Chemistry, University of North Bengal, Darjeeling 734 013, India

HIGHLIGHTS

- Strong synergism in surface property of SAIL, C_{16}-3-MeImCl in presence of 1-Naphthol, 2-Naphthol and 2,3-Dihydroxynaphthalene.
- Probing the micro-structural interactions by UV–vis Spectroscopy, Fluorescence anisotropy, ^{1}H NMR and DFT study.
- Formation of temperature responsive entangled wormlike micelles with strong viscoelasticity.
- Formation of metal tolerant viscoelastic gel of the ionic liquid/additive in presence of the π-conjugated hydroxy aromatic additive.

GRAPHICAL ABSTRACT

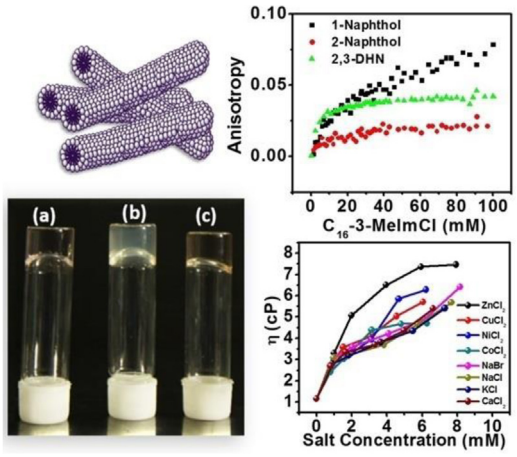

ARTICLE INFO

Article history:
Received 29 August 2016
Received in revised form 7 December 2016
Accepted 13 December 2016
Available online 14 December 2016

Keywords:
Hydroxy aromatic additives
Cation-π interaction
Surface active ionic liquid
Micellar shape transition
Wormlike micelles
Thermo-sensitive
Metal ion impurities

ABSTRACT

The nature of transition from ordinary micelles (of nanometer length scale) of surface active ionic liquid 1-Hexadecyl-3- methylimidazolium chloride, to wormlike micelles (WLM) (micrometer length scale), mediated by hydroxy aromatic π-electron systems 1-Naphthol, 2-Naphthol and 2,3-Dihydroxynaphthalene (2,3-DHN) in salt free condition have been studied under Newtonian as well as non-Newtonian flow regimes. Conductance and tensiometry show that the additives lower the CMC of the ionic liquid. The interaction parameter (β) of the systems at different mole fraction evaluated on basis of Rubingh's Regular solution approach were negative at all SAIL/Additive compositions. UV–vis spectroscopy showed that micelle-bound additives formed hydrogen bonds with interfacial water molecules. Increase in steady state fluorescence anisotropic measurements revealed that the additives increasingly partitioned within the micelles. ^{1}H NMR study confirmed that although the additives reside at the palisade layer, they perturb the micellar core as well. At higher concentration (100 mM, 1:1), systems formed transparent viscoelastic gel. Rheological study of the viscoelastic gels showed that their zero shear viscosity is a function of temperature. 2,3-DHN interacted most strongly with the SAIL micelles, both in Newtonian and non-Newtonian regimes. This was corroborated by DFT study of binding energy. Hydrogen bonding of the hydroxy functionality along with strong cation-π interaction between the aromatic

* Corresponding author.
E-mail address: ssahanbu@hotmail.com (S.K. Saha).

http://dx.doi.org/10.1016/j.colsurfa.2016.12.025

moieties and the imidazolium ring are considered as the main driving forces behind the morphology change. The viscosity of C_{16}-3-MeImCl/1-Naphthol increased as function of salt concentration unlike C_{16}-3-MeImCl/NaSal system. A possible mechanism is suggested and discussed. The present study sheds light on understanding the molecular interactions behind the structural change from spherical to elongated micelles, in both microscopic and macroscopic scale, triggered by hydroxy naphthalenes under salt-free condition. The metal tolerance of the gels has huge application prospects as fractured fluids in oil-mining industry.

1. Introduction

Due to their unique chemical and physical properties and high tunability [1], ionic liquids (ILs) have drawn increasing interest as alternative media in a variety of catalytical, separation and electrochemical methods [2]. The transfer of a compound through an interface is a major part of the extraction process which is controlled by molecules adsorbed at the interface. The presence of surface active ionic liquid (SAIL) aggregates could modulate the efficiency of these processes including partial extraction of the product into micelles. Under certain conditions such as concentration, salinity, temperature, presence of counter ions, etc., the globular micelles may undergo uniaxial growth and form very long and highly flexible aggregates, referred to as "wormlike" or "thread-like" micelles [3]. Due to their cylindrical morphology and high flexibility, wormlike micelles (WLM) have emerged as a novel carrier system that provide larger core volume to load drugs and is, therefore, able to flow readily through capillaries and pores [4]. Since WLMs have larger drug loading capacity and longer circulation time it may be highly useful and novel strategy for drug delivery to start as WLMs and later degrade to spherical micelles, which are already known to be extremely useful for therapeutic applications [5,6]. Better prospect of controlled drug release warrants more insight on mechanism and kinetics of such degradability of wormlike micelles.

Study on micelle formation of the surface active ionic liquid, (SAIL) 1-Hexadecyl-3-methylimidazolium chloride, C_{16}-3-MeImCl and the cationic surfactant Cetylpyridinium chloride, C_{16}PyCl in the temperature range 15–75 °C, have shown that although aggregation of C_{16}PyCl should have been more favorable than C_{16}-3-MeImCl as C_{16}PyCl is more hydrophobic than the corresponding SAIL, this is not the case [7]. The strong hydrogen-bonding between the counter ion and the relatively acidic hydrogen of the imidazolium ring distinguishes imidazole-based SAILs from other conventional cationic surfactants. Also, due to presence of asymmetric organic cations, the lattice energy of 1-alkyl-3-methyl-imidazolium [C*n*MIM] salts is reduced which result in low melting point ionic liquids, commonly called room temperature ionic liquid (RTIL) (melting point < 100 °C) [8]. Literature shows that the coexistence of incompatible hydrophobic moieties such as fluorocarbon and hydrocarbon chains are a basic requirement but often not sufficient for the formation of the two distinct types of micelles i.e. spherical and WLM in aqueous solutions. On the other hand, synergistic micellization is observed when ionic surfactants are mixed with non-ionic or with oppositely charged surfactants. Both surface and bulk properties of these systems have been studied using different experimental techniques [9–11]. Strong synergistic gains in viscoelastic properties of mixtures of anionic and cationic surfactants compared to the parent surfactants have been reported. ILs (especially those with long hydrophobic chains) have been reported to show amphiphilic properties in aqueous solution [12–14]. Aromatic hydrotopes like salicylate, tosylate, chlorobenzoate, hydroxynaphthalene carboxylates and nitrobenzoate are reported to induce wormlike micelle formation in cationic surfactant solution. In particular, various hierarchically self-assembled structures such as tubes, ribbons, vesicles and lamellar structures can be fabricated in mixtures of surfactants and hydrotopes [15]. Synergistic effect of aromatic hydrotopes on the solution properties of ammonium gemini surfactants were reported [16]. Recently, highly temperature sensitive wormlike micelle-to-hydrogel and vice-versa transition in the ionic liquid 1-Hexadecyl-3-methylimidazolium chloride, triggered by the aromatic hydrotope, Sodium salicylate (NaSal), have been reported [17]. It is evident from literature that interaction of aromatic hydrotopes with surfactant yield interesting properties of aggregates which are tunable via external stimuli like temperature, pH etc [18]. However, majority of the reports involve ionic medium and presence of salts, and there are very less reports regarding study of interaction of ionic liquids with non-ionic hydrotopes and on the use of additives in improving the micellization characteristics of ionic liquids. It has also been reported that hydroxy aromatic compound viz., 1-Naphthol and 2-Naphthol interact with the structurally reoriented water molecules on micellar surface of the cationic surfactant CTAB via hydrogen bond formation and induce viscoelasticity in CTAB solution [19,20]. It was observed that 1-Naphthol and 2-Naphthol showed surface active behavior [20]. The surface active property of the aromatic promoters leaves room for understanding of the molecular interactions between the aromatic hydrotopes/additives and the surfactant systems comprising of aromatic extended conjugated systems especially because the hydroxy aromatic group as well as the imidazolium moiety, both form the fundamental skeleton of two non-essential amino acids viz. tyrosine and tryptophan respectively. We intend to further investigate the effect of the hydroxy aromatic compounds, viz., 1-Naphthol, 2-Naphthol and 2, 3-Dihydroxynaphthalene on the aggregation characteristics of the ionic liquid system namely, 1-Hexadecyl-3-methylimidazolium chloride (C_{16}-3-MeImCl). This ionic liquid has superior individual surface and bulk property compared to its ordinary surfactant analogues viz. Cetylpyridinium bromide (CPB) and CTAB. The pK_a of the additives are >9.15 and therefore, in aqueous solution of ionic liquids (pH- 6.5–7.5), they remain in protonated non-ionic form. Herein we report the quantitative estimation of the surface parameters of the aromatic compounds: 1-Naphthol, 2-Naphthol and 2,3-Dihydroxynaphthalene and investigate their effect in modifying the aggregation characteristics of the ionic liquid C_{16}-3-MeImCl under salt-free condition. An interesting aspect of these additives, is their fluorescent nature; which enables them to be used as self-probes. Modification of their spectral properties in presence of the ionic liquid may provide insight of the probe-ionic liquid interaction at the micro-structural level. Interactions in micro-environment of the additives are explored spectroscopically (UV–vis Spectroscopy, Fluorescence anisotropy and ^{1}H NMR) and the effect of the additives on aggregate morphology of the ionic liquid micelle are investigated. For more specific insight about the binding interactions of the individual additives with the ionic liquid, molecular dynamics calculations using DFT are carried out.

Effect of metal salts on viscosity of the SAIL/Additive system have been investigated.

2. Materials and methods

1-Hexadecyl-3-methylimidazolium chloride, was purchased from Across chemicals (USA) and was used as received. 1 and 2-Naphthols (Fluka, Germany) and 2,3-Dihydroxynaphthalene (Fluka, Germany) were further purified by vacuum sublimation followed by crystallization from 1:1 aqueous methanol. Methanol was distilled prior to use. Double distilled water (conductance below 2 μS/cm, pH ~6.5–7) was used for all experimental purposes. D_2O was purchased from Aldrich, USA (Purity > 99.9%). All conductometric measurements were carried out on Metler Toledo Digital Conductivity bridge (MC226) using a dip cell with cell constant 1.0 cm^{-1}. Tensiometric studies were done with Krüss GmbH K9 tensiometer following the ring detachment method. Constant temperature was maintained during the experiments with Remi ultra thermostat (CB-700) with precision (±0.1 K).

The rheological experiments were done using cone-plate geometry with 4^{00} truncation angle, with diameter 25 mm and 0.105 mm sample gap in MCR 302 (Anton Paar) equipped with Peltier temperature control system.

Steady state fluorescence anisotropy study was carried out in bench top spectrofluorimeter from Photon technologies International (Quantamaster-40) with excitation and emission slit widths fixed at 0.3 nm and 2.0 nm respectively. Steady state anisotropy (r) was determined using the following expressions [21]:

$$r = \frac{I_{VV} - G.I_{VH}}{I_{VV} + 2G.I_{VH}} \text{ and } G = \frac{I_{HH}}{I_{VH}} \quad (1)$$

where I_{VV} and I_{VH} represent the intensities obtained with the excitation polarizer oriented vertically and the emission polarizer oriented vertically and horizontally respectively; I_{HV} and I_{HH} refer to the similar parameters as mentioned above for the horizontal positions of the excitation polarizer.

^1H NMR experiments were performed in Bruker ADVANCE spectrometer operating at 300 MHz frequency at 298 K. Signals are quoted as δ values in ppm using residual protonated solvent signals as internal standard (D_2O: δ 4.79 ppm). Data are reported as chemical shift.

2.1. Sample preparation

Since Naphthol(s) and its derivative 2,3-Dihydroxynaphthalene are only sparingly soluble in water, a methanolic solution of higher concentration was initially made. Experimental solutions were prepared routinely by transferring the required volume of solution (in pure methanol) in the experiment vial first, and then the alcohol was evaporated off completely before the addition of aqueous surfactant solution [20]. For rheometry, surfactant was added to the dried additive followed by requisite volume of solvent. Sample concentration for all the systems was 100 mM with 1:1 surfactant: additive mole ratio i.e. concentration of each of the components was 100 mM. The mixture was then stirred at 60 °C for three hours for homogenization and equilibrated for 36 h. During measurement, samples were equilibrated for 10 mins at each temperature [22]. For NMR study, respective solutions were made in D_2O and 0.6 mL of the same was used for each measurement.

3. Results and discussion

3.1. Surface active properties of π-conjugated additives

The variation of surface tension of aqueous solution of the hydroxy aromatic compounds 1-Naphthol, 2-Naphthol and 2,3-Dihydroxynaphthalene (2,3-DHN) is obtained from tensiometric study. It is evident from Fig. 1 that the surface tension of water decreases linearly as a function of concentration of 1-Naphthol, 2-Naphthol or 2,3-DHN and reaches a limiting value above critical aggregation concentration (CAC) in each case. The equilibrium surface tension of the additive solutions is 12–15 mN m^{-1} lower than pure water's which confirms their surface activity. The CAC for 1-Naphthol, 2-Naphthol and 2,3-DHN is found to be 4.66 mM, 3.62 mM and 3.06 mM respectively at 303 K.

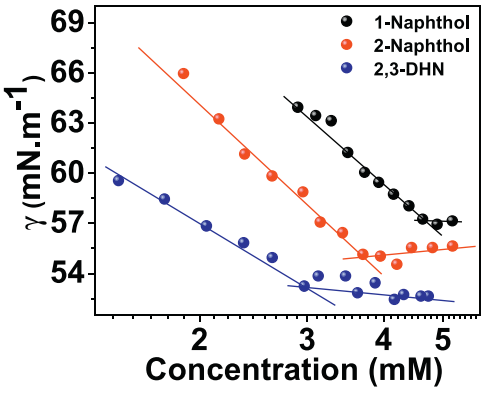

Fig. 1. Tensiometric profile of additives (1-Naphthol, 2-Naphthol and 2, 3-Dihydroxynaphthalene (2,3-DHN)) in log scale at 303 K.

Table 1 lists the CAC values along with the surface tension at CAC (γ_{CAC}), the maximum surface excess concentration (Γ_{max}) and the minimum surface area per organic molecule (A_{min}). (Mathematical background of evaluation of surface parameters is provided under Section 1.1 of SI). Both CAC and γ_{CAC} values decrease slightly in the order 1-Naphthol > 2-Naphthol > 2,3 DHN, which indicates stronger surface activity and wetting ability at the surface in the opposite order (Table 1). The minimum surface area per molecule (A_{min}) marks the effectiveness of a compound to populate the air-water interface. Higher the value of A_{min}, greater is the tendency to "wet" the surface. A_{min} for 2,3-DHN is found to be 0.55 $nm^2 \cdot mol^{-1}$, almost twice that of 1 and 2-Naphthols, which are almost identical i.e. 0.28 and 0.29 nm^2 mol^{-1} respectively. The γ_{CAC} for 1-Naphthol, 2-Naphthol and 2,3-DHN are respectively 57.02, 55.37 and 52.85 mM m^{-1}. The values indicate in case of 2,3-DHN, the surface activity is the highest while that for 1-Naphthol it is lowest. The maximum surface excess (Γ_{max}) denotes the number of surface active molecules present at the interface in excess of the bulk. Γ_{max} for 2,3-DHN is 3.02 mol m^{-2} while that of 1 and 2-Naphthol are 5.64 and 5.93 mol m^{-2} respectively i.e. approximately half the number of dihydroxy naphthalene populate the surface compared to mono hydroxy analogue. This suggests that the 2,3-DHN molecules are arranged in staggered or oblique manner at the water/air interface whereas the 1 and 2-Naphthols may possibly be arranged more or less perpendicularly. While lesser number of 2,3-DHN molecules populate the surface compared to that of Naphthols due to their oblique arrangements, the surface activity vis-a-vis hydrophobic force operating at the surface becomes higher leading to lowering of γ_{CAC} value.

3.2. Synergistic improvement of surface and bulk properties of C_{16}-3-MeImCl in presence of naphthols

The effects of π- conjugated hydroxy aromatic additives 1-Naphthol, 2-Naphthol and 2,3-DHN on the critical micelle concentration, (CMC) of the cationic ionic liquid 1-Hexadecyl-3-methylimidazolium chloride (C_{16}-3-MeImCl) are studied, both by conductivity and surface tension measurements (Fig. S1). The CMC of C_{16}-3-MeImCl (0.89 mM) is in agreement with the reported value

Table 1
Interfacial parameters of 1-Naphthol, 2-Naphthol and 2,3-DHN in aqueous medium at 303 K.

Additive	CAC (mM)	$10^3 \Pi_{CAC}$ (mN m^{-1})	$10^6 \Gamma_{max}$ (mol m^{-2})	A_{min} (nm^2·mol^{-1})
1-Naphthol	4.66	17.2	5.64	0.29
2-Naphthol	3.62	19.2	5.93	0.28
2,3-DHN	3.06	21.1	3.02	0.55

[7]. The CMC of C_{16}-3-MeImCl decreases significantly as a function of additive (the hydroxy aromatic compounds) concentrations and the systems display strong synergism in their aggregation behavior. The maximum drop in CMC is observed from 0.89 mM to 0.45 mM, 0.52 mM and 0.65 mM in presence of 1-Naphthol, 2-Naphthol and 2,3-DHN respectively inspite of much higher CAC of these additives (Fig. S1(a)). The observation demonstrates a fairly strong interaction between the additives and the SAIL micelles. From Fig. S1(b), it is seen that the CMC decrease with increasing mole fraction of additives upto $\alpha_{Additive} = 0.5$, and increases thereafter. It seems apparent that hydrophobicity of the aromatic ring of the additives is involved in strong interaction with the hydrocarbon tail of SAIL in the micelle. All these additives have similar aromatic architecture for which their effectiveness in reducing the CMC is found to be nearly identical. Earlier, Bergstrom and Eriksson have shown by theoretical calculation based on the theory of regular solution mixtures, that for mixed systems consisting of monovalent ionic surfactant and a non-ionic surfactant, the CMC *vs.* composition curve exhibits a skew with maximum shallow at $\alpha = 0.5$ i.e. at equimolar composition, at total surfactant concentration below 0.2 M, wherein the reduced charge density, $S_r >> 1$. S_r dominates the electrostatic free energy per unit charge of the system which arises out of the interaction of additive and surfactant with solvent molecules and amongst themselves [23]. Interestingly, similar nature of curves are obtained in the present mixed systems comprising of C_{16}-3-MeImCl and hydroxy aromatic compounds. It may be argued that the π-conjugated additives, in this case, behave as cosurfactant to lower the CMC of the present systems.

3.3. Interaction parameters

To quantitatively investigate the interaction between the surface active components viz. 1-Naphthol, 2-Naphthol and 2,3-DHN with the SAIL, C_{16}-3-MeImCl, the interaction parameter (β) and activity coefficients of the respective components in the micellar region is evaluated based on Rubingh's Regular solution theory (RST) [24]. The central assumption of RST is that excess entropy of mixing is zero and that the departure from ideal mixing is described by the single interaction parameter, β, which account for the enthalpy of mixing. β, reflects the interaction between the head groups of the surfactant and the additives involved. More negative value of β indicates stronger interaction between the surfactant and the surface active components [25] (Mathematical background of Regular Solution approach is provided under Section 1.2 of SI).

For components which are non-aggregating in nature, their solubility limit can be taken as the phase-separation point and the regular solution theory can be extended onto them [26]. In cases where the additive is highly water soluble yet non-aggregating in nature the high value of solubility incur a high value of x_1, which predicts an unusually high value of interaction parameter [27]. In the present systems, however, quantitative analysis of the mixture in the usual framework of RST is valid because of the surface active nature of the additives and the observed well defined CAC values for each of them. The interaction parameters and activity coefficients of components at different additive mole fraction are, therefore, determined following equation 5 of SI and summarized in Table 2. It is seen that in all the cases, β have negative values at all additive mole fractions ($-2.9 > \beta > -5.7$). While for 1-Naphthol, β increases from −3.45 to −5.73 at mole fraction 0.1–0.7; in 2-Naphthol and 2,3-DHN, β reaches minima (highest negative) near a composition $\alpha_{additive} \cong 0.5$ there after it decreases (Table 2). This implies that interaction of 1-Naphthol with the micelles of the SAIL is favored with increasing additive concentration whereas in case of 2-Naphthol and 2,3-DHN, the synergism is highest near equimolar composition of the components. The activity coefficients of the surfactant and the additives are less than unity (Table 2) for all additive compositions, which indicates the deviation from ideal behavior. The behavior seems at par with their ability to lower the CMC of the SAIL. 1-Naphthol is found to lower the CMC to a higher extent compared to 2-Naphthol and 2,3-DHN. This further confirms the strong synergism between the additives and the SAIL micelles.

3.4. Mode of interaction: absorption spectroscopy and fluorescence anisotropy study

3.4.1. UV absorption spectroscopy

To explore the interactions at the molecular level, responsible for the synergism, spectral modifications of the additives viz. 1-Naphthol, 2-Naphthol and 2,3-DHN are studied as a function of SAIL micelle concentration (Fig. 2(a–c)).

Aromatic moiety like naphthalene (and its derivatives) has two strongly overlapped bands in the UV–vis region viz., longitudinally polarized $^1L_a \longleftarrow {}^1A$ and transversely polarized, $^1L_b \longleftarrow {}^1A$ band [21]. Thus conjugation extended to —OH group in transverse direction in 1-Naphthol and that in longitudinal direction in case of 2-Naphthol and 2,3-DHN ought to affect the ^1L_a and ^1L_b bands respectively [20]. Significant red shift in the λ_{max} for all the three additive systems (shown in inset) (Fig. 2(a–c)) is observed in presence of SAIL micelles. The isobestic points indicate equilibria to exist between micelle bound and free additive (probe) molecules (Fig. S2). The red shifts are respectively 4.6 nm for 1-Naphthol with λ_{max} at 293.1 nm, 2.3 nm for 2-Naphthol with λ_{max} at 273 nm and 3 nm for 2,3-DHN with λ_{max} at 324 nm. This significant red shift in near UV absorbances in the additives, which arises out of two strongly overlapped π- π* transitions indicates a lesser π-π* separation (Fig. 2) on addition of SAIL in the post-micellar region (above 1.44 mM in 1-Naphthol, 1.16 mM for 2-Naphthol and 2,3-DHN). Such shift continues to occur till most of the probe molecules are partitioned within the micellar phase at high SAIL/Additive ratio (90:1). The role of Hydrogen bonding in such modification of spectral property is noteworthy. The —OH group of the naphthols can act both as proton donor or acceptor in forming intermolecular hydrogen bonds. During hydrogen bond formation of hydroxy group, in which —OH act as donor, electron density on the oxygen increases, which is further induced towards the aromatic ring decreasing the π-π* separation resulting in the observed red shift in the absorption spectra [20].

The results suggest that the considerably polar hydroxyl group of the micelle-embedded additive molecules, protrude out of the micellar interface and engage in hydrogen bond with interfacially located water molecules thereby acting at hydrogen donor. Significant values of binding constants are also observed for C_{16}-3-MeImCl micelles/Additive probes. (Fig. S2). The hydrogen bonds steer the rigidity of re-oriented water structures, and force the additives to position firmly in between the surfactant head-groups thereby screening their positive charge.

Table 2
Interaction parameter (β), activity coefficients (f_1 and f_2) of C_{16}-3-MeImCl with 1-Naphthol, 2-Naphthol and 2,3-DHN at 303 K.

$\alpha_{Additive}$	1-Naphthol			2-Naphthol			2,3-DHN		
	β_m	f_1	f_2	β_m	f_1	f_2	β_m	f_1	f_2
0.3	−3.45	0.171	0.185	−2.95	0.221	0.236	−2.87	0.222	0.025
0.4	−4.08	0.099	0.168	−3.41	0.139	0.235	−3.21	0.156	0.257
0.5	−5.40	0.033	0.134	−4.23	0.071	0.207	−3.76	0.089	0.258
0.6	−5.44	0.027	0.161	−3.63	0.089	0.295	−3.48	0.095	0.322
0.7	−5.73	0.018	0.176	−3.84	0.065	0.326	−3.69	0.070	0.355

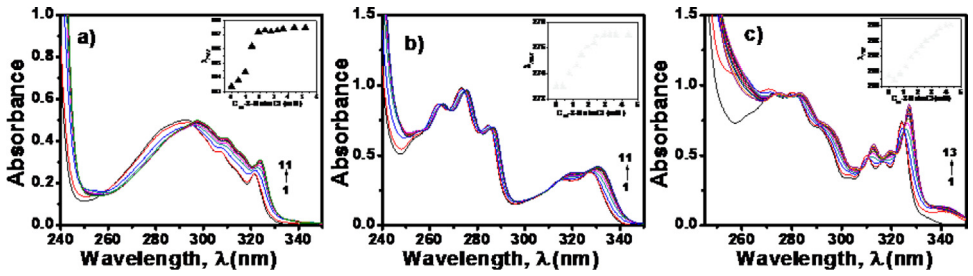

Fig. 2. a) Absorption spectra of 1-Naphthol (0.5 mM) in water at varying concentrations of C_{16}-3-MeImCl at 298 K. [C_{16}-3-MeImCl]: (1) 0.0 (2) 0.49 (3) 0.97 (4) 1.44 (5) 1.90 (6) 2.35 (7) 2.79 (8) 3.22 (9) 3.63 (10) 4.43 (11) 5.21 mM; b) Absorption spectra of 2-Naphthol (0.5 mM) in water at varying concentrations of C_{16}-3-MeImCl at 25° C. [C_{16}-3-MeImCl]: (1) 0.0 (2) 0.39 (3) 0.78 (4) 1.16 (5) 1.53 (6) 1.90 (7) 2.26 (8) 2.61 (9) 2.95 (10) 3.29 (11) 3.62 mM; c) Absorption spectra of 2,3-DHN (0.5 mM) in water at varying concentrations of C_{16}-3-MeImCl at 25° C. [C_{16}-3-MeImCl]: (1) 0.00 (2) 0.39 (3) 0.78 (4) 1.16 (5) 1.53 (6) 1.90 (7) 2.26 (8) 2.61 (9) 2.95 (10) 3.29 (11) 3.62 (12) 3.94 (13) 4.27 mM.

3.4.2. Fluorescence anisotropy

Fluorescence anisotropy is an important tool to monitor the changes in microenvironment of the probe in cases involving the structural transition of fluorophores [28]. Since the lifetimes of fluorescence emissions are of similar order as the rate of tumbling of molecules in solution, physical processes like rotational diffusion lead to depolarization of fluorescence and this is a function of solution viscosity and the size and shape of the molecule. 1-Naphthol, 2-Naphthol and 2,3-DHN are already known to be very effective fluorophores [21,29,30] and therefore study of fluorescence anisotropy, would be interesting, in order to understand the microscopic changes in the environment comprising of the SAIL micelles. To ensure complete insertion of the probe molecules within the micelles, the surfactant concentration is varied from 4.7 mM to 100 mM, (much above the CMC of the SAIL) and the concentration of the self-probes viz. 1-Naphthol, 2-Naphthol and 2,3-DHN are fixed at 0.4 mM. The excitation wavelength for 1-Naphthol, 2-Naphthol and 2,3-DHN are respectively 323 nm, 324 nm and 326 nm while emission for the same are obtained at 465 nm, 478 nm and 351 nm respectively. 1-Naphthol (pK_a 9.34) undergo ultrafast deprotonation in aqueous media due to which the emission intensity of its neutral form (λ = 360 nm) is extremely low [31]. Therefore, anisotropic studies are done considering the anion emission of 1-Naphthol at 465 nm. For similar reason, the most intense peak at 409 nm is considered for 2-Naphthol (pK_a 9.51) whereas that for 2,3-DHN (pK_a 9.10) the single emission band with λ_{max} at 340 nm is considered. The initial anisotropy of the probes in pure aqueous medium is found to be very low and it increases with increase in the SAIL concentration and attains limiting value (Fig. 3) (for 2-Naphthol and 2,3-DHN).

The increase in anisotropy values reflects an impended rotational diffusion of the fluorophores under high micro viscous environment [32].

Anisotropy- concentration profiles show different degree of polarization for different fluorophores in the SAIL micelles (Fig. 3). Anisotropy is highest for 1-Naphthol, it does not exhibit the plateau, while 2-Naphthol and 2,3-DHN reach plateau in anisotropy-concentration profile at high SAIL concentrations. Under the condition, when the probe are encapsulated within the micellar core, no further change in its rotational dynamics is entailed, resulting in near constancy of the anisotropy values. Such situation prevails for 2-Naphthol and 2,3-DHN at SAIL concentration of 20 mM onward, while in case of 1-Naphthol, micellar encapsulation seems to be less favorable and increases with SAIL concentration upto 100 mM i.e. location of the probe in 1-Naphthol, registered stronger hindrance to rotational freedom. However, the scattering of data-points for 2-Naphthol and 2,3-DHN in the anisotropy-concentration profile indicates that unlike 1-Naphthol, the anisotropy of the above probes are not the sole function of encapsulation in the micelles vis-à-vis concentration of SAILs only.

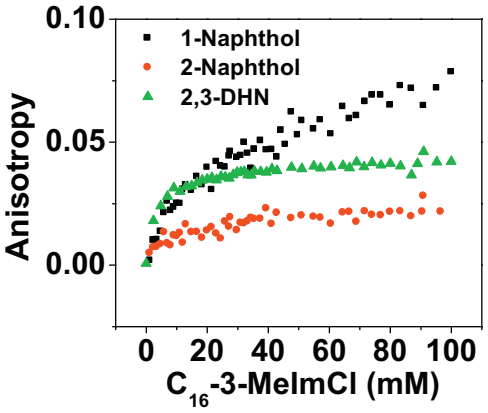

Fig. 3. Steady state fluorescence anisotropy of 0.4 mM 1-Naphthol, 2-Naphthol and 2,3-DHN as function of C_{16}-3-MeImCl concentration at 298 K.

3.5. Improvement in viscous properties of C_{16}-3-MeImCl/Naphthol(s) systems at enhanced concentration

Upon increasing the concentration of the 1:1C_{16}-3-MeImCl/Naphthol(s) systems to 100 mM, significant changes in physical properties are observed. The mixture becomes highly viscous and shows recoiling of entrapped air bubbles. Upon equilibrating the SAIL/Additive mixtures for 24 h, transparent

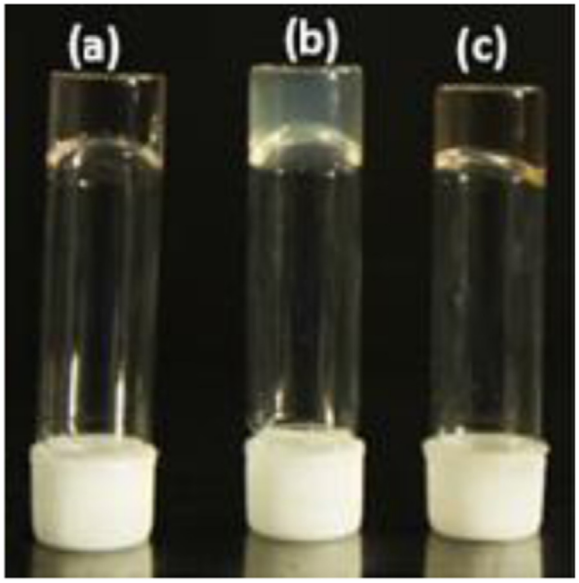

Fig. 4. Macroscopic appearance of viscoelastic gels of 100 mM 1:1 solutions of C_{16}-3-MeImCl and a) 1-Naphthol; b) 2-Naphthol and c) 2,3-DHN at 298 K.

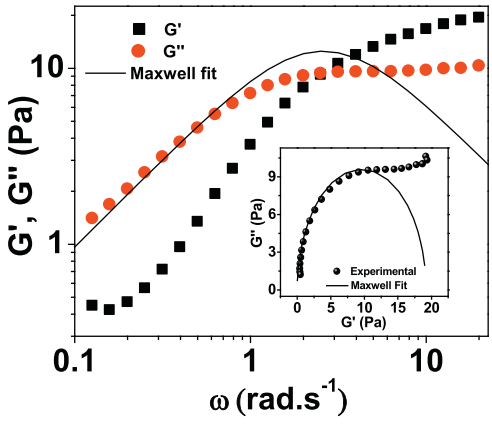

Fig. 5. Representative profile of dynamic rheology of C_{16}-3-MeImCl/1-Naphthol system (1:1, 100 mM) as function of angular frequency at 328 K.

gel is formed. The gels show arrested flow even after holding upside-down (Fig. 4).

The appearance of viscoelasticity suggests the presence of entangled wormlike micelles in the systems [32,33]. In order to understand the changes in physical characteristics, rheological study of the SAIL/Additive gels are carried out. The response of elastic and loss modulus as a function of angular frequency shows that the systems behave like typical viscoelastic fluid with loss modulus (G″) predominating at lower frequencies and elastic or storage modulus (Gí) predominating at higher frequencies [16]. A representative plot is shown in Fig. 5.

Upon increase in temperature, the crossover frequency increases (ω_c) i.e. the frequency at which Gí and G″ intersect (Fig. S3(a-c)). The inverse of ω_c gives the relataxion time (τ_R) which is the time required by the system to regain its equilibrium structure after an external stress is applied. With increase in temperature, τ_R decreases, implying that the systems adopt faster routes of stress-relaxation. The trend in relaxation time, show that SAIL/Additive composed of 2,3-DHN relaxes much slower followed by 1-Naphthol and 2-Naphthol respectively (Fig. S4). [34]

The dynamics of the viscoelastic micellar systems have been most successfully described by the Cate's "living polymer model" which is the combination of the reptation model of polymer dynamics and the effect of reversible scission on viscoelastic properties [35–37]. According to this model the relaxation of the viscoelastic micelles involves two time scales viz. reptation time (τ_{rep}) corresponding to curvilinear diffusion of a wormlike micellar chain along its own contour and breaking time(τ_b) which is the result of micellar chain scission. When $\tau_b \ll \tau_{rep}$, there occurs many breakages and recombination before the chain segment relaxes by reptation. The system is then defined by a single stress relaxation time,

$$\tau_R = (\tau_{rep} \times \tau_b)^{1/2} \quad (2)$$

and is characterized as a Maxwell Fluid.

For a fluid with near-Maxwell character, the elastic (or storage modulus), G′ and viscous (or loss modulus), G″ are related to angular frequency, ω as [36]

$$G'(\omega) = G_0\omega^2\tau_R^2 / \left(1 + \omega^2\tau_R^2\right) \quad (3)$$

$$G''(\omega) = G_0\omega\tau_R / \left(1 + \omega^2\tau_R^2\right) \quad (4)$$

where G_0 is the storage modulus at high frequency, where it exhibits a plateau, also called the plateau modulus. It is proportional to the number density of the entanglement points and hence characterizes the network structure [37]. (More details provided under Section 3.1 of SI)

The oscillatory flow spectra of all the SAIL/Additive systems could be fitted to the theoretical curve obtained on basis of Maxwell's model (Fig. 5). The semi-circular nature of Cole-Cole plot further proves that the system behaves as Maxwell fluid (Fig. 5 inset). Deviation of G″ from Maxwell model at higher ω indicates that the wormlike micelles are in dynamic equilibrium and the process of breaking and recombination takes place rapidly [38]. At this condition, the system adopts faster relaxation time given by Rouse or breathing modes. The characteristic parameters of the wormlike micellar network viz. the hydrodynamic correlation length, ξ, which is a measure of the network mesh size of the entangled micelles; the persistence length, l_p; entanglement length, l_e and average micellar length, L are related as-

$$\xi = \left(k_B \times T/G_0\right)^{1/3} \quad (5)$$

$$l_e = \xi^{\frac{5}{3}}/ \quad (6)$$

$$\frac{G_0}{G''_{min}} = \frac{L}{l_e} \quad (7)$$

where, k_B is Boltzman constant, T is the temperature, G''_{min} is the local minimum observed in G″ curve at frequency aboveω_c.

Assuming near Maxwell behavior for the systems [39] the micellar characteristics of the C_{16}-3-MeImCl/Additive (1:1, 100 mM) systems have been evaluated using the above relations and are presented in Table 3. From the values of τ_b and τ_{rep}, it is clear that $\tau_b \ll \tau_{rep}$, which further testifies the presence of single relaxation mode and hence wormlike micelles, in the systems. The reptation time, in case of C_{16}-3-MeImCl/2,3-DHN system is much higher, varying within 1316.6–2.65 s (approx. 10 order higher) compared to C_{16}-3-MeImCl/1-Naphthol (τ_{rep} = 111.03 – 0.34 s) and C_{16}-3-MeImCl/2-Naphthol (τ_{rep} = 48.87 – 3.99 s) with temperature (Table 3). Higher the time, slower is the process adopted by the system in order to relax. Results show that the system comprised of C_{16}-3-MeImCl/2,3-DHN undergoes slowest reptation. Slow relaxation is also associated with linearity of the micelles [35]. It can be said that C_{16}-3-MeImCl/2,3-DHN form longer micelles than C_{16}-3-MeImCl/1-Naphthol and C_{16}-3-MeImCl/2-Naphthol systems. From the severe drop in τ_{rep} with temperature in all the C_{16}-3-MeImCl/Additive systems, (Table 3) it is clear that temperature has profound effect on the relaxation mode of the systems. In order to

Table 3
Parameters G''_{min}, τ_R, τ_b, τ_{rep}, ξ, L as obtained from rheological data for C_{16}-3-MeImCl with 1-Naphthol, 2-Naphthol and 2,3-DHN as additive at different temperatures.

Temp K	G''_{min} Pa	τ_R s	τ_b s	τ_{rep} s	ξ x 10^6 m	L nm
1-Naphthol						
318	11.5	4.22	0.16	111.03	2.13	315–473
323	8.46	1.79	0.12	26.67	2.68	217–408
328	10.02	0.38	0.10	1.49	2.82	160–300
333	20.97	0.07	0.02	0.34	2.65	212–397
2-Naphthol						
318	4.63	4.39	0.395	48.87	3.23	225–422
323	11.74	0.83	0.079	8.67	2.91	123–230
328	24.90	0.28	0.040	1.97	2.98	202–379
330.5	5.71	0.19	0.063	0.60	3.05	224–42
333	1.46	2.01	1.010	3.99	3.49	590–1107
2,3-DHN						
323	12.46	8.03	0.049	1316.6	1.91	413–774
325.5	15.87	3.35	0.039	285.08	2.01	278–522
328	18.84	2.87	0.040	205.82	2.04	170–319
330.5	20.55	0.76	0.015	37.08	1.91	255–478
333	11.08	0.51	0.099	2.65	2.81	149–280

understand the temperature dependence of the wormlike micellar characteristics, oscillatory flow measurements as functions of various forms of stress at different temperatures are studied. The shear dependent flow-curves are extrapolated to zero shear rate to obtain the zero shear viscosity (Fig. S5(a–c)).

The samples exhibit a constant viscosity below a critical shear rate above which shear thinning is observed, which corresponds to the non-Newtonian flow behavior typical to wormlike micelle [37]. The critical shear rate, γ_c, shifts to lower values on increasing the temperature with corresponding increase in zero shear viscosity (η_0). η_0 becomes maximum at particular temperature specific to the additives (Fig. S5(a–c)). With further increase in temperature, η_0 decreases and the Newtonian region shifts forward i.e. γ_c, increased.

The molecular origin of the observed changes in viscoelastic behavior is the change in topology of the SAIL aggregates and shape of its micelles due to the presence of the hydroxy aromatic additives. The packing parameter, P [26] for spherical micelles <1/3 while that for elongated micelles is $\frac{1}{3}$ <P< $\frac{1}{2}$. P is a dimensionless fundamental parameter, which determines the shape of molecular aggregates. (Details provided under Section 3.2 of SI) At higher concentrations of the SAIL micelles and additives (100 mM, 1:1) the inter-micellar interaction between the components increases to a great extent. Since the local H-bonding network of water at the charged micellar interface differ much from that in the bulk, these water molecules are much less polar (dielectric constant ~30) with restricted mobility [20]. The aromatic ring of the Naphthols and 2,3-DHN embed in between the imidazolium head group of the SAIL micelles and impart strong screening effect on the electrostatic charges of the micellar head groups which reduces the electrostatic double layer around the micelle. The strong hydrogen bonding with the −OH group of the naphthol(s) and its derivatives with the interfacial water optimally orients the aromatic π-system of 1Naphthol, 2-Naphthol and 2,3-DHN perpendicularly for stronger screening of the electrostatic repulsion between the imidazolium headgroups via cation−π interaction [40]. This addition of Naphthol(s)/2,3-DHN into the micelles apparently decreases the effective area of the head groups causing an increase in A_0 and lowers the packing parameter. Thus, the globular micelles flip into cylindrical micelles with lower spontaneous curvature [41]. WLM are eventually formed because small cylindrical rods are thermodynamically unstable in aqueous media since their end-cap energy is higher compared to that of the body of the rods. Presence of the long WLM's on entanglement, impart the observed viscoelasticity in the medium. With rise in temperature, the tendency of the additives to get solubilized within the palisade layer of the SAIL micelles increases which further lowers the interfacial curvature of the molecular assembly. This leads to the formation of longer worms with corresponding increase in viscosity [42–44] (Fig. S6).

When a linear micelle breaks the energy penalty is compensated by formation of two new end caps. The increased curvature of an end cap which spreads the head groups apart is favored over the concave curvature of a branch point which drives the charged head groups of the surfactants closer together, resulting in formation of branches. The gain in entropy, with temperature, in the branch points is greater than in the end caps, which enables faster and easier route to stress relaxation by sliding of the branches alongside the cylindrical body of the wormlike micelles [32]. These branch points restrict the alignment of micelles when under shear and cause an increase in the critical shear rate while lowering the zero shear viscosity above the critical temperature. The observed critical temperature for the C_{16}-3-MeImCl/Additive systems are: 308 K for 1-Naphthol with η_0 674 Pa s, 313 K for 2-Naphthol with η_0 211 Pa s and 318 K for 2,3-DHN with η_0 1819 Pa s. Tendency of 2,3-DHN to embed within the micellar core is, therefore, higher compared to 1 and 2-Naphthol, which subsequently lead to corresponding highest increase in zero shear viscosity with temperature (Fig. S6).

The flow activation energy, (E_A) describes the end-cap energy required for reversible micellar scission and also, a measure of compactness of the WLM and is related to τ_R and temperature as [35],

$$\tau_R = A \times \exp\left(E_A/R \times T\right) \quad (8)$$

$$\text{or,} \quad \log \tau_R = \log A + (E_A/R \times T) \quad (9)$$

where A is the pre-exponential factor and is a constant, R is the universal gas constant taken as 8.314 J mol^{-1}. K^{-1} and T is the temperature. E_A is found to be 241.13, 218.20 and 249.61 kJ mol^{-1} for SAIL WLM in presence of 1-Naphthol, 2-Naphthol and 2,3-DHN respectively (Fig. S7). Above trend of E_A implies that the most compact assembly occurs in case of 2,3-DHN, which causes the "slowest" movement of the worms.

3.6. ^{1}H NMR study: the location of residence of the additive within SAIL micelles

Proton NMR (^{1}H NMR) spectroscopy is an important tool for identifying the time-averaged location of aromatic solubilized species within the surfactant micelles, based on the dependence of chemical shifts of protons in surfactant and aromatic units on the composition of the aqueous phase [45]. The present study is aimed to investigate the effect of addition of the naphthol additives on the protonic environment of C_{16}-3-MeImCl micelles. Fig. 6(a) shows the ^{1}H NMR spectra of 10 mM C_{16}-3-MeImCl in D_2O.

The concentration is much above the critical micellar concentration of C_{16}-3-MeImCl (0.89 mM), therefore it is assumed that the system consists of micelles of the ionic liquid. The spectra of C_{16}-3-MeImCl is similar to that of 10 mM CTAB. [49,50]. Here, the most downfield resonance at ppm 7.36 is due to the aromatic protons of the imidazolium ring (H2, H3 and H4) (Fig. 6(a)). The α protons (H5) of the alkyl chain are deshielded due the vicinity of the aromatic ring, and appear at 4.09 ppm. The intense signal at 3.77 ppm corresponds to the N-methyl protons (H1) attached to the imidazolium ring. The relatively less intense resonance at 1.75 ppm is due to the β protons (H6) whereas the γ protons (H7) appear as a hinge at 1.18 ppm. The signals for the intermediate methylene protons (H8-H19) merge together and appear as an intense signal at 1.12 ppm while the terminal methyl group (ω, H20) appear farthest upfield at 0.72 ppm. Fig. 6b depicts the spectra of the mixture of 10 mM C_{16}-3-MeImCl and 10 mM 1-Naphthol in D_2O with

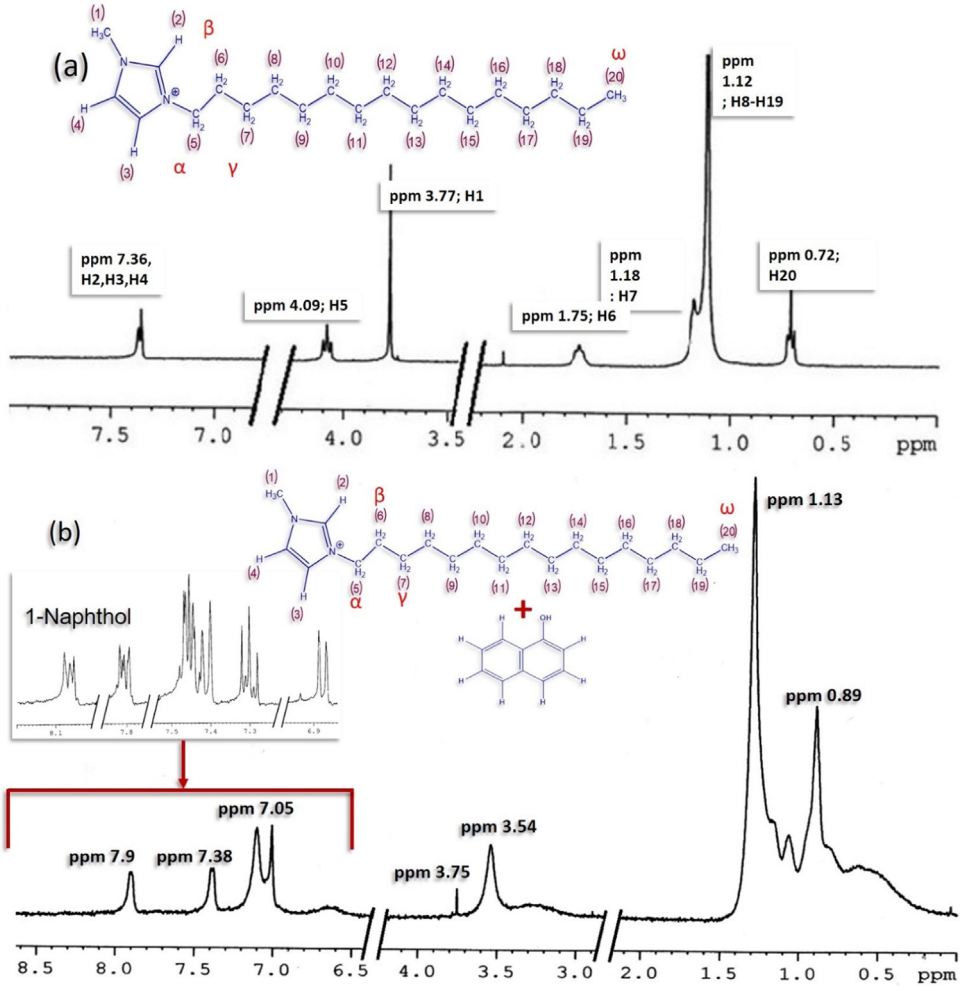

Fig. 6. a): ^{1}H NMR spectra of 10 mM C_{16}-3-MeImCl in D_2O at 25 °C; b) ^{1}H NMR spectra of mixture of 10 mM C_{16}-3-MeImCl and 10 mM 1-Naphthol in D_2O at 298 K.

the spectra of 1-Naphthol in D_2O in the inset. The aromatic protons of 1-Naphthols resonate in between 7.10 and 7.76 ppm (Inset) and appear highly splitted. It is evident that in the mixture, signals due to aromatic protons merge, broaden and appear upfield with three main signals (two singlet and one doublet) at 7.9, 7.38 and 7.05 ppm respectively. The large upfield shift of the resonances indicates that the protons are located in relatively non-polar environment compared to that in water [19,46]. The broadening of the peaks imply restricted motion of the naphthol molecules in the viscoelastic phase on the NMR time scale [19]. The α protons of the ionic liquid resonate highly upfield at 3.54 ppm while the *N*-methyl protons do not seem affected, resonating at 3.77 ppm.

The chemical shift in the terminal methyl group shows opposite trend, resonating at down field 0.89 ppm. Resonances due to β protons and the intermediate methylene groups merge to a single intense and broad peak at 1.13 ppm. The observed upfield shifts are supposedly induced by ring current of the aromatic ring of the naphthol [47,48]. The large shift of the α and β protons confirms that the aromatic part of the additives are intercalated in the outer micellar part [46,49]. Previously, study of ^{1}H NMR of CTAB micelles (10 mM) have shown that only the protons adjacent to the polar quaternary ammonium head groups of CTAB were affected and shifted upfield in presence of phenols (5 mM) while terminal methyl group and other methylene protons remains unaffected. The aromatic protons of phenols appeared upfield in presence of CTAB and so did the α and β protons of CTAB, hence it was concluded that the phenols reside at the vicinity of the micellar interface without affecting protons beyond γ position of the alkyl chain [49]. In the present study, a downfield shift of the resonance of terminal protons is observed in all the C_{16}-3-MeImCl/Additives systems (Figs. 6b and S8(a and b)). The broadening of peak near 1.13 and 0.89 ppm together with the respective upfield and downfield chemical shifts show that both intermediate and terminal protons are perturbed due to the presence of naphthol. This suggests an orientation of the naphthol ring between the alkyl chains such that the ring current affects the terminal protons as well (particularly by those naphthol moieties embedded near endcaps). Due to formation of cylindrical micelles, the alkyl chains of C_{16}-3-MeImCl move apart creating greater space for the spatial distribution of the terminal methyl groups which accounts for the observed downfield shift [50]. This difference in behavior from phenol, [49] is due to the presence of extended conjugation of the extra aromatic ring adding to the hydrophobicity of naphthols (and 2,3-DHN). The hydroxy-naphthalene derivatives have greater hydrophobic length compared to phenol which allows easier partitioning of the same within the alkyl chains. Similar observations were found with 2-Naphthol and 2,3-DHN as well (Fig. S8(a and b)).

3.7. Binding energy: DFT study

To further understand the differences in electrostatic interactions between the two components of each system viz., the

imidazolium head group of C_{16}-3-MeImCl and the naphthalene moiety of the additives, DFT calculations were done using Gaussian 09 package [65] with hybrid functional B3LYP using 6-31G (d, p) basis set. For technical limitation the hydrocarbon chain was truncated beyond C10 (since the electrostatic interactions considered are primarily between the surfactant head group and the aromatic ring of the additive). The calculated binding energies for the imidazolium moiety and the additive molecules was found to be -10.05 kcal mol^{-1}, -9.68 kcal mol^{-1} and -10.31 kcal mol^{-1} for 1-Naphthol, 2-Naphthol and 2,3-DHN respectively. The values indicate that 2,3-DHN bind to imidazolium head group more strongly followed by 1-Naphthol and 2-Naphthol i.e. the magnitude of electrostatic interaction with the ionic liquid is highest in case of 2,3-DHN and lowest in case of 2-Naphthol. It can be said that due to two hydroxy functionality, 2,3-DHN binds stronger with the head group of the ionic liquid compared to the mono-naphthols. This result corroborates the trend observed in the zero shear viscosity with temperature and the flow activation energy of the systems (Section 3.5). The difference in magnitude arises from the fact that though all the additives have identical aromatic backbone, they differ in the electrostatic surface potential owing to position of the hydroxy functionality, (Fig. S9) which plays major role in stability of the imidazolium-hydroxy aromatic moieties. The present study gives an overview of the extent of interaction between the imidazolium head group and the additive moiety in terms of binding energy.

3.8. *Application: metal ion tolerance of SAIL-π-conjugated additive systems – improved viscous characteristics in presence of metal ion impurities*

Hydraulic fracturing is a method of using pump rate and hydraulic pressure to fracture or crack a subterranean formation in a process for enhancing the recovery of hydrocarbons from the formation. Recently it has been shown that aqueous drilling and treating fluids may be gelled or have their viscosity increased by the use of non-polymeric viscoelastic WLM. These materials are advantageous in many ways over the use of the conventional polymer gelling agents in that they do not leave a filter cake on the formation face, do not coat the proppant or create microgels [51–55]. Since electrostatic interaction plays major role in partitioning Sodium salicylate (NaSal) in cationic micelles, such process is not favorable in absence of electrolyte or high salinity because of charge screening of head groups. Moreover, salicylate forms stable complexes with such metal ions which are present in rock environment [56]. The salicylate moiety acts as an active bidentate donor ligand to form chelates with many heavy and transition metal ions. Its efficiency as the fractured fluid in presence of salinity and the metal salts is thus highly compromised. The Naphthols, (including 2,3-DHN), are a new class of promoters which may act under salt free condition. The study of their effectiveness in presence of metal ions is, therefore, of considerable interest in order to address the limitation of NaSal as the WLM triggering agent. In this connection, wormlike micellar solutions of C_{16}-3-MeImCl and 1-Naphthol were prepared in presence of metal salts and the viscosities at steady shear rate of 304 s^{-1}, were measured. All the metal ions are employed as chloride salts, in order to ensure identical effect of anions, if any, on the rheology of the system and also due to the fact that impact of chloride ions on the microstructural transition of surfactant micelles is, in general, small [57]. For the purpose of comparison, similar study is done in the SAIL/NaSal system. The viscosity profiles as a function of metal concentrations are shown in Fig. 7.

The addition of transition metal salts progressively decreases the viscosity of the SAIL/NaSal system which is indeed significant (Fig. 7(a)). The extent of the lowering of viscosity as a function of metal ion follows the order: $ZnCl_2 < CoCl_2 < NiCl_2 < CuCl_2$. This can be explained in light of degree of complex forming tendency of NaSal with metal ions in aqueous solutions. The trend follows the Mellor and Maley series of stability of metal complexes [58]. The fact that viscosities are highly reduced (maximum reduction in viscosity encountered from ~7.0 cP to ~3.5 cP, Fig. 7(a)) which also implies that although addition of metal salts increases Cl^- counter ion in the system, counter ion binding, if any, could not ultimately enhance micellar growth. It seems apparent that unavailability of free salicylate ions in presence of metal, for promoting microstructural transition of spherical micelle to WLM becomes key factor in reducing viscosity and augmenting effect, if any, of counter ion condensation is trounced.

The diminishing charge density on the head groups in presence of counter ions reduces the electrostatic interaction between micelles and salicylate ions causing later to remain in the vicinity of the interface only. This further stabilizes the spherical micelles and lowers the viscosity. Therefore, the effect of alkali metal salts is not surprising. Alkali metal salts have been known to induce micellar growth and conspicuous effect of anions on charge screening is reported earlier [59]. The alkali metal ions cannot form complex with salicylate, yet the drop of viscosity as a function of salt concentration is found for all the salts (Fig. 7(b)) in the present study. In the present system, anions lower the viscosity in a trend: $Cl^- < Br^- < SO_4^{2-}$. It seems apparent that same reason is invoked here also. Effect of confiscating salicylate ion by Cl^- prevails over the effect of counter ion binding on sphere-to-rod transition. Recently, in studying the effect of anions on rheology of WLM of Cetyltrimethylammonium salicyalate (CTASal) system, it is also shown that the anions decrease the relaxation time of the systems [60,61]. However, Chloride counter ions of C_{16}-3-MeImCl are reported to participate in hydrogen bonding with the solvent H_2O molecules as well as with the imidazolium head group [61–64]. Therefore, it can be said that the condensation of counter ions

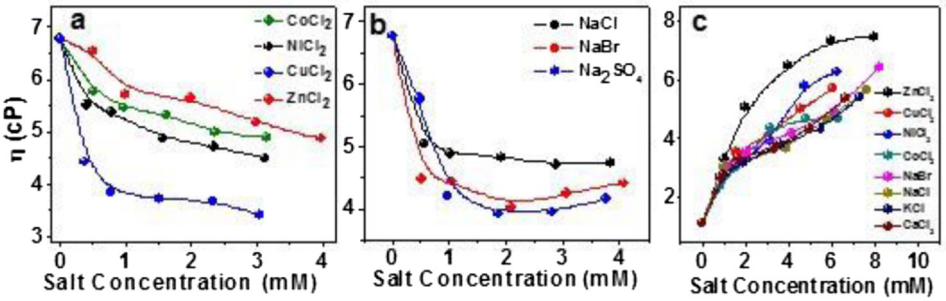

Fig. 7. a) Viscosity of C_{16}-3-MeImCl (5 mM)-NaSal(3.5 mM) system as a function of metal ion concentration at 303 K and 304 s^{-1}. (b) Viscosity of C_{16}-3-MeImCl(5 mM)/NaSal(3.5 mM) system as a function of anion concentration at 303 K and 304 s^{-1}. (c) Viscosity of C_{16}-3-MeImCl/1-Naphthol (1:1, 7.5 mM) system as a function of metal salt concentration at 303 K and 304 s^{-1} shear rate.

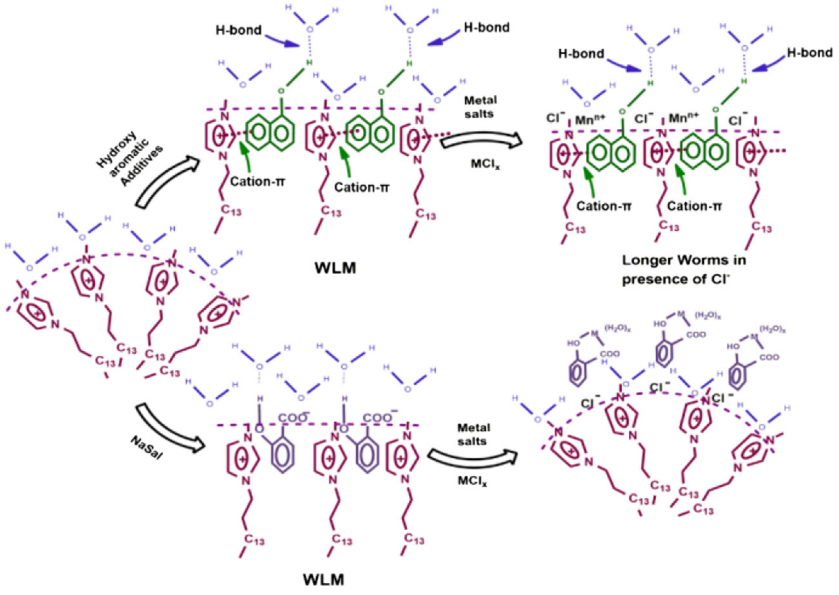

Fig. 8. Schemetic representation of possible microstructural changes in aqueous SAIL/Additive (1-Naphthol) solutions and SAIL/NaSal, on addition of metal salts and the underlying forces.

from the added alkali metal salts, on the WLM surface following the order $Cl^- < Br^- < SO_4^{2-}$ leads to the corresponding decrease in viscosity.

On the other hand, it is indeed interesting to note that in the present study, the viscosities of C_{16}-3-MeImCl/1-Naphthol system increases considerably with the increase in metal salt concentration. The nature of interaction in this system is probably H-bonding and cation-π interaction along with hydrophobic forces. Therefore, counter ion cannot remove 1-Naphthol from micellar phase. Further, 1-Naphthol, being a non-chelating agent promoter, does not interfere with the metal ions and the linear morphology of the micelles is maintained (Fig. 7(c)). A schematic representation of the possible molecular interactions is given in Fig. 8.

However the reason underlying the increase in viscosity is not entirely apparent although it can be understood, from the above discussion, that counter ion binding is definitely involved in micellar growth in the present system. Nevertheless, the situation is indeed complex in nature. The effectiveness of counter ion binding is dependent on a number of factors from the tendency of ion-pair formation for alkali metal salt solutions to the ease of formation of aquo-complex formation in transition metals. The observed trend in viscosity enhancement (Fig. 7(c)) is the result of a number of such multiple factors. However, it is clear that, the efficiency of Naphthols as viscoelasiticity inducer is not compromised by the presence of metal impurities and salinity and unlike NaSal it enhances and could be a potential agent to replace NaSal as fractured fluid for oil recovery.

4. Conclusion

Strong synergism is observed between the surface active ionic liquid, 1-Hexadecyl-3-methylimidazolium chloride and the π-conjugated additives viz., 1-Naphthol, 2-Naphthol and 2,3-Dihydroxynaphthalene, in improving the surface and bulk properties of the system Significant attractive interaction exist between π-electron clouds of the additives and charged imidazolium head groups via cation-π interaction. Fluorescence anisotropy study suggests partitioning of the additives within the SAIL micelles while UV–vis and ^{1}H NMR study support the positioning of the additives at the palisade layer of the micelles and their involvement in hydrogen bonding with interfacial water molecules. The dynamic oscillatory flow measurements confirm the formation of viscoelastic wormlike micelles while flow activation energy supports the efficiency of the π conjugated aromatic additives in triggering wormlike micelles in the order 2-Naphthol < 1-Naphthol < 2,3-Dihydroxynaphthalene. The viscoelasicity of the SAIL/Additive systems is tuneable by temperature as the systems respond to a critical temperature with highest zero shear viscosity, above which they relax faster forming branched micelles. Results of DFT study show that 2,3-DHN has maximum binding energy followed by 1-Naphthol and 2-Naphthol to the imidazolium moiety. Moreover, the systems are found to be metal tolerant. The viscosity of the present system is found to increase in the presence of metal salts. This observation promises potentiality of the system in enhanced oil recovery as fractured fluids in the presence of metal ion impurities. This study reports, fine-tuning of the temperature sensitive wormlike micelles developed under the salt-free condition which has huge prospects as usage in storage and carriage media of suitable drugs.

Acknowledgements

We thank Science & Engineering Research Board (SERB), DST, Govt. of India (SanctionNo.SB/S1/PC-034/2013) for financial assistance. GC thanks University Grants Commission for Basic Scientific Research (UGC-BSR) Fellowship.

Appendix A. Supplementary data

Supplementary data associated with this article can be found, in the online version, at http://dx.doi.org/10.1016/j.colsurfa.2016.12.025.

References

[1] M. Freemantle, Designer solvents Ionic liquids may boost clean technology development, Chem. Eng. News 76 (13) (1998) 32–37.
[2] R. Sheldon, Catalytic reactions in ionic liquids, Chem. Commun. 23 (2001) 2399–2407.

[3] H. Rehage, H. Hoffmann, Rheological properties of viscoelastic surfactant systems, J. Phys. Chem. 92 (16) (1988) 4712–4719.
[4] Y. Kim, P. Dalhaimer, D.A. Christian, D.E. Discher, Polymeric worm micelles as nano-carriers for drug delivery, Nanotechnology 16 (2005) S484–S491.
[5] D.A. Christian, S. Cai, O.B. Garbuzenko, T. Harada, A.L. Zajac, T. Minko, D.E. Discher, Flexible filaments for in vivo imaging and delivery: persistent circulation of filomicelles opens the dosage window for sustained tumor shrinkage, Mol. Pharm. 6 (5) (2009) 1343–1352.
[6] K. Kataoka, A. Harada, Y. Nagasaki, Block copolymer micelles for drug delivery: design, characterization and biological significance, Adv. Drug Deliv. Rev. 47 (1) (2001) 113–131.
[7] O.A.El. Seoud, P.D. Galgano, Micellar properties of surface active ionic liquids: a comparison of 1-hexadecyl-3-methylimidazolium chloride with structurally related cationic surfactants, J. Colloid Interface Sci. 345 (1) (2010) 1–11.
[8] A. Modaressi, H. Sifaoui, M. Mielcarz, U. Domanska, M. Rogalski, Influence of the molecular structure on the aggregation of imidazolium ionic liquids in aqueous solutions, Colloids Surf. A: Physicochem. Eng. Aspects 302 (2007) 181–185.
[9] T. Asakawa, H. Hisamatsu, S. Miyagishi, Experimental verification of demixing micelles composed of fluorocarbon and hydrocarbon surfactants via the fluorescence-quenching method, Langmuir 12 (5) (1996) 1204–1207.
[10] R.H. Clapperton, A study of fluorocarbon–hydrocarbon surface active agent mixtures by NMR spectroscopy, Langmuir 10 (1) (1994) 51–56.
[11] M.B. Ghoulam, N. Moatadid, A. Graciaa, G. Marion, J. Lachaise, Hydrocarbon/fluorocarbon mixed micelle diagram from surface tensiometry, Langmuir 12 (21) (1996) 5048–5051.
[12] S.R. Raghavan, G. Fritz, E.W. Kaler, Wormlike micelles formed by synergistic self-assembly in mixtures of anionic and cationic surfactants, Langmuir 18 (10) (2002) 3797–3803.
[13] E.W. Kaler, K.L. Herrington, A.K. Murthy, J.A.N. Zasadzinski, Phase behavior and structures of mixtures of anionic and cationic surfactants, J. Phys. Chem. 96 (16) (1992) 6698–6707.
[14] R.D. Koehler, S.R. Raghavan, E.W. Kaler, Microstructure and dynamics of wormlike micellar solutions formed by mixing cationic and anionic surfactants, J. Phys. Chem. B 104 (47) (2000) 11035–11044.
[15] D. Grabner, L. Zhai, Y. Talmon, J. Schmidt, N. Freiberger, O. Glatter, B. Herzog, H. Hoffmann, Phase behavior of aqueous mixtures of 2-Phenylbenzimidazole-5-sulfonic acid and cetyltrimethylammonium bromide: hydrogels, vesicles, tubules, and ribbons, J. Phys. Chem. B 112 (10) (2008) 2901–2908.
[16] L. Wattebled, A. Laschewsky, Effects of organic salt additives on the behavior of dimeric (Gemini) surfactants in aqueous solution, Langmuir 23 (20) (2007) 10044–10052.
[17] Y. Lin, Y. Qiao, Y. Yan, J. Huang, Thermo-responsive viscoelastic wormlike micelle to elastic hydrogel transition in dual-component systems, Soft Matter 5 (16) (2009) 3047–3053.
[18] Q. You, Y. Zhang, H. Wang, H. Fan, J. Guo, M. Li, The formation of pH-SensitiveWormlike micelles in ionic liquids driven by the binding ability of anthranilic acid, Int. J. Mol. Sci. 16 (12) (2015) 28146–28155.
[19] S.K. Saha, M. Jha, M. Ali, A. Chakraborty, G. Bit, S.K. Das, Micellar shape transition under dilute salt-free conditions: promotion and self-fluorescence monitoring of stimuli-responsive viscoelasticity by 1- and 2-s, J. Phys. Chem. B 112 (15) (2008) 4642–4647.
[20] M. Ali, M. Jha, S.K. Das, S.K. Saha, Hydrogen-bond-induced microstructural transition of ionic micelles in the presence of neutral s: pH dependent morphology and location of surface activity, J. Phys. Chem. B 113 (47) (2009) 15563–15571.
[21] J. Lackowicz, Fluorescence anisotropy, in: Principles of Fluorescence Spectroscopy, Springer, 2006, pp. 353–381.
[22] S.H. Tung, Y.E. Huang, S.R. Raghavan, Contrasting effects of temperature on the rheology of normal and reverse wormlike micelles, Langmuir 23 (2) (2007) 372–376.
[23] M. Bergström, J.C. Eriksson, Theoretical analysis of synergistic effects in mixed surfactant systems, Langmuir 16 (18) (2000) 7173–7181.
[24] D.N. Rubingh, Mixed micelle solutions, in: Solution Chemistry of Surfactants, Springer, 1979, pp. 337–354.
[25] M.J. Rosen, Molecular interactions and synergism in mixtures of two surfactants, in: Surfactants and Interfacial Phenomena, John Wiley, 2004, pp. 379–414.
[26] J.H. Clint, Mixed-micelle formation, in: Surfactant Aggregation, Springer, 1992, pp. 130–146.
[27] I.A. Khan, A.J. Khanam, Z.A. Khan, Kabir-ud-Din, Mixing behavior of anionic hydrotropes with cationic gemini surfactants, J. Chem. Eng. Data 55 (11) (2010) 4775–4779.
[28] W.R. Laws, L. Brand, Analysis of two-state excited-state reactions. The fluorescence decay of 2-naphthol, J. Phys. Chem. 83 (7) (1979) 795–802.
[29] S. Erkki, H. Ilkka, Fluorescence spectroscopy assay means with fluorescent chelate of a lanthanide, US 4374120 A.
[30] D. Mandal, S.K. Pal, K. Bhattacharyya, Excited-State proton transfer of 1-naphthol in micelles, J. Phys. Chem. A 102 (48) (1998) 9710–9714.
[31] J.J. Yan, R.P. Tang, B. Zhang, X.Q. Zhu, F. Xi, Z.C. Li, E.Q. Chen, Gelation originated from growth of wormlike living polymer of symmetrically dendronized large-ring crown ether in dilute solutions, Macromolecules 42 (21) (2009) 8451–8459.
[32] R. Grenek, M.E. Cates, Stress relaxation in living polymers: results from a Poisson renewal model, J. Chem. Phys. 96 (6) (1992) 4758–4767.
[33] E. Sabadini, R.F.S. Ungarato, P.B. Miranda, The elasticity of soap bubbles containing wormlike micelles, Langmuir 0 (3) (2014) 727–732.
[34] A. Parker, W. Fieber, Viscoelasticity of anionic wormlike micelles: effects of ionic strength and small hydrophobic molecules, Soft Matter 9 (2013) 1202–1213.
[35] M.E. Cates, S.J. Candau, Statics and dynamics of wormlike surfactant micelles, J. Phys. Condens. Matter 2 (1990) 6869–6892.
[36] D.L. Diaz, R. Castillo, The wormlike micellar solution made of a zwitterionic surfactant (TDPS), an anionic surfactant (SDS), and brine in the semidilute regime, J. Phys. Chem. B 114 (27) (2010) 8917–8925.
[37] R.G. Shrestha, L. Abezguaz, D. Danino, K. Sakai, H. Sakai, M. Abe, Structure and dynamics of poly(oxyethylene) cholesteryl ether wormlike micelles: rheometry, SAXS, and Cryo-TEM studies, Langmuir 27 (21) (2011) 12877–12883.
[38] F. Kern, F. Lequeux, R. Zana, S.J. Candau, Dynamical properties of salt-free viscoelastic micellar solutions, Langmuir 10 (6) (1994) 1714–1723.
[39] M.E. Cates, Reptation of living polymers: dynamics of entangled polymers in the presence of reversible chain-scission reactions, Macromolecules 20 (9) (1987) 2289–2296.
[40] D. Chinedu, V.B. Umeasiegbu, R. Krishnamoorti, pH-induced re-entrant microstructural transitions in cationic surfactant-hydrotrope mixtures, Langmuir 32 (3) (2016) 655–663.
[41] C.A. Dreiss, Wormlike micelles: where do we stand? Recent developments, linear rheology and scattering techniques, Soft Matter 3 (8) (2007) 956–970.
[42] M. In, G.G. Warr, R. Zana, Dynamics of branched threadlike micelles, Phys. Rev. Lett. 83 (11) (1999) 2278–2281.
[43] P.A. Hassan, S.R. Raghavan, E. Kaler, Microstructural changes in SDS micelles induced by hydrotropic salt, Langmuir 18 (7) (2002) 2543–2548.
[44] J. Gasjo, E. Anderson, J. Forsbeing, E.F. Aziz, B. Brena, C. Johansson, J. Nordgren, L. Duda, J. Adersson, F. Hennies, J. Rubensson, P. Hansson, Electronic structure of water molecules confined in a micelle lattice, J. Phys. Chem. B 113 (24) (2009) 8201–8205.
[45] L.A. Bernardez, Investigation on the locus of solubilization of polycyclic aromatic hydrocarbons in non-ionic surfactant micelles with ^{1}H NMR spectroscopy, Colloids Surf. 324 (1–3) (2008) 71–78.
[46] U.R.K. Rao, C. Manohar, B.S. Valaulikar, R.M. Iyer, Micellar chain model for the origin of the visoelasticity in dilute surfactant solutions, J. Phys. Chem. 91 (12) (1987) 3286–3291.
[47] J.P. Mata, V.K. Aswal, P.A. Hassan, P. Bahadur, A phenol-induced structural transition in aqueous cetyltrimethylammonium bromide solution, J. Colloid Interface Sci. 299 (2) (2006) 910–915.
[48] K. Xu, H.Q. Ren, G.M. Zeng, L.L. Ding, J.H. Huang, Investigation of interaction between phenol and cetylpyridinium chloride micelle in the absence and in the presence of electrolyte by ^{1}H NMR spectroscopy, Colloids Surf. A 356 (1–3) (2010) 150–155.
[49] P. Sabatino, A. Szczygiel, D. Sinnaeve, M. Hakimhashemi, H. Saveyn, J.C. Martins, P.V. Meeren, NMR study of the influence of pH on phenol sorption in cationic CTAB micellar solutions, Colloids Surf. A: Physicochem. Eng. Aspects 370 (1–3) (2010) 42–48.
[50] R. Chaghi, L.C. de Menorval, C. Charnay, G. Derrien, J. Zajac, Interactions of phenol with cationic micelles of hexadecyltrimethylammonium bromide studied by titration calorimetry, conductimetry, and ^{1}H NMR in the range of low additive and surfactant concentrations, J. Colloid Interface Sci. 326 (1) (2008) 227–234.
[51] Y. Jhing, Viscoelastic wormlike micelles and their applications, Curr. Opin. Colloid Interface 7 (5–6) (2002) 276–281.
[52] A.Z. Abidin, T. Puspasari, W.A. Nugroho, Polymers for enhanced oil recovery technology, Procedia Chem. 4 (2012) 11–16.
[53] D. Hourdet, G. Ducouret, S. Varghese, M.V. Badiger, P.P. Wadgaonkar, Thermodynamic behavior of hydrophobically modified polyacrylamide containing random distribution of hydrophobes: experimental and theoretical investigations, Polymer 54 (11) (2013) 2676–2689.
[54] D.A.Z. Wever, F. Picchioni, A.A. Broekhuis, Polymers for enhanced oil recovery: a paradigm for structure–property relationship in aqueous solution, Prog. Polym. Sci. 36 (11) (2011) 1558–1628.
[55] Z. Zhao, T. Liu, P. Luo, Y. Li, J. Liu, J. Cheng, Y. Yu, Performance and field implementation of a new fracturing fluid consisting of hydrophobically associating polyacrylamide and anionic surfactant, J. Polym. Eng. 36 (1) (2016) 13–21.
[56] V.M. Egorov, D.I. Djigailo, D.S. Momotenko, D.V. Chernyshov, I.I. Torocheshnikova, S.V. Smirnova, I.V. Pletnev, Task-specific ionic liquid trioctylmethylammonium salicylate as extraction solvent for transition metal ions, Talanta 80 (3) (2010) 1177–1182.
[57] L. Abezgauz, K. Kuperkar, P.A. Hassan, O. Ramon, P. Bahadur, D. Danino, Effect of Hofmeister anions on micellization and micellar growth of the surfactant cetylpyridinium chloride, J. Colloid Interface Sci. 342 (1) (2010) 83–92.
[58] D.P. Mellor, L. Maley, Order of stability of metal complexes, Nature 161 (1948) 436–437.
[59] S.C. Flores, J. Kherb, N. Konelick, X. Chen, P.S. Cremer, The effects of hofmeister cations at negatively charged hydrophilic surfaces, J. Phys. Chem. C 116 (9) (2012) 5730–5734.
[60] M.I. Alkschbirs, A.M. Percebom, W. Loh, H.W. Junior, M.B. Cardoso, E. Sabadini, Effects of some anions of the Hofmeister series on the rheology of cetyltrimethylammonium-salicylate wormlike micelles, Colloids Surf. A: Physicochem. Eng. Aspects 470 (2015) 1–7.

[61] R. Angelico, S. Amin, M. Monduzzi, S. Murgia, U. Olssone, G. Palazzo, Impact of branching on the viscoelasticity of worm like reverse micelles, Soft Matter 8 (42) (2012) 10941–10949.
[62] L. Cammarata, S.G. Kazarian, P.A. Salter, T. Welton, Molecular states of water in room temperature ionic liquids, Phys. Chem. Chem. Phys. 3 (23) (2001) 5192–5200.
[63] G. Zhang, X. Chen, Y. Zhao, Y. Xie, H. Qiu, Effects of alcohols and counterions on the phase behavior of 1-Octyl-3-methylimidazolium chloride aqueous solution, J. Phys. Chem. B 111 (40) (2007) 11708–11713.
[64] A. Downard, M.J. Earle, C. Hardacre, S.E.J. McMath, M. Nieuwenhuyzen, S.J. Teat, Structural studies of crystalline 1-Alkyl-3-Methylimidazolium chloride salts, Chem. Mater. 16 (1) (2004) 43–48.
[65] M.J. Frisch, G.W. Trucks, H.B. Schlegel, G.E. Scuseria, M.A. Robb, J.R. Cheeseman, G. Scalmani, V. Barone, B. Mennucci, G.A. Petersson, H. Nakatsuji, M. Caricato, X. Li, H.P. Hratchian, A.F. Izmaylov, J. Bloino, G. Zheng, J.L. Sonnenberg, M. Hada, M. Ehara, K. Toyota, R. Fukuda, J. Hasegawa, M. Ishida, T. Nakajima, Y. Honda, O. Kitao, H. Nakai, T. Vreven, J.A. Montgomery Jr., J.E. Peralta, F. Ogliaro, M. Bearpark, J.J. Heyd, E. Brothers, K.N. Kudin, V.N. Staroverov, R. Kobayashi, J. Normand, K. Raghavachari, A. Rendell, J.C. Burant, S.S. Iyengar, J. Tomasi, M. Cossi, N. Rega, J.M. Millam, M. Klene, J.E. Knox, J.B. Cross, V. Bakken, C. Adamo, J. Jaramillo, R. Gomperts, R.E. Stratmann, O. Yazyev, A.J. Austin, R. Cammi, C. Pomelli, J.W. Ochterski, R.L. Martin, K. Morokuma, V.G. Zakrzewski, G.A. Voth, P. Salvador, J.J. Dannenberg, S. Dapprich, A.D. Daniels, Ö. Farkas, J.B. Foresman, J.V. Ortiz, J. Cioslowski, D.J. Fox, Gaussian 09, Gaussian, Inc., Wallingford, CT, 2009.

LANGMUIR

Article

pubs.acs.org/Langmuir

Solvent-Induced Molecular Folding and Self-Assembled Nanostructures of Tyrosine and Tryptophan Analogues in Aqueous Solution: Fascinating Morphology of High Order

Gulmi Chakraborty, Madhurima Paul Chowdhury, and Swapan K. Saha*

Department of Chemistry, University of North Bengal, Darjeeling 734 013, India

Supporting Information

ABSTRACT: Hydrophobic derivatives of tyrosine and tryptophan, viz. octyl and dodecyl esters of tyrosine and octyl ester of tryptophan, are synthesized, and the interfacial and bulk properties in aqueous media are investigated as models for the membrane proteins. Molecular modeling by the density functional theory method is carried out to understand the molecular conformation and geometry for the purpose of determining the packing parameters. Water-induced molecular folding of the esters of both tyrosine and tryptophan, as observed using rotating frame nuclear Overhauser effect spectroscopy, indicates that the segregation of the hydrophobic and hydrophilic blocks in water is the key to the development of fascinating interfacial property displayed by the aromatic amino acid esters. The unusually high-order morphology of the aggregates, as observed using high-resolution transmission electron microscopy, is highly uncommon for single-chain amphiphiles and points to the fact that the self-assembly behavior of the present systems resembles that of block copolymers. The study of the growth of mesosized hollow aggregates with internal bilayer structures from tyrosine and tryptophan-based model systems would add to the understanding of biochemistry and biotechnology relevant to the cell membrane. The potential of biocompatible nanostructured motifs as the drug carriers is discussed. The highly functional role played by the aromatic amino acids at the membrane−water interface will be considered with the present amphiphilic models for future perspective.

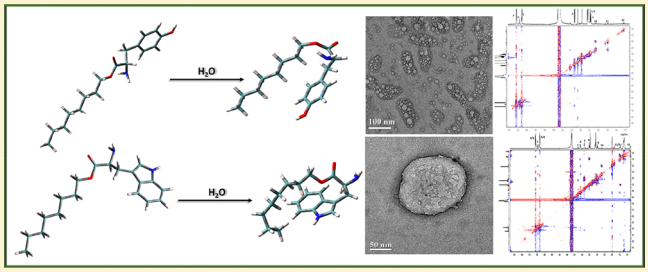

1. INTRODUCTION

The environmental concern for the widespread use of a large number of surfactant classes, including those of linear alkylbenzene sulfonates, alkylphenol ethoxylates, and dialkyl quats, has led to legislation in many countries with the aim of gradually phasing out these materials from commercial and industrial scenarios.[1−3] The apprehension is not only due to poor biodegradability under anaerobic conditions, concerning the use of anaerobically stabilized sewage sludge as fertilizers in agriculture, but also due to strong inhibitory effects of some of the above surfactant classes on the metabolic activity of autotrophic ammonia-oxidizing bacteria with respect to the nitrogen cycling reaction in soil and water.[4,5] As a result, there is a trend throughout the world to produce more environmentally benign surfactants, although so far, only limited success has been achieved to produce the so-called green surfactants for industrial purposes at affordable prices. The strategy for preparing environment-friendly surfactant molecules could be to start with the biologically active molecules, viz. amino acids or vegetable oil derivatives.[1,6] The end products of these chemical processes will form an interesting domain of natural, surface active biomolecules and create interests not only to chemists and biologists but also to environmentalists .[7−13] These compounds would naturally find a large number of basic and industrial applications too. Because the precursor amino acid molecules have biocompatible properties and a large variety of chemical functionalities, the surfactant molecules containing the amino acids in their molecular architecture would retain the same remarkable properties. Notwithstanding the prevailing situation, the amino acid-based new surfactants would be water-soluble, biodegradable, nontoxic, and chiral, with little or no adverse impact on soil and aquatic environment.[5,6,14−16] All of these properties ensure their eventual development to cater the need in food, pharmaceutical, and cosmetic sectors, which are the major users of various surfactant classes. However, in spite of the optimism that has been raised in the development of amino acid-based surfactants, the volume of industrial production is still meagre. Further, surprisingly, one of the very important amino acid class, viz. aromatic amino acids, has not been focused for preparing amino acid-based surfactant systems. Therefore, it would indeed be prudent to explore the possibility of surface-active properties of long-chain derivatives of aromatic amino acids, especially those of tryptophan and tyrosine, to apply these materials as environment-friendly surfactants. This, quite naturally, would not be confined to spherical aggregates and their uses concerning laundry detergent only, and rather, the applications of biocompatible and environment-gentle

Received: May 17, 2017
Revised: June 8, 2017
Published: June 9, 2017

DOI: 10.1021/acs.langmuir.7b01651
Langmuir 2017, 33, 6581−6594

surfactants would be quite diverse. The increasing need for drug-delivery systems that improve specificity and activity and at the same time reduce toxicity to ensure maximum treatment safety has led to the development of a great variety of drug vector formation. Since the first reported nonionic surfactant vesicles (ninosomes) nearly 3 decades ago, there have been a number of studies on ninosomes as potential drug carriers, principally focusing on the absence of electrostatic driving force in such systems to create any undesirable secondary interaction interface.[17] The combination of polar aromatic amino acids and nonpolar long chain compounds (esters of tyrosine and tryptophan) might lead to the association into vesicles on hydration as a result of the existence of high interfacial tension between water and the hydrocarbon portion of the amphiphile. Therefore, the high promises that are expected to be created for these supramolecular assemblies, if they are formed in amino acid-based systems, would translate into the demand for advanced highly functionalized drug-delivery materials having bio-origin.

Another highly challenging fact pertinent to aromatic amino acid-based surfactants, however, prompts from their biological relevance and strongly functional roles played by aromatic amino acids in transmembrane proteins at the membrane interface. Biological membranes are complex assemblies of lipids and proteins in which phospholipids form the major building blocks. The components of supreme importance in cell membranes are various types of proteins that are associated with the lipid bilayer to form functional membranes and perform different important tasks inculcated by the cell. Some of these crucial proteins are transmembrane proteins, anchored proteins, or peripheral proteins. The transmembrane proteins, viz. α-helical bundles and β-barrel proteins, localize aromatic amino acids (especially tyrosine, tryptophan, and histidine) at the membrane/water interface where they form functionally significant hydrogen bonds (H-bonds) with interfacial water.[18−23]

The discrimination between the nonpolar interior and the polar exterior of the lipid bilayer is made by the transmembrane proteins via the typical hydrophobic and hydrophilic domains that are present in their molecular architecture. The hydrophobic region, which contains a stretch of 20−25 hydrophobic and/or uncharged amino acids, spans the membrane bilayer. The hydrophilic region, on the other hand, is exposed to one or both sides of the membrane and contains hydrophilic amino acids, including amino acid vesicles. The interplay between the hydrophobic and hydrophilic forces in the membrane proteins is the key to the function and activity of these protein molecules that typically resemble conventional surfactants or amphiphilic molecules in this respect. Although the amphiphilic behavior of the membrane proteins is indeed significant, it is difficult, if not impossible, to study in situ because of the inherent complexity of the membrane systems. Long-chain alkyl esters of aromatic amino acids, especially those of tyrosine and tryptophan, could be good models of membrane proteins, and a few studies on the fluorescence behavior of such a model system, viz. tryptophan octyl ester, are reported in the literature.[24−29] However, no scientific report of such model systems involving tyrosine or other aromatic amino acids is available. In spite of their importance, the surface active property of the model systems has not been reported. Therefore, the initial motivation is to consider the surface activities of long-chain esters of tyrosine and tryptophan and to study the behavior of the aromatic π systems at the interface. It is indeed a fact that these materials are not easily available at present, not even from well-known chemical manufacturers. This may be one of the reasons for the lack of interest shown to these model systems. In the present paper, we have reported the method for the synthesis of octyl esters of tyrosine and tryptophan residues and dodecyl ester of tyrosine and investigated a detailed aspect of the surface activity and the related phenomena, including their conformations, molecular interactions in the aqueous medium, aggregation behavior, and morphology of the self-assembled nanostructures of the aggregates.

2. MATERIALS AND METHODS

2.1. Materials. L-Tyrosineoctyl ester (TYOE), L-tyrosinedodecyl ester (TYDE), and L-tryptophanoctyl ester (TROE) were synthesized in our laboratory according to Scheme 1. L-Tyrosine and L-tryptophan were purchased from HiMedia (India). $SOCl_2$ and *n*-dodecanol were purchased from Aldrich (USA). *n*-Octanol was purchased from Lancaster (England). Pyrene was purchased from Fluka (Switzerland) and purified before use via column chromatography using hexane as the eluent. Hexane was purchased from SDFCL (India); NaCl, NaOH, and Na_2SO_4, for synthesis, were purchased from Merck (India). The purity of all chemicals was greater than 99%, and they were used as received (except pyrene). All experiments were done with deionized and doubly distilled water with pH 6.5−7 and specific conductance below 2 $\mu S \cdot cm^{-1}$.

2.2. Methods. *2.2.1. Tensiometry.* Tensiometric measurements were recorded on a Krüss K9 tensiometer (Germany), based on the Du-Noüy ring detachment method, fitted with an OMNIset temperature bath with a precision of ±0.1 °C. Before each measurement, the platinum ring was thoroughly cleaned with 1:1 acetone/water solution and heated under an oxidizing flame until a glowing temperature was attained. After every addition, the experimental solution was stirred for 5 min for homogeneity and equilibrated for 10 min. For each measurement, three to five subsequent readings were taken for concordance. The standard deviation was <0.1 $mN \cdot m^{-1}$.

2.2.2. pH Measurements. The pH values of the solutions were measured using a Systronics digital pH meter (model: 335, India) calibrated with standard buffers of pH 4.0 and 9.2. The solutions were equilibrated for 5 min after the addition of the alkali, until a steady pH meter reading was observed.

2.2.3. Fluorescence Spectroscopy. Steady-state fluorescence emission study was carried out in a bench top spectrofluorimeter from Photon Technologies International (QuantaMaster-40, USA) with excitation and emission slitwidths fixed at 3.0 and 2.5 nm, respectively. The samples were taken in a Hellma quartz cuvette of optical length 1.0 cm.

2.2.4. Nuclear Magnetic Resonance (NMR) Spectroscopy. ^1H NMR experiments were performed using a Bruker (Germany) ADVANCE spectrometer operating at 300 MHz frequency (for characterization) and at 400 MHz for the two-dimensional (2D) rotating frame nuclear Overhauser effect spectroscopy (ROESY) study. Signals are quoted as δ values in ppm using residual protonated solvent signals as the internal standard (D_2O: δ 4.79 ppm). The respective solutions were made in D_2O, and 0.6 mL of the same was used for each measurement. Data are reported as a chemical shift.

2.2.5. High-Resolution Transmission Electron Microscopy (HR-TEM). HR-TEM images were obtained with a Jeol JEM 2100 microscope (Japan) operating at an accelerating voltage of 200 kV. All images were taken at suitable defocus condition to obtain maximum contrast. A drop of the sample solution was added to a 200 mesh copper lacey support grid coated with the carbon film. The excess sample was manually blotted carefully with a Whatman 42 filter paper for 2 s. The grid was dried at 60 °C for 1 h before experimentation.

2.2.6. Dynamic Light Scattering (DLS). DLS was performed on a Zetasizer Nano ZS light scattering apparatus (Malvern Instruments

DOI: 10.1021/acs.langmuir.7b01651
Langmuir 2017, 33, 6581−6594

Scheme 1. Synthetic Route of L-Tyrosine Alkyl Ester, n = 8 (TYOE) and 12 (TYDE)

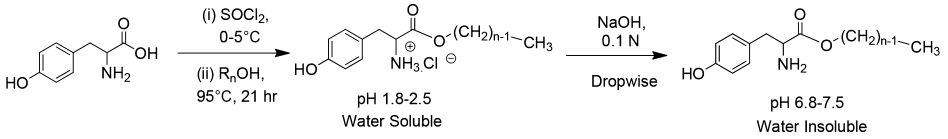

Scheme 2. Synthetic Route of TROE

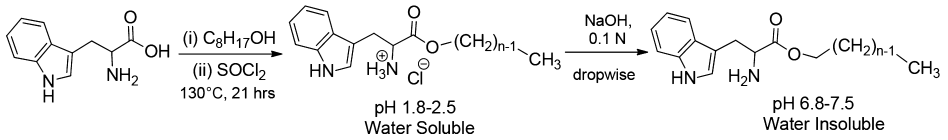

Ltd., UK) with the He−Ne laser (632.8 nm, 4 mW) at a scattering angle of 173°. The temperature was maintained constant at 303 K.

2.3. Synthesis of TYOE and TYDE. To 0.6 mol of *n*-alcohol (95 mL of *n*-octanol and 135 mL of *n*-dodecanol, respectively, for TYOE and TYDE) at −5 °C, 0.055 mol (4 mL) thionyl chloride was added dropwise, and the mixture was stirred for 10 min (Scheme 1). To this mixture, 0.05 mol (9 g) L-tyrosine was added, and the resulting mixture was stirred and refluxed at 95 °C for 21 h under a nitrogen atmosphere. The mixture was then allowed to stand at room temperature. The white solid that appeared was washed with diethyl ether several times (to remove excess *n*-alkanol) and filtered via vacuum suction. It was then dissolved in water and pH was adjusted to 7 (±0.2) by dropwise addition of ∼0.1 N NaOH solution. The white cloudy solution was taken in a separating funnel, to which ethyl acetate was added, and the mixture was shaken well and allowed to stand overnight. A clear, transparent layer of water and ethyl acetate was obtained.

The organic part of the mixture was collected over Na_2SO_4. The solvent was evaporated in a water bath, and the product was dried in a vacuum pump for 6 h.[30] The yellow semisolid product for TYOE (yield ≈ 72%, 6.5 g) and the white crystalline product for TYDE (yield ≈ 75%, 6.7 g) were obtained, and these were characterized using ^{1}H and ^{13}C NMR spectroscopies.

2.3.1. TYOE. ^{1}H NMR (300 MHz, $CDCl_3$): δ (ppm) 7.3 (1H, −OH), 7.01 (d, 2H, 8.4 Hz), 6.69 (dd, 2H, 2.1 Hz), 4.17−4.10 (m, 2H), 3.74−3.66 (m, 1H), 3.2 (broad, $-NH_2$), 3.05 (dd, 1H, 5.1 Hz), 2.94−2.79 (m, 1H), 2.06 (t, 2H), 1.64 (t, 2H), 1.31−1.25 (m, 10H), 0.898 (t, 3H, 6.6 Hz).

^{13}C NMR (300 MHz, $CDCl_3$): δ (ppm) 174.9, 130.35 (for two C, twice intensity), 127.9, 115.7, 77.45, 77.02, 76.60, 65.43, 55.54, 39.71, 29.18, 28.55, 25.88, 22.62, 14.17, 14.07.

2.3.2. TYDE. ^{1}H NMR (300 MHz, $CDCl_3$): δ (ppm) 7.2 (s, −OH), 6.99 (d, 2H, 8.4 Hz), 6.66 (d, 2H, 8.4 Hz), 4.12 (t, 2H, 6.6 Hz), 3.71 (q, 1H, 5.1 Hz), 3.03 (broad, $-NH_2$), 3.05 (dd, 1H, 4.8, 5.1 Hz), 2.8 (q, 1H, 7.1 Hz), 1.63 (t, 2H, 6.6 Hz), 1.28 (d, 18H, 5.1 Hz), 0.88 (t, 3H, 6.3 Hz).

^{13}C NMR (300 MHz, $CDCl_3$): δ (ppm) 174.9, 155.4, 130.34, 127.79, 115.77, 77.46, 77.03, 76.61 65.46, 55.53, 39.71, 31.91, 29.63, 29.58, 29.51, 29.34, 29.24, 28.57, 25.89, 22.68, 14.11.

2.4. Synthesis of TROE. To 63 mL (0.4 mol) of *n*-octanol maintained at −5 °C, 2.2 mL of $SOCl_2$ (0.03 mol) was added dropwise and stirred for 30 min. Thereafter, 6 g of L-tryptophan (0.03 mol) was added, and the mixture was stirred and refluxed at 130 °C under a nitrogen atmosphere for 21 h. The white solid obtained was washed with diethyl ether several times and dried.[31] It was then treated with ethyl acetate, and a strong NaOH solution was added dropwise to adjust pH to 7.0 (±0.2)

The ethyl acetate part was collected over Na_2SO_4 and washed with saturated NaCl solution several times and dried under vacuum for 24 h (Scheme 2).[32] The white solid product (TROE) was obtained and characterized using ^{1}H NMR and ^{13}C NMR techniques. The yield of the product was ∼92% (8.1 g).

^{1}H NMR (300 MHz, $CDCl_3$): δ (ppm) 8.2 (s, NH_2), 7.73 (d, 1H, 7.92 Hz), 7.47 (d, 1H, 7.92 Hz), 7.37 (s, 2H), 7.26 (m, 1H), 4.19 (t, 1H, 6.75 Hz), 3.93 (q, 2H, 4.98 Hz), 3.58 (q, 2H, 4.98 Hz), 3.37 (q, 1H, 5.13 Hz), 3.19−3.14 (m, 1H), 1.72 (s, 6H), 1.34 (s, intense, 6H), 0.99 (t, 3H, 6.93 Hz).

^{13}C NMR (300 MHz, $CDCl_3$): δ (ppm) 171.23, 136.31, 127.46, 123.1, 122.1, 119.46, 118.72, 111.29, 110.92, 65.29, 62.99, 54.91, 31.8, 30.6, 29.4, 29.3, 25.88, 22.66, 14.12.

2.5. Sample Preparation. For experiments at low concentration regimes [concentration < 5 times critical aggregation concentration (cac)], the amino acid esters were directly dissolved in water. For experiments at high concentration regimes (concentration > 5 times cac), the samples were dissolved in pure methanol, followed by the addition of water. The final methanol content in water never exceeded 4%.

3. RESULTS AND DISCUSSION

3.1. Molecular Modeling of TYOE, TYDE, and TROE. Since the geometry of the individual amphiphile molecule determines the packing parameter, vis-à-vis morphology of the self-assembled aggregates in aqueous solutions, the structural aspects of TYOE, TYDE, and TROE are important and have been studied using density functional theory (DFT) calculations in Gaussian 09 package using the hybrid functional B3LYP and 6-31G as the basis set.[33] According to the above measurements, the most stable conformations of aromatic amino acid esters are observed in which the aromatic moieties are bent/folded toward the hydrocarbon chains at different angles. The optimized conformations of TYOE, TYDE, and TROE are shown in Figure 1. The hydrophobic alkyl chain lengths for TYOE, TYDE, and TROE as obtained from the DFT calculations are 9.74, 14.87, and 9.74 Å, respectively. The respective aromatic planes arise approximately 1.29 Å below the plane containing the alkyl chain of TYOE and TYDE and approximately 1.01 Å in the case of TROE. The bending angles between the aromatic plane and the alkyl chain are 152.5°, 154.6°, and 98.1° for TYOE, TYDE, and TROE, respectively. This shows that TYOE and TYDE are comparatively much less aligned (vertically) toward the hydrocarbon skeleton compared with TROE. Single point energy calculations were done to compute the energetics of the most stable conformation in vacuum. The total thermal internal energy of the most stable conformations, that is, those which display minimum internal energy in vacuum via energy minimization, are 280.5, 356.06, and 297.55 kcal·mol^{-1} for TYOE, TYDE, and TROE, respectively. (Theoretical details are provided in section S1.1.) It is noteworthy that the structural geometry of tryptophan octyl ester was studied previously using the molecular mechanics calculation.[28] It has been shown that, in vacuum, the stable conformations were all folded. Extended conformation did occur in water for they were stabilized by electrostatic and van der Waals interaction between the solvent

DOI: 10.1021/acs.langmuir.7b01651
Langmuir 2017, 33, 6581−6594

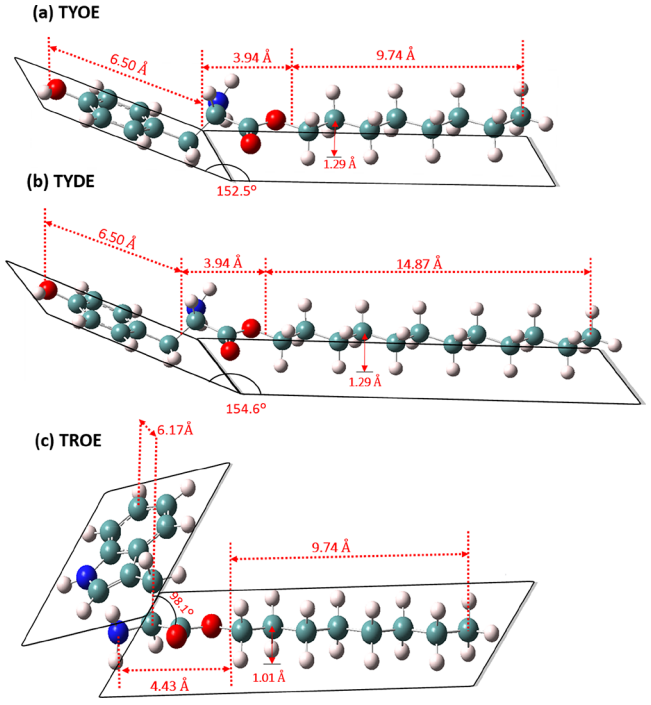

Figure 1. Optimized geometries of (a) TYOE, (b) TYDE, and (c) TROE using DFT B3LYP methodology and 6-31G basis set. Color code: blue = nitrogen, red = oxygen, green = carbon, and gray = hydrogen.

and TROE molecules. Such interactions are weaker for folded conformations. Nevertheless, there is a difference in the potential energy of ~5 kcal·mol^{-1} between the extended and folded conformations of TROE in the presence of the solvent. This again favors the folded conformation.

3.2. Interfacial and Bulk Properties of TYOE, TYDE, and TROE. Measurement of interfacial tension is a reliable and popular tool, which provides direct insight into the molecular behavior of a moiety through careful study of its bulk property. To explore the nature of the amino acid esters, viz. TYOE, TYDE, and TROE, in solution, tensiometric study was undertaken. Figure 2a–c shows that the surface tension of water decreases steadily with increasing concentrations of TYOE, TYDE, and TROE and reaches a constant value at a critical concentration in each case, like a conventional surfactant. At room temperature, viz. 303 K, sharp break points at 1.81, 1.31, and 0.046 mM concentrations of TYOE, TYDE, and TROE are observed, respectively. The equilibrium surface tension of the solutions at the critical points, γ_{cac}, is 45.0 mN·m^{-1} for TYOE, 38 mN·m^{-1} for TYDE, and 52.5 mN·m^{-1} for TROE. These surface tension values are indeed much lower than that of pure water, that is, 70.8 mN·m^{-1} at 303 K. This result indicates that the amino acid esters are surface active in nature. The absence of a minimum around the break point confirms the purity of the synthesized ester.[34] Generally, the nature of the head group and the alkyl chain length of the nonionic surfactant govern critical micelle concentration (cmc)/cac values [the term, in general, is used in this work because of the occasional presence of different types of aggregates together (see section 3.4)].[35] In the present study, it is observed that the cac values for the two tyrosine esters (1.81 mM for octyl and 1.31 mM for dodecyl esters) are not only close to cmc values normally found for many conventional single-tailed surfactants but also follow the well-understood trend of synergism as a function of the chain length.[36] However, tryptophan ester (TROE) exhibits a surprisingly strong self-assembling tendency in water displaying a cac value of 0.046 mM. The γ_{cac} values for the three aromatic amino acid esters indicate that none of these amphiphiles pack the air–water interface much densely, most probably because of their obliquely bent head group geometry (see also section 3.3).[37] Among the three, TYDE molecules are packed most densely, whereas TROE molecules are packed least densely. The pC_{20} values have been determined from the surface tension plots.[38] The pC_{20} is defined as $pC_{20} = -\log C_{20}$, where C_{20}

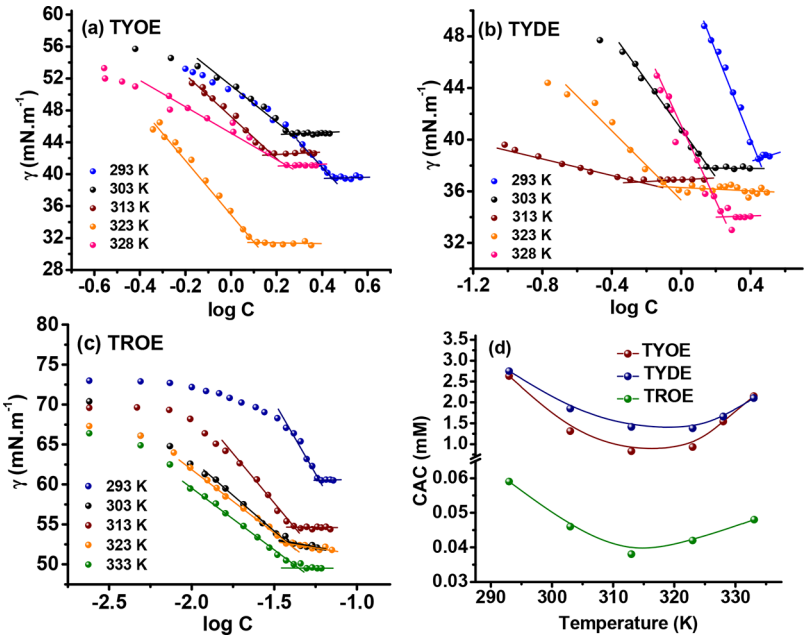

Figure 2. Surface tension profile as a function of temperature for (a) TYOE, (b) TYDE, and (c) TROE. (d) Variation of cac with temperature for different amino acid esters.

DOI: 10.1021/acs.langmuir.7b01651
Langmuir 2017, 33, 6581–6594

Table 1. Temperature Dependence of cac and Surface Parameters, viz. Surface Pressure at cac (Π_{cac}), Surface Excess, (Γ_{max}), Area Minimum (A_{min}) of TYOE, TYDE, and TROE in Aqueous Medium

temperature (K)	cac (mM)	$10^3 \times \Pi_{cac}$ (mN·m^{-1})	$10^6 \times \Gamma_{max}$ (mol m^{-2})	A_{min} (nm^2·molecule^{-1})
		TYOE		
293	2.75	33.2	1.96	0.85
303	1.81	26.1	2.55	0.65
313	1.41	26.9	3.45	0.48
323	1.38	36.7	4.87	0.30
328	1.66	25.9	2.55	0.46
		TYDE		
293	2.63	39.6	2.21	0.75
303	1.31	33.4	3.79	0.44
313	0.83	36.9	5.80	0.29
323	0.93	31.8	5.59	0.30
328	1.54	33.1	3.65	0.46
		TROE		
293	0.059	12.6	6.81	0.24
303	0.046	18.3	2.93	0.57
313	0.038	17.8	3.42	0.48
323	0.042	12.8	2.15	0.79
333	0.045	17.7	2.58	0.66

stands for the concentration required to reduce the surface tension of water by 20 mN·m^{-1}. C_{20} is the minimum concentration needed to lead to a saturation of the surface adsorption and thus can be used as the signature for the efficiency of the amphiphile adsorption at the air−water interface. Higher value of pC_{20} implies greater surface active nature. The pC_{20} values for the present aromatic amino acid amphiphile systems are found to be 0.05, 0.50, and 1.30 for TYOE, TYDE, and TROE, respectively. It implies that TROE demonstrates much higher surface activity compared with the tyrosine analogues. The cac of the present systems is a typical weak function of temperature like the cmc of the conventional surfactants (Figure 2d).[39] In the present case, it decreases with temperature initially and then increases, passing through a shallow minimum. The observed decrease in the surface tension is probably caused by the orientation of amino acid esters at the air−water interface. The rapture of hydrogen bonds between the amphiphiles and the water molecules, caused by the initial rise in temperature, increases the effective hydrophobicity of amino acid ester molecules, thus favoring their aggregation. The increase in cac at higher temperatures is due to the breakdown of the structured "ice-bergs" of water, thus increasing the entropy of aggregation.[40−42] The noted decrease in the equilibrium surface tension values corresponds to higher surface energy with increase in temperature. Other surface parameters underlining the surface behavior of the surface active amino acid esters in the aqueous medium are calculated via Gibbs adsorption equation[43,44] (theoretical background provided under section S1.2) and presented in Table 1. The maximum surface excess (Γ_{max}) denotes the number of surface active molecules present at the air−water interface in excess of the bulk. Γ_{max} shows a significant increase of nearly 2.5 times, from 1.96×10^{-6} to 4.87×10^{-6} mol m^{-2} in the case of TYOE and 2.21×10^{-6} to 5.59×10^{-6} mol·m^{-2} for TYDE in the temperature range of 323−328 K, but in the case of TROE, it decreases from 6.8×10^{-6} to 2.6×10^{-6} mol·m^{-2} within the temperature range of 293−333 K (Table 1). A_{min}, which is the minimum surface area occupied by a molecule at the interface, decreases from 0.85 to 0.46 nm^2·molecule^{-1} for TYOE and 0.75 to 0.46 nm^2·molecule^{-1} for TYDE, whereas it increases from 0.24 to 0.66 nm^2·molecule^{-1} for TROE (Table 1). The increase in the A_{min} value, in the case of TROE, suggests that the molecules are oriented more obliquely at the interface and explains the decrease in the number of excess TROE molecules with temperature. The TYOE and TYDE molecules, on the other hand, assume perpendicular orientations, and consequently, their Γ_{max} is higher.[37] The observation indicates that the head group of the amino acid ester moieties plays a significant role in determining the orientation of the molecules at the interface.

The morphology/phase-transitions of self-assembled aggregates of amphiphilic compounds are dependent on the packing parameter (p)[45]

$$p = v/l{\cdot}a_0 \quad (1)$$

where v and l are the volume and length of the hydrophobic alkyl chain, respectively, and a_0 is the area of the hydrophilic head group of the surfactant molecule. The numerical value of p determines the degree and extent of morphological transition of the aggregates formed in the surfactant solution; for example, to form global micelles, $p \leq 1/3$; for wormlike micelles, $1/3 < p \leq 1/2$; for bilayers, $1/2 < p \leq 1$; and for reverse micelle structures, $p > 1$.[46] The effective head group area, a_0, of the surfactant molecules, is generally obtained from the variation of surface tension as a function of concentration[47] and is given by A_{min} (Table 1). The volume of the hydrophobic chains, v, can be determined empirically from Tanford's equation as follows[48]

$$v = 27.4 + 26.9n \quad (2)$$

where n is the number of carbon atoms in the chain.

For, n = 8 and 12 (for octyl esters of tyrosine and tryptophan and dodecyl ester of tyrosine), v assumes the values of 242.6 and 350.2 Å^3, respectively. Using these values and the value of A_{min} from Table 1, assuming perpendicular orientation only, p is found to be 0.38 for TYOE, 0.53 for TYDE, and 0.43 for TROE. The values indicate that in the case of TYOE, p is slightly above the limit of 0.33 (for micelles) and is therefore expected to aggregate as nearly spherical micelles and ellipsoidal clusters, whereas both TYDE and TROE would have strong inclination to pack as bilayers or vesicles.[49]

DOI: 10.1021/acs.langmuir.7b01651
Langmuir 2017, 33, 6581−6594

Table 2. Thermodynamic Parameters, viz. Standard Gibbs Free Energy Change of Aggregation (ΔG^0_{agg}), Standard Enthalpy Change of Aggregation (ΔH^0_{agg}), Standard Entropy Change of Aggregation (ΔS^0_{agg}), and Standard Free Energy Change of Adsorption (ΔG^0_{ads}) of TYOE, TYDE, and TROE in Aqueous Medium

temperature (K)	ΔG^0_{agg} (kJ·mol^{-1})	ΔH^0_{agg} (kJ·mol^{-1})	ΔS^0_{agg} (J·mol^{-1} K^{-1})	ΔG^0_{ads} (kJ·mol^{-1})
		TYOE		
293	−10.33	+56.56	+228.31	−27.24
303	−12.29	+38.41	+167.31	−22.51
313	−14.48	+16.73	+99.17	−22.27
323	−13.27	−8.56	+14.59	−20.81
328	−13.22	−22.77	−29.11	−23.40
		TYDE		
293	−11.42	+36.19	+162.50	−29.34
303	−12.88	+17.74	+101.08	−21.69
313	−13.55	+0.78	+45.78	−19.91
323	−13.48	−15.65	−6.71	−19.17
328	−14.17	−30.63	−50.17	−23.23
		TROE		
293	−33.51	−9.32	+82.55	−35.36
303	−35.89	−9.05	+88.58	−42.21
313	−36.94	−7.71	+93.38	−42.18
323	−37.85	−6.12	+98.23	−43.94
333	−38.89	−4.31	+103.84	−45.97

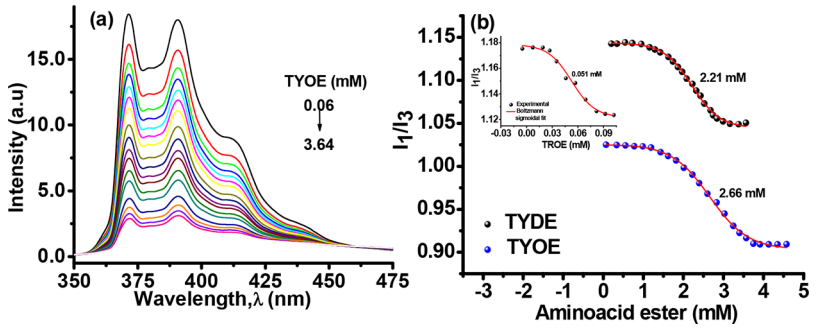

Figure 3. (a) Variation of emission intensity of 2 μM aqueous pyrene as a function of the TYOE concentration at 303 K (representative plot) and (b) relative intensities of the vibronic band (I_1/I_3) of pyrene fluorescence in aqueous solutions of TYOE, TYDE, and TROE at 303 K. The solid circles indicate the experimental curve, and the dashed line indicates Boltzmann sigmoidal fit.

3.2.1. Thermodynamics. The energetics of aggregation and interfacial adsorption have been studied as a function of temperature (Table 2) using Gibbs adsorption isotherm[50] and mass action model[51] of surfactant aggregation, respectively. The mathematical details and equations are provided under section S1.2.1. The standard free energy of aggregate formation per mole of monomer unit[52] for TYOE, TYDE, and TROE in the aqueous medium is evaluated based on the mass action model and summarized in Table 2. The high negative ΔG^0_{agg} value for TROE aggregation, compared with that for tyrosine analogues, shows that the aggregation process is much favored in the former. The self-assembly of amphiphilic molecules in polar solvents such as water generally involves interesting thermodynamic maneuver. On the one hand, the endothermic melting of the ordered solvent cluster due to hydrophobic effect of the amphiphile dominates over the exothermic association of hydrophilic parts leading to positive entropy change. The hydrophilic part, on the other hand, preferentially hydrates in solvent water via hydrogen bond formation with water molecules. Thus, a greater enthalpic compensation is brought about compared with that if the hydrophilic parts are interacted among each other leading to electrostatic repulsion between adjacent hydrophobic blocks. The balance between all such forces drives the formation of aggregates of different sizes, shapes, and orders. Thus, during aggregation, compared with tyrosine analogues, the endothermic melting of ordered water molecules around the nonpolar tail of TROE is much greater than the subsequent exothermic assembly of the molecules (Table 2). Although hydrophobic and electrostatic interactions dominate ΔH^0_{agg}, ΔS^0_{agg} is contributed by the transfer of the hydrocarbon chains of the monomers into the aggregate core.[53] Thus, the temperature favors the decrease of the exothermic repulsion between the tryptophan head groups in TROE. Further, the association of monomers, readjustment of the hydration sphere of the head groups within the aggregates, and reorganization of the hydrocarbon chains at the aggregate core increases the overall degree of freedom of the system causing a net rise in the entropy.[54] The linear enthalpy−entropy compensation relationship was observed with compensation temperature, T_c, as 308, 313, and 246 K for TYOE, TYDE, and TROE, respectively (Figure S1). Further, the negative values of ΔG^0_{ads} indicate that the phenomenon of interfacial adsorption is also spontaneous in nature. In the case of TYOE and TYDE, ΔG^0_{ads} shows a nonregular trend with temperature, whereas in the case of TROE, the value increases as a function of temperature. This shows that temperature favors the process of adsorption in TROE. Furthermore, the more negative values of ΔG^0_{ads} compared with ΔG^0_{agg} for TYOE, TYDE, and TROE at

DOI: 10.1021/acs.langmuir.7b01651
Langmuir 2017, 33, 6581−6594

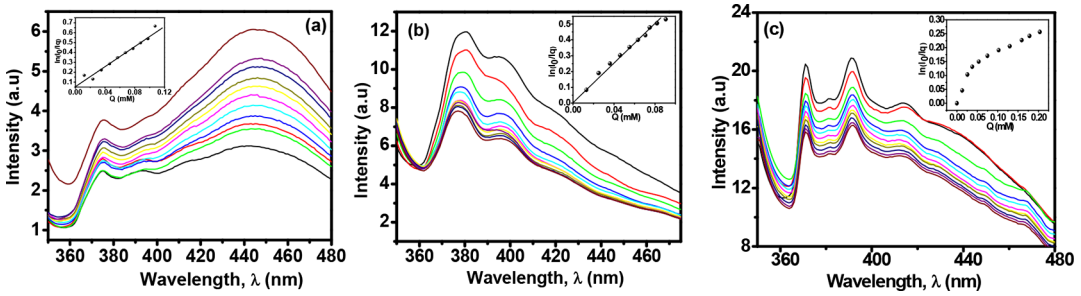

Figure 4. Variation of fluorescence emission spectra of 2 μM pyrene in aqueous solutions of the amino acid esters: (a) 8.09 mM TYOE, (b) 4.24 mM TYDE, and (c) 0.21 mM TROE at 303 K. The insets display linear plots of $\ln(I/I_0)$ for 2 μM pyrene in aqueous solutions of the respective amino acid esters as a function of CPC (Q) concentrations.

all temperatures indicate that the adsorption process in all amino acid esters is more spontaneous in comparison to their corresponding aggregation.[44]

3.2.2. Steady-State Fluorescence Emission. Steady-state fluorescence emission study was performed to verify the cac values of the amino acid aggregates and to ascertain the microenvironment of the molecular aggregates in solution. Figure 3a depicts the variation in the fluorescence emission intensity of 2 μM aqueous pyrene solution upon increasing the concentration of TYOE (representative plot). Plots for TYDE and TROE are provided in Figure S2. The lowering of emission intensity signifies considerable binding of pyrene to the TYOE molecules. The relative intensities of the vibronic bands, I_1/I_3, of pyrene emission are plotted as a function of the concentrations of amino acid esters (Figure 3b).

A sigmoidal variation is observed in all three cases (Figure 3b). The values were fitted according to Boltzmann distribution to obtain the inflexion point, which has been considered as the cac.[55] The cac values obtained by this method are 2.66 mM for TYOE, 2.21 mM for TYDE, and 0.051 mM for TROE. These values differ to a considerable extent from those obtained from the surface tension measurement (Table 1). However, such difference of results between the two methods is not uncommon.[6] The I_1/I_3 value, which is shown to be a measure of the polarity of the fluorophore location, ranges from 0.91 to 1.02 in TYOE, 1.04 to 1.14 in TYDE, and 1.12 to 1.18 in TROE (Figure 3b). The values are consistent with those observed for pyrene in the nonpolar solvent, toluene (1.11) and in the nonpolar micellar core of traditional anionic surfactant, sodium dodecyl sulfate (1.14).[55] The vibronic bands of the fluorescence emission spectrum of pyrene are highly sensitive to the local polarity; the I_1/I_3 values in the micelle-solubilized pyrene increases with the solvent polarity.[56] Therefore, it is evident that the pyrene molecules partition into a preferably nonpolar location at the core of the aggregates. This also corroborates the fact that the lowering of the emission intensity upon increased amphiphile concentration, as observed in Figure 3a, is a sign of partitioning more and more fluorophore into the aggregate core. Further, I_1/I_3 varies in the order TYOE > TYDE > TROE, implying that the aggregate core is more polar in TROE followed by TYDE and least polar in TYOE.

3.2.3. Aggregation Number. The steady-state fluorescence quenching technique was used to determine the aggregation number ($N_{agg.}$) of the aggregates of amino acid esters. The equilibrium of the amino acid esters between the aqueous and the self-assembled pseudophases follows the Poisson distribution. The following equation is applied to analyze the fluorescence quenching data[57]

$$\ln I = \ln I_0 - \frac{C_Q}{C_a} \tag{3}$$

or,

$$\ln I = \frac{\ln I_0 - N_{agg.}C_Q}{C_T - \text{cac}} \tag{4}$$

where C_Q, C_a, and C_T are the concentrations of the quencher, aggregate, and total amino acid esters, respectively, whereas I and I_0 are the fluorescence intensities in the presence and absence of the quencher. Figure 4 shows the emission spectra of pyrene in aqueous solutions of amino acid esters in the presence of varying quencher concentrations (cetylpyridinium chloride, CPC). The emission intensity of pyrene decreases with the increase in the quencher concentration in all three amino acid esters. From the slope of the plots of $\ln(I/I_0)$ versus the quencher concentration (insets of Figure 4a–c) and the cac values, $N_{agg.}$ is determined using eq 4. To avoid the possibility of microstructure transition, the concentration of amphiphile is kept 4.5 times of cac, whereas higher concentration is usually desirable. However, the results of the quenching experiment suggest that both pyrene and the quencher, CPC, are partitioned well within the aggregate core under the above concentration condition. The shape of the emission spectra of pyrene is modified in the presence of CPC; the vibronic structure becomes ill-defined, and the spectra are red-shifted due to the interaction of pyrene molecules with the pyridinium head groups of CPC within the aggregates. The aggregation numbers obtained by this method are 35 and 18, respectively, for TYOE and TYDE, whereas for TROE, $N_{agg.}$ could not be determined because of the nonlinear nature of the $\ln(I/I_0)$ versus the quencher concentration plot (inset of Figure 4c). It seems apparent that the experimental plots (insets of Figure 4a,b) for TYOE and TYDE are consistent and yield the values of N_{agg}. Nevertheless, the aggregation numbers are unusually small, especially for TYDE aggregates. Moreover, the deviation, of plots of $\ln(I/I_0)$ versus the quencher concentration (for TROE) from linearity is undoubtedly indicative of the morphology transition of the aggregates at the experimental concentration. It is therefore tempting to examine the molecular interaction (by 2D NMR) and the detail morphology (by HR-TEM) at similar and higher concentration regimes of the amino acid analogues.

3.3. Molecular Interactions: 2D NMR (Concentration > 5 Times cac). NMR spectroscopy is a powerful and reliable tool for the investigation of molecular aggregates.[58] NMR techniques have been successfully utilized in determining parameters such as the size, shape, degree of association,

DOI: 10.1021/acs.langmuir.7b01651
Langmuir 2017, 33, 6581–6594

Scheme 3. Chemical Representation and Proton Numbering of TROE and TYOE

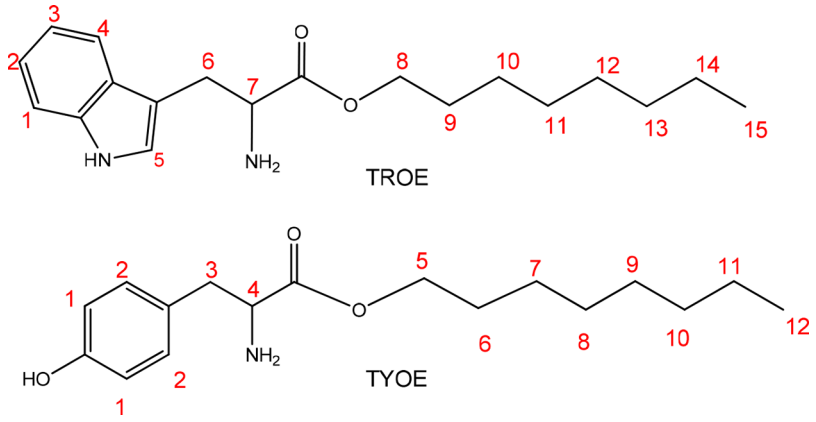

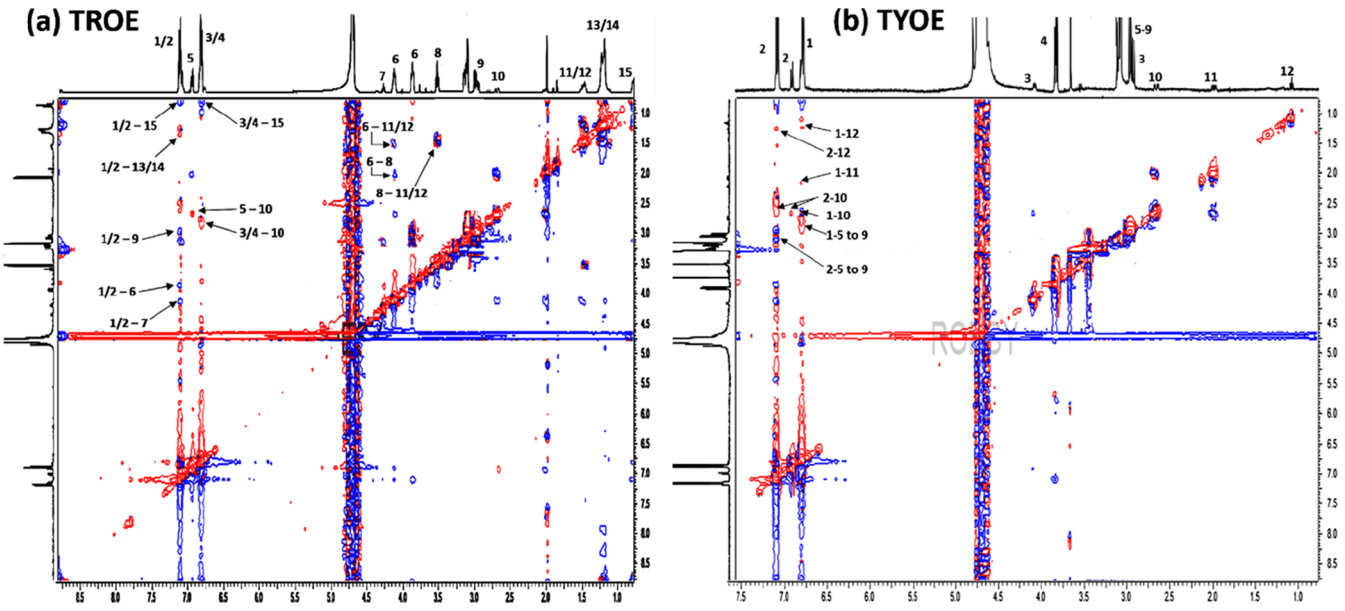

Figure 5. Two-dimensional $^1H-^1H$ ROESY spectra of (a) 0.5 mM TROE and (b) 7.2 mM TYOE in D_2O at 303 K.

structure, and so forth of various self-assemblies.[59−62] ROESY is one of the 2D NMR techniques that correlates signals arising via dipolar interaction from protons that are close in space (<5 Å). The intensity of the cross-peaks of ROESY spectra reflects the extent of magnetization transfer between the nuclei and is proportional to the internuclei distance.[63] Herein, the 2D ROESY spectroscopic analysis is utilized to study the microstructure of the amino acid esters, viz. TYOE and TROE, in solution (D_2O). The chemical representation and proton numbering of TYOE and TROE are shown in Scheme 3.

The presence of key cross-peaks in the ROESY spectra of TYOE and TROE (Figure 5) suggests that strong interaction occurs between various protons of the respective molecules. In Figure 5a, the intense cross peaks 3/4−15 and 1/2−15 correlate the aromatic protons of the indole ring of the tryptophan moiety with the terminal alkyl protons.

Cross-peaks, viz. 1/2−13/14, 3/4−10, and 1/2−9 are observed between the aromatic protons and the intermediate aliphatic protons of the octyl chain of TROE. These correlations suggest that the aromatic face of the TROE molecule containing the benzene ring of the indole moiety lies in close proximity to the aliphatic protons of the alkyl chain of TROE, including the terminal methyl protons. The optimized geometries of amino acid esters (section 3.1) in vacuum especially that of TROE also showed that the aromatic ring remains folded. Previously, theoretical studies using molecular mechanics calculations[28] have shown that an extended conformation of TROE molecule is energetically unfavorable and that the TROE molecule exists as a folded conformer in vacuum and in water box, with the amino and carboxylate groups located at one end creating a polar extremity. Similar conformation of TROE is observed herein from the ROESY spectrum. The interaction of aromatic protons with the terminal methyl group further suggests that the aliphatic chain tends to bend toward the aromatic ring exhibiting a folded structure. Strong hydrophobic interactions between the aromatic ring and the aliphatic chain might be the driving force behind the "bending inwards" of the terminal alkyl protons and the observed cross-peaks in the ROESY spectrum. This conformation of TROE may be stabilized by the favorable van der Waal interaction and possible hydrogen bonding between the solvent water molecules and the polar amino and carboxyl groups of TROE, which lie at the micellar interface. Furthermore, the two H6 protons exist in two magnetically nonequivalent environments. One is closer to the polar amino

DOI: 10.1021/acs.langmuir.7b01651
Langmuir 2017, 33, 6581−6594

Scheme 4. Key $^{1}H-^{1}H$ Intramolecular ROESY (◄·····►) Correlations in (a) TROE and (b) TYOE[a]

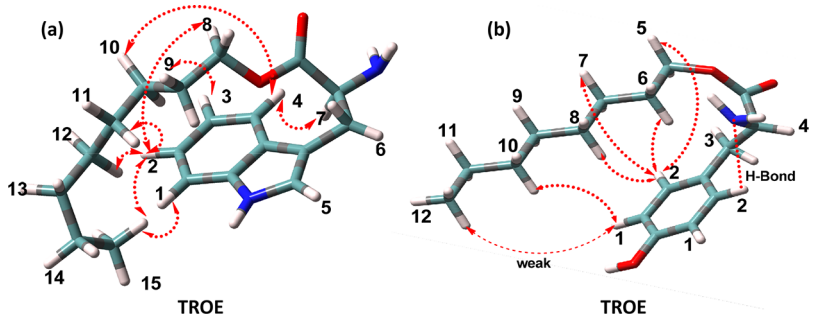

[a]Color code: blue = nitrogen, red = oxygen, green = carbon, and gray = hydrogen.

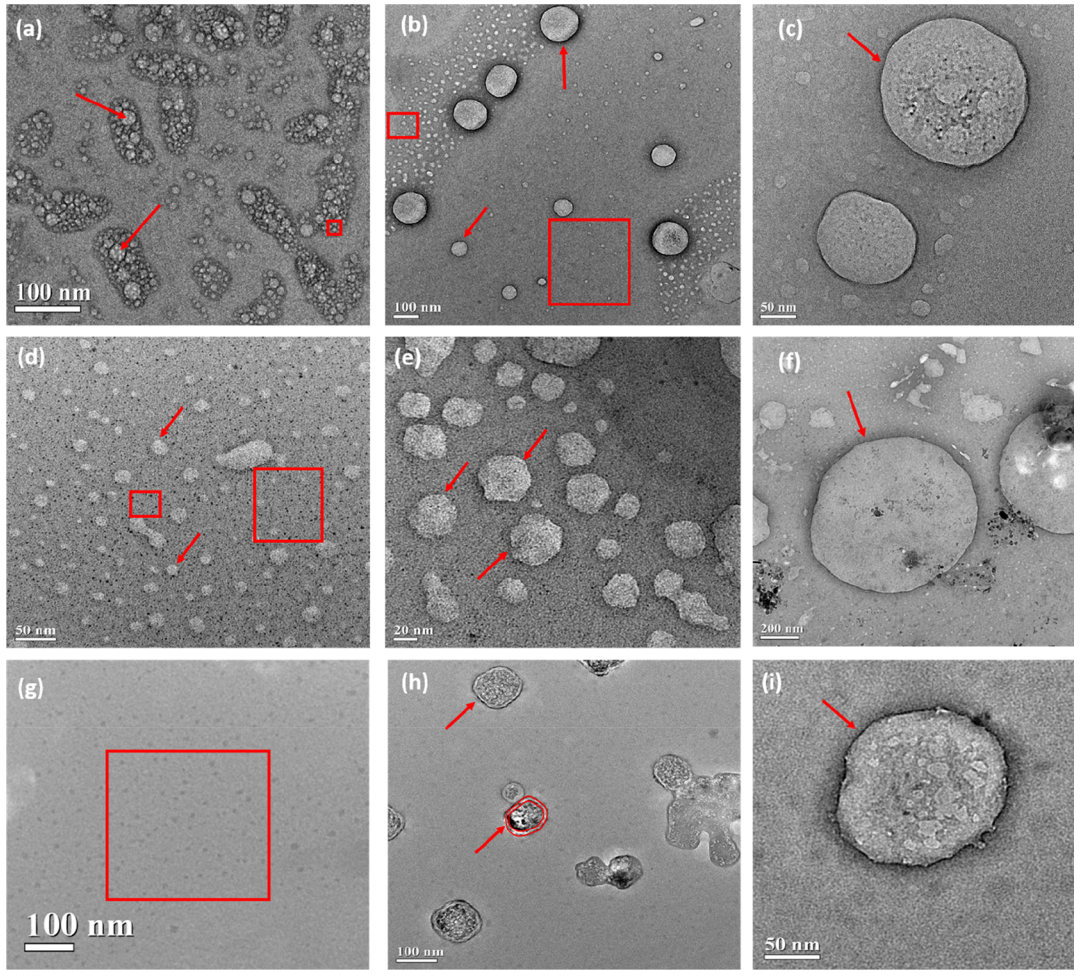

Figure 6. HR-TEM micrographs of (a–c) 7.2 mM TYOE in the aqueous medium in different fields of view: (a) clusters of vesicular aggregates, (b) dispersed micellar aggregates of size <10 nm indicated by boxes and presence of large vesicles of diameter >50 nm indicated by arrows, and (c) presence of giant spherical vesicles of diameter ∼200 nm; (d–f) 9.0 mM TYDE in different fields of view: (d) presence of aggregates of micellar dimension (arrows and boxes), (e) mesosize aggregates with regular hollow internal structures (trigonal dodecahedron/icosahedron?), and (h) giant vesicle of diameter ∼200 nm; and (g–i) 0.5 mM TROE in different fields of view: (g) uniformly distributed micellar aggregates, (h) vesicles with a distinct bilayer membrane of thickness ≈ 5–7 nm of predominantly square geometry, with hollow concentric circles indicating bilayer thickness, and (i) large spherical vesicle of diameter ∼150 nm.

group and appears downfield at δ 4.2 ppm, whereas the other is oriented away from the amino group and appears relatively upfield at δ 3.9 ppm (Figure S3a). In the ROESY spectrum, a correlation between the more downfield H6 protons is observed with H8 and H11/H12 protons of the alkyl chain. Moreover, several other weak cross–peaks, viz. 1/2–6, 1/2–7, and 5–10, are also observed correlating the aromatic protons with the protons at the polar end of the head group. These interactions suggest that molecular interactions may also occur between two adjacent TROE molecules.

In the case of TYOE, two fascinating aspects were observed. First, in spite of consisting of two types of magnetically nonequivalent aromatic protons, viz. H1 and H2 (Figure 5b), the ^{1}H NMR spectra displayed low intensity resonance signals

DOI: 10.1021/acs.langmuir.7b01651
Langmuir 2017, 33, 6581–6594

for a third type aromatic proton at δ 7.00 ppm (Figure S3b). This indicates that some of the H2 protons may be hydrogen-bonded to the amino group in its vicinity. The 2D ROESY spectrum reveals that this hydrogen-bonded proton interacts with H10 of the aliphatic chain giving rise to cross-peaks at 6.99−2.75. A very weak correlation peak is observed between the aromatic H1 proton and the terminal methyl protons, viz. H12. This shows that the aliphatic chain terminal is located away from the proximity of the aromatic ring contrary to that observed in TROE. Second, unlike commonly observed for aliphatic proton resonances and as observed in the spectra of TYOE in the nonpolar solvent $CDCl_3$ where it appears at δ 1.33 ppm (Figure S1a), the chain protons H5−H9 appear highly downfield in D_2O and merge into a single peak observed at 3.16 ppm (Figure S3b). No intense peak at the nonpolar end suggesting otherwise is evident. The observation indicates that the chain protons of TYOE experience unusually high polar environment in the aqueous medium compared with that of TROE. Intense cross-peaks correlating these protons, viz. H5−H9, with the aromatic nonbonded H2 proton is observed. It seems likely that in TYOE, the aromatic moiety bends the carbonyl group inward along with the ester−oxygen facing the interface.[64] Because of the incorporation of rigidity in the structure owing to the hydrogen bonding, the aromatic group remains less closely packed compared with that of TROE. The highly polar environment experienced by H5−H9 in TYOE may be explained by the close proximity of the $-NH_2$ group in the vicinity and the presence of larger number of polar solvent molecules compared with that of TROE.

On the basis of the 2D NMR observation, a probable structure of TROE and TYOE as present within the aggregates and the intramolecular interaction between different protons is shown in Scheme 4.

3.4. Morphology of Aggregates: HR-TEM and DLS (Concentration > 5 Times cac). The aggregate morphology of the amino acid esters was visualized using HR-TEM[6] (Figure 6). To ensure complete aggregation and microstructure transformation, aqueous solutions of the amino acid esters were prepared with concentrations 5−10 times of their respective cac values. The TEM micrographs show the presence of aggregates of different sizes having diverse microstructural features. In TYOE, spherical micelles of size 5−10 nm (representative indication by red square) and small spherical vesicles of size 20−30 nm (representative indication by red arrow) are observed to pack together in the form of ellipsoidal domains (Figure 6a). Furthermore, the vesicles form stacked-up structures, as evident from their overlapped contour (indicated by red arrow).[65,66] The absence of a well-defined membrane around the periphery of the large ellipsoidal assembly suggests that the formation of this cluster is driven by solvophobic repulsive interactions between the micelles or vesicles and the solvent molecules. It may also be seen that large spherical vesicles, of average diameter of ∼100 nm, are present alongside the smaller micellar aggregates, which are dispersed throughout the field of view (Figure 6b). Larger vesicles of diameter >200 nm are also present (Figure 6c). Similar coexistence of small micelles (size <8 nm) and vesicles (diameter 20−25 nm) is evident in TYDE (Figure 6d) as well. A closer inspection of the HR-TEM picture of TYDE aggregates reveals the presence of mesosize aggregates with regular hollow internal structures that look like trigonal dodecahedron/icosahedron geometry (Figure 6e). The aggregates in TYDE are spheroidal and have a diameter of ≈10−20 nm. These are comparatively more homogeneously distributed (Figure 6d) than TYOE. Besides, there are large number of smaller aggregates of micellar dimension (black dots) evenly distributed within the field of view (Figure 6). However, giant spherical vesicles (diameter ≈ 200 nm) similar to those in TYOE are also observed in TYDE (Figure 6f). In TROE, micellar aggregates of size <10 nm are found dispersed in the medium (Figure 6g indicated by the red square), whereas larger vesicles of average dimension of ∼60−80 nm, having cubic geometry (indicated by the red arrow), are found to coexist (Figure 6h). Giant vesicles similar to those in TYOE and TYDE are also observed in another field of view (Figure 6i). The membrane bilayer thickness observed in the larger vesicles of TYOE, which are relatively less abundant than the smaller ones, is about ∼4−6 nm. TROE consists of large vesicles with well-defined bilayer boundaries. The bilayer membrane thickness of TROE is ∼8−10 nm. The vesicles of TROE are sparsely distributed compared with those of TYOE and TYDE, and this may be due to the much lower concentration of TROE (0.5 mM) compared with TYOE (7.2 mM) and TYDE (9 mM) of the experimental samples.

The presence of large vesicular aggregates in TYOE, TYDE, and TROE was also examined using DLS at 303 K (Figure 7).

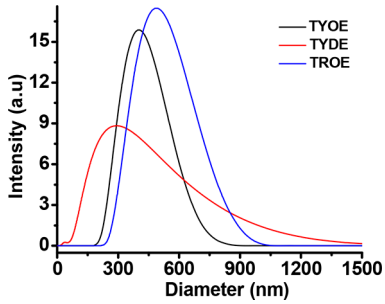

Figure 7. Size distribution of aggregates in aqueous solutions of 7.2 mM TYOE, 9.0 mM TYDE, and 0.5 mM TROE as obtained from DLS measurements at 303 K.

For better understanding, the sample concentrations were kept identical to that used during the HR-TEM measurement. It is evident that giant aggregates of size 200−600 nm are present in all three amino acid esters. The average hydrodynamic diameters (d_h) of TYOE, TYDE, and TROE are obtained as 451, 353, and 540 nm, respectively. The results confirm the aggregation of the amino acid esters into giant vesicles.

Unlike conventional single-tailed surfactant systems, TYOE, TYDE, and TROE aggregates display rich morphologies as observed from the HR-TEM study in the absence of any promoter/additive. The key difference of aromatic amino acid esters from the conventional surfactants is that, unlike the latter, amino acid esters contain blocks of hydrophobic and hydrophilic moieties in their molecular structures. This molecular picture is similar to that witnessed in block copolymer amphiphiles, the self-assembled aggregates of which have attracted wide interests because of the creation of a plethora of morphologies.[17,66,67] For these systems that contain a multiple number of hydrophobic and hydrophilic blocks, the morphologies are determined by the curvature created in the assembly via relative volume of such water-insoluble and water-soluble domains. The balance between the hydrophobic and hydrophilic interactions gives rise to an optimum surface area (a_0) of the hydrophobic block at the interface between the hydrophobic and hydrophilic domains.

DOI: 10.1021/acs.langmuir.7b01651
Langmuir 2017, 33, 6581−6594

Scheme 5. Schematic Representation of Possible Morphology and Orientation of TROE Molecules in the Bilayer and Micelles

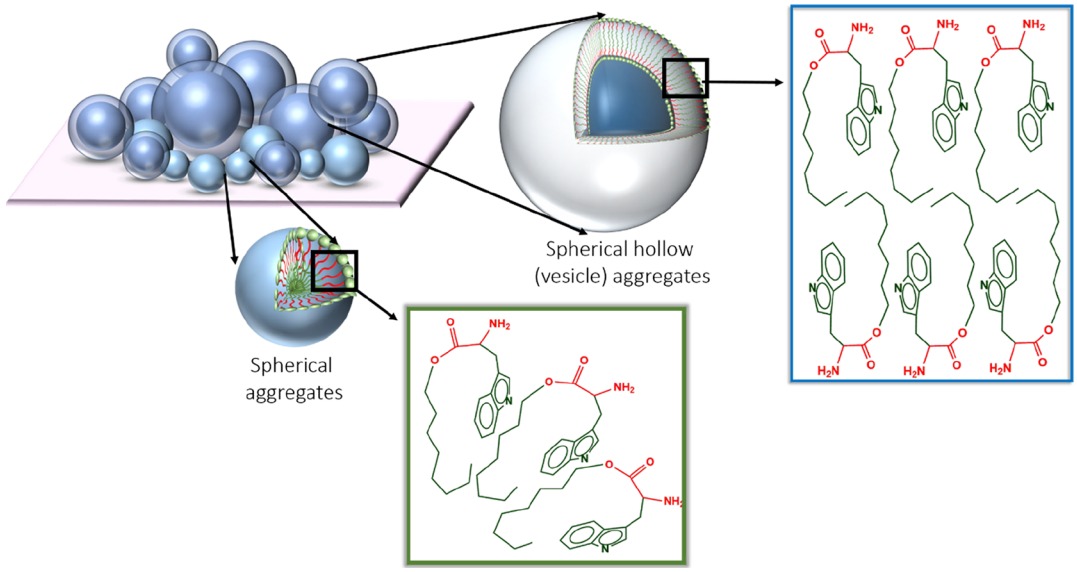

This area together with the length and volume of the hydrophobic block contributes to the packing parameter. In the present amphiphilic systems, viz. TYOE, TYDE, and TROE, containing hydrophobic and hydrophilic blocks in the molecule, the geometries and the degree of order of the aggregate nanostructures depend on the amphiphile concentration and the volume ratio of the water-insoluble and water-soluble blocks—"the insoluble soluble ratio (ISR)".[67] As a result, at a low concentration, because of the soluble domain compatibility with the solvent, the system may be soluble. On the other hand, at the cac or higher concentrations, the molecules containing multiple number of blocks self-assemble to form either a dispersed isotropic globular phase or larger aggregates with higher order morphology. From the length of hydrophobic and hydrophilic domains for TYOE, TYDE, and TROE, as determined by DFT calculations (Figure 1), the corresponding ISR values for these amphiphiles are found to be 4.12, 5.42, and 3.93, respectively (assuming identical cross-sectional area). It may, therefore, be presumed that the surface activity of the above systems would be in the order TYDE > TYOE > TROE, unless major structural discrimination is encountered by them in the presence of a polar solvent. However, because of the segregated structure in the presence of the solvent, the present system deviates from the above trend. Therefore, instead of kinetically trapped nonequilibrium structures of small vesicles formed by conventional double-tailed surfactants with inverted cone/truncated conelike molecular form, thermodynamically stable vesicles and bilayers are formed in present amphiphile systems because of their intrinsic polydispersity. Such polydispersity leads to selective segregation of hydrophobic blocks in the inside of vesicles, whereas hydrophilic blocks segregates on the outside. The preferred curvature of the bilayer is stabilized in this way. The effect is enhanced in smaller vesicles because the tendency to segregate would be greater as the interfacial curvature is increased. The various morphologies that are observed in the present systems are primarily a result of the inherent molecular curvature and how this influences the packing of the amphiphiles in the assemblies. A schematic representation of the possible morphology and orientation of the molecules in the bilayer and in the micelles is shown in Scheme 5. The vesicles that are formed in the present amino acid ester-based amphiphile systems are found to be stable (examined up to 10 days and found stable in terms of size). The conformation of individual amino acid ester molecule as observed by DFT computation is modified in aqueous aggregates. As revealed from the 2D NMR study, these molecules are further folded in the aggregates because of the interplay between the hydrophobic and hydrophilic forces, including H-bonding between the polar groups present in the hydrophilic blocks and the water molecules at the interface. Therefore, the driving force of the self-assembly formation is the hydrophobic and hydrophilic interactions along with the noncovalent interactions, including H-bonding. The thermodynamic maneuver (enthalpy and entropy) plays a vital role just like the aggregation process as involved in block copolymers and common surfactants in polar solvents. Hydrogen bond formation in aqueous amphiphilic systems have attracted much attention recently, both experimentally and theoretically, because it has been proved of crucial importance on the structural and dynamic properties of self-assembled nanostructural motifs.[68] The array of intramolecular and intermolecular interactions among the blocks within TYOE, TYDE, and TROE assemblies in water generates the sophisticated structures. These interactions for the formation and stability of rich morphologies also undoubtedly include the H-bonding network that is formed among interfacially located hydrophilic blocks as well. The difference between the molecular packing predicted from Israelachvili's approach[46] (section 3.1) and that observed in the solvent is, therefore, due to the molecular folding induced by the solvent. In the presence of a solvent, the amino acid esters with the folded aromatic ring behave as the pseudo-double-tailed surfactants with truncated cone geometries, and the hydrophilic blocks oriented toward the interface act as the "head groups". Such orientation is favored because of the strong hydrogen bonding of the polar head groups with the solvent water molecules.[68] Therefore, due to molecular folding in the presence of water, vis-à-vis segregation of hydrophobic and hydrophilic blocks, the conventional approach of the calculation of the packing parameter and the prediction of aggregation morphology in terms of individual molecular geometry is not valid, and hence does not follow in the present study.[69]

DOI: 10.1021/acs.langmuir.7b01651
Langmuir 2017, 33, 6581−6594

4. CONCLUSIONS

Molecular geometries of the models for membrane proteins, viz. TYOE, TYDE, and TROE, as determined via energy minimization by DFT calculations, exhibit partial bending of the aromatic ring (phenol or indole) toward the hydrocarbon chain of the molecules. Occurrence of a hydrophilic block (consisting of ethereal oxygen, carbonyl, and amine groups) between two strongly hydrophobic blocks (consisting of the phenol/indole ring and the hydrocarbon chain) in the molecular architectures and the obliquely bent molecular geometry lead to the formation of a distinctive amphiphilic system that unveils strong surface active properties in aqueous solutions. The 2D NMR spectroscopy in D_2O reveals that the unique molecular geometry of these tyrosine and tryptophan analogues facilitates strong segregation domain of the two hydrophobic blocks to form within the same molecule, and this leads to further folding of the molecules via noncovalent interactions, including hydrogen bonding. The display of the rich morphology of the exclusive aggregates, as has been witnessed in the present systems, is not only rare for single-chain amphiphiles but the biocompatibility of the aromatic amino acid esters makes them highly potential contenders for drug delivery vehicles and drug vectors as well. The demonstration of chemically segregated domains with exceptional chemistries and topographies leading to the formation of bilayer and membrane motifs commands fundamental features of cell membranes and may have important relevance in biotechnology. Further, it points out to the fact that membrane proteins are not just integral dopants in the membrane system but very much set their role as the building blocks of the cell membrane and may act as the stabilizer of the membrane structure as well.

■ ASSOCIATED CONTENT

Supporting Information

The Supporting Information is available free of charge on the ACS Publications website at DOI: 10.1021/acs.langmuir.7b01651.

Theoretical details regarding energy calculations via DFT methodology, evaluation of surface parameters and thermodynamics, and figures related to thermodynamics and spectroscopic data (PDF)

■ AUTHOR INFORMATION

Corresponding Author

*E-mail: ssahanbu@hotmail.com.

ORCID

Swapan K. Saha: 0000-0002-1846-9531

Notes

The authors declare no competing financial interest.

■ ACKNOWLEDGMENTS

We thank the Science & Engineering Research Board (SERB), DST, Govt. of India (sanction no. SB/S1/PC-034/2013) for financial assistance. G.C. thanks the University Grants Commission for Basic Scientific Research (UGC-BSR) Fellowship. We gratefully acknowledge NEHU, SAIF for providing HR-TEM facility.

■ REFERENCES

(1) Bordes, R.; Holmberg, K. Amino acid-based surfactants—Do they deserve more attention? *Adv. Colloid Interface Sci.* **2015**, *222*, 79−91.

(2) Infante, M. R.; Clapes, P.; Perez, L.; Pinazo, A.; Moran, M. D. C. Amino Acid-based surfactants. In *Novel Surfactants: Application and Biodegradibility*, 2nd ed.; Holmberg, K., Ed.; CRC Press, 2003; pp 193−216.

(3) Pérez, L.; Pinazo, A.; Pons, R.; Infante, M. Gemini surfactants from natural amino acids. *Adv. Colloid Interface Sci.* **2014**, *205*, 134−155.

(4) Angelidaki, I.; Toräng, L.; Waul, C. M.; Schmidt, J. E. Anaerobic bioprocessing of sewage sludge, focusing on degradation of linear alkylbenzene sulfonates (LAS). *Water Sci. Technol.* **2004**, *49*, 115−122.

(5) Brandt, K. K.; Hesselsoe, M.; Roslev, P.; Henriksen, K.; Sorensen, J. Toxic Effects of Linear Alkylbenzene Sulfonate on Metabolic Activity, Growth Rate, and Microcolony Formation of Nitrosomonas and Nitrosospira Strains. *Appl. Environ. Microbiol.* **2001**, *67*, 2489−2498.

(6) Rao, K. S.; Singh, T.; Trivedi, T. J.; Kumar, A. Aggregation Behavior of Amino Acid Ionic Liquid Surfactants in Aqueous Media. *J. Phys. Chem. B* **2011**, *115*, 13847−13853.

(7) Xu, W.; Song, Q.; Xu, J.-F.; Serpe, M. J.; Zhang, X. Supramolecular Hydrogels Fabricated from Supramonomers: A Novel Wound Dressing Material. *ACS Appl. Mater. Interfaces* **2017**, *9*, 11368−11372.

(8) Liu, K.; Xing, R.; Zou, Q.; Ma, G.; Möhwald, H.; Yan, X. Simple Peptide-Tuned Self-Assembly of Photosensitizers towards Anticancer Photodynamic Therapy. *Angew. Chem., Int. Ed.* **2016**, *55*, 3036−3039.

(9) Wang, J.; Shen, G.; Ma, K.; Jiao, T.; Liu, K.; Yan, X. Dipeptide concave nanospheres based on interfacially controlled self-assembly: from crescent to solid. *Phys. Chem. Chem. Phys.* **2016**, *18*, 30926−30930.

(10) Jiao, Y.; Li, W.-L.; Xu, J.-F.; Wang, G.; Li, J.; Wang, Z.; Zhang, X. A Supramolecularly Activated Radical Cation for Accelerated Catalytic Oxidation. *Angew. Chem., Int. Ed.* **2016**, *55*, 8933−8937.

(11) Zou, Q.; Abbas, M.; Zhao, L.; Li, S.; Shen, G.; Yan, X. Biological Photothermal Nanodots Based on Self-Assembly of Peptide−Porphyrin Conjugates for Antitumor Therapy. *J. Am. Chem. Soc.* **2017**, *139*, 1921−1927.

(12) Shao, J.; Wen, C.; Xuan, M.; Zhang, H.; Frueh, J.; Wan, M.; Gao, L.; He, Q. Polyelectrolyte multilayer-cushioned fluid lipid bilayers: a parachute model. *Phys. Chem. Chem. Phys.* **2017**, *19*, 2008−2016.

(13) Shao, J.; Xuan, M.; Dai, L.; Si, T.; Li, J.; He, Q. Near-Infrared-Activated Nanocalorifiers in Microcapsules: Vapor Bubble Generation for In Vivo Enhanced Cancer Therapy. *Angew. Chem., Int. Ed.* **2015**, *54*, 12782−12787.

(14) Miyagishi, S.; Nishida, M. Influence of chirality on micelle formation of sodium N-acylalanates and sodium N-lauroylvalinates. *J. Colloid Interface Sci.* **1978**, *65*, 380−386.

(15) Takehara, M.; Yoshimura, I.; Yoshida, R. Surface-active N-acylglutamate: IV. Physicochemical properties of triethanolamine long chain N-acylglutamates. *J. Am. Oil Chem. Soc.* **1974**, *51*, 419−423.

(16) Ohta, A.; Nakashima, S.; Matsuyanagi, H.; Asakawa, T.; Miyagishi, S. Krafft temperature and enthalpy of solution of *N*-acyl amino acid surfactants and their racemic modifications: effect of the counter ion. *Colloid Polym. Sci.* **2003**, *282*, 162−169.

(17) Roy, A.; Kundu, N.; Banik, D.; Sarkar, N. Comparative Fluorescence Resonance Energy-Transfer Study in Pluronic Triblock Copolymer Micelle and Niosome Composed of Biological Component Cholesterol: An Investigation of Effect of Cholesterol and Sucrose on the FRET Parameters. *J. Phys. Chem. B* **2016**, *120*, 131−142.

(18) Kelkar, D. A.; Chattopadhyay, A. The gramicidin ion channel: A model membrane protein. *Biochim. Biophys. Acta* **2007**, *1768*, 2011−2025.

DOI: 10.1021/acs.langmuir.7b01651
Langmuir 2017, 33, 6581−6594

(19) Yau, W.-M.; Wimley, W. C.; Gawrisch, K.; White, S. H. The Preference of Tryptophan for Membrane Interfaces. *Biochemistry* **1998**, *37*, 14713−14718.
(20) Levine, Z. A.; Venable, R. M.; Watson, M. C.; Lerner, M. G.; Shea, J.-E.; Pastor, R. W.; Brown, F. L. H. Determination of Biomembrane Bending Moduli in Fully Atomistic Simulations. *J. Am. Chem. Soc.* **2014**, *136*, 13582−13585.
(21) Sainz, B., Jr.; Rausch, J. M.; Gallaher, W. R.; Garry, R. F.; Wimley, W. C. The Aromatic Domain of the Coronavirus Class I Viral Fusion Protein Induces Membrane Permeabilization: Putative Role during Viral Entry. *Biochemistry* **2005**, *44*, 947−958.
(22) McMahon, H. T.; Gallop, J. L. Membrane curvature and mechanisms of dynamic cell membrane remodelling. *Nature* **2005**, *438*, 590−596.
(23) Kollmitzer, B.; Heftberger, P.; Rappolt, M.; Pabst, G. Monolayer spontaneous curvature of raft-forming membrane lipids. *Soft Matter* **2013**, *9*, 10877−10884.
(24) Sengupta, B.; Sengupta, P. K. Influence of Reverse Micellar Environments on the Fluorescence Emission Properties of Tryptophan Octyl Ester. *Biochem. Biophys. Res. Commun.* **2000**, *277*, 13−19.
(25) Chattopadhyay, A.; Mukherjee, S.; Rukmini, R.; Rawat, S. S.; Sudha, S. Ionization, partitioning, and dynamics of tryptophan octyl ester: implications for membrane-bound tryptophan residues. *Biophys. J.* **1997**, *73*, 839−849.
(26) Chattopadhyay, A.; Arora, A.; Kelkar, D. A. Dynamics of a membrane-bound tryptophan analog in environments of varying hydration: a fluorescence approach. *Eur. Biophys. J.* **2005**, *35*, 62−71.
(27) Arora-Sharawat, A.; Chattopadhyay, A. Effect of structural transition of the host assembly on dynamics of a membrane-bound tryptophan analogue. *Biophys. Chem.* **2007**, *129*, 172−180.
(28) de Foresta, B.; Gallay, J.; Sopkova, J.; Champeil, P.; Vincent, M. Tryptophan Octyl Ester in Detergent Micelles of Dodecylmaltoside: Fluorescence Properties and Quenching by Brominated Detergent Analogs. *Biophys. J.* **1999**, *77*, 3071−3084.
(29) Tortech, L.; Jaxel, C.; Vincent, M.; Gallay, J.; de Foresta, B. The polar headgroup of the detergent governs the accessibility to water of tryptophan octyl ester in host micelles. *Biochim. Biophys. Acta* **2001**, *1514*, 76−86.
(30) Yang, Y.; Zhou, Y.; Ge, J.; Wang, Y.; Chen, X. Synthesis, characterization and infrared emissivity property of optically active polyurethane derived from tyrosine. *Polymer* **2011**, *52*, 3745−3751.
(31) Ley, J. P.; Bertram, H.-J. Synthesis of Lipophilic Clovamide Derivatives and Their Antioxidative Potential against Lipid Peroxidation. *J. Agric. Food Chem.* **2003**, *51*, 4596−4602.
(32) Hassani, M.; Cai, W.; Holley, D. C.; Lineswala, J. P.; Maharjan, B. R.; Ebrahimian, G. R.; Seradj, H.; Stocksdale, M. G.; Mohammadi, F.; Marvin, C. C.; Gerdes, J. M.; Beall, H. D.; Behforouz, M. Novel Lavendamycin Analogues as Antitumor Agents: Synthesis, in Vitro Cytotoxicity, Structure−Metabolism, and Computational Molecular Modeling Studies with NAD(P)H:Quinone Oxidoreductase 1. *J. Med. Chem.* **2005**, *48*, 7733−7749.
(33) Frisch, M. J.; Trucks, G. W.; Schlegel, H. B.; Scuseria, G. E.; Robb, M. A.; Cheeseman, J. R.; Scalmani, G.; Barone, V.; Mennucci, B.; Petersson, G. A.; Nakatsuji, H.; Caricato, M.; Li, X.; Hratchian, H. P.; Izmaylov, A. F.; Bloino, J.; Zheng, G.; Sonnenberg, J. L.; Hada, M.; Ehara, M.; Toyota, K.; Fukuda, R.; Hasegawa, J.; Ishida, M.; Nakajima, T.; Honda, Y.; Kitao, O.; Nakai, H.; Vreven, T.; Montgomery, J. A., Jr.; Peralta, J. E.; Ogliaro, F.; Bearpark, M.; Heyd, J. J.; Brothers, E.; Kudin, K. N.; Staroverov, V. N.; Kobayashi, R.; Normand, J.; Raghavachari, K.; Rendell, A.; Burant, J. C.; Iyengar, S. S.; Tomasi, J.; Cossi, M.; Rega, N.; Millam, J. M.; Klene, M.; Knox, J. E.; Cross, J. B.; Bakken, V.; Adamo, C.; Jaramillo, J.; Gomperts, R.; Stratmann, R. E.; Yazyev, O.; Austin, A. J.; Cammi, R.; Pomelli, C.; Ochterski, J. W.; Martin, R. L.; Morokuma, K.; Zakrzewski, V. G.; Voth, G. A.; Salvador, P.; Dannenberg, J. J.; Dapprich, S.; Daniels, A. D.; Farkas, O.; Foresman, J. B.; Ortiz, J. V.; Cioslowski, J.; Fox, D. J. *Gaussian 09*; Gaussian, Inc.: Wallingford, CT, 2009.
(34) Clint, J. H. Mixed-micelle formation. In *Surfactant Aggregation*; Springer, 1992; pp 130−146.
(35) Huibers, P. D. T.; Lobanov, V. S.; Katritzky, A. R.; Shah, D. O.; Karelson, M. Prediction of Critical Micelle Concentration Using a Quantitative Structure−Property Relationship Approach. 1. Nonionic Surfactants. *Langmuir* **1996**, *12*, 1462−1470.
(36) Okano, L. T.; El Seoud, O. A.; Halstead, T. K. A proton NMR study on aggregation of cationic surfactants in water: effects of the structure of the headgroup. *Colloid Polym. Sci.* **1997**, *275*, 138−145.
(37) Chakraborty, G.; Paulchowdhury, M.; Bardhan, S.; Saha, S. K. Surface activity and modifying effects of 1-Naphthol, 2-Naphthol and 2,3-Dihydroxynaphthalene on self-assembled nanostructures of 1-Hexadecyl-3-methylimidazolium chloride. *Colloids Surf., A* **2017**, *516*, 262−273.
(38) Dong, B.; Li, N.; Zheng, L.; Yu, L.; Inoue, T. Surface Adsorption and Micelle Formation of Surface Active Ionic Liquids in Aqueous Solution. *Langmuir* **2007**, *23*, 4178−4182.
(39) Chen, L. J.; Lin, S.-Y.; Huang, C.-C. Effect of Hydrophobic Chain Length of Surfactants on Enthalpy−Entropy Compensation of Micellization. *J. Phys. Chem. B* **1998**, *102*, 4350−4356.
(40) Galamba, N. Water's Structure around Hydrophobic Solutes and the Iceberg Model. *J. Phys. Chem. B* **2013**, *117*, 2153−2159.
(41) Graziano, G. Comment on "Water's Structure around Hydrophobic Solutes and the Iceberg Model". *J. Phys. Chem. B* **2014**, *118*, 2598−2599.
(42) Shinoda, K.; Kobayashi, M.; Yamaguchi, N. Effect of "Iceberg" formation of water on the enthalpy and entropy of solution of paraffin chain compounds: the effect of temperature on the critical micelle concentration of lithium perfluorooctane sulfonate. *J. Phys. Chem.* **1987**, *91*, 5292−5294.
(43) Sarmoria, C.; Puvvada, S.; Blankschtein, D. Prediction of critical micelle concentrations of nonideal binary surfactant mixtures. *Langmuir* **1992**, *8*, 2690−2697.
(44) Ghosh, S.; Burman, A. D.; De, G. C.; Das, A. R. Interfacial and Self-Aggregation of Binary Mixtures of Anionic and Nonionic Amphiphiles in Aqueous Medium. *J. Phys. Chem. B* **2011**, *115*, 11098−11112.
(45) Tanford, C. *The Hydrophobic Effect: Formation of Micelles and Biological Membranes*; Wiley-Interscience: New York, 1973.
(46) Israelachvili, J. N.; Mitchell, D. J.; Ninham, B. W. Theory of self-assembly of hydrocarbon amphiphiles into micelles and bilayers. *J. Chem. Soc., Faraday Trans. 2* **1976**, *72*, 1525−1568.
(47) Xu, W.; Wang, T.; Cheng, N.; Hu, Q.; Bi, Y.; Gong, Y.; Yu, L. Experimental and DFT Studies on the Aggregation Behavior of Imidazolium-Based Surface-Active Ionic Liquids with Aromatic Counterions in Aqueous Solution. *Langmuir* **2015**, *31*, 1272−1282.
(48) Tanford, C. Micelle shape and size. *J. Phys. Chem.* **1972**, *76*, 3020−3024.
(49) Oliver, R. C.; Lipfert, J.; Fox, D. A.; Lo, R. H.; Doniach, S.; Columbus, L. Dependence of Micelle Size and Shape on Detergent Alkyl Chain Length and Head Group. *PLoS ONE* **2013**, *8*, No. e62488.
(50) Clint, J. H. Mixed-micelle formation. In *Surfactant Aggregation*; Springer, 1992; pp 130−146.
(51) Moroi, Y. Mass action model of micelle formation: Its application to sodium dodecyl sulfate solution. *J. Colloid Interface Sci.* **1988**, *122*, 308−314.
(52) Chatterjee, A.; Moulik, S. P.; Sanyal, S. K.; Mishra, B. K.; Puri, P. M. Thermodynamics of Micelle Formation of Ionic Surfactants: A Critical Assessment for Sodium Dodecyl Sulfate, Cetyl Pyridinium Chloride and Dioctyl Sulfosuccinate (Na Salt) by Microcalorimetric, Conductometric, and Tensiometric Measurements. *J. Phys. Chem. B* **2001**, *105*, 12823−12831.
(53) Galgano, P. D.; El Seoud, O. A. Micellar properties of surface active ionic liquids: A comparison of 1-hexadecyl-3-methylimidazolium chloride with structurally related cationic surfactants. *J. Colloid Interface Sci.* **2010**, *345*, 1−11.
(54) Das, S.; Naskar, B.; Ghosh, S. Influence of temperature and organic solvents (isopropanol and 1,4-dioxane) on the micellization of cationic gemini surfactant (14-4-14). *Soft Matter* **2014**, *10*, 2863−2875.

DOI: 10.1021/acs.langmuir.7b01651
Langmuir 2017, 33, 6581−6594

(55) Kalyanasundaram, K.; Thomas, J. K. Environmental effects on vibronic band intensities in pyrene monomer fluorescence and their application in studies of micellar systems. *J. Am. Chem. Soc.* **1977**, *99*, 2039−2044.
(56) Mehta, S. K.; Bhasin, K. K.; Kumar, A.; Dham, S. Micellar behavior of dodecyldimethylethyl ammonium bromide and dodecyltrimethylammonium chloride in aqueous media in the presence of diclofenac sodium. *Colloids Surf., A* **2006**, *278*, 17−25.
(57) Turro, N. J.; Yekta, A. Luminescent probes for detergent solutions. A simple procedure for determination of the mean aggregation number of micelles. *J. Am. Chem. Soc.* **1978**, *100*, 5951−5952.
(58) Kaur, G.; Chiappisi, L.; Prévost, S.; Schweins, R.; Gradzielski, M.; Mehta, S. K. Probing the Microstructure of Nonionic Microemulsions with Ethyl Oleate by Viscosity, ROESY, DLS, SANS, and Cyclic Voltammetry. *Langmuir* **2012**, *28*, 10640−10652.
(59) Fraenkel, Y.; Gershoni, J. M.; Navon, G. Acetylcholine interactions with trypytphan-184 of the α-subunit of the nicotinic acetylcholine receptor revealed by transferred Nuclear overhauser effect. *FEBS Lett.* **1991**, *291*, 225−228.
(60) Kreke, P. J.; Magid, L. J.; Gee, J. C. 1H and 13C NMR Studies of Mixed Counterion, Cetyltrimethylammonium Bromide/Cetyltrimethylammonium Dichlorobenzoate, Surfactant Solutions: The Intercalation of Aromatic Counterions. *Langmuir* **1996**, *12*, 699−705.
(61) Jiang, Z.; Jia, K.; Liu, X.; Dong, J.; Li, X. Multiple Responsive Fluids Based on Vesicle to Wormlike Micelle Transitions by Single-Tailed Pyrrolidone Surfactants. *Langmuir* **2015**, *31*, 11760−11768.
(62) Ali, M.; Jha, M.; Das, S. K.; Saha, S. K. Hydrogen-Bond-Induced Microstructural Transition of Ionic Micelles in the Presence of Neutral Naphthols: pH Dependent Morphology and Location of Surface Activity. *J. Phys. Chem. B* **2009**, *113*, 15563−15571.
(63) Wangsakan, A.; McClements, D. J.; Chinachoti, P.; Dickinson, L. C. Two-dimensional rotating-frame Overhauser spectroscopy (ROESY) and 13C NMR study of the interactions between maltodextrin and an anionic surfactant. *Carbohydr. Res.* **2004**, *339*, 1105−1111.
(64) Lavoie, S.; Gauthier, C.; Mshvildadze, V.; Legault, J.; Roger, B.; Pichette, A. DFT Calculations and ROESY NMR Data for the Diastereochemical Characterization of Cytotoxic Tetraterpenoids from the Oleoresin of Abies balsamea. *J. Nat. Prod.* **2015**, *78*, 2896−2907.
(65) Liu, Q.; Chen, S.; Chen, J.; Du, J. An Asymmetrical Polymer Vesicle Strategy for Significantly Improving T1 MRI Sensitivity and Cancer-Targeted Drug Delivery. *Macromolecules* **2015**, *48*, 739−749.
(66) Mai, Y.; Eisenberg, A. Self-assembly of block copolymers. *Chem. Soc. Rev.* **2012**, *41*, 5969−5985.
(67) Smart, T.; Lomas, H.; Massignani, M.; Flores-Merino, M. V.; Perez, L. R.; Battaglia, G. Block copolymer nanostructures. *Nano Today* **2008**, *3*, 38−46.
(68) Singh, P. C.; Inoue, K.-I.; Nihonyanagi, S.; Yamaguchi, S.; Tahara, T. Femtosecond Hydrogen Bond Dynamics of Bulk-like and Bound Water at Positively and Negatively Charged Lipid Interfaces Revealed by 2D HD-VSFG Spectroscopy. *Angew. Chem., Int. Ed.* **2016**, *55*, 10621−10625.
(69) Nagarajan, R. Molecular Packing Parameter and Surfactant Self-Assembly: The Neglected Role of the Surfactant Tail. *Langmuir* **2002**, *18*, 31−38.

DOI: 10.1021/acs.langmuir.7b01651
Langmuir 2017, 33, 6581−6594